THE UNIVERSITY
of EDINBURGH

Biochar characteristics and its roles in optimizing anaerobic digestion

Mingyu Hu

THE UNIVERSITY *of* EDINBURGH

Thesis submitted for the degree of
Doctor of Philosophy

The University of Edinburgh
School of Geoscience

Declaration

I declare that this thesis has been composed solely by myself and it has not been previously submitted to any other degree or professional qualification, in part or in whole. Except stated otherwise by reference or acknowledgement, I declare that the work contained herein is my own.

Mingyu Hu

Date: 5th 03 2023

Acknowledgements

Firstly, I would like to express my sincere gratitude to my supervisors Prof Ondřej Mašek and Dr Andrew Free for their advice, supports and guidance throughout the project. Their insightful feedback pushed me to wider my research from various perspectives.

I would like to acknowledge my colleagues from my placement at Leibniz institute for Agricultural Engineering and biotechnology (ATB) for their wonderful collaboration. I would particularly like to thank the research group of Hoffmann, in particular Maja Schultze, Dr Christine Herrmann and Dr Patrice Ramm, and the research group around Dr. rer.agr Thomas Hoffmann in the department of Post-Harvest Technology for their help with the STSM project. I would also like to thank the student Natalie Steller who helped with the experiments as part of her internship project at the ATB Potsdam. In addition, I would also like to thank Gavin Sim, the crew lab staff, John Morman, Stephen Mowbray and Andrey Gromov for their help around my PhD thesis lab work.

I would like to thank my parents for their support and sympathetic ear. You are always there for me. Finally, special thanks go to my partner Ziqiao Liao, who provided stimulating discussions and emotional support, and Suhagi for happy distractions to rest my mind off campus.

Abstract

Over decades anaerobic digestion (AD) has been successfully established as technology to treat organic wastes. The perspective of turning organic wastes into biogas, a source of renewable energy and profit, through a low-cost process, has gained increased interest around this technology. The AD as biological process is strongly dependent on the environmental conditions such as temperature, pH, presence of inhibitors, and nutrients content, that, in particularly unfavourable situations, can attribute to undesirable drop in performance and even for detrimental failures. Therefore, several strategies such as feedstock pre-treatment and process optimization have been developed to secure AD performance. However, these approaches do not remove inhibitor from the process, which may result in accumulation of the inhibitor and further destabilization of the AD system. From this point of view, it is beneficial to develop methods that remove and/or reduce the mobility and bioavailability the inhibitor within the digestion process. In this study, char derived from lignocellulosic wastes was added to anaerobic digestion to elucidate their roles on process performance and efficiency. The results of this analysis suggest that changes of AD performance (i.e. biogas production and intermediates concentrations) are strongly correlated to biochemical characteristics of char materials. Furthermore, the impact of changes in inhibitor concentrations on the digester's performance was observed, and found that inhibition tolerance of AD was improved by the presence of selected char materials. However, contrary to the initial hypothesis based on previous studies in related hydrochar application, the addition of RH hydrochar led to reduction in biogas production but an enhanced methane content in biogas was observed. Except from batch AD tests, a larger-scale AD system (semi-continuous stirring tank reactor) was used to determine the possibility of biochar on enhancing digestate

structure and reduce the sensitivities towards environmental factors such as pH and other inhibitors. The further outcome from scale-up study revealed that biochar had improved ammonium tolerance (1.59 mg NH_4-N/kg) by recovering 12-16.4% biogas production. This study also investigated effects of iron impregnated-thermal activation on physiochemical properties of the resultant biochar. Effects of these modified biochars on gas production and volatile fatty acids concentration was also measured and significant changes was observed. Overall, char material had a positive effect on AD system stability and promoted bio-methanation during the long run operations.

Lay summary

The worldwide high energy demand is primarily rely on the production and consumption of fossil fuels. However, high greenhouse gas emissions, severe air pollution, insecure fossil-based energy crisis, and rapid growth of global transportation fuel demand have raised significant concerns about the development of bioenergy. According to the Intergovernmental Panel on Climate Change (IPCC) and International Energy Agency (IEA) net-zero analysis, the global average of carbon dioxide, methane, and nitrogen compounds rises sharply to a undesirable level (IPCC , 2021; Sun *et al.*, 2021). To accomplish the goals of the United Nations Framework Convention on Climate Change, the 26th Conference of the Parties (COP26), limiting global warming to 1.5^{o}C requires fundamental change in all economic and social sectors. To fulfil these aims, numerous techniques have been proposed, one of which is the employment of negative emission technology (NET), which is a process of converting biomass to bioenergy. Despite the fact that the first generation of biofuels were produced from edible food crops, the utilisation of lignocellulosic biomass and organic wastes for biofuel generation is a potential proposal for reducing environmental issues and minimising waste disposal. Meanwhile, the physiochemical properties of resulting products from thermal conversion are strongly related to the feedstock types, process parameters, and production methods. Therefore, the goal of this project is to examine the impact of feedstock type and manufacturing processes on the characteristics of biochars. Meanwhile, alternative bioenergy conversion technique is anaerobic digestion, which uses microorganisms to convert organic matter to biogas. Yet, anaerobic digestion encounters several challenges, such as low biomass concentration, inhibitions, and system instability; hence, there is interest in overcoming these obstacles and improving AD performance. As such a conclusion, in

this thesis, various biowastes, including digestate from a wastewater treatment plant and animal wastes, were employed to establish several reactors with the addition of biochar. The ultimate aim was to make recommendations on feedstock and production conditions in order to produce an appropriate additive for promoting methane generation. Changes in digestate chemistry and biogas productivity were used to evaluate AD performance in these tests. In this work, it was revealed that the application of biochar in AD may considerably increase ammonium tolerance and improve biogas productivity. The results also showed that activation by impregnation-pyrolysis could improve the surface functionalities of biochar and successfully generate iron oxides on its surface, enabling for a higher biogas generation rate during the AD process. Overall, the findings of this study are very encouraging for the use of biochar in the AD process; nevertheless, further research is needed to assess the underlying biological mechanism of biochar for optimising microbial activity.

Chapter structure

This thesis is comprised of eight chapters. The aims and hypothesis were investigated throughout the five experimental chapters and three of them have been prepared in journal article format. The details of each chapter are showing as follows: Chapter 1 provides a foreword of thesis and a background to energy demands and emerged sustainable energy technologies. It also addresses aims, hypothesis and chapter structure of the thesis. Literature on waste-to-energy techniques, challenges of biological energy conversion, as well as biochar and its use in anaerobic digestion were also reviewed in Chapter 1. It also details research gaps and areas for future research. Chapter 2 provides detailed information on materials and the methodologies used for all experiments and analyses in this project. Chapter 3 investigates the role of surface functionality of standard biochar in the removal of ammonium. It also relates the sorption capacity to the properties of standard biochar on pH titration. Chapter 4 determines the potential effects of biochar derived from different types of feedstocks on co-digestion performance and system stability. In chapter 5 the characterization of hydrochar and its application on sewage sludge digestion were investigated. Chapter 6 details the iron-doping modification and its role on AD system stability. Chapter 7 summaries the key findings of the thesis and acknowledges the limitations of the research as well as provides suggestions on further studies.

Table of Contents

List of abbreviations

Abbreviation	Definition
AC	Ash content
AD	Anaerobic digestion
AL	Alkali lignin
ATB	Leibniz institute for Agricultural Engineering and biotechnology
ATR-FTIR	Attenuated Total Reflectance - Fourier Transform Infrared Spectroscopy
BMP	Biomethane Potential Test
CEC	Cation exchange capacity
C/N	Carbon to Nitrogen ratio
COD	Chemical oxygen demand
CSTR	Continuous stirred tank reactor
DIET	Direct interspecies electron transfer
DIR	Dissimilatory iron reduction
DOC	Dissolved organic carbon
EC	Electrical conductivity
EDC	Electron donating capacity
EPS	Extracellular polymeric substances
FAN	Free ammonia nitrogen
FC	Fixed carbon
GC-FID	Gas chromatography with flame-ionisation detection
H/C	Hydrogen-to-Carbon ratio
HD	Hardwood and digestate
HRT	Hydraulic retention time

HTC	Hydrothermal carbonization
IEA	International Energy Agency
IPCC	Intergovernmental Panel on Climate Change
ICP-OES	inductively coupled plasma optical emission spectrometry
MC	Moisture content
O/C	Oxygen-to-Carbon ratio
OSR	Oilseed rape pellets
PZC	Point of zero charge
RH	Rice husk
SD	Standard deviation
SS	sewage sludge granule
TAN	Total ammoniacal nitrogen
TGA	Thermogravimetric analysis
THP	Thermal hydrolysis plant
TKN	Total Kjeldahl Nitrogen
TOC	Total organic content
TSS	Total suspended solids
UKBRC	UK Biochar Research Centre
UV-vis	UV-visible spectrophotometer
VFA	Volatile fatty acids
VM	Volatile matter
VSS	Volatile suspended solids
WSP	Wheat straw pellets
WT	Weight
WWTP	Wastewater treatment plant

XRD	X-ray diffractometer

List of Figures

List of Tables

1. Introduction

1.1. Background

Currently, fossil-based energy resources, such as petroleum, coal, and natural gas, are responsible for about three-quarters of the world's primary energy consumption, each corresponding to 33, 24, and 19%, respectively whereas renewable energy sources (i.e., solar, wind, and biofuel) only contributed a mere 13% (Appels *et al.*, 2011; IEA, 2011). According to the International Energy Agency, the global energy demand still largely relies on the use of fossil fuels, which is expected to account for 80% of the global energy demand by 2040 (IEA, 2017). In spite of their qualities, the generation of heat and power by using fossil fuels is the main cause of anthropogenic emission of greenhouse gases (GHG) at a large scale accounting for 25% of total global GHG emissions (IPCC, 2014). Meanwhile, fossil fuels are unevenly distributed and facing depletion challenge, for instance over 200 billion tonnes (Gt) of coal (both hard and lignite) are remaining unburned in the United States and the Former Soviet Union countries while developing countries such as China and India have a twenty-five percentages points higher rate of coal utilization (McGlade & Ekins, 2015). Consequently, it would increase the concerns about energy security and their availability for the future generation. All the above-mentioned issues contributed to the urge for new solutions that can reduce the environmental negative impacts of conventional energy system, thus alternating a sustainable energy sector.

Renewable resources such as biomass, solar and wind would play a crucial role in increasing sustainability by the reduction of the net emissions of carbon dioxide (CO_2) to the atmosphere and improving the economy of those regions challenged to fossil fuels insecurity. Among them, biomass could be the most suitable candidate to serve

as a low-cost feedstock for fuel production. However, increasing important moral and ethical questions have arisen from the use of 1st generation biomass such as sugarcanes, starch crops and vegetable oils for the engineering practice of fuel production, due to competition with food demands and consumption. It is necessary to develop sustainable biofuels without competing food supplies. Table 1-1 lists various biofuel generations and their pros and cons.

Table 1-1. Selected pros and cons for each biofuel generations.

Generations of Biofuels	Primary	Secondary	Tertiary
Biomass sources	Edible Biomass: Sugar Beet, Sugarcane, Wheat, Corn, potato wastes, and sugar beets	Non-edible feedstocks sources include wood, agricultural residues, organic waste, food waste and grass	Algae
Advantages	Well implemented around the world	Not come directly from food crops; Less requirements of land; A replacement for conventional petroleum based fuels	Ability to grow whole year around; Less water consumption rate; Higher growth potential; The ability to grow under harsh conditions such as saline, costal seawater
Disadvantages	In competition with food market; Biomass for the 1st generation biofuels requires lots of land to cultivate	Considerably high production costs; Requirement of clear and long-term policy frame work; Lack of adequate harvesting, storage and transport systems for process and distribution biomass in large scales	Additional dewatering and other pre-treatment methods required before extracting lipid; High cultivation cost as compared to conventional crops; High energy input

Lignocellulosic biomass is the predominate renewable resource, which could be commonly found in most natural ecosystem and agricultural/forestry related industries. Due to its large abundance and availability, it has gained increased interests for

substitution of fossil fuels (Perlack, 2005; Serrano-Ruiz *et al*., 2010). Table 1-2 lists various types of lignocellulosic biomass with some examples. Lignocellulosic biomass has three main constituents: cellulose, hemicellulose and lignin with varied amount of other inorganic constituents and extractives (including alkaline earth and alkali metallic species) (Eom *et al.*, 2011). Unlike easily degradable cellulose and hemicellulose, lignin has been found fairly stable and resistant to chemical attack by forming a hydrophobic cross-linked network between hydrogen bonded crystalline cellulose and hemicellulose polysaccharides (Hatfield & Fukushima, 2005). Considering the chemical complexity and structural rigidity of lignocellulosic biomass, various techniques have been employed to convert this resource into valuable products and transportation fuels, by subjecting to several processes, such as enzymatic saccharification and degradation into fermentable sugars with additional physical and chemical treatment to overcome its recalcitrant nature (Malherbe & Cloete, 2002; Taha *et al.*, 2016). Encountered those obstacles, lignocellulosic biofuels cannot yet be produced economically at the commercial scale due to the increased operational and productional cost (Chowdhury & Loganathan, 2019).

Table 1-2. Lignocellulosic biomass feedstocks available for energy purposes.

Supply sector	Type	Examples
Agriculture	Lignocellulosic energy crops	Herbaceous crops (e.g. switchgrass, miscanthus, reed)
	Crop residues	Crop straw (e.g. rice straw, wheat straw, corn stalk, cotton stalk)
	Oil, sugar and starch energy crops	Rape seed; Sugarcane; Corn
Forest	Dedicated forestry	Short rotation plantations (e.g. willow, poplar, eucalyptus)
	Forestry by-products	Barks; wood blocks; wood chips from tops and branches; wood chips from thinning; logs from thinning
Industry	Lignocellulosic agricultural-industrial residues	Rice husks; sugarcane bagasse; corn cob
	Wood industry residues	Industrial waste wood; sawdust from sawmills
Other	Lignocellulosic wastes	Residues from parks and gardens (e.g. pruning, grass, fallen leaves)

1.2. Lignocellulosic residues and wastes

Lignocellulosic residues and wastes can be found as undesired components from agriculture and forestry, or as by-products generated from anthropological activities (Khanal *et al.*, 2010). To be more detailed, biomass residues include primary, secondary, and tertiary wastes. Primary residues are solid vegetal residues generated from harvesting or plantation, including straw, corn stover, leaves and stems. Secondary residues are the fraction discarded from the agricultural process or the food chain. Rice husk, sugarcane bagasse and woodchips are typical secondary biomass residues. On the other hand, tertiary residues are generated from the consumption by human or animals, such as municipal solid wastes, fat, greases, and these residues can be further converted into wastewater and sewage sludge (Lee *et al*., 2019). Figure

1-1 illustrates typical biomass conversion technologies and their primary products and end-uses.

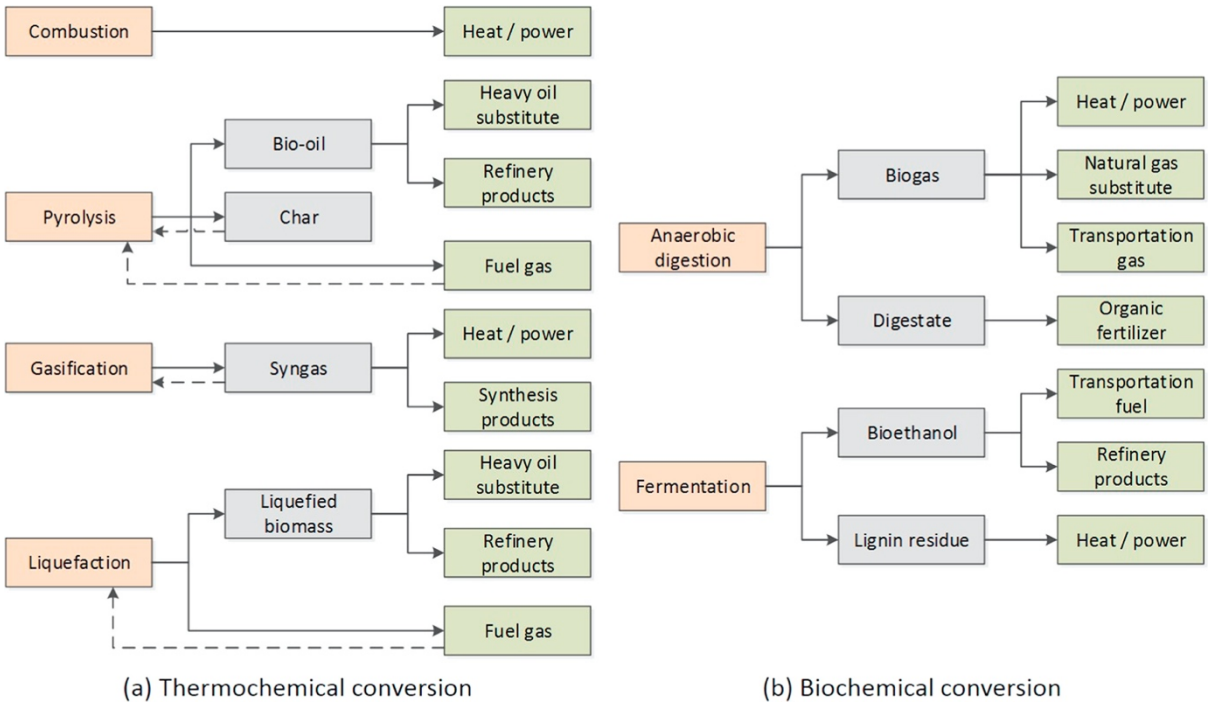

Figure 1-1. Thermochemical and biochemical conversion of lignocellulosic biomass (Cai, 2017).

1.2.1. Agricultural residues

Agricultural residues such as rice husk, wheat straw, corn stover that are generated through the cultivation and harvesting have been recognized as an available and inexpensive renewable lignocellulosic fibre feedstocks for biofuels (Adhikari, *et al.*, 2018). The role of agricultural residues has been verified by several studies in terms of its environmental benefits in thermochemical conversion, biohydrogen generation, and bioethanol production (Limayem & Ricke, 2012; Pooja, *et al.*, 2018; Saratale *et al.*, 2019; Sarkar *et al.*, 2012). For instance, around 140-350 Mt of agricultural residues including corn stover and wheat straw are mainly used in the industrial facilities, and 54.95% of these residual biomass have the potential for bioenergy generation in the USA (Daly *et al.*, 2018; Perea-Moreno *et al.*, 2019). The developing countries such as

Brazil, China and India accounted for 53.95% of global agricultural residues (Tripathi *et al.*, 2019), which can ensure potential practice of bioenergy production. In tropical regions like south America and Africa, sugarcane residues including bagasse and leaves are abundant, and recognized as a good alternative for the heat and electricity unitization, or the production of bio-ethanol and biochar (Chandel *et al.*, 2012; Lim et al., 2020).

1.2.2. Municipal sewage sludge

Sewage sludge is a by-product generated from the wastewater treatment plant (WWTP) after primary and secondary treatment processes, which contains high concentrations of organic substances and biogenic elements (Smoliński *et al.*, 2019). With increased population, a significant amount of sewage sludge can be generated due to the intensive anthropological activities. In the European countries, around 50 million tonnes of sewage sludge are produced annually while the USA is producing 40 million tonnes (Kelessidis & Stasinakis, 2012). In China, an annual sewage sludge production of about 60 million tonnes is estimated, and the majority of these are landfilled or used as agricultural fertiliser (Tao *et al.*, 2018). The dominant fraction in primary and secondary sludges is nitrogen-rich material ranging between 25 and 40%, and followed with lignin-rich compounds accounted for 20-30% (Navia & Mittelbach, 2012). Up to the present, three main types of sludge are produced during the activated sludge wastewater treatment process including: a primary sludge which composed floating grease and solids materials; a secondary sludge which is a combination of microbial cells and suspended solids generated from biological settlement tank; a tertiary sludge produced from anaerobic digestion (Manara & Zabaniotou, 2012; Navia & Mittelbach, 2012). Several studies verified that sewage sludge can be used as a soil

amendment for agricultural and phytoremediation purposes, and has the potential for biodiesel production due to its high content of lipid (Smoliński *et al.*, 2019; Bora *et al*., 2020). In addition to that, the presence of heavy metals, toxic compounds, and microbial pathogens in sewage sludge may restrict its application and cause unwanted toxic effects on plant growth and/or public hygiene (Kominko *et al.*, 2017; Johnson and Affam, 2019). Thus, it is important to introduce integrated options for sludge management.

1.3. Waste-to-Energy (WTE) technology

Waste-to-Energy approaches such as incineration, pyrolysis, gasification, anaerobic digestion, bio-methanation, and landfill gas recovery serve as effective lignocellulosic biomass conversion treatments, while giving rise to energy valorisation (Cai, 2017). This section mainly focuses on thermal and biochemical conversions.

1.3.1. Thermal conversions

There are three main commercially thermal processes for upgrading the biomass into various energy products from: combustion, gasification and pyrolysis (de Jong and van Ommen, 2014; Lewandowski *et al*., 2020). Figure 1-2 shows the different thermal treatment pathway to obtain desired end products. Although the combustion and gasification system are wildly available in most industrialized and developing countries for many years, there are considerable drawbacks. Generally, combustion and gasification require higher energy input at high temperatures of 800-1000^{o}C (Akhtar *et al.*, 2018). Furthermore, biomass with low content of lignin exhibits incomplete combustion and lower char yield by prolonging the burning (Dorez, Ferry, Sonnier, Taguet, & Lopez-Cuesta, 2014).

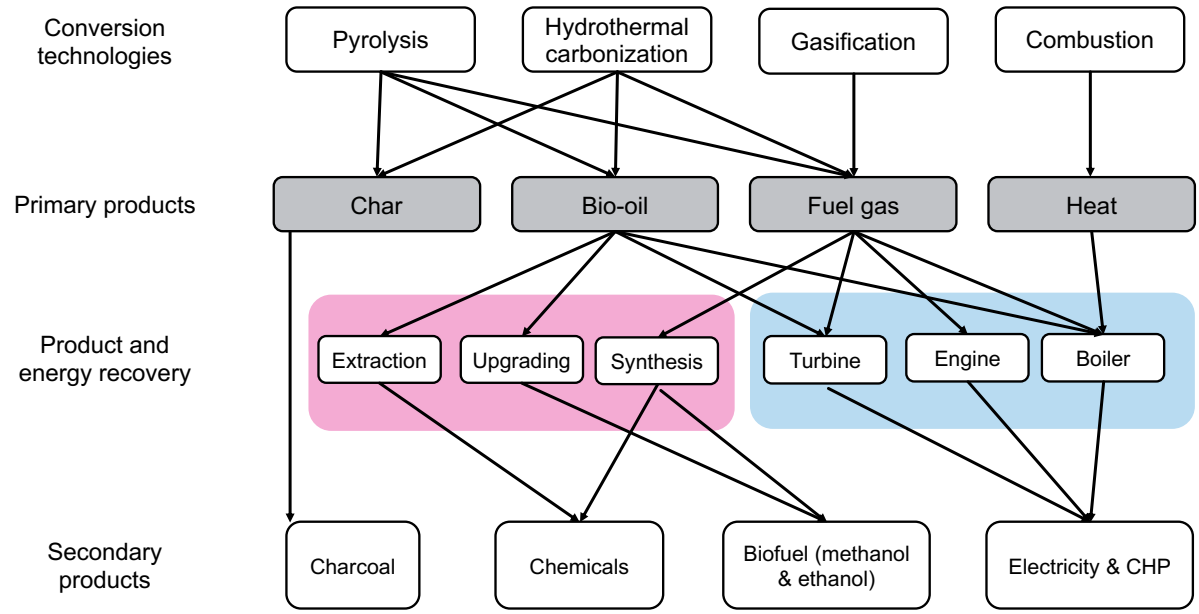

Figure 1-2. Products from thermal biomass conversion (Bridgwater, 2012).

Alternatively, pyrolysis appears to favour the biomass conversion with lower operational temperature of 280-850°C and reasonable vapor residence times. In pyrolysis, half the organic matter in biomass is decomposed to low molecular weight liquids or gases products, while the rest of the substances can be dominantly distributed into pyrolytic residue (termed biochar) in a solid form in the absence of oxygen (H. Yang, Yan, Chen, Lee, & Zheng, 2007). Table 1-3 represents the various products from pyrolysis of lignocellulosic biomass. Pyrolysis process can be divided into three stages including pre-pyrolysis, main-pyrolysis and the formation of carbonaceous products (Tomczyk, Sokołowska, & Boguta, 2020). In detail, the moisture and light volatiles in the biomass are evaporated at 200°C in the first stage. At the same time, formations of hydroperoxide and functional groups such as -COOH and -CO occur when the chemical bonds break. The hemicelluloses and cellulose are then devolatilized and decomposed at temperature ranging from 200 to 500°C during the second stage. When the temperature reaches up to 500°C, the lignin and other organic matter with stronger chemical bonds are then degraded. Therefore, the char

is formed in three sequent pathways: solid-solid interaction at the second stage, solid and organic vapour or tars reaction, and gas-solid interaction (Pattanotai *et al*., 2015).

Table 1-3. Various products obtained from pyrolysis of different lignocellulosic biomass.

Type of lignocellulosic biomass	Type of pyrolysis	Operational temperature (°C)	Reactor	Type of products	Products yield	Reference
Rice straw	Flash carbonization	800-1200	Fixed bed reactor	Biochar	20.8-61.54%	(Chen *et al*., 2017)
Rice husk	Fast	500	Semi-batch pyrolysis	Bio-oil	2.60%	(Kusworo, 2020)
Oil palm empty fruit bunches	Fast	500	Semi-batch pyrolysis	Bio-oil	4.30%	(Kusworo, 2020)
Coconut shell	Flash/fast	400 to 600	Fixed bed reactor	Biochar	33.6-28.6%	(Sarkar, 2020)
Wood waste	Continuous microwave-assisted pyrolysis	800	Lab-scale reactor	Syngas	67%	(Zhou *et al*., 2020)

Hydrothermal carbonization (HTC) is a promising thermochemical process for biomass utilization and biofuel production. Several literature have mentioned the sequent chemical reactions (Figure 1-3) include hydrolysis, dehydration, decarboxylation, condensation polymerization, and aromatization appear during HTC process (Funke and Ziegler, 2010; Nizamuddin *et al.*, 2017). Biomass substances are hydrolysed to oligomers saccharides of cellulose and monomers such as phenolic fragments in the first stage. Hemicellulose is hydrolysed at lower temperature of 180°C. On the other hand, cellulose and lignin are degraded at around 200°C. By the meantime, hydrothermal degradation results in the formation of highly reactive products such as acetic acid (Mok & Antal, 1992). These products are then utilized

into oligomer during the interaction between lignin and hemicellulose fragments. The hydroxyl group in the condensation of fragments is eliminated in the dehydration stage, and sequentially lowered the H/C and O/C ratios. Carboxyl and carbonyl groups that obtained from the hydrolysis of cellulose are degraded in the decarboxylation process. The solid phase (hydrochar) are produced from humic acids, bitumen and a fraction of undegraded component of cellulose during the course of ongoing polymerization (Sevilla & Fuertes, 2009). At the same time, carbohydrates in hemicellulose and cellulose are able to form aromatic structures under alkaline conditions at temperatures ranging from 200-300°C. These aromatic structures potentially provide a building base for the formation of the resulting hydrochar during the aromatisation process. The presence of water facilitate the chemical carbonization by serving as a reacting medium and a oxidised composite under thermal conditions (Nizamuddin *et al.*, 2017).

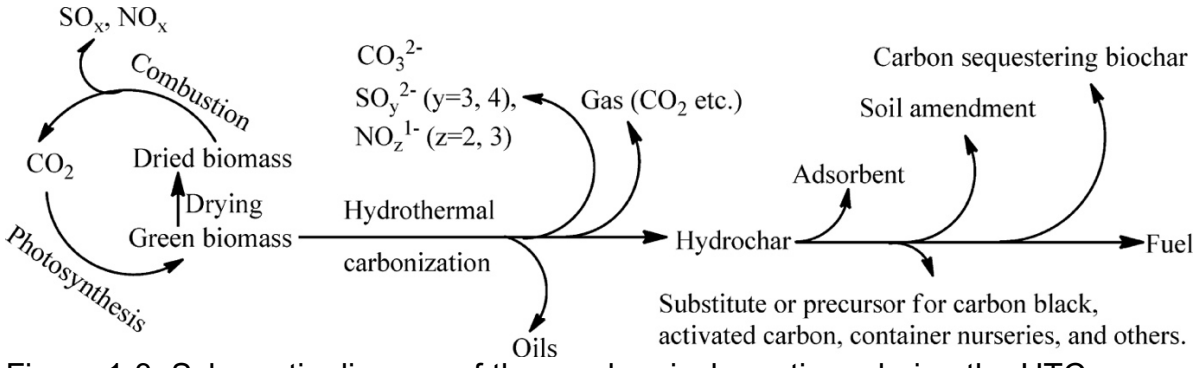

Figure 1-3. Schematic diagram of thermochemical reactions during the HTC process and potential application (Kang *et al.*, 2012b).

As compared to other thermal conversion techniques, HTC performs at a mild operating condition in the temperature range of 100-300°C, attributed to lower energy input (Kang *et al*., 2012a). HTC can also be applied to wet biomass as water serves as the solvent with varied dissolved gases such as CO_2, nitrogen oxides, and sulfur oxides (Kang *et al.*, 2012a) (Table 1-4). In pyrolysis process, drying pre-treatment is

required for biomass with relatively high moisture content whilst may increase heat inputs for vaporization (Akhtar & Amin, 2011). HTC therefore offers alternatives for biomass utilization and biofuel production together with the overall economic values. Meanwhile, biomass with high content of crystalline cellulose can be effectively carbonized in the HTC process due to the presence of hot water as a reactant, solvent and catalyst by donation of hydrogen ions (Funke & Ziegler, 2010; Titirici & Antonietti, 2010). Thus, HTC has positive potential to a wilder industrial application for energetic purposes.

Table 1- 4. Selected studies of hydrothermal carbonization for carbon-rich material formation.

Feedstock	Temperature (°C)	Time (hrs)	Products	Carbon yield (%)	Reference
Rice husk	300	16	Biochar	47.32	(Kalderis, 2014)
Corn stalk	200	40	Hydrochar microspheres	56.97	(Lei, 2016)
Lignin	265	20	hydrochar	68.43	(Kang, 2012)
Tamarix ramosissima	250	4	Carbon microspheres	72.08	(Xiao, 2012)
Kenaf Fiber	225	10	Biochar	60.2	(Zakaria, 2016)
Cellulose	250	2	Carbonaceous microspheres	71.46	(Sevilla, 2009)

1.3.2. Effects of process parameters on physiochemical properties of the resultant char

The key physicochemical properties of biochar and hydrochar include pH, elemental content, particle size distribution, surface area and porosity, surface functional groups

and electrical conductivity (EC). The characteristics and yields of the emitted products from thermal conversion have reported to depend on several operating parameters such as temperature, heating rate, and residence time as well as the feedstock type (Yaman, 2004; Apaydin-Varol and Pütün, 2012; Garcia-Nunez *et al.*, 2017; Tomczyk *et al*., 2020). Increasing both pyrolysis time and temperature result in a higher carbonization degree of the char product, while decreasing the char yield and its surface functionality (Mohan *et al.*, 2014). Mašek *et al.* (2013) reported that the increased pyrolysis temperature from 350^{o}C to 550^{o}C facilitated the stability of biochar obtained from pine, mixed larch, spruce chips, and wood chips by increase the concentration of stable carbon. Meanwhile, they also found that the increasing heating rate has negligible effects on the yield of stable carbon. Study by Zhang *et al.* (2015) has also reported that the total carbon content of biochar derived from straw and lignosulfonate increased with increasing pyrolysis temperature while the volatile matter and production yield of char decreased. In addition to that, biochar obtained from higher temperature possesses diverse physical structure, greater ash content and larger surface area (Chen *et al.*, 2014). Conversion temperature can also result in the transformation of electron donating moieties from the phenol surface functional groups to aromatic C=C surface functional groups when temperature elevated from 400^{o}C to 800^{o}C (Xu *et al.*, 2020). The selected effects of the biomass nature and the pyrolysis conditions on characteristics of the char product were summarised in Table 1-5.

Table 1-5. Effects of properties with increasing values on the pyrolysis product (Santhoshkumar and Anand, 2019)

Parameter	Yield with increasing value of the parameter	Physicochemical properties	Other comments
Heating rate	Decrease the char yield; Increase the syngas and bio-oil yields	Increase the surface area and the porosity; activate the oxygen and hydrogen contents	
Temperature	Decrease the char yield; Increase the syngas yield	Increase the concentration of a larger aromatic ring on the surface of char; Improve the char's structure	Decrease the CO_2 concentration in the syngas
Residence time	Increase the char production	Reduce the surface functionality of char; decrease the active sites on char surface; cause the loss of structural ordering	
Biomass nature	No effect	The initial biomass pertains the structure and physicochemical properties of the char	

The major types of feedstocks used for biochar and/or hydrochar productions are agricultural and forestry residues, municipal solid wastes (MSW), and animal manures (Lu *et al.*, 2012; Nizamuddin *et al.*, 2017; Sipra *et al.*, 2018; Hassan *et al.*, 2020; Ippolito *et al.*, 2020; Tomczyk *et al*., 2020; Lin *et al.*, 2021). Furthermore, using marine algae and sewage sludge granule as feedstocks for pyrolysis and/or HTC has also gained a wide interests due to the abundance and availability of these materials (Chen *et al.*, 2017; Liu *et al.*, 2018; Barry *et al.*, 2019; Aravind *et al.*, 2020). Sewage sludge is a by-product obtained from municipal and industrial wastewater treatment which also consists high concentrations of heavy metals and nutrients (Hossain *et al.*, 2011). Therefore, pyrolyzing sewage sludge can not only reduce its weight and volume, but also produce value-added biofuels while prevent any potential health risks associated with its disposal.

The physical structure of biochar obtained from lignocellulosic biomass can inherit the architecture of the feedstock, and consequently affects its potential applications (Sohi *et al.*, 2010). While non-woody biomass including agricultural residues, animal wastes, marine algae and sewage sludge have considerably higher content of moisture which can alter production process, and influence the char's physicochemical characteristics (Tripathi *et al.*, 2016). Meanwhile, feedstock material that are rich in hydrogen, such as sugar, can develop a cross-link system during pyrolysis (Mészáros *et al*., 2007). The resultant biochar therefore cannot inherit the original structure of the feedstock and may have lower porosity. Pyrolyzing feedstock with lower moisture content can enhance poly-aromatization and form biochar with graphite-like structure (Darmstadt *et al.*, 2000). Meanwhile, feedstock material containing higher nutrients, such as animal wastes can result in nutrients accumulation in biochar as compared to

lignocellulosic biomass. Sarfaraz *et al.* (2020) reported that biochar produced from animal wastes have relatively high nitrogen content as compared to the plant materials, because of the presence of more nitrogen concentration in the parent material. They also found that high phosphate concentration (3.33-4.88%) in the biochar produced from swine manure and poultry litter biochar than those in the biochars obtained from rice straw and corn straw. Meanwhile, feedstock type can influence total ash content and the carbon-to-nitrogen (C/N) ratio of biochar (Bourke *et al.*, 2007; Gaskin *et al.*, 2008; Singh *et al.*, 2010; Amonette and Joseph, 2012; Qambrani *et al.*, 2017).

1.3.3. Influences of thermal techniques on char properties

Due to the different formation mechanisms of biochar and hydrochar, they may have distinctive characteristics. As discussed earlier, hydrochar produced by using hot water as solvent generally has a lower C content and lower ash content, because the ash content in hydrochar dissolved in the liquid phase (Zhang *et al.*, 2019). Furthermore, hydrochar has lower surface area due to the persistence of the decomposition products on the surface of hydrochar and then bloke partial of pores (Fang *et al.*, 2018). However, the surface functionality of hydrochar is greater than that of biochar due to the presence of carbonaceous nanoparticles with a hydrophobic-core and hydrophilic shell on the surface of hydrochar (Keiluweit *et al.*, 2010). Hydrochar may also have higher pore volume attributing to the high inorganic matter content of hydrochar (Dieguez-Alonso *et al.*, 2018). Table 1-6 shows a selection of factors influencing the thermal conversion process and the resultant char's properties.

Table 1-6. A selection of factors influencing the thermal conversion process and the resultant char's properties (Kambo & Dutta, 2015).

	Char yield (%) with the increased value of parameter		**C/H and C/O ratios with the increased value of parameter**		**Porosity with the increased value of parameter**	
Parameter	**Pyrolysis**	**HTC**	**Pyrolysis**	**HTC**	**Pyrolysis**	**HTC**
Process temperature	Decrease	Decrease	Increase	Increase	Increase when temperature less than 500^{o}C, further decrease with high pyrolysis temperature	Increase up to 230^{o}C, then decreased
Heating rate	Decrease	-	Increase	-	Increase from 5-100^{o}C/min, further decrease	-
Residence time	Decrease	Decrease	Increase	Increase	Increase	Increase
Pressure	Decrease	Increase	-	-	Decrease	Decrease
Moisture content of feedstock	Decrease	Not affected	-	-	May require extra energy input for drying	Not affected

1.3.4. Modification and/or activation

In spite of the potential application of biochar for environmental uses, increased researchers has been attracted to the modification of biochar in order to enhance its functions and environmental benefits (Ok *et al.,* 2015). In this section, we mainly focus on the magnetic modification of biochar.

Magnetic modification is performed on the basis of facilitating the separation ability of biochar particles after treatment process. The existing techniques for producing magnetic biochar include precipitation and combined thermal-chemical treatment (Chen *et al*., 2011; Zhang *et al.*, 2013). Hao *et al.* (2018) developed a magnetic biochar through co-precipitation of ferrous and ferric salts and followed by heating at 60^{o}C. The engineered magnetic biochar exhibited higher phenol removal efficiency with increased mass magnetic susceptibilities compared with pristine biochar (Hao *et al.*, 2018). Similarly, Zhang *et al.* (2013) reported an enhancement in ferromagnetic property of magnetic biochar produced from thermal pyrolysis of ferric salt treated biomass at 600^{o}C by embedding nanosized γ-Fe_2O_3 particles in biochar matrix. They also found that the resulting engineered biochar improved the removal of arsenic. Meanwhile, it has been shown that magnetic biochar has a rougher surface and higher surface area than the pristine biochar while decreased pore volume (Khan *et al.*, 2020). Similar observations were also reported in the literature (Wang *et al.*, 2011; Zhang *et al.*, 2013; Zhao *et al.*, 2019; Zheng *et al.*, 2020). Regardless of this, understanding the effects of magnetic modification on the biochar characteristics and its applications is not an easy task and as such our knowledge of transformation through different pathway is still developing.

1.3.5. Biochemical conversions

Biochemical conversion uses microorganisms or enzymes such as Glycoside Hydrolases, Polysaccharide Lyases, Carbohydrate Esterases, Lignin Oxidases, and Lignin Degrading Auxiliary enzymes families to convert biodegradable waste into biofuels and biochemicals (Lee *et al.*, 2019). The typical process options include anaerobic digestion, bioethanol fermentation and bio-hydrogen production. This section focuses on anaerobic digestion (AD) and selected factors influencing the AD process.

Anaerobic digestion (AD) involves the degradation and stabilization of organic substrates by a microbial consortium of various microorganisms under anaerobic condition and leads to energy recovery in the form of biogas. The valorised biogas, as a renewable energy source, mainly consists carbon dioxide and methane. It can be upgraded to natural gas by purification in the natural gas grid or in a combined heat and power (CHP) installation for the simultaneous generation of heat and electricity (Appels *et al.*, 2008; Appels *et al.*, 2011). Meanwhile, AD is identified as an efficient technique to reduce or eliminate a large proportion of pathogens and pollutants. Cao *et al.* (2015) found that anaerobic digestion has great potential to digest plants used in remediation with a 100 mg kg^{-1} Cu levels and provide bioenergy recovery with the maximum methane production of 5722 mL/g.

According to the European Biogas Association (EBA), up to 17783 biogas plants are installed and operating in Europe, with a total installed electric capacity (IEC) of 10532 MWe by 2017 (EBA, 2018). Among the European countries, Germany is the leading force in biogas market with 10971 plants, and followed by Italy with 1655 plants (EBA,

2017). In 2020, there are 579 operational AD facilities in the UK, with a total capacity of around 466.086 Megawatt electrical (MW_e) (Anaerobic Digestion, 2018). In developing countries such as Asia-Pacific regions and Africa, the majority of anaerobic digestion plants are implemented in domestic or farm-based facilities (Patinvoh & Taherzadeh, 2019). Among these countries, China has the highest numbers of household digesters (up to 26.5 million), with capacity of 10.5 billion m^3 biogas production (Chen *et al.*, 2010). In India, strategies and policies were also made to encourage the implementation of family-sized and community AD plants, and installed a total of 5 million biogas plants by 2018 (Mittal *et al.*, 2018). Meanwhile in Nigeria, an estimated of 482 Mwe of electricity can be generated by the anaerobic digester by 2030 (Suberu *et al.*, 2013). These observations showed that the biogas plant would not only escalate waste management, but also benefit with developing countries and rural areas where experiencing the shortage of energy supplies.

Anaerobic digestion has been recognised as a complex process with a number of sequential and parallels steps under anoxic conditions (Hagos *et al.*, 2017). There are four stages taking place during the process of anaerobic digestion: hydrolysis, acidogenesis, acetogenesis, and methanogenesis (Chiappero *et al.*, 2020). A simplified schematic diagram of the four digestion stages is showed in Figure 1-4.

In hydrolysis, complex polymers included polysaccharides, lipids, suspended organic matters and proteins are decomposed into component units such as glucose, amino acids, soluble organic matters and fatty acids though enzymatic cleavage (Xu *et al*., 2019). These hydrolytic products are able to diffuse through the cell membrane and used as nutrient sources for acidogenic microorganisms. However, certain substrates

such as lignocellulosic biomass may be difficult to degrade due to its complex structure formed among lignin, cellulose and hemicellulose compounds, and result in reduced hydrolysis rate (Lin *et al.*, 2010).

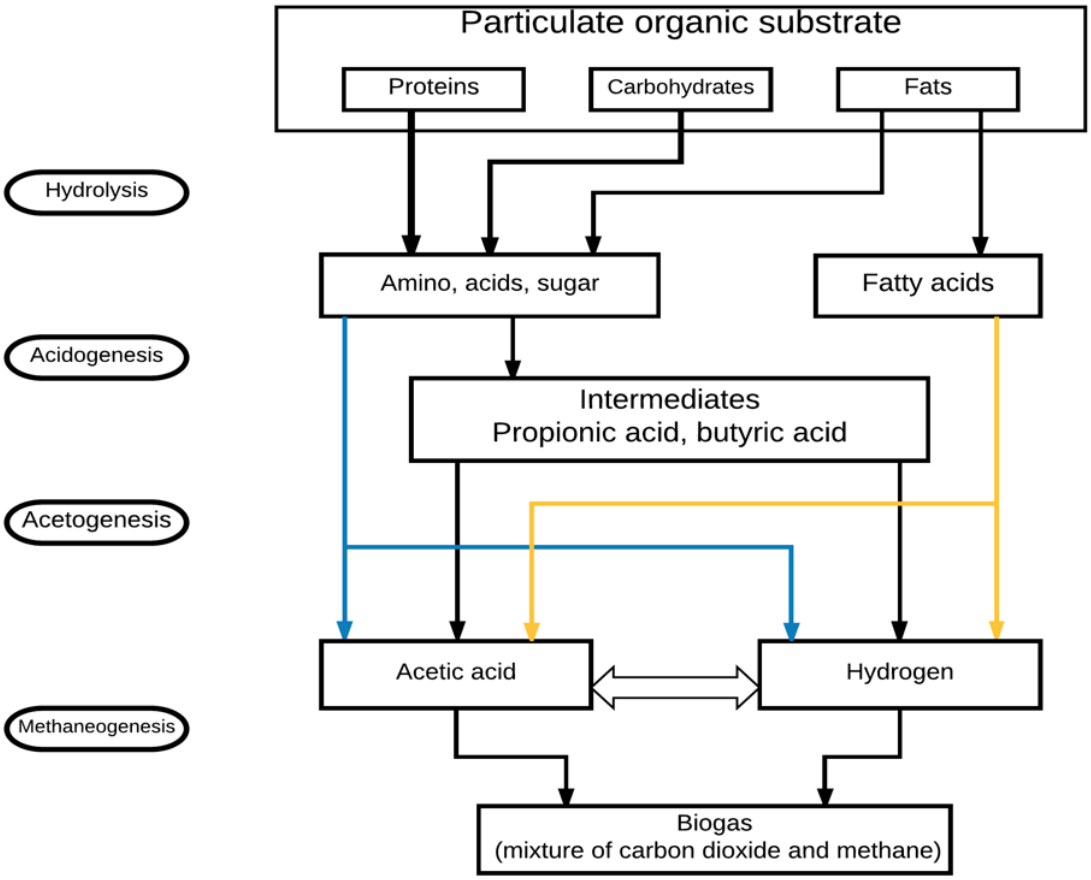

Figure 1- 4. Degradation steps of anaerobic digestion bioprocesses.

After diffusing into the cell membrane of acidogenic microorganisms, those soluble compounds are degraded into short chain volatile acids, ketones, alcohols, hydrogen and CO_2 (Anukam *et al.*, 2019). The volatile fatty acids (VFAs) formed in the acidogenesis stage serve as a substrate for CH_4-forming microorganisms. This degradation process resulted in forming a number of organic acids including acetates, propionate and butyrate, and smaller amount of ethanol and lactate (Meegoda *et al.*, 2018). The next stage is acetogenesis that acetogenic microorganisms digest the acid phase products into acetate (CH_3COO^-) and hydrogen (de Bok *et al.*, 2005; Schink,

1997). The rate of acid production during the acidogenesis stage depends greatly on the operational conditions of the digester. Unlike other stages, the rate of acidogenesis is generally faster than all other stages of AD, with the maximum conversion time of 36 hours (Deublein & Steinhauser, 2010). With the rapidity of this stage in mind, the intermediate products generated in this process which are used as precursor in next step have great influence on the final product during methanogenesis process (Adekunle & Okolie, 2015). These products are further consumed as substrates for acetoclastic methanogenesis in the third phase. In this process, the short chain volatile fatty acids (VFAs) and alcohols are converted into acetate, hydrogen and carbon dioxide; while the long chain VFAs are converted into acetate and hydrogen (Wellinger *et al*., 2013). It should be noted that acetogenesis collaborates with the next group in the methanogenesis stage, and associates with the hydrogen interspecies transfer (Zhang & Zang, 2019).

In the methanogenic phase, intermediate products are converted to biomethane and carbon dioxide. It should be noted that methanogenic activities carry out in higher pHs than all other stages of anaerobic digestion (Khelaifia *et al.*, 2013). Furthermore, methanogenesis has been found as the slowest biochemical reaction than other reactions, which taking up to 5-16 days (Meegoda *et al.*, 2018). In the batch digester, the duration of methanogenesis may even take longer up to 40 days which is evaluated by the rate of biogas production (Zhu *et al.*, 2019).

1.3.6. Types of Anaerobic Digestion System

Various types of anaerobic digestion system have applied in agricultural and industrial sectors such as single stage and two-stage batch digester (Figure 1-5). In one-stage

system, all substrates are loaded simultaneously, and all of the biological reactions occur in the same reactor sequentially; the digestate is then discarded when the biogas production is negligible (Meegoda *et al*., 2018). On the other hand, the two-stage digestion system typically consists of a hydrolysis reactor and a methanogenic reactor. The substrate is fed into the first reactor where hydrolysis and acidification take place. The acidified effluent is then transferred to the second reactor and utilized by microorganisms (Van *et al.*, 2020).

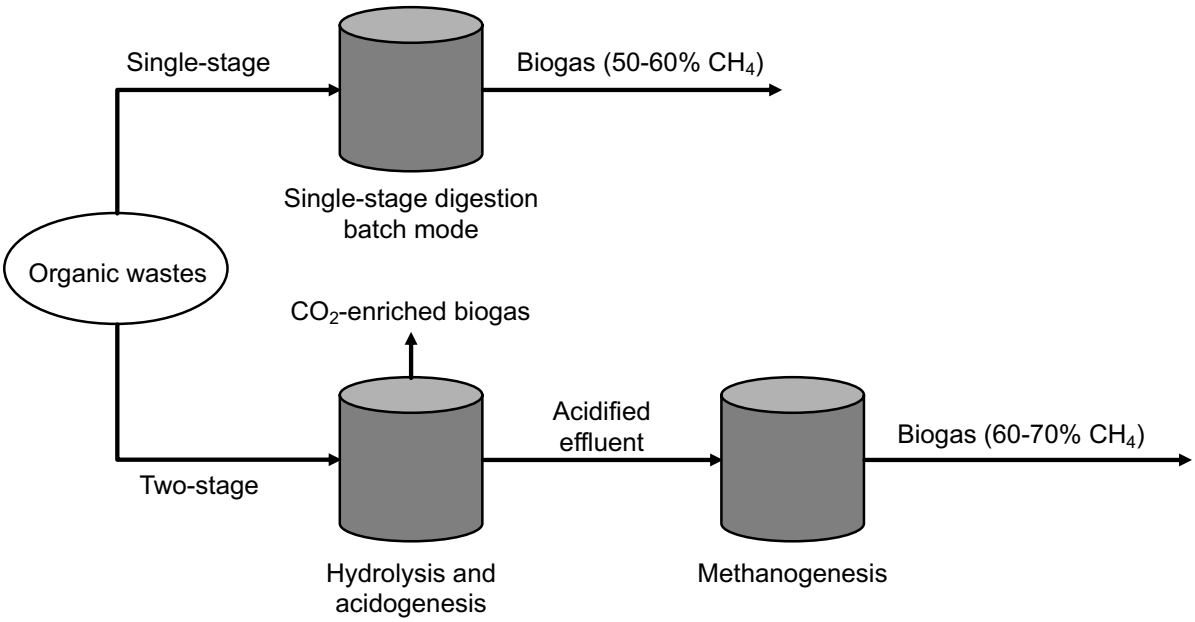

Figure 1-5. Schematic diagram of single-stage and two-stage anaerobic digestion systems. Adapted from Van *et al*. (2020).

1.3.7. Process stability and efficiency

Although as a well-established technique, AD faces several challenges affecting process performance and biogas stability. Many factors can influence the biogas system, directly and indirectly, including water and nutrient content, the composition of feedstock, buffer capacity and inhibitory agents (Baştabak & Koçar, 2020).

The main factor directly affects the process stability and efficiency is substrate source. A range of biomass feedstocks are available to use in AD, including energy crops, forest residues, and waste from food processing industries and wastewater treatment (Bacenetti *et al.*, 2013). However, the efficiency of digestion strongly depends on the composition and characteristics of substrates. For example, a high lignin content of biomass can lead to low biogas yield during the AD process due to the potential generation of AD inhibitorial phenolic compounds (Mosier *et al*., 2005; Sawatdeenarunat *et al*., 2015; Triolo *et al*., 2012). Likewise, certain plants such as tomato, cucumber and grape have relatively high C/N content, which could potentially cause accumulation and inhibition in the digestion process (Paul & Dutta, 2018). Meanwhile, animal waste can be used as a feedstock in anaerobic digesters which tends to have a plentiful source of easily degradable organic substance (Başţabak & Koçar, 2020). On the other hands, animal wastes tend to have high levels of protein and lipid, attributed to nitrogen accumulation, thus increasing the risk of ammonia inhibition, which could cause system failure (Momayez *et al.*, 2019). Table 1-7 summarized typical types of biomasses used as substrates for biogas plants worldwide.

The substrate to inoculum ratio is another determinant for the stable operation of the AD process. It can be evaluated by the organic loading rate (OLR) which determines the quantity of influent substrate per unit reactor volume in a given unit time period (Grangeiro *et al.*, 2019). An optimal OLR is key link in increasing the biogas production (Fuess *et al.*, 2016; Hafez *et al.*, 2010). The OLR is not only influenced by the substrate concentration, but also by the flow rate and the digester volume. Meanwhile, higher

OLR can result in increased experimental time and delayed methane production during AD of sewage sludge in single-stage system (Pellera & Gidarakos, 2016).

Table 1-7. Main types of biomasses utilized by the anaerobic digestion plants worldwide. Adapted from Appels *et al.* (2011) and Nsair *et al.* (2020).

Feedstock	% Dry matter	C:N (%:%)	Biogas yields (L kg^{-1} wet)	Methane content (L kg^{-1} wet)	Electricity production (kWh t^{-1} wet)
Pig manure	4-9	6	20-35	10-21	40-71
Cattle manure	20-25	22.71	60-120	33-36	112-257
Poultry manure	34-50	11.54	130-270	70-140	257-551
Maize silage	28-39	40-85	170-230	68-120	347-469
Grass silage	15-50	9-25	102-200	46-109	208-408
Wheat straw	91-94	100-150	-	135-237	146-266
Corn stover	66-89	60	-	261-402	293-451
Rye	62-93	47	130	70	265
Orange peels	92.3-96.8	102.86	-	460	-
Whole mandarins	89.0-97.3	25-80	-	500	-
Sewage sludge	93.91-95.55	10.86-17.16	-	590	-

1.3.8. Process inhibitors

Ammonia (NH_3) and ammonium (NH_4-N) have been recognized as the foremost inhibitors, which can reach to undesirably high concentrations during the hydrolysis of proteins available in nitrogen-rich substrates such as animal wastes, municipal wastes and dairy wastes (Rajagopal *et al.*, 2013). Furthermore, the ammonium concentration

which may inhibit microorganisms activities applied in the literature varies at a wild range (Banks *et al.*, 2011). For example, under mesophilic conditions, the maximum methanogenic activity was affected and declined by 75% at higher total ammoniacal nitrogen (TAN) concentration ranging from 1500-5000 mg/L (Chen *et al.*, 2016; Jiang *et al.*, 2019). However, ammonium inhibition can occur during AD of municipal solid waste (MSW) at lower TAN concentration of 1200 mg L^{-1} (Labatut & Pronto, 2018). Belmonte *et al.* (2011) reported that the free ammonia (FA) concentrations of 215 and 468 mg L^{-1} deteriorated the digestion of swine wastewater by reducing 50% methane production rate under mesophilic and thermophilic conditions. Meanwhile, the high concentration of NH_4^+-N can lead to the significant formation of FA in anaerobic conditions (Yang *et al.*, 2018; Liu *et al.*, 2019). The concentration of NH_4^+-N ranging from 1.0 to 2.0 g N L^{-1} increased the FA concentration up to 30-560 mg NH_3-N L-1 during the AD of sewage sludge under slightly alkalic conditions (pH 7.5-8.6) (Wei *et al*., 2017). These changes are attributed to an equilibrium formed between the FA and ammonium ion, which can be expressed in the following equation:

$$NH_{4(aq)}{}^{+} \leftrightarrow NH_{3(aq)} + H_{(aq)}{}^{+} \quad (1).$$

Meanwhile, ammonia inhibition enhanced the accumulation of acetate and propionate and consequently decreased the pH, which resulted irrelevant microorganisms enrichment (Chen *et al*., 2016). Meanwhile, the sensitivity of the microbial consortia to ammonia and ammonium inhibitions fluctuates at a wild range. Studies observed that acetoclastic methanogens can be inhibited at a low ammonia concentration, while hydrogenotrophic methanogens can tolerate higher amount of FA (Westerholm *et al.*, 2012; Zhang *et al.*, 2017).

Besides ammonia inhibition, the accumulation of volatile fatty acids (VFAs) can also hinder the AD process. The VFAs, as metabolic intermediates, are carboxylates with low molecular weight produced at stages of acidogenesis and acetogenesis (Wainaina *et al*., 2019). They include a mixture of straight-chain fatty acids, such as acetic acid, propionic acid and butyric acid, etc, from the metabolism of the amino acids, which also are precursors for methane generation (Fu & Holtzapple, 2010; Shi *et al.*, 2017). The production of typical VFAs can be expressed in the following equations:

$$C_6H_{12}O_6 + 2H_2O \rightarrow 2CH_3COOH\ (acetate) + 4H_2 + 2CO_2 \text{ (1);}$$

$$C_6H_{12}O_6 + 2H_2 \rightarrow 2CH_3CH_2COOH\ (propionate) + 2H_2O \text{ (2);}$$

$$C_6H_{12}O_6 \rightarrow 2CH_3CH_2CH_2COOH\ (butyrate)\ + 2H_2 + 2CO_2 \text{ (3);}$$

$$C_6H_{12}O_6 \rightarrow 3CH_3COOH\ (acetogenesis) \text{ (4);}$$

$$4H_2 + 2CO_2 \rightarrow CH_3COOH + \ 2H_2O\ (acetogenesis) \text{ (5).}$$

Acetic acid is the predominant VFA accounting for 30-80% due to abundance of homoacetogens which can grow in a wide range of physicochemical conditions such as high or low temperatures and wide alkalinities (Annamalai *et al.*, 2020; Mateos *et al.*, 2018). Propionic acid is another frequently reported carboxylic acid that can accumulate during the AD process. The rate of propionate degradation can be significantly inhibited by environmental conditions such as ammonium concentrations and pH by up to 31% (Bonk *et al.*, 2018). Similar to other inhibitors, high concentrations of VFAs can negatively permeate the cell wall and break the gram-positive bacteria under low-pH conditions, further deteriorating the AD process (Shi *et al.*, 2017; Yuan & Zhu, 2016). For example, previous study found that up to about 30 g COD L^{-1} of VFAs accumulated when treating distillery wastes, inhibited methane production at a moderate level of organic loading rate (Wang *et al.*, 2019). Likewise, Shi *et al.* (2017) observed that the accumulation of VFAs resulted in a 85% decrease in the biogas

production rate during the digestion of fruit and vegetable wastes with an organic loading rate of 3.0 kgVS L^{-1} day^{-1} under mesophilic conditions. Meanwhile, the overall VFAs utilisation and accumulation can be severely affected by pH in a complex way. Studies found that the total VFAs concentration reached to the maximum limit at pH ranging from 5.0 to 6.0 regardless of the type of inoculum in the AD of food waste (Wang *et al.*, 2014). In contrast, the highest VFAs concentration was observed from the digestion of low-strength synthetic wastewater at pH 7.0 (Khan *et al.*, 2019). Furthermore, Jie *et al.* (2014) reported that the lowest rate of VFAs degradation was recorded at pH 10.0 during the digestion of excess sludge. Therefore, it can be hypothesized that different types of microbial species which present in different inoculums has varied sensitivity and tolerance toward to the VFA degradation.

1.4. Use of biochar in anaerobic digestion

Biochar attracts increasing attentions as the means of enhancing AD efficiency and stability (Chiappero *et al.*, 2020; Fagbohungbe *et al.*, 2017a) (Table 1-8). The application of biochar can potentially increase process efficiency in three major ways: (1) adsorbing inhibitors; (2) increasing the buffering capacity of AD; (3) serving as an additional surface for microbial adherence; and (4) facilitating electron transfer between microorganisms. Figure 1-6 summarised the potential benefits of biochar on each stage during AD process.

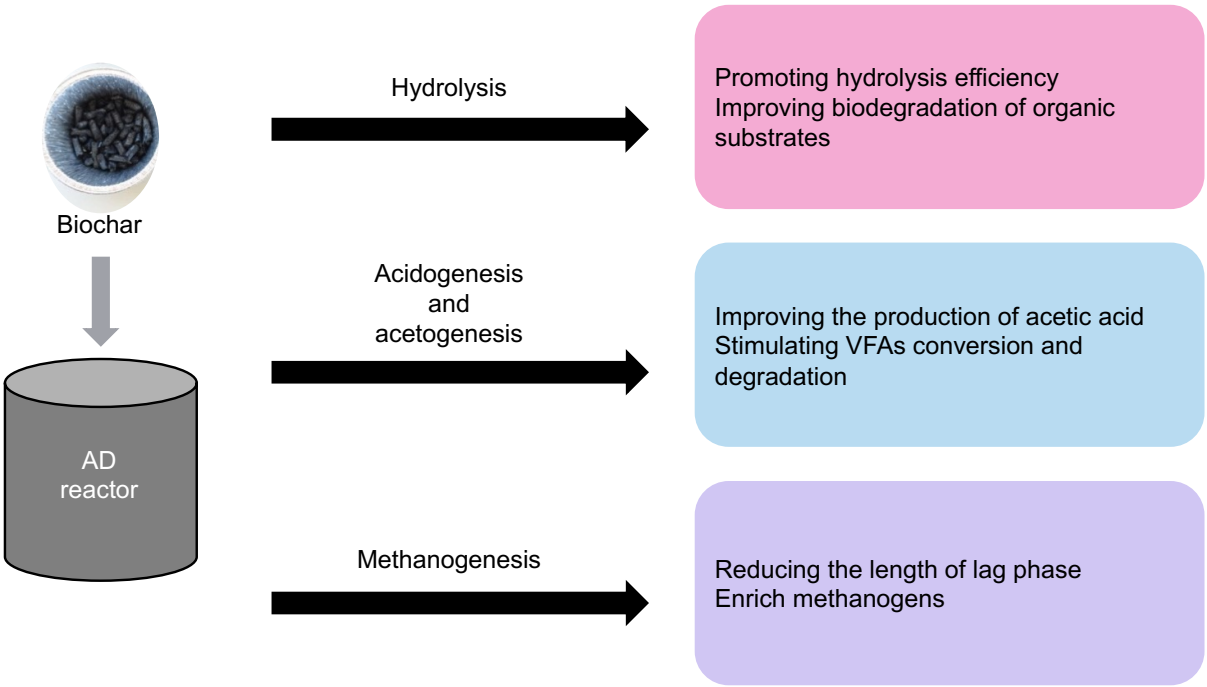

Figure 1-6. Potential impacts of biochar on each AD step (Pan *et al.*, 2019).

As aforementioned, substrate-induced inhibitors including ammonia, limonene and phenol can either be degraded or converted into other metabolites as precursors of inhibitors (Duetz *et al.*, 2003). The acclimatization process with microbial cells can naturally occur under anaerobic conditions. However, it generally takes long time to achieve stable acclimation for the whole consortia of cells, which increases the capital cost of commercial AD plant. The application of adsorbents such as activated carbon and zeolite showed the possibility of suppressing and mitigating substrate-induced inhibition (Masebinu *et al.*, 2019a). Similar to those carbonous materials, biochar is considered as a cheaper alternative to sorb those inhibitors. For instance, previous study recorded that biochar was able to sorb ammonium and remain bioavailable for plant growth (Taghizadeh-Toosi *et al.*, 2012). It was also reported that the application of wood and rice husk biochar increased ammonium removal in digestion of pig manure with maximum adsorption of 44.64 mg/g and 39.8 mg/g respectively *(Kizito et al.*, 2015). Meanwhile, Wang *et al.* (2018) studied the effects of sawdust biochar on

methane production in AD of dewatered activated sludge and food waste, and found a promoted syntrophic VFAs oxidation and stabler pH conditions. Likewise, Jang *et al.* (2018) investigated the digestion of dairy manure under mesophilic and thermophilic conditions with supplementation of dairy manure-derived biochar. They found the application of biochar lowered the concentrations of total VFAs and propionic acid up to 50%, indicating the ability of biochar on alleviating acids accumulation (Jang *et al.*, 2018). Whereas, it has been found that biochar addition can enhance the production of VFAs products. Lü *et al.* (2016) observed that production of propionic acid was enhanced by biochar supplements. Similar results were also reported by Giwa *et al.* (2019).

Table 1- 8. Selected studies on applications of biochar in AD systems.

Biochar	Pyrolysis conditions	Substrate	Operation conditions (°C)	Inhibition substances (concentrations)	Reference
Wheat straw pellets	550°C	Food waste and sludge	35	VFAs (more than 40 g/L)	(Kaur, 2020)
Sawdust waste	500°C for 1.5h	Food waste and sludge	35	VFAs (57.9 chemical oxygen demand/L)	(Wang *et al.*, 2020)
Vermicompost	500°C for 2.0h	Chicken manure and kitchen waste	35	VFAs (More than 12 g/L)	(Wang *et al.*, 2017)
Rice husk	550°C for 2.0h	Corn stover and chicken manure	35	Ammonia (more than 6 g/L)	(Yu, 2021)
Macadamia nut shells	350°C for 2.0h	Food waste	Room temperature	Ammonium (1.5 g/L)	(Su, 2019)
Fruitwood	800-900°C	Ammonium wastewater	35	Ammonia (up to 7 g-N/L)	(Lü, 2016)

The VFAs inhibition also associates with ammonia inhibition during AD process. As aforementioned, exceed concentration of ammonia can inhibit methanogens activity resulting in VFAs accumulation, consequently reducing pH and TAN concentration (Pan *et al.*, 2019). Xu *et al.* (2021) suggested that the application of hydrochar at 6 g/L reduced ammonia inhibition with increased tolerance level of maximum ammonia

concentration from 2.68 to 3.38 g/L during digestion of pig carcass. Similar observations was reported by Wang *et al.* (2017) that biochar derived from vermicompost at 500^{o}C stimulated the VFAs degradation and maintained their concentrations at a feasible level of 2835.8 mgL^{-1} during AD process. In contrast, no or only marginal effects of hydrochar on ammonia emission from cattle slurry and poultry manure were recorded in previous studies (Gronwald *et al.,* 2018; Mumme *et al.*, 2014). Ma *et al.* (2019) reported an increased concentration of ammonia nitrogen during AD of dried chicken manure with biochar addition. The role of biochar and/or hydrochar on mitigating ammonia inhibition is not fully clear due to its adverse effects on ammonia nitrogen. Therefore, it is necessary to understand the interaction of char with inhibitors during AD process.

Biochar has also proposed as redox mediator accelerating the reduction of organic chemicals such as chlorinated aliphatic compounds and nitro herbicides (Kappler *et al.*, 2014; Zhang *et al.*, 2018). Biochar can serve as electron acceptors to stimulate the syntrophic metabolism among electroactive microorganisms such as *Anaerolineaceae* and *Methanosaeta* (Jang *et al.*, 2018; Martínez *et al.*, 2018; Li *et al.*, 2018). Furthermore, hydrochar derived from agricultural residues has found to generate active oxygen species for the degradation of organic contaminant via the surface redox active sites during the electron donating process (Chen *et al.*, 2017; Yan *et al.*, 2018). However, biochar may negatively affect the AD process at high levels of 20 wet%. Li *et al.* (2019) reported an adverse effect of biochar on AD performance by reducing the contact between microbes and organic substrates. It is assumed to be cause by the over-acceleration of hydrolysis and acidogenesis with biochar addition

which resulted in intermediates accumulations and consequently inhibiting the methanogens activity (Pan *et al.,* 2019).

Overall, there are various factors and parameters to consider when applying biochar and/or hydrochar to the AD system and there is a need for systematic studies to determine the effects of feedstock types, thermal conversion types and process conditions on the resultant char's physicochemical properties. This is a vita prerequisite in determining the role of the char products during AD process. This work intends to fill those gaps.

1.5. Aims and objectives

The primary aim of this project was to elucidate the effects of char and/or hydrochar on process performance and system stabilities of anaerobic digestion. The hypothesis for this analysis was that the functions of char would be reflected through changes in the inhibitors and AD products. The secondary aim of this project was to find char with potential useful characteristics for industrial applications, such as the production of iron-modified char which enhances the recycle potential of char and improve economic feasibility.

2. Materials and methods

2.1. Char samples

Four standard biochars were obtained from the UK Biochar Research Centre (UKBRC) at the University of Edinburgh. The standardized production procedure can be found on the website of UKBRC (Mašek, Buss & Sohi, 2018). All used type of standard biochars were produced at 550^{o}C and 750^{o}C from four feedstocks: rice husk (RH), wheat straw pellets (WSP), oil seed rape (OSR) and sewage sludge (SS). The analysis of the standard biochars for determining chemical composition of biochar, pH and heavy metals concentrations were conducted at UKBRC. Biochar samples derived from the mixture of hardwood and digestate briquette were produced externally by the Leibniz institute of Agricultural Engineering and Bioeconomy (ATB), located at Potsdam Germany. The four hydrochars used in this project were produced from rice husk, wheat straw pellets, oil seed rape and alkali lignin (Sigma-Aldrich) (Table 2-1).

Table 2-1. Summary of biochar/hydrochar samples tested in this project.

Feedstock	Conversion method	Conversion conditions (°C)	Modification	Chapter
Rice husk	Pyrolysis	550	Unmodified	3, 4
Wheat straw pellets	Pyrolysis	550	Unmodified	3, 4
Hardwood and digestate briquette	Pyrolysis	500	Unmodified	4
Oilseed rape pellets	Hydrothermal carbonization	250	Unmodified	4
Alkali lignin	Hydrothermal carbonization	250	Unmodified	5
Rice husk	Hydrothermal carbonization	250	Unmodified	5
Wheat straw pellets	Hydrothermal carbonization	250	Unmodified	5
Rice husk	Pyrolysis	550	Iron-impregnation and thermal activation	6
Sewage sludge	Pyrolysis	550	Iron-impregnation and thermal activation	6

2.2. Digestate and substrates

Digestate used for all AD tests which were conducted in University of Edinburgh was obtained from a commercial AD reactor at Seafield Wastewater Treatment Plant (WWTP) located in Edinburgh. The plant is capable of processing 300 million litres of wastewater every day and producing up to 2300 Kw of sustainable electricity using a combined heat and power plant and thermal hydrolysis. This WWTP consists of five units, including settlement tank, primary and secondary tanks, thermal hydrolysis plant (THP) and continuous stirred-tank (CSTR) AD reactors. The sludge fed to the AD reactors was sourced from mentioned tanks and thickened to an 18-20% total suspended solids (TSS) cake with the discharged effluent of secondary tank. The

thickened sludge is then fed to the THP for sterilization and biological degradation at high temperature and pressure conditions. The resultant sludge is diluted to roughly 10% TSS and used as a substrate for the CSTR. The CSTR digesters are operated at mesophilic temperatures with a hydraulic retention time (HRT) of 22-28 days and maintained at a constant volume by discharging the overflow digestate to a holding tank. The discharged digestate is separated into a final cake (33% TSS) and liquor which is returned to the primary tank. The thickened sludge and overflow digestate were collected prior to each AD experiment and stored in sealed containers at 4^{o}C until required.

Digestate sample was collected from a farm-based AD plant at “Lehr- und Versuchsanstalt für Tierzucht und Tierhaltung e.V.”, Germany to be used in experiments described in Chapter 4. The reactor handles two different sources, including cattle slurry and maize silage (1:1 %/%) at 40±2^{o}C. Cow slurry and maize silage chips were used as substrates for the CSTR digesters, and these were also obtained from the same site. The maize silage chip samples were ground and sieved through a 2-cm mesh before storage. All samples were stored in sealed containers at 4^{o}C for further use.

Table 2-2. Experimental conditions used for anaerobic batch and semi-continuous experiments.

Chapter	Inoculum	Substrate	TSS (%)		VSS (%)		ISR (gVSS/gVSS)	Biochar Dosage
			Inoculum	Substrate	Inoculum	Substrate		
3	Sewage sludge based digestate	Activated sludge	2.51	3.05	72.9	90.4	2	0.1, 1.0%
4	Farm-based digestate	Cow slurry, maize silage	8.69	2.42 (cow slurry); 31.3 (maize silage)	74.2	75.5 (cow slurry); 95.6 (maize silage)	2	0.2% (batch); 6.0%wt (CSTR)
5	Sewage sludge based digestate	Activated sludge	2.51	3.05	72.9	90.4	3	2 g/L
6	Sewage sludge based digestate	Activated sludge	2.51	3.05	72.9	90.4	2	0.2, 0.5, 1.0%wt

2.3. Thermal conversion methods and procedures

2.3.1. Pyrolysis

Pyrolysis of the mixture of hardwood pellets and digestate at ratio of 1:1 (% wet mass) was conducted by external company at the ATB, Germany. The pyrolysis was carried out using a Pyreg pyrolysis unit (Pyred-500 III, with annual production of 250 t biochar) with consist of a cylindrical furnace and a combustion unit. During the pyrolysis, the reactor was powered by an electric motor and heated constantly to 500^{o}C. Due to the configuration limitation of this pyrolysis unit, no inert gas was purged during pyrolysis process. Noticeably, small amount of oxygen might be trapped in the reactor during operation, potentially leading to thermal oxidation of the feedstock. The resultant solid

products were collected in a cyclone and syngas was channelled into the combustion chamber and burned by preheated combustion air though flameless oxidation.

2.3.2. Hydrothermal carbonization (HTC)

Hydrothermal carbonizations of rice husk, wheat straw pellets, oilseed rape pellets and alkali lignin were conducted at the ATB, Germany. Hydrothermal carbonization were carried out using a stirred pressured reactor (Parr model 4520, Moline, IL, USA) with a capacity of 1 litre working volume. A Parr controller (model 4848, Moline, IL, USA) was used to monitor the operation temperature and pressure. The HTC unit consists an external resistance heater and internal sensors. HTC reaction was conducted at 250^{o}C to obtain larger surface area and higher porosity (Dieguez-Alonso *et al.*, 2018). Also, the selection of only 250^{o}C was due to the facts that at intermediate temperature ranges from 250 to 374^{o}C, the hydrothermal conversion process is defined as hydrothermal liquefaction and the predominant product is liquid fuel known as biocrude (Elliott *et al.*, 2015). The heating rate was set at 2 K min^{-1} and constant stirred at 90 rpm. It usually takes 3 hours to reach reaction temperature from 50 to 250^{o}C. After HTC, the heater was turned off, the heating jacket was removed. The reactor was immersed in a water bath and cooled to 50^{o}C or below before opening. The slurry was filtered through filter paper (ROTH type 113P) for 30 min. The resulting hydrochar was dried at 60^{o}C overnight and stored in sealed containers until further uses.

The yield (S% on the dry basis) of hydrochar/biochar and carbon recovery (%) calculated by the following equations:

$$S\ (\%)\ = \frac{hydrochar\ /\ biochar\ (g)}{feedstock\ (g)}\ (6);$$

$$C\ recovery\ (\%)\ = \frac{S \times C_{char}}{C_{feedstock}} \times 100\%\ (7).$$

Where,

C_{char} = the carbon content of hydrochar/biochar;

$C_{feedstock}$ = the carbon content of biomass feedstock.

2.3.3. Modification of biochar

The standard biochars (UKBRC, University of Edinburgh) derived from rice husk and sewage sludge were used to produce magnetic biochars. The iron doping modification was prepared by following the impregnation and activation procedure described by Park *et al.* (2018). Iron-doping modification of the standard biochar samples was conducted as described in Chapter 6 in order to achieve magnetization of biochar and alter the physiochemical properties of the pristine biochars. In brief, biochar was impregnated with ferric chloride hexahydrate (97% w/w, Sigma Aldrich) in a 5% Fe-to-biochar ratio, and the mixed solution was agitated at room temperature for 2 hours. The Fe-impregnated biochar was dried at 60^{o}C overnight. The dried samples were then loaded to the reactor tube and activated at 550^{o}C for 20 min. The resulting solids were collected and stored in a sealed glass vessel until further analyse.

The thermal activation was conducted using a lab-scale pyrolysis unit (UKBRC Stage I) comprised of a vertical quartz tube static bed reactor of 50 mm inner diameter and 200 mm sample bed depth with capacity of up to 100 g biomass (Crombie, Mašek, Sohi, Brownsort, & Cross, 2013). The pyrolysis unit was heated by a 12-kW infrared gold image furnace with a proportional-integral-derivative (PID) controller (ULVAC RHL-P610C, ULVAC, Methuen, MA, USA), with temperature control based on a

thermocouple inserted 10 mm from the inner surface within the test sample. The testing sample were charged to the reactor tube before assembling the whole pyrolysis unit and pre-purged with nitrogen gas for 10 mins. The nitrogen gas was injected through the bottom of the reactor tube in order to ensure an oxygen-absence condition during the pyrolysis. These purged nitrogen gasses were also used as an inert carrier gas passing through volatiles and syngas through a series of condensation vessels at a steady flow of 0.33 L/min. The condensation stage consists of four units or 'heat traps' to obtain four fractions of syngas at decreasing temperature increments from 240 to 120^{o}C. The heat traps were heated using heating tapes to prevent blocking of the glass tubes due to excessive condensation of pyrolysis vapours, while the first cold trap was cooled by constant externally waterflow and the following two cold traps were cooled with a mixture of acetone and liquid nitrogen at temperatures ranging from -30^{o}C to -60^{o}C. LabVIEW software was used for monitoring variations in temperature and pressure. After activation, the heater was switched off and cooled naturally to room temperature before opening. For this project, only the resulting biochars were collected and analysed.

2.4. Characterization of Char materials

2.4.1. Surface functional groups

The standard and modified biochars and hydrochars were analysed using Attenuated Total Reflectance-Fourier-transformed infrared (ATR-FTIR) spectroscopy to identify the surface functionality. The surface functional groups on a material determined by FTIR analysis is based on the absorbance of infrared light at various wavelengths. Prior to spectral acquisition the dry sample were grounded to fine powder by using a ball mill (MM200; Retsch, Castleford, UK). The same milling technique was used for

all samples to minimize variation from this source. The resulting powder was stored in a glass vessel until required.

FTIR spectra was recorded using a Bruker Vertex 70 spectrometer in the region of 4000 to 600 cm^{-1}, for 512 scans at a resolution of 4 cm^{-1}. Scan times were 1 s, and 5 – 10 accumulations were collected to obtain reasonable signal-to-noise ratio. The spectrometer equipped with a platinum ATR accessory connecting to a diamond crystal. 1 µg of finely powdered samples were placed on a glass slide and covered the surface of diamond crystal, ensuring that the entirely of the crystal was covered. In order to ensure the effervescent ATR wave penetration, sufficient sample was employed to achieve the minimum crushed thickness of 5 µm. A background spectrum was collected on the clean diamond crystal before each sample measurement. Absorbance was measured using a DLaTGS detector under room temperature (20 ± 2^{o}C). The crystal stage and glass slide were cleaned with acetone and air-dried between samples to reduce any potential erroneous spectral features. Spectra were recorded and processed using OPUS software (version 7.0, Bruker) and exported in CSV format. Each spectrum was presented in the absorbance form. Assignment of the peaks in each spectrum to a chemical formula was based on the absorbance value ($-\log(R/R_0)$, where R is the reflectance of the sample and R_0 is the reflectance of the background) and compared to the standard value.

2.4.2. Crystalline phases

Standard biochar and magnetic biochar samples were further analysed using x-ray diffraction (XRD) crystallography as described in Chapter 6 in order to determine the effects of iron-doping modification on the crystalline phases in the samples. The

presence of crystalline components was determined according to their resonance in the presence of X-rays at varying incidence angles. Prior to XRD analysis, all biochar samples were finely ground to a homogenous powder using an agate pestle and mortar. A Bruker D8 Advance diffractometer was used for the analysis though CuKα primary radiation generated at an accelerating voltage of 40 kV. 1 g of powdered sample was placed in a plastic disc and scanned in a range of 2-60^{o} 2θ. The dwell time was set to 1 s/0.01 2θ to ensure the sufficient diffraction. The diffracted X-rays were recorded by a Sol-x energy dispersive detector.

2.4.3. Proximate analysis

Prior to proximate analysis, biochar samples were finely milled to a homogenous powder. Digestate sample was freeze-dried and grounded to powder using an agate pestle and mortar. Thermal gravimetric analysis (TGA/DSC 1; Mettler-Toledo, Leicester, UK) was used for the proximate analysis of biochar samples and corresponding digestate samples. The procedure was used as follows: approximately 10-15 mg sample was loaded in a ceramic crucible and purged with nitrogen gas for 10 min inside the furnace to remove oxygen. The sample was heated for 10 min at 105^{o}C to determine moisture content. The temperature was then increased to 900^{o}C at 25^{o}C min^{-1} for a further 10 min to determine volatile matter. The nitrogen gas flowrate was kept at 50 mL min^{-1} in both steps. For the final step, the sample was combusted at 900^{o}C for 15 min in an air atmosphere for oxidation of remaining carbon content. Fixed carbon was determined by subtracting moisture, volatile and ash value on a weight basis.

2.4.4. Ultimate analysis

The elemental composition in magnetic biochar sample was determined by the ultimate analysis. An elemental analyser (Flash 2000; CE Elantech Inc, Lakewood) was used for determining C, H, N, O and S concentrations in biochar.

2.4.5. Heavy metal concentrations

Magnetic biochar was further analysed using inductively coupled plasma optical emission spectrometry (ICP-OES) in order to determine the total metal concentration. Prior to ICP-OES analysis, the biochar sample was prepared by following a 'modified dry ashing' method described by Enders and Lehmann (2012). The preparation method was adjusted to improve the quality of ICP-OES analysis by yielding a higher elemental concentration (Buss *et al.*, 2016). In detail: biochar sample was heated for 8 h at 500^{o}C and cooled to room temperature. The sample (roughly 10 g) was then placed in a steam bath with 5 mL of HNO_3 (70% concentration; analytical grade, Fisher Scientific) and removed moisture. A mixed solution contained 1 mL HNO_3 and 4 mL H_2O_2 (30% concentration; analytical grade, Fisher Scientific) was then added to the dried sample. After drying, 2 mL HNO_3 solution was added to dissolve the resulting solids. The resultant solution was filtered to remove particles and diluted with deionized water to achieve 50 mL final volume. Control without biochar were also prepared by following the same method. Notedly, the high-temperature chemical pre-treatment would result in a potential loss of elements such as As and Hg during the process (Bridle, Hammerton, & Hertle, 1990). Therefore, this method limits to analysis focusing on elements with low boiling points. An ICP-OES (Perkin Elmer Optima 5300DV) was used to determine 20 elements in the digested sample, including A, B, Ca, Cd, Co, Cr, Cu, Fe, Hg, K, Mg, Mn, Mo, Na, Ni, P, Pb, Se and Zn. The element

concentration in digested sample was determined by comparing their intensities to intensities of an internal standard derived from the ICP multi-element standard solution VI (Certipur®, Merck) and converted into mg L^{-1}. The concentration in biochar was further converted into mg Kg^{-1} using the origin mass and the solution volume. The limit of detection (LOD) was also measured by using 10 mL deionized water as blank. The standard deviation of intensities in blank was used to determine the slope of the calibration and calculated for the solution in mg L^{-1}. Analysis for each sample was conducted in triplicate.

2.4.6. Analysis of water-related and pressure functionated electrical conductivity

2.4.6.1. Water-related electrical conductivity

Electric conductivity (EC) of biochar sample was obtained according to Rajkovich *et al.* (2012). Briefly, 1 g of finely ground biochar was loaded in a centrifuge tube with 20 mL deionized water and shaken for 1.5 h at 150 rpm on a bench-top shaker to ensure sufficient equilibration between solution and biochar. Water-related EC was then determined with a Hach HQ40d portable meter connected to a conductivity probe (CDC 401).

2.4.6.2. Pressure-related electrical conductivity

Electrical conductivity in functions of pressure was measured using a 2-point probe method (Gabhi *et al.*, 2017; Giorcelli and Bartoli, 2019). It should be noted that contact resistance may cause uncertainty and must be eliminated from the total resistance (Gabhi *et al.*, 2020). It is achieved by gradually reducing the thickness of a sample and measuring the resistance of samples of different thickness. The resistivity was derived

from the slop of the linear relationship (R_{int}) between the measured resistance (V) and sample thicknesses (L) (Cristiani *et al.*, 2020).

$$R_{int} = \frac{\Delta V}{\Delta L} \quad (8)$$

The measurement chamber was composed of two copper parts, 11.5 mm in diameter and 40 mm in length, encapsulated in a plastic cylinder with an outer diameter of 41 mm. The inner diameter of plastic cylinder is slightly higher that allows the two rods to slide inside the cylinder. The plastic cylinder was firstly placed on the top of the lower rod, which formed an internal chamber to locate biochar sample. The upper rod was positioned on the top of biochar sample to close this chamber. Conductive probes were mounted inside the copper rods which used to connect to a multi-meter. The electrical resistance was measured at increasing loads by a compression machine (Instron universal testing system) with a loading head of 500 N. The loading rate was set to 1 N/s to ensure sufficient time to obtain a stable reading according to ASTM standard C695-2010. The movement of the loading head was recorded by the compression machine in mm and second units. The multi-meter used was TECH 72-7720 with three outlets connected to the conductive probes. The electrical resistance value was recorded only after a stable reading was achieved. The resistivity (P) was calculated from the measured resistance I against the area of the rods contact and the distance between the rods (Equation 9), which converted to the electrical conductivity (S) by equation 10.

$$P = \frac{RA}{L} \quad (9);$$

$$S = \frac{L}{P} \quad (10).$$

Where,

R = electrical resistance (Ω);

A = area of the sample (m^2);

L = height of the sample (m);

S = electrical conductivity (S/m).

2.4.7. Acid-base titration

The dissociation property and concentration of acid-base groups of biochar was determined via acid-base titration following studies of Silber *et al.,* (2010) and Chen *et al.*, (2015). A batch titration method was used in this project. In brief, biochar sample was finely grounded and sieved through 0.25-0.5 mm. A given amount of the resultant sample (115.0 mg) was weighed and placed in a 23.5 mL glass vial. Then, 11.5 mL NaOH solution (0.05 mol L^{-1}, analytical grade reagent, Sigma Aldrich) was added to the vial. The mixture was added 0-11.5 mL of 0.119 mol L^{-1} HCl solution (Sigma Aldrich) to achieve different pH levels, and followed by adding different amount of deionized water to reach a final working volume of 23.0 mL. The mixture was incubated and horizontally shaken at 110 rpm on a bench-top shaker at 25^{o}C under light restriction condition for 5 days. After incubation, the sample was centrifuged at 3,000 x g for 10 minutes to separate solid and liquid phased, and measured by an Orion 3-star benchtop pH meter (Thermo Fisher Scientific, USA).

2.4.8. Water-extractable dissolved organic carbon and total organic carbon

The extraction of dissolved organic carbon (DOC) was performed according to Liu *et al.,* (2019). In brief, 100 mg of the char products were mixed with 10 mL of deionized water, and the suspension was shaken at 30 rpm for 7 days at room temperature (20 $\pm$ 1 ^{o}C). Aluminium foil was used to wrap the container avoiding light exposure. Then, the suspensions were filtered through a 0.45-μm syringe membrane and further centrifuged at 10,000 x *g* for 10 min to remove the colloidal biochar particles. The

supernatant was then collected and defined as DOC here. All the DOC samples were diluted 20-fold with deionized water to meet the detection limits. The DOC concentrations were measured by a Shimadzu TOC-V_{cpn} TOC analyser (Shimadzu, Japan). The blank samples with only deionized water was also analysed and used for correcting the DOC concentrations of each sample. All the DOC samples were further analysed by a Varian Cary 100 scan UV-visible spectrophotometer (Varian, USA) between 200 to 800 nm. The blank samples were measured prior to each DOC sample serving as a correction of the UV-vis absorbance spectra. The E2/E3 ratio was used to estimate aromaticity and molecular weight (Peuravuori, 1997). It was calculated by absorbance at 255 nm divided by absorbance at 365 nm, and defined as the decadic absorption coefficient (*a*, cm^{-1}). Meanwhile, the spectra slope coefficients between 275-295 nm were determined by fitting the absorption spectra to the slope of Napierian absorption coefficient. The Napierian absorption coefficient was calculated according to Helms *et al.* (2008).

$$a = A/L \quad (11);$$

$$a = 2.303A/L \quad (12);$$

$$\alpha_\lambda = \alpha_{\lambda_0} e^{-S(\lambda-\lambda_0)} \quad (13);$$

$$SR = S_{275-295}/S_{350-400} \quad (14).$$

Where,

a = absorption coefficient (m-1);

A = the UV-vis absorbance;

L = the path length (m);

λ_0 = the reference wavelength;

$S_{275\text{-}295}$ = the absorption spectra slope at 275 and 295 nm;

$S_{350\text{-}400}$ = the absorption spectra slope at 350 and 400 nm.

2.4.9. pH measurements

The pH measurement was conducted according to Rajkovich *et al.*(2012). Briefly, 1 g of biochar was added to 20 mL deionized water, and the suspension was shaken at 150 rpm for 24 hours to achieve equilibrium. Then the mixture was filtered to separate solid and liquid phases. The filtrate was measured by an Orion 3-star benchtop pH meter (Thermo Fisher Scientific, USA). These analyses were performed in triplicates.

2.4.10. Mass specific magnetic susceptibility

The mass specific magnetic susceptibility was analysed to determine the capacity of separating magnetic particles from the liquid phase in functions of the magnetic properties (Mašek *et al.*, 2020). In this project, the mass specific magnetic susceptibility of magnetic biochar was measured using a magnetic susceptibility meter set at 4.6 kHz.

2.4.11. Ammonium adsorption

To investigate the ammonium adsorption ability of the biochar samples, 2 g of each biochar was added to a 45 mg L^{-1} NH_4^+-N solution of 200 mL (ammonium nitrate, analytic grade reagent, Sigma Aldrich), and the vial was shaken at 25^{o}C for 24 hours. The resultant solution was filtered through a 0.22 μm syringe filter and measured by a continuous flow analyser to determine the ammonium concentration.

In order to determine the thermodynamic and dynamic properties of $NH4^+$ on biochar, adsorption kinetics analysis was investigated by adding 2 g biochar to a 500 mL glass flask contained 200 mL ammonium solution (45 mg L^{-1} NH_4^+-N). The mixture was shaken horizontally at 110 rpm on a bench-top mechanical shaker at 25^{o}C. A given

amount of sample (5 mL) was withdrawn from the mixture at different time intervals, such as 0.5, 1, 2, 3, 4, 6 and 24 hours. The suspension was then filtered with a 0.22 μm membrane filter, and the supernatant was retained. The adsorption amount of NH_4^+-N per unit mass of biochar in functions of duration was calculated by the following equation:

$$Q_t = \frac{(C_0 - C_t) \times V}{m} \quad (15).$$

Where,

Q_t = the amount of NH_4^+ adsorbed at a given time interval (mg g^{-1});

C_0 = the initial concentration of NH_4^+-N solution (mg L^{-1});

C_t = the NH_4^+-N concentration of the sample at time t (mg L^{-1});

V = the volume of the ammonium solution (L);

m = the weight of biochar sample (g).

In order to examine the maximum adsorption capacity of the biochar sample to ammonium ion, adsorption isotherm tests were performed by adding biochar sample (0.4 g) to a 50 mL centrifuge tube containing 40 mL of ammonium solution with different initial concentration (5, 10, 25, 50, 100 mg L^{-1}). The mixture was then shaken at 110 rpm in a bench-top shaker for 24 hours at 25ºC, and filtered with 0.22 μm membrane filter. Ammonium concentration in the supernatant was determined by a continuous flow analyser. The adsorption capacity was calculated by the following equation:

$$Q_e = \frac{(C_0 - C_e) \times V}{m} \quad (16).$$

Where,

Q_e = the equilibrium adsorption capacity of NH_4^+-N (mg g^{-1});

C_0 = the initial ammonium concentration (mg L^{-1});

C_e = the ammonium concentration at equilibrium (mg L^{-1});

V = the solution volume (L);

m = the weight of the biochar sample (g).

Pseudo-first-order, pseudo-second-order and intra-particle diffusion models (Wang *et al.*, 2020) was used to evaluated the adsorption kinetic data in this project.

$$Q_t = Q_e \times (1 - e^{\frac{-k_1 t}{2.303}}) \text{ (17);}$$

$$\frac{t}{Q_t} = \frac{1}{k_2 Q_e^t} + \frac{t}{Q_e} = \frac{1}{V_0} + \frac{t}{Q_e} \text{ (18);}$$

$$Q_t = k_d t^{\frac{1}{2}} + C \text{ (19).}$$

Where,

Q_e = the equilibrium adsorption capacity of ammonium (mg g^{-1});

Qt = the amount of adsorbed ammonium ion (mg g^{-1});

k_1 = a pseudo-first-order constant (min^{-1});

k_2 = a pseudo-second-order constant (min^{-1});

kd = an intra-particle diffusion rate constant ($g/mg/h^{1/2}$);

C = a constant.

The results of adsorption isotherm experiment were fitted to Freundlich, Langmuir Temkin isotherm models using the following equations:

$$Q_e = \frac{Q_m C_e k_L}{1 + k_L C_e} \text{ (20);}$$

$$Q_e = k_F C_e^{\frac{1}{n}} \text{ (21);}$$

$$Q_e = \frac{RT}{B_t} lnA_t + \frac{RT}{B_t} lnC_e \text{(22);}$$

Where,

Q_m = the maximum sorption capacity of ammonium ion (mg g^{-1});

k_L = the Langmuir adsorption constant (L mg^{-1});

k_F = the Freundlich adsorption constant ($mg^{1-1/n}L^{1/n}g^{-1}$);

n = the Freundlich linearity constant;

A_t = equilibrium binding constant (L/mg).

2.5. Anaerobic digestion experiments

2.5.1. Batch AD experiments

Batch AD experiments were performed as accordance with the "VDI 4630 – Fermentation of organic materials Characterization of the substrate, sampling, collection of material data, fermentation tests" standard (Helffrich & Oechsner, 2003). The digester consists of a 100 mL glass syringe with 20 mL working volume (Figure 2-1). Each syringe was sealed with stopcocks to guarantee the anaerobic condition and allow access to biogas and digestate sampling. The air-tight condition was also ensured by inserting a silicone-grease-coated plunger. The syringe digesters were placed in a desktop shaker and incubated under mesophilic condition (37±2°C).

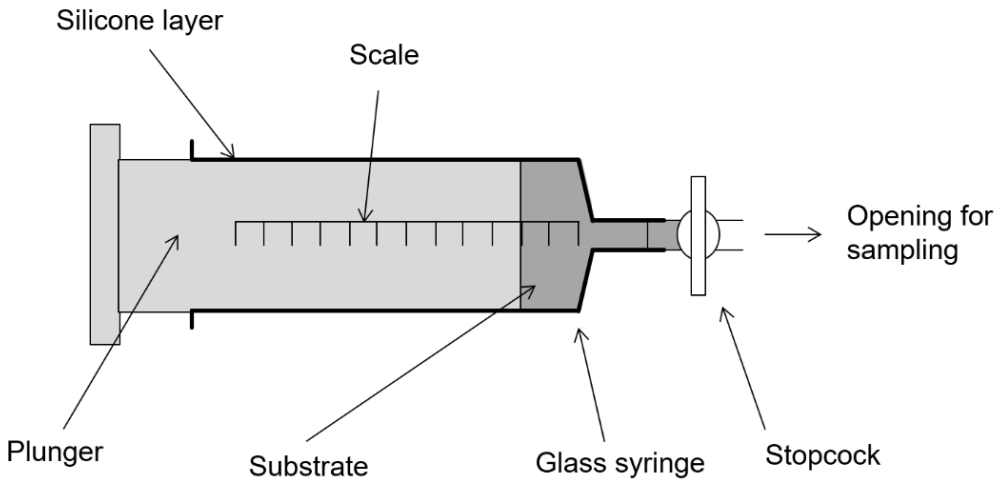

Figure 2-1. Schematic diagram of syringe digester.

2.5.2. Semi-continuous AD experiments

In this project, the continuous stirred tank bioreactor was used for determined the effects of biochar on anaerobic digestion performance and system stability. This digester was selected due to larger volumes are more appropriate to stimulate the realistic operation conditions (Pearse *et al.*, 2018). It also provided efficient homogenization of the entire digestate and facilitated dispersion of intermediates and any end products by adequate mixing (Kariyama *et al.*, 2018).

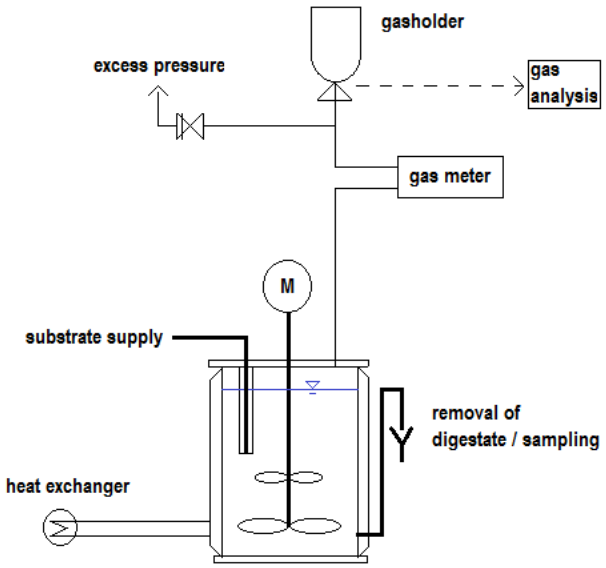

Figure 2-2. Schematic diagram of CSTR reactor.

All continuous feeding experiments described in Chapter 4 were carried out using CSTR reactor. The digesters consist of a 10 L stainless steel cylinder with 8 L working volume. Each digester was coated with a heating jacket which connected to a water bath. Agitation was performed using a paddle rotating at a rate ranging from 100 to 200 rpm, powdered by a geared motor drive unit which was installed at the top of the reactor. This system also equipped with a drum-type gas meter (Ritter, Germany) which consisted of an engine oil filled U-tube and a counter to measure gas production. Biogas was collected by a 40 L gasbag (Sigma Aldrich, Germany) connecting to the

gas meter. The total working volume in each digester was retained at 8 L by withdrawing daily through the sample port fitting in the bottom of the reactor.

Prior to continuous feeding operation the reactors were operated without feeding for 7 days. In the adapting period, no substrates were added in order to enrich the biomass in methane producing microorganisms and to prevent foaming, a method that has been widely adopted (Dareioti & Kornaros, 2014). The operation was subsequently switched to continuous mode to deliver the hydraulic retention time (HRT) of 14 days. This HRT were selected to keep clogging minimal and performance relatively good. At the same time, biochar was introduced into three of the four CSTRs at a ratio of 6% w/w. The reactor without biochar supplementation was used as a control. The starting organic loading rate (OLR) was 3 gVS L^{-1} per day. For the biochar-treated reactors, biochar was added five times a week to maintain consistent biochar concentrations. At the same time of each day, the reactors were opened to discharge digestate and feed fresh substrate. The CSTRs were maintained under mesophilic conditions (37±1^{o}C) by heating using a hot water batch.

2.5.3. Chemical analysis of gas and digestate samples

2.5.3.1. Total suspended solids and volatile suspended solids

Total suspended solids (TSS) and volatile suspended solids (VSS) were measured by following standard methods (Gilcreas, 1967). Briefly, samples of digestate (20 g) were weighed in ceramic crucible and heated to 105^{o}C for 24 hours in a Universal Oven (Memmert). The dried samples were then weighed and heated at 550^{o}C for 2 hours until achieving a stable final weight. The resultant solids were transferred to an air-

tight glass vessel and weighed after cooling down. The TSS and VSS values were calculated by following equations.

$$\%TSS = \frac{W_{105} - W_{crucible}}{W_{initial} - W_{crucible}} * 100 \text{ (23);}$$

$$\%VSS = \frac{W_{550} - W_{crucible}}{W_{105} - W_{crucible}} * 100 \text{ (24).}$$

Where,

$W_{crucible}$ = the weight of empty crucible (mg);

$W_{initial}$ = the weight of wet sample and crucible (mg);

W_{105} = the weight of dried residue and crucible after drying at 105°C (mg);

W_{550} = the weight of residue and crucible after ignition (mg).

2.5.3.2. Biogas and biomethane monitoring

In this project, methods used for determining the rate and volume of biogas and biomethane include volume displacement and gas meter. In case of volume displacement, the overpressure inside the syringe reactors pushed the plunger until achieving a balance in the pressure build-up to the atmospheric pressure. The volume of biogas was read off the syringe in mm and converted to standard temperature and pressure as described by Wirth and Mumme (2014). The major advantage of this method was that the carbon dioxide solubility and oxygen access can be kept to a minimum. In the gas meter method, it was only used for monitoring gas production from the CSTR digesters. The headspace pressure build-up inside the reactor was converted by a pressure transducer equipped in the gas meter and recorded in L.

Methane production was monitored by two methods: biogas composition analysis and liquid replacement. In Chapter 3-5, the methane in biogas obtained from syringe digesters was measured using an Advanced Gasmitter® digital infrared methane

analyser (Pronova) when biogas volume reached to detection limits (≥20 mL). The methane, carbon dioxide and hydrate sulphide concentrations in biogas generated from the CSTR reactor were determined by using a NIR sensor (University of Hohenheim, Germany). This equipment was selected due to it was more suitable for larger volume (>1 L).

In the liquid displacement as used in Chapter 6, the methane concentration was measured by absorbing carbon dioxide in an alkaline liquid as described by Pham *et al.* (2013). The method was adjusted to suit the small quantity of biogas produced from syringe digester in order to improve the final methane concentration analysis. Briefly: about 20 mL 0.5 M KOH solution were filled in a 50-ml glass syringe which equipped with a stopcock. This syringe was further added with a 0.2 μm PTFE filter (Cole-Parmer) and connected to the digester. Biogas was then injected through the liquid and filled the syringe. Then, the adsorption occurred due to KOH solution can absorb CO_2 and H_2S, and caused a reduction in gas volume in the measuring syringe. The different between initial and final volume corresponded to the wet methane. The dry methane production was obtained in terms of standard temperature and pressure by following equation:

$$V_{dry} = V_{wet} \times \frac{(P - P_{water}) \times T_0}{P_0 \times T} \quad (25).$$

Where:

V_{wet} = the gas volume as read off (mL);

P = the pressure of the gas phase during measurement (hPa);

P_{water} = the vapour pressure of water as a function of the ambient temperature (hPa);

P_0 = the standard pressure (1013 hPa);

T_0 = the standard temperature (273^{o}K);

T = the incubation temperature at the time of reading (^{o}K).

2.5.3.3. Kinetic study of gas production

To quantitatively analyse the production of methane in different treatment, the modified Gompertz and logistic function models were used to fit the cumulative biomethane data (Rana, Bhushan, & Prajapati, 2020).

$$\mathrm{M} = \mathrm{P} \times exp\{-exp\,[\frac{\mathrm{R_{max}} \times \mathrm{e}}{\mathrm{P_0}}(\,t_0 - \mathrm{t}) + 1]\}\ (\ 26\ );$$

$$M\ = \frac{P}{1+\,exp(4*R_{max}*\frac{\lambda - t}{P}+2)}\ \ (\ 27\ ).$$

Where,

M = biomethane production (mL/g);

P = CH_4 production potential (mL/g);

R_{max} = the maximum CH_4 production potential (mL/g);

λ = the lag phase (days)

t = duration time (days);

e = 2.718281828.

All parameters were fitted via GraphPad Prism software (Prism 9, USA).

2.5.3.4. Analysis of volatile fatty acids (VFAs) concentrations

A given amount of digestate sample (0.5 µL) was centrifuged with a bench-top 1-15 Microfuge (Sigma Zentrifugen) at 18,000 X g for 15 minutes to separate the solid and aqueous phase. The supernatant was then filtered with a 0.2 µm PTFE filter (Cole-Parmer) and acidified with 100 µL 10% phosphate acid (Sigma Aldrich). The resultant solution was added with 250 µL of internal standard solution (2-ethlybutyric acid 1:1,000 in deionized water). Then, 450 µL deionized water was added and vigorously

mixed with the resultant solution. Calibration solution was prepared by adding 200 µL standard VFAs mix (Merck) which consisted of acetic acid, butyric acid, formic acid, heptanoic acid, hexanoic acid, iso-butyric acid, isovaleric acid, 4-methylvaleric acid, propionic acid and valeric acid in 320 µL deionized water. The diluted solution was then acidified using 80 µL 20% phosphate acid and added with the internal standard (200 µL). These solutions were stored at 4^{o}C until required.

The determination of VFAs was performed by using a gas chromatograph (HP 5890 II). In brief, 1 µL of the solution was injected into the split injector at 250^{o}C using an autosampler. Then, analytes were separated by a Permabond FFAP column (30 m X 0.32 mm X 0.5 µm film thickness) with helium flow of 1 mLmin^{-1}. The GC oven was preheated at 50^{o}C for 5 minutes and increased to 250^{o}C at a heating rate of 10^{o}C min^{-1}. Detection was conducted using a flame ionization detector at 1 scan s^{-1} in the range between 29 to 450 m/z. Quantification was performed by integrating characteristic ions obtained from total ion chromatograms and normalizing peak areas with the area of the internal standard. The integration analysis was conducted with Chrome statistical software. The concentration of each VFAs was converted into mg L^{-1}. In order to eliminate errors generated during method development, blanks with only reagents were also analysed and used for calculating critical VFAs values for digestate samples. The final VFAs concentration (V) was calculated by following equation:

$$V = V_0 \times V_I \times R \quad (28).$$

Where:

V_0 = The VFAs concentration obtained from the integration (mg L^{-1});

V_I = the concentration of internal standard (mg L^{-1});

R = dilution ratio of digestate sample.

2.5.3.5. Analysis of ammonium concentration

Prior to analysis, the digestate sample was centrifuged at 18,000 x g for 10 minutes to separate solid and liquid fractions. The supernatant was filtered with a 0.45 µm PTFE filter (Cole-Parmer) and diluted with deionized water until achieving detection limits. Calibration solution was prepared from ammonium sulfate (analytical reagent grade) at a concentration of 10 mmol L^{-1}. Orthophtaldiadehyde (OPA) solution was prepared by adding 2 g standard OPA in 50 mL of ethanol (Sigma Aldrich) and vigorously shaking until completely dissolved under dark conditions, and stored in a glass vessel at 4°C. Borate buffer solution was made from disodium tetraborate decahydrate at a concentration of 3 g L^{-1} and filtered using a 0.45 µm membrane filter (Whatman®), and stored in a polyethylene vial at the room temperature. Sulfite solution was also used as a supporting reagent which made from 8 g L^{-1} sodium sulfite.

The determination of ammonium concentration was conducted using a continuous flow analyser (SEAL analytical AACE 6.07). This instrument consists five channels including a sampler, a pump, five-reagent mixing, a heating bath and photometers. It should be noted that this instrument only measures nutrients at low concentration levels (µm). The method used in this project was based on the reaction of OPA and sulfite following by Kérouel and Aminot, (1997). In brief, the sample was run at a sampling rate of 20 mL per hour and a sample-to-wash ratio of 1:1. The nitrate channel equipped with a bubble segmentation to remove oxygen from the airflow using an oxygen absorber (activated iron, Sigma Aldrich). The sample was then reacted with OPA in the presence of borate buffer and sulphite solution at 75°C. Consequently, this reaction resulted in the generation of fluorescent species, and measured by a fluor-monitor with a 460 nm fluorescence lamp and a 370 nm excitation filter. The output of

the fluorometer was then converted proportionally to the ammonium concentration (mg L^{-1}).

Total Kjeldahl nitrogen (TKN) is the sum of organic nitrogen and ammonia. The TKN in digestate was measured after Kjeldajl nitrogen digestion using re-dosed reagent cuvettes (Hach) (Behera, 2006). Briefly, inorganic and organic nitrogen are oxidized to nitrate by digestion with peroxodisulfate. The nitrate ions react with 2.6-dimethylphenol in a solution of sulfuric and phosphoric acid to form a nitrophenol. Oxidized forms of nitrogen in the original sample are determined in second vial and subtracted and measured spectrophotometrically on a DR5000 Spectrophotometer (Hach) which reads the cuvette barcodes, selects the necessary wavelengths and calculates the desired test parameter.

2.5.3.6. Other chemical analysis

After fermentation, the digestate sample was analysed for pH using an Orion 3-star benchtop pH meter (Thermo Fisher Scientific, USA). The digestate sample was freeze dried and ground to finely powder, and stored at room temperature until required for proximate analysis.

2.6. Statistical analysis

Statistical comparisons between groups, such as in the gas volume and composition analyses, were made using the t-test function in GraphPad Prism version 9.4.1 (Motulsky, 2003). The tests were two-tailed, assuming a heteroscedastic distribution of values, such as larger averages will produce larger errors than smaller averages. Standard deviations were calculated using the Microsoft Excel STDEV function.

Adsorption kinetic, adsorption isothermal, and kinetic model of biogas production (modified Gompertz) analyses were done using the GraphPad Prism Data Analysis function.

3. Adsorption mechanisms of ammonium to biochar derived from rice husk and wheat straw pellets and their applications in anaerobic digestion of municipal sewage sludge

3.1. Introduction

Biological treatment process in wastewater treatment plants (WWTPs) mainly comprises two approaches, namely wastewater treatment for removing organic carbon and nutrients, and the sludge treatment for disposing waste activated sludge (WAS). Biological treatment offers several advantages such as lower chemical and energy requirement while achieving satisfactory removal efficiency and higher economic feasibility compared to chemical treatment methods. Meanwhile, nitrogen compounds mainly exists in the form of ammonium in the wastewater, and derive from wastewater influent and anaerobic fermentation liquid received from WAS treatment. Studies have shown that the concentration of ammonium ion in domestic wastewater can be up to 200 mg L^{-1}, of which organic nitrogen accounts for 60% of the total (Tang *et al.*, 2019; Cheng *et al.*, 2020). In addition, the concentration of ammonium inevitably causes the presence of free ammonia (NH_3) and unionised form of ammonium (NH_4^+). For instance, a typical anaerobic fermentation liquor from WAS treatment with ammonium concentration of 1.0-2.0g/L (pH=7.5-8.6) at 33^oC led to an FA concentration of 30-560 mg/L. Hence, high ammonium wastewater needs to be properly treated due to its potential risks to human health and water body via eutrophication (Britto, 2002; Sui, 2016). Current treatment of the nitrogen-rich wastewater are mainly comprised of nitrification and denitrification of the nitrogen compounds. This method requires high energy inputs and high operational costs, where the aeration for nitrification alone occupies up to 50% of total energy and 60% of the capital cost (Foley, 2010; Ledezma, 2015). In addition to that, a substantial

chemical supplements are needed as acting as the electron donor in the nitrification-denitrification process. Therefore, it implies a high affinity towards ammonium, high removal efficiency, low-cost, simplicity of application and operation as well as environmental friendliness.

Biochar is a carbon-rich product from the thermal decomposition of various types of feedstock, including agricultural residues, sewage sludge and animal manure under oxygen absent condition. Great interest has shown on using biochar to remove ammonium from liquids due to its unique physiochemical properties (Sarkhot, 2013; Sika and Hardie, 2014; Salimova *et al.*, 2020). Tang *et al.* (2019) demonstrated biochar derived from anaerobic sludge at 450^{o}C on ammonium removal efficiency in municipal wastewater, and showed a 1.2 mg NH_4-N/g ammonium removal capacity. A higher ammonium removal efficiency (22.6 mg NH_4-N/g) was also reported by Vu *et al*. (2017) by using HNO_3-modified biochar derived from corncob at 400 ^{o}C. As such, biochar produced from different feedstocks and pyrolysis temperature shows varied adsorption strength.

Meanwhile, as aforementioned, anaerobic digestion (AD) has been extensively applied to treat wastewater sludge due to its high potential for energy recovery, promotion of sanitation, and provision of nutrient-rich fertilizers (Yellezuome, 2022). Briefly, wastewater sludge is hydrolysed into volatile fatty acids (VFAs) and fermented as methanogenesis precursor (Liu, 2015). In the meantime, nitrogen-rich substrates such as proteins, urea, and nucleic acid are disintegrated and converted to ammonium, therefore resulting a high degree of ammonium accumulation (González-Fernández, 2009). Wei *et al.* (2017) reported that ammonium concentration of anaerobic

fermentation of sludge treatment could be up to 1.5 g/L, leading to a free ammonia (FA) content of 70 mg/L at 33^{o}C (pH=8). The presence of FA has been reported as a strong inhibitor to hinder anaerobic digestion efficiency by decreasing the specific microbial activities and reconfiguring the microbial community structure. Meanwhile, the free ammonia and ammonium inhibition in AD have reported a huge disparity in the inhibitory limits, ranging from 27 to 1450 mg FA /L and from 1.1 to 11.8 g/L of total ammoniacal nitrogen (Capson-Tojo, 2020).

Several studies have reported using biochar as an additive in AD system to improve biogas generation, methane concentration, and microbial enrichment (Cai *et al.*, 2016; Dang *et al.*, 2016; Fagbohungbe *et al.*, 2017b; Masebinu *et al.*, 2019b). For instance, Luo *et al.* (2015) investigated mesophilic AD of glucose with addition of biochar derived from fruitwoods at 800^{o}C and found biochar shortened the methanogenic lag phase, and the maximum methane production rate increased by 86.6%. Shen *et al*. (2016) reported that the addition of biochar derived from pine wood and white oak biochar at 500-700^{o}C enhanced the activities of methanogenic microbial and reduced the CO_2 content in biogas due to the honeycomb-like porous structure of biochar with desirable chemical properties. However, the impacts of biochars on pH changes and ammonia-ammonium shifts during AD process have not been fully understood.

This work aimed to investigate the influence of biochar physiochemical properties and surface functionality on ammonium inhibition. The chemical state, composition, and dissociation characteristics of the functional groups on the surface of biochar were also be investigated using acid-base titration in this study. Their effects on the anaerobic digestion of sewage sludge were also be explored.

3.2. Results and discussions

3.2.1. Characterisation of biochar

Functional groups such as carboxylic and phenolic groups have been recognized as the main sources of alkaline biochar derived at low temperature, presenting as deprotonated conjugate bases (Fidel, 2017). However, carbonate groups greatly contributed to the alkalinity of biochar made at high temperature (500-700^{o}C) (Chen *et al.*, 2015b). In the meantime, oxygen-containing groups especially carboxyl groups (CGs) on biochar surfaces have proven as the main ion-exchange sites by modulating the uptake and release of nutrient ions in surrounding environments (Lee, 2010; Silber, 2010). Deprotonation and protonation of carboxyl groups can directly regulating the pH buffering capacity of biochars, and surface charges from their dissociation are related to the ability of biochar particles to disperse into water solution. An acid-base titration curve can reveal pH-dependent proton exchange of acid-base groups with water to indicate the dissociation property and content of acid-base groups (Jr, 2002; Konkena, 2012). Hence, the chemical states, contents and dissociation properties of carboxyl groups on tested biochar surface were analysed by acid-base titration.

Acid based titration curves of biochar and D.I water and the proton consumed curves for biochar RH and WSP were determined as shown in Figure 3-1. The suspension pH of WSP biochar decreased less than suspension pH of biochar as the amount of HCl added increased, implying that WSP biochar had slightly higher buffering capacity to protons. When the pH decreased from 10.0 to 8.0, the amount of protons consumed by RH biochar was 1.2±0.07-fold larger than that of WSP biochar. These results are in line with Shi *et al*. (2017) that biochar derived from rice straw consumed less amount of protons than peanut stover biochar. The solid carbonates in anaerobic digestion

reacted with protons at a wild range from 5-8 (Wang, 2017). The carbonates in biochar was expected to react with protons in a similar manner. In our work, the inflection point at pH 10.15 in the curve for the reaction of WSP biochar with protons verified the pH range in which carbonates in the biochar consumed protons, while RH biochar showed an inflection potin at pH 8.80. This implied that in the pH range of 8.0-10.0 carboxyl groups on the biochars may not be the main contributors to the pH buffering due to the acid dissociation (pK_a) of carboxyl groups occurring at pH 5.0-6.0 (Chen, 2014). Another possibility is that the oxygen-containing groups are gradually reduced with the increase of pyrolytic temperature. Chen *et al.* (2014) suggested that for biochar produced at 100-350^oC, the acid-base groups dissociation directly controls the pH buffering properties of biochar, and the resulting surface charges can regulate biochar in nutrient retention and biochar particle dispersing properties. While for biochar produced at 500-700^oC, the effect of acid-base dissociation on organic matter dissolution may be eliminated.

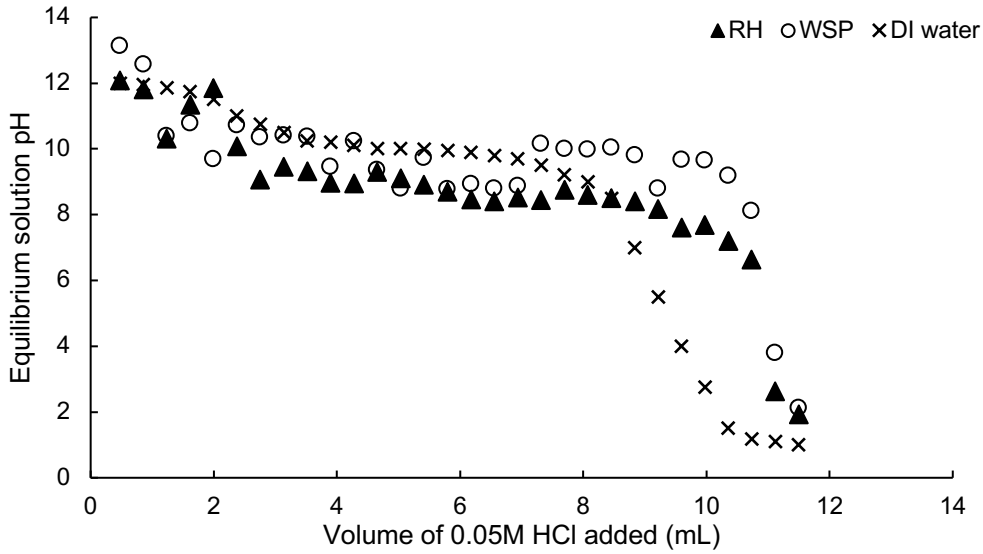

Figure 3-1. Changes in biochar suspension pH as a function of the volume of 0.12 mol/L HCl added at the end of a 5 d equilibrium experiment.

The point of zero charge (PZC) is an inherent electrokinetic property of biochar, which can influence the adsorption process under certain pH conditions. The difference between initial pH and differential pH (△pH) was plotted against the pH_{in} values , and the pH at PZC (pH_{PZC}) corresponded to the point of intersection in the resulting curve (Figure 3-2). The pH values at the PZC were 9.34 for RH biochar and 10.89 for WSP biochar. Our findings are consistent with literature pH_{pzc} values of different biochars (Table 3-1). The greater PZC values of tested biochar could be attributed to the release of alkaline salts such as Na, K, Ca and Mg, from the feedstock during the pyrolysis process, which could favour anionic adsorption (Ahmad, 2012). Meanwhile, this also indicates that the biochar's surface would be positively charged when the pH of solution were adjusted to below each biochar's PZC values.

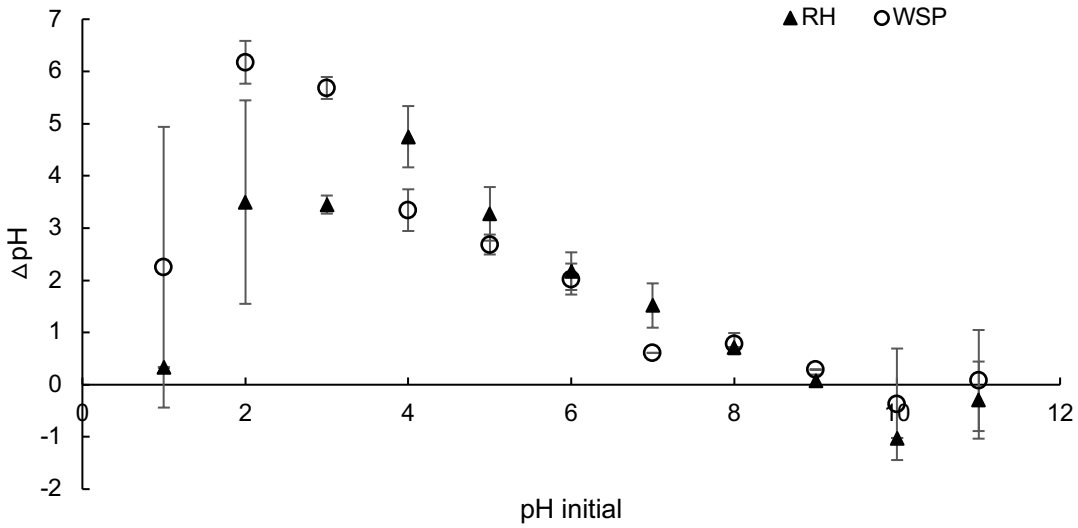

Figure 3-2. pH at PZC for RH and WSP biochar. Data are expressed as mean±standard deviations.

Table 3-1. Comparisons of pH_{pzc} values of difference biochars.

Biochar feedstock	Pyrolysis Temp (°C)	pH_{pzc}	Reference
wheat straw	550	7.8	(Liu *et al*., 2012)
Scrap papers	600	11	(Xu *et al*., 2020)
Date palm fronds waste	800	11.38	(Zubair, 2020)
Peanut shell	500	9.93	(Wang *et al*., 2019)
Mango leaves	800	7.7	(Vyavahare, 2019)

FTIR analysis was performed to analyse the functional groups in tested biochars, and the resulting spectra are shown in Figure 3-3. Peaks at 3400 cm^{-1} assign to the associated hydroxyl (O-H) stretching vibration peak or moisture molecules in both biochar samples, which was attributed from carbohydrates in the biomass. Furthermore, peaks at 910-650 cm^{-1} correspond to the out-of-plane bending vibration of C-H bond on the benzene ring substitution region which were also found in FTIR spectra of both biochars. In addition, an asymmetric stretching vibration at 1628 cm^{-1} represents a C-O or C=O group on a benzene ring, which has seen in both biochar sample; whilst this peak was more identified in biochar WSP. In addition, the adsorption peak at 1383 cm^{-1} is an in-plane flexural vibration of an aromatic $-CH_3$ group on a benzene ring, appeared in biochar WSP. Beside, we saw an increasing draft in the baseline at high wavenumbers in the spectra of biochar RH. Literature has reported similar phenomena in the study of maize stalk and corn stover biochars (Sharma *et al.*, 2004; Zhu *et al*., 2015).

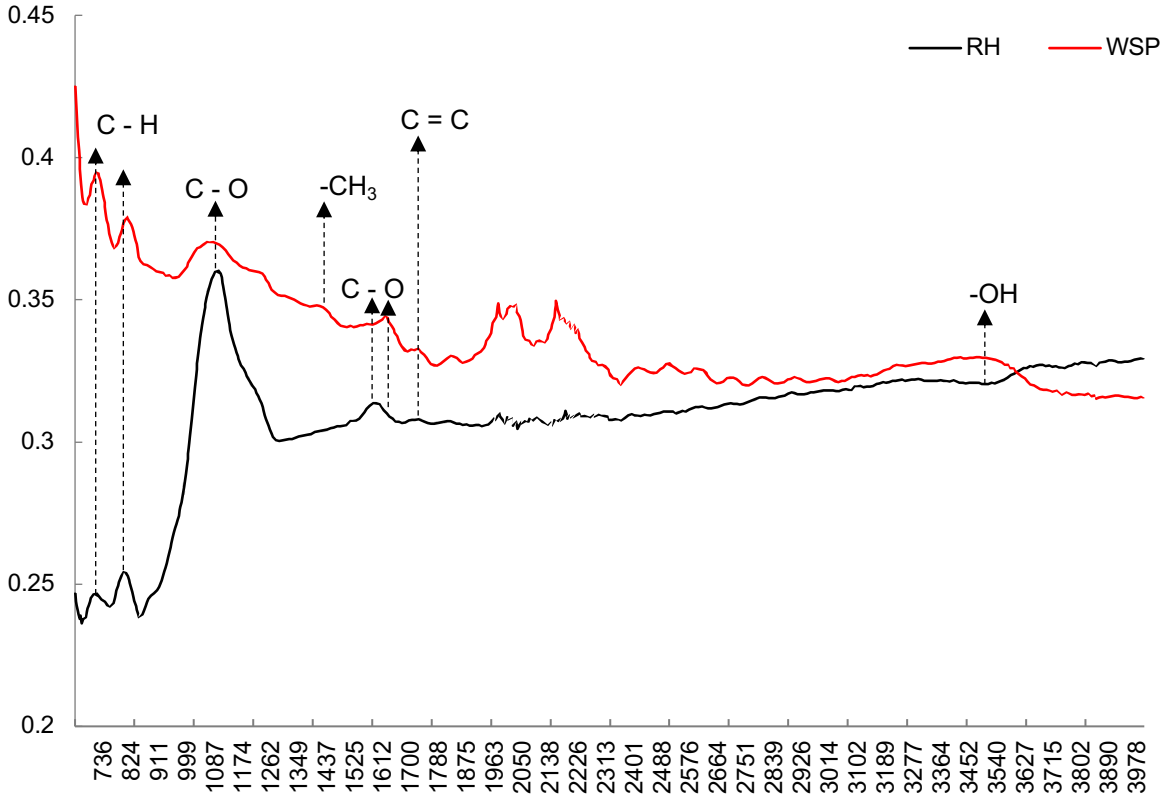

Figure 3-3. FTIR spectra of biochar derived from rice husk and wheat straw pellets.

3.2.2. Adsorption analysis

Three different models of Langmuir, Freundlich and Temkin were used to describe adsorption isotherms (Table 3-2 and Appendix Figure 2). The Langmuir model assumes monolayer adsorption on homogeneous sites inside of the adsorbent, and once a molecule occupies a site, no additional adsorption can occur there. While Freundlich equation is used to describe chemical adsorption process onto the heterogeneous surface (Gong, 2017). Temkin model assumes the adsorption heat of all molecules decreases linearly with the increase in coverage of the adsorbent surface (Piccin, 2011). The experimental data did not fit well with the Langmuir model, with the R^2 below 0.90, while fitted the Temkin best with R^2 of 0.9993 and 0.9994 for RH and WSP biochar, respectively. It indicated that the adsorption of ammonium was mainly

controlled by chemisorption by indirect sorbate/sorbate interactions (Al-Ghouti, 2020). Therefore, the possible mechanism of ammonium adsorption on RH and WSP biochar might be electrostatic interaction between ammonium and surface charge of biochar (Kim, 2021). Meanwhile, the Freundlich isotherm model showed a higher correlation coefficient for ammonium adsorption on WSP biochar, suggesting that the adsorption of ammonium onto WSP biochar might be a process of multilayer adsorption. Meanwhile, our findings shows that the tested biochar had a moderate sorption capacity for ammonium. Hale *et al*. (2013) reported that the maximum adsorption capacity of cacao shell and corn cob biochars were 0.24mg.g and 0.56 mg/g. Digested sludge biochar had a 1.40 mg/g adsorption capacity for ammonium (Tang, 2019), while the maximum adsorption capacity of wood biochar for ammonium were 44.64 mg/g (Kizito, 2015).

Table 3-2. Adsorption isotherm parameters for tested biochars.

Biochar	**Langmuir**			**Freundlich**			**Temkin**	
	K_L	Q_{max} (mg g^{-1})	R^2	n	K_F	R^2	K_t(L/mg)	R^2
RH	4.66	0.069	0.901	1.04	0.254	0.9764	0.02177	0.9993
WSP	4.61	0.415	0.9139	0.88	0.218	0.999	0.020758	0.9994

It should be noted that biomass-based biochar without pre-/post-treatment might not provide high adsorption capacity in acidic or neutral environments (Huang *et al*., 2018). For example, researchers suggested that the maximum ammonium removal efficiency of biochar derived from rice husk and other plant shells is under 40% (Kizito *et al.*, 2015; Wang *et al.*, 2020). Activation and/or modification by metal ions and acids could greatly enhance ammonium removal efficiency.

Table 3-3. The adsorption capacity of ammonium of different biochars.

Biochar feedstock	Modified methods	NH_4-N (mg/g)	Reference
Hardwood shavings	unmodified	5.3	(Sarkhot, 2013)
Thalia dealbata	CO_2	17.6	(Zeng, 2013)
Sawdust	$LaCl_3$	4.1	(Wang, 2015a)
Phragmites australis	CO_2	4	(Zeng, 2013)
Cacao shell	unmodified	0.24	(Hale, 2013)
Corn cob	unmodified	0.56	(Hale, 2013)
Pitaya peel	unmodified	2.65	(Hu, 2020)
Orange peel	unmodified	4.71	(Hu, 2020)

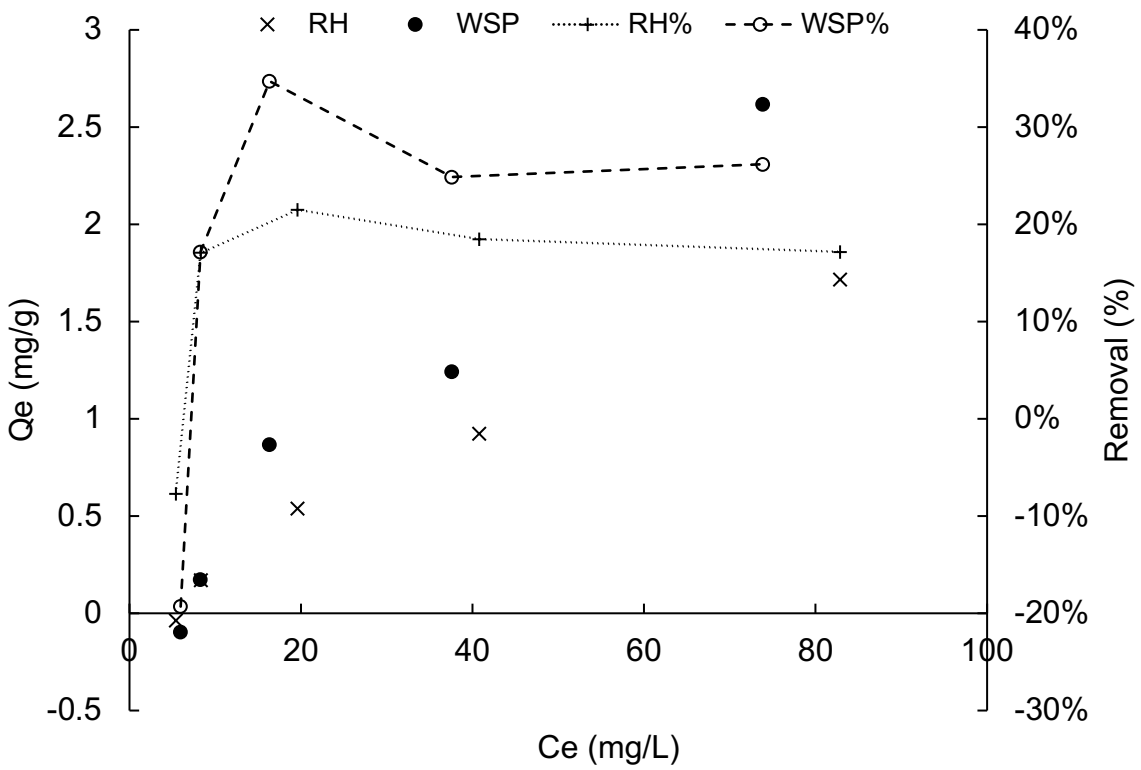

Figure 3-4. Adsorption of ammonium by biochar RH and WSP.

In order to investigate reaction mechanisms, the ammonium adsorption data were fitted with kinetic model (pseudo second order model and intra-particle diffusion model)

(Table 3-4 and Appendix Figure 1). The pseudo-second order did not fit well for RH biochar with a squared correlation coefficient (R^2) of 0.92 indicating more than one steps might be involved in the adsorption process. Although the correlation coefficient value of pseudo second-order kinetic curve for WSP biochar was 0.98, the experimental Q_e value did agree with the theoretical ones. It was interesting to find that ammonium adsorption on both biochars were not fit the intra-particle diffusion well throughout the entire process with squared correlation coefficient (R^2) less than 0.90.

Table 3-4. Adsorption kinetic parameters for tested biochar.

Biochar	Pseudo 1st order			Pseudo 2nd order			Intra-particle diffusion		
	K_1	Q_e (mg/g)	R^2	K_2	Q_e (mg/g)	R^2	K_{diff} (mg/g/$h^{1/2}$)	C (mg/g)	R^2
RH	-0.025	0.498	0.2516	5.144	0.929	0.9225	0.3503	0.2715	0.6252
WSP	-0.065	0.868	0.9143	1.345	1.708	0.9833	0.5364	0.4769	0.7956

The mechanism of ammonium adsorption onto different biochars was still not fully understood due to it involved physical adsorption, interaction of functional groups, ion exchange adsorption and several other approaches (Gong, 2017). To sum, the main ammonium adsorption mechanisms on the tested biochar in this study was chemisorption. Similar to other literatures, NH_4^+-N adsorption on biochar is greatly influenced by oxygen-containing functional groups on biochar surface (Takaya *et al.*, 2016; Huang *et al.*, 2018; Wang *et al.*, 2020; Munar-Florez *et al.*, 2021). Combined with infrared spectra, the nitrogen atoms can be coordinated with the carboxyl and hydroxyl groups on benzene ring, or amino groups on the benzene structure substituted region (Pereira *et al*., 2015). Overall, biochar WSP showed a better adsorption capacity for ammonium than biochar RH, indicating its potential as an adsorbent for ammonium removal.

3.2.3. Biogas batch experiments with addition of biochar

To evaluate the effect of biochar as a functional additive and to optimize the additive dosage of biochar on anaerobic digestion of sewage sludge, the gas production and methane content were monitored in a series of batch tests at different ammonium concentration (1, 3, and 6 g/L) with different dose of biochar (0.1 and 1.0%wt). Of note is that the biogas volume from the 1st test was lower than the detection limits of methane meter (>20 mL) and therefore the biogas composition was only assessed at day 11. The 2nd test was conducted with the initial ammonium concentration of 3 g/L. Methane content in biogas was monitored throughout the course of 2nd experiment with measurements taken at day 11, 25, 43, and 54. Moreover, additional ammonium stress were introduced to the AD system at the beginning time in Test 3 by adjusting ammonium concentration to 6 g L^{-1}. The composition of biogas was measured at day 11, 25 and 43. All treatment groups were conducted in duplicates.

All the treatment groups from the 1st test started producing biogas from day 0, except from reactor with addition of WSP biochar at a biochar dose of 0.1%wt showed a 1-day lag phase (Figure 3-5). Meanwhile, with increasing biochar dose of 1.0%wt, WSP biochar-amended reactor achieved maximum daily biogas production (0.20 mL/g/d), which was 3-fold higher than the control groups (0.07 mL/g/d). The daily biogas production for most of treatment groups showed a slight fluctuation in the first two days and followed by a sharp decrease by day 9, which suggested that during this phase, the microorganisms in these reactor went through an acclimated duration. Considering that the source of seed inoculum came from an AD unit with municipal wastewater sludge as substrate, great change of substrate characteristics likely caused the microbial succession in initial stage of operation under low organic loading rate. This

is consistent with previous studies (Wang, 2020). Moreover, daily gas production from AD of sewage sludge increased slightly as the biochar dose increased, which biogas production rates increased by 53.1% by day 15. Although both biochar additions enhanced cumulative biogas production by 26.9±0.9% for RH biochar and 33.6±0.4% for WSP biochar, the increased dosage of biochar did not show such influences on cumulative biogas production.

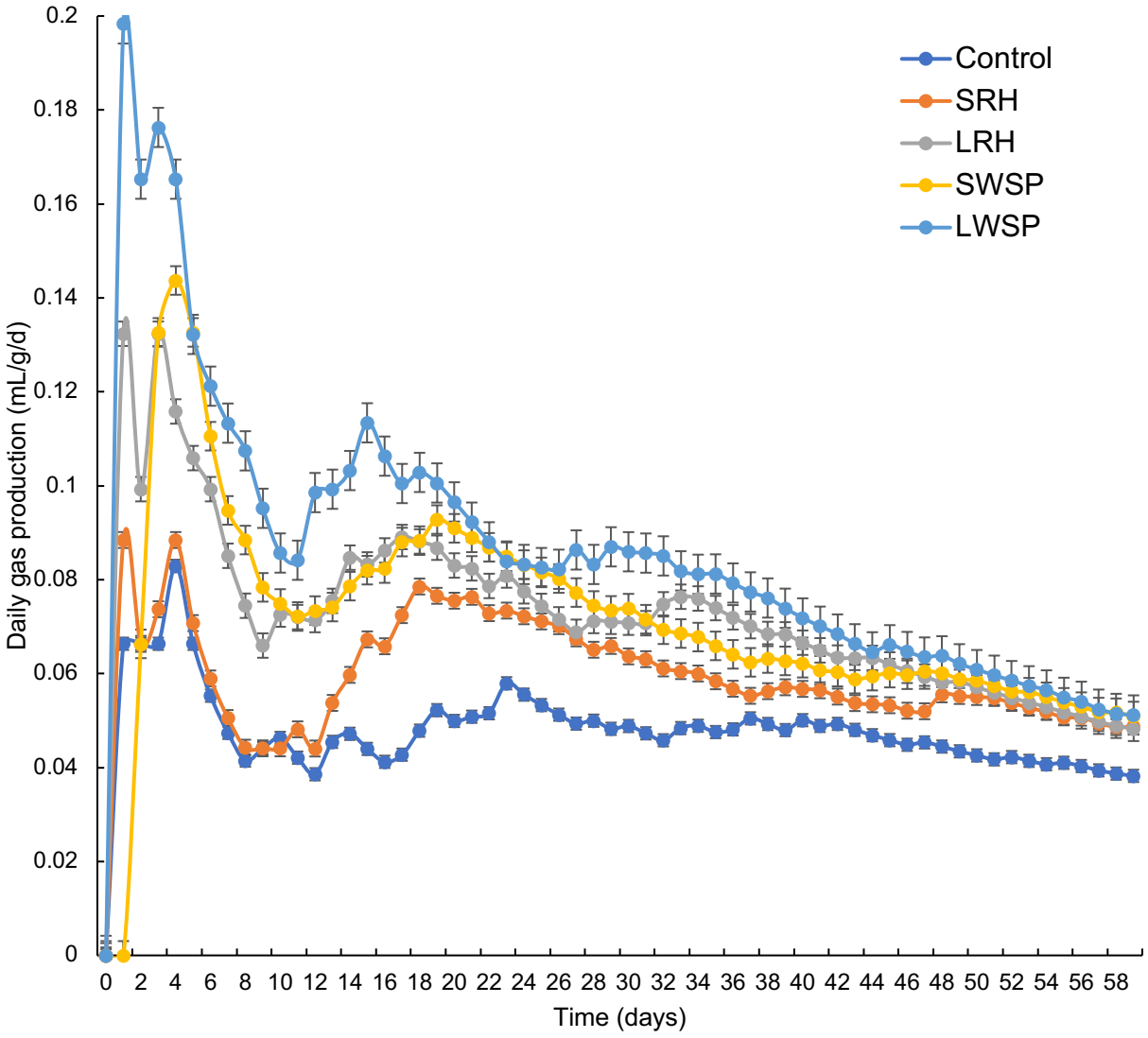

Figure 3-5. daily biogas production under ammonium concentration of 1 g L-1, 'S;L' = the dosage of biochar at 0.1 and 1.0 wt%.

It has been reported that methane content in biogas generated from anaerobic digestate of sewage sludge typically ranges from 60 to 65% with the rest greatly consisted of carbon dioxide (Liebetrau *et al.*, 2018). The methane content from the test reactors reached considerably higher than typically reported for sewage treatment anaerobic digestate at 73.7 $\pm$ 2.39%. Differences in the methane concentration between the test conditions were also observed; control group had a mean methane content of 58 $\pm$ 1.18% whereas biogas from biochar WSP and RH reactors at biochar dose ratio of 0.1%wt contained 73.71% and 75.04% methane respectively. Meanwhile, with increased biochar dosage (1.0%wt), biogas had higher methane content of 75.76% for WSP biochar-amended reactor, while a decrease in methane content was observed in RH biochar-assisted reactor. The enhanced methanogenesis with addition of WSP biochar can be attributed to the pH buffering capacity (Jang, 2018). Furthermore, FTIR results showed that phenazines presented onto the surface of WSP biochar, indicating that the redox-active phenazine organic structure can be another possibility to promote methanogenesis by facilitating the syntrophic oxidation of volatile fatty acids via direct electron transfer (DIET) (Beckmann, 2016). In addition to that, RH biochar additive showed a promoting potential for methane content (75.04%) at a lower biochar dose, indicating that, from the viewpoint of engineering applications, RH biochar could be an economic-feasible additive for AD systems.

Table 3-5. Methane content (%) of the biogas from biochar-treated reactors and the control. 'S;L' = the dosage of biochar at 0.1 and 1.0 wt%.

Day	PC	SRH550	LRH550	SWSP550	LWSP550
11		75.04 ± 1.49	70.36 ± 6.71	73.71 ± 2.7	75.76 ± 2.3
43	58.0 ± 0.84				

Similar to the 1st biogas experiment, all reactors immediately started producing biogas. The daily gas production followed an order: SRH≈LWSP≈LRH>SWP>Control. Again negligible effects of RH biochar dosage were observed on AD of sewage sludge, and both of them (0.1% and 1.0%) have similar daily gas production of 5.35 and 5.41 mL/g, respectively. This implied that the functions of RH biochar on promoting biogas production was mainly contributed to chemical interaction during the AD process at ammonium concentration of 3g/L. Meanwhile, the presence of alkaline-earth metals such as Ca, Mg and alkali metals such as Na, K, in RH biochar may promote chemical sorption of CO_2 via mineralogical reactions, leading to a higher gas yield (Xu, 2016). Chiappero *et al*. (2021) investigated biochar derived from rich husk and sewage sludge and activated at 900°C with CO_2 on anaerobic digestion of wastewater sludge, and found that activated biochars with higher surface area and the presence of alkali metals boosted gas yield and improved the methane yield up to 105%. In contrast, with increasing biochar dosage, the cumulative gas production from WSP biochar-added reactor was improved by 1.1-fold compared to the control, which might be attributed to acid-buffering function of WSP biochar. Wang *et al.* (2017) reported that buffering capacities of biochar derived from vermicompost were positively correlated

to their loading proportion, and 5.0% of their biochar worked the best for enhanced methane production.

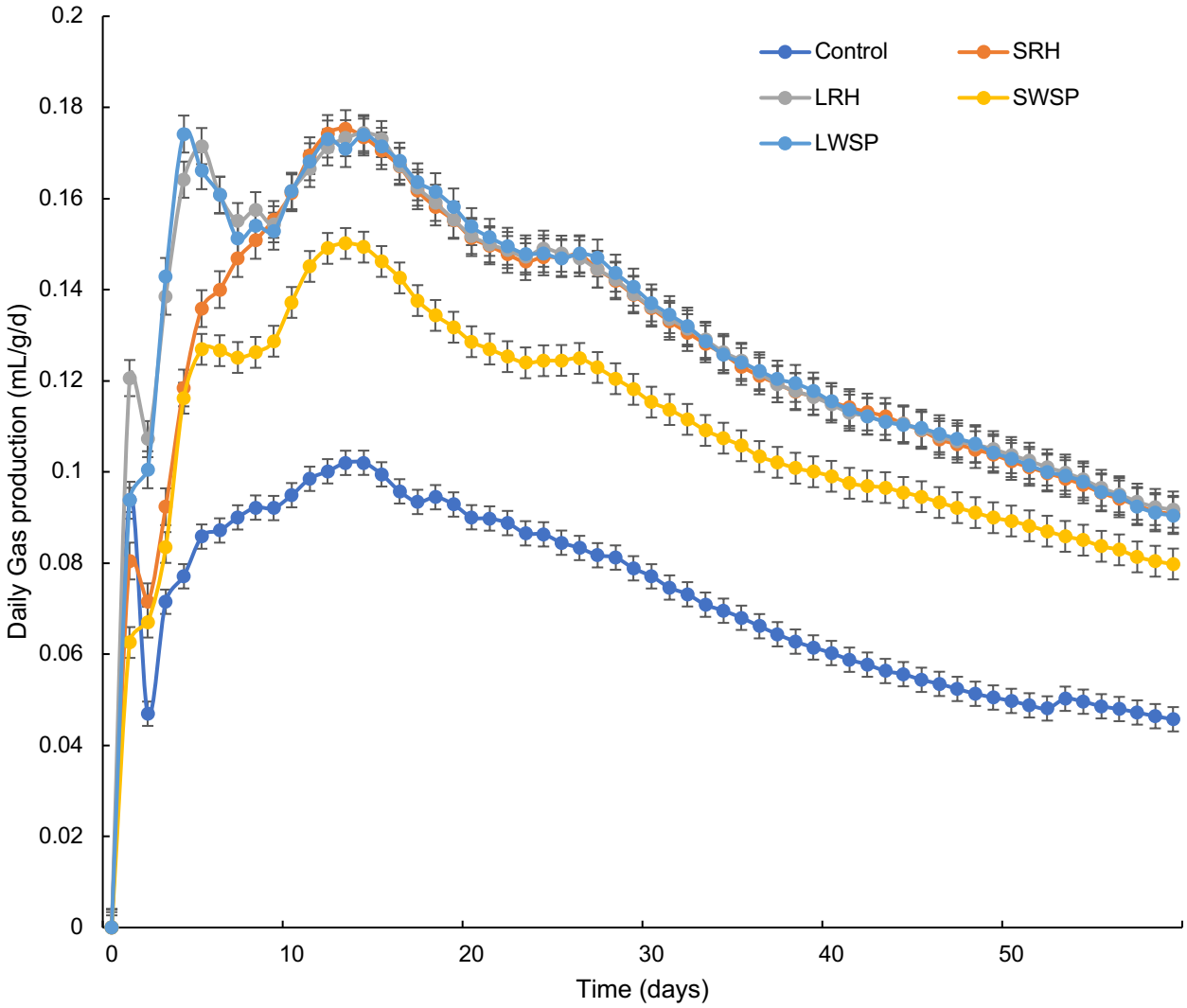

Figure 3-6. Daily biogas production (mL/g) with initial ammonia concentration of 3.0 g L-1 in Test 2. 'S;L' = the dosage of biochar at 0.1 and 1.0 wt%.

With increasing ammonium concentration (up to 6 g/L), the cumulative gas production from the control group was increased by 2.05±0.26 folds compared to the 1st and 2nd AD tests. Our findings are in agreement with findings by Zaied *et al.* (2020) that the addition of strong alkaline bases such as ammonium bicarbonate to AD increased the

oxidation-reduction potential and enhance the buffering potential. According to their results, the additional dosing (up to 10 mg L^{-1}) of ammonium bicarbonate led to a 29.80% increase in biogas production from palm oil mill effluent (Zaied *et al*., 2020). Siddique and Zularisam (2012) also reported that biogas yield was increased by 27.77% with addition of 10 mg L^{-1} ammonium bicarbonate during the AD of petrochemical wastewater under mesophilic temperature conditions, and ammonium bicarbonate improve carbon-to-nitrogen ratio and ensure a stable pH during AD process. However, unlike previous tests, all the reactors with addition of biochar WSP were inhibited by reducing 8.6%-21.8% cumulative gas production. Moreover, a higher dosage of WSP biochar caused severer inhibition on AD of sewage sludge. Li *et al*. (2019) investigated effect of biochar on AD of mono-cardboard and found that the addition of biochar with higher dosage led to a decreased methane production and extended the lag phase. Similar results were reported by Qin *et al.* (2017a) that biochar derived from rice straw at 500^{o}C with a biochar dosage of 0.5%wt resulted in a reduced cumulative methane production and decreased maximum methane production rate from batch AD of organic fraction of municipal solid wastes. The negative effect might be attributed to adsorption capacity of biochar, which reduced the contact between microbes and substrates (Li, 2019). Another possibility is that hydrolysis and acidogenesis-acetogenesis are accelerated to the unbearable extent by excessive biochar, resulting in accumulated intermediates to inhibit the methanogenesis (Pan, 2019). On the other hand, biochar RH-treated reactor improved AD by producing considerably higher cumulative gas yield (5.26±0.05 mL g^{-1}) than the control (5.03±0.02 mL g^{-1}). This might be due to that minerals such as Mg, Na, K, P, and N leached from biochar can enhance syntrophic metabolic process among various bacteria (Ambaye, 2021). Another possibility for enhanced biogas production is the cations from alkali metals and

alkaline-earth metals influence the reduction of CO_2 to carbonates, resulting in facilitated methane formation through hydrogenotrophic methanogens (Resasco, 2017; Stams, 2009).

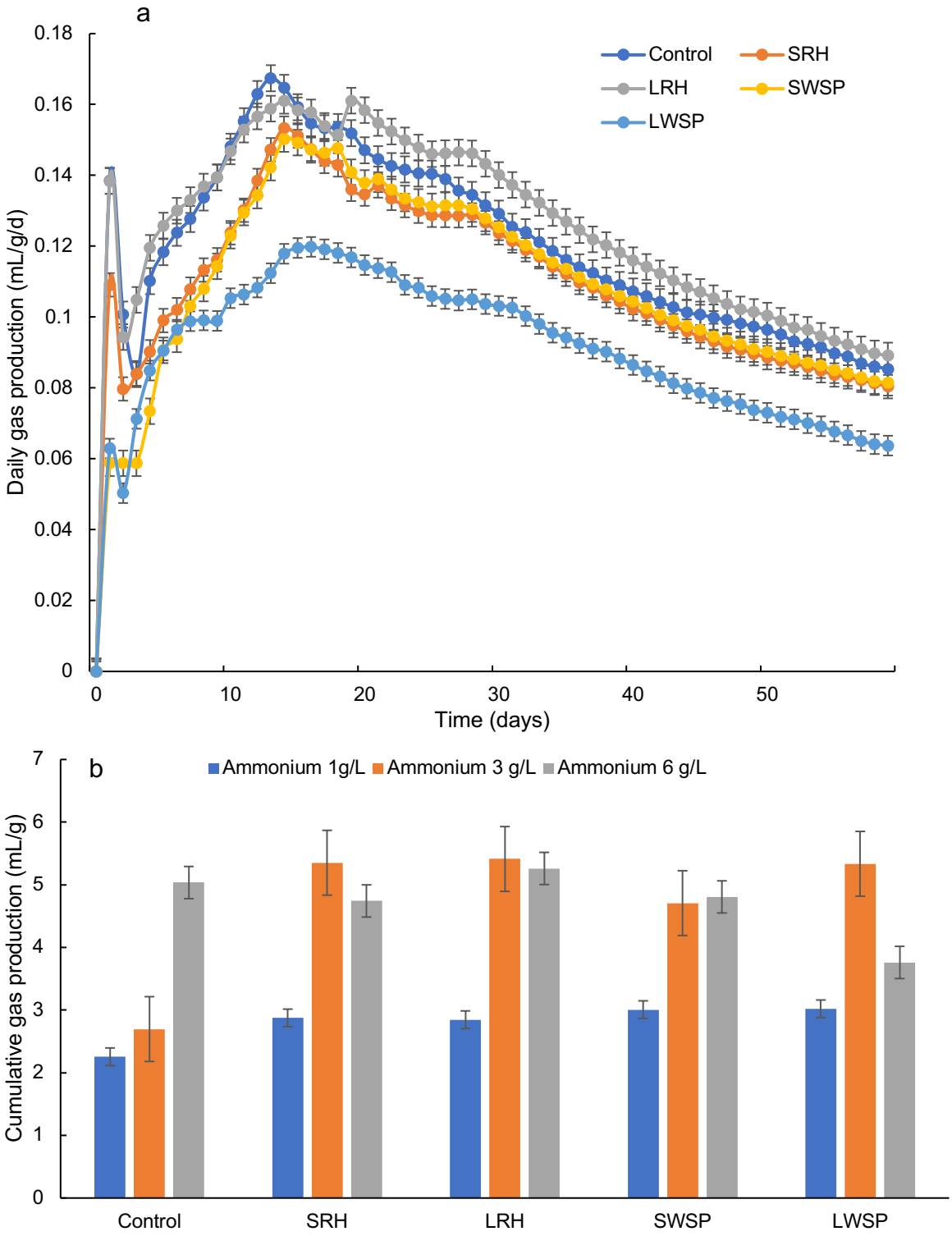

Figure 3-7. Daily biogas production (mL/g) with initial ammonium concentration of 6.0 g/L (a) and cumulative biogas production (mL/g) (b).

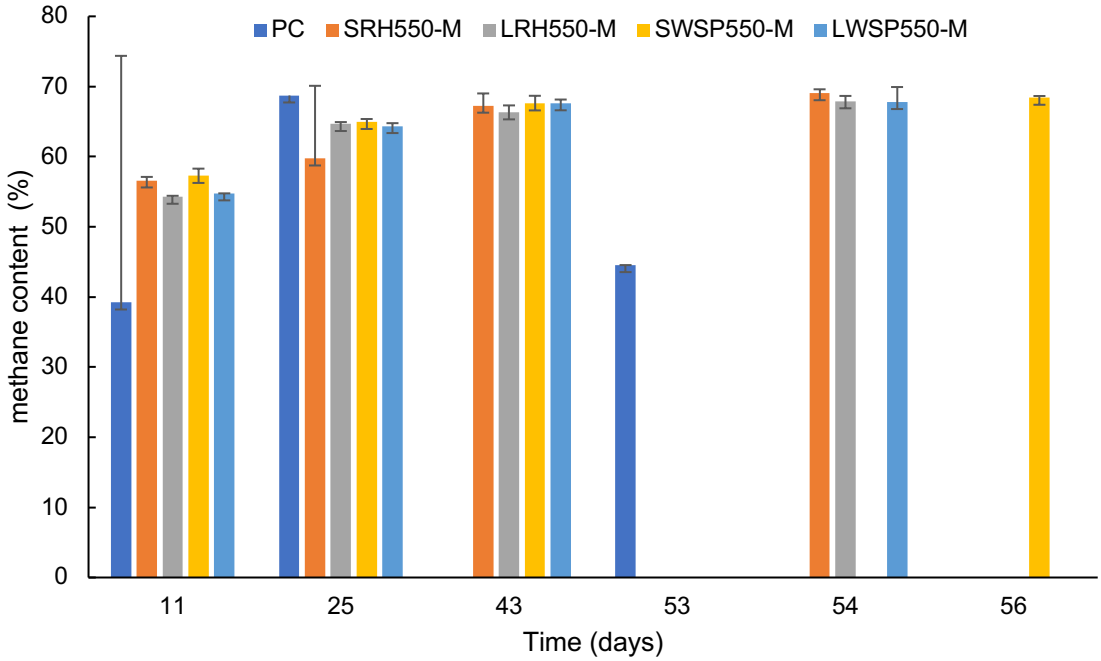

Figure 3-8. Methane content of biogas from the reactors under ammonia concentration of 3.0 g L-1 in Test 2, mean of triplicates. 'S;L' = the dosage of biochar at 0.1 and 1.0%wt.

With the increasing ammonium concentration, an inhibition in methane content was observed in the control groups, resulted in decreased methane content of 12.4% for AD with initial ammonium concentration of 3.0 g/L. In contrast, when the initial ammonium concentration reached up to 6 g/L, the average methane content in biogas from the control group was improved by 1-fold than that of Test 1, and achieved to an average of 63.7±8.4%. Similar results were reported by Cai *et al.* (2021) that the cumulative methane yield was higher at TAN 5g/L than at TAN 3g/L at mesophilic conditions. This phenomenon was contributed to enhanced activity of microorganisms caused by a higher temperature (32-39^{o}C) offsets the higher toxicity of free ammonia Lin *et al*. (2016) also reported the similar phenomenon in anaerobic digestion. Meanwhile, the standard deviation in methane content from the control group in Test 2 was considerably high as it was unknown if the biogas production would be disturbed

by regular sampling and therefore give a varied reading. The addition of WSP and RH biochars enhanced methane content (an average of 63.7±0.5%) in biogas at initial ammonium concentration of 3 g/L by an average of 1.25±0.01 folds compared to the control (50.8±0.5%). Noticeably, no significant difference on methane production in functions of biochar types and doses were observed. Although the increased dosage of WSP biochar led to a reduction of biogas production, this is not the case with the methane production. When the initial ammonium concentration increased to 6 g/L, the addition of RH and WSP biochar at a biochar dose of 1.0 %wt resulted in a slightly lower methane content (61.7% and 62.3%) than the control group (63.7%). Dudek *et al.* (2019) reported that biochar derived from brewer's spent grain overdose inhibited gas production. This also confirms that there appears to be a limit beyond which the properties of biochar contributing to inhibiting the fermentation process.

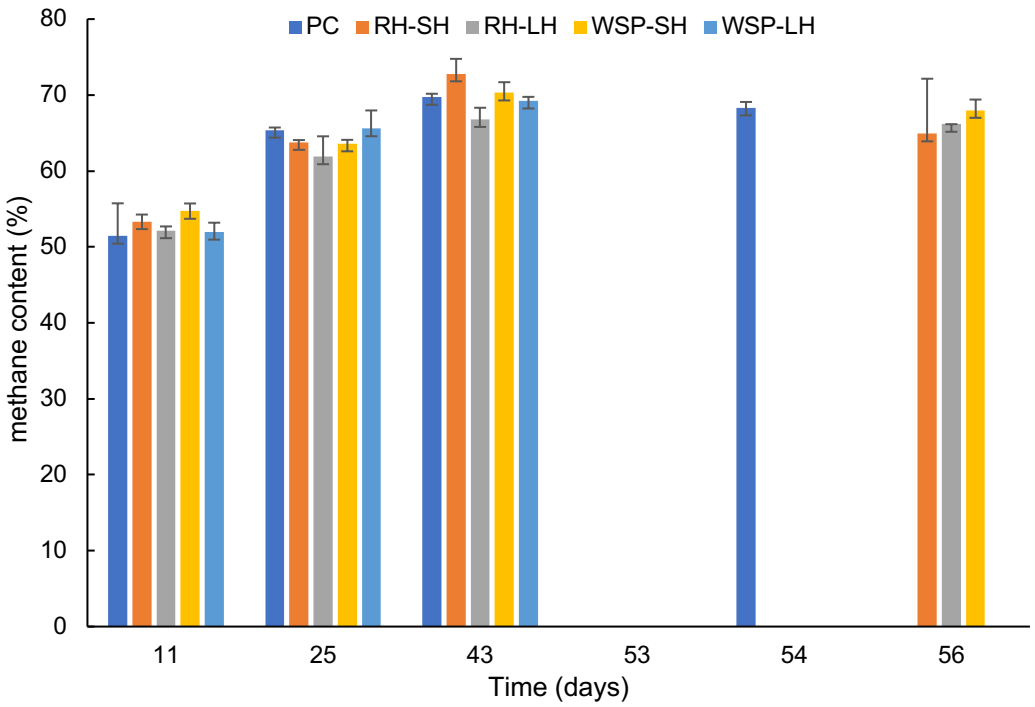

Figure 3-9. Methane content of biogas from the reactors under ammonia concentration of 6.0 g L-1 in Test 3, mean of triplicates. 'S;L' = the dosage of biochar at 0.1 and 1.0 wt%.

It is important to note that although different enhancement in biogas profiles were shown in each biochar treatment; there are several limitations in this study. In order to minimise the impact on the reaction rate, chemical analysis and gas composition analysis is performed less frequently. This, however, shows the limitations of laboratory equipment, as the gas composition and solid fraction may be excluded from the analysis. As a result, we only see the gas composition when a particular amount of gas has generated, rather than on a regular basis. To achieve a more accurate measurement of AD performance, it is advised that future studies should precisely define the methodological application of gas composition analysis in small volume experimental settings. Furthermore, in this experiment, the biochar was not treated to any pre-treatment or pre-inoculation with digestate prior to its use in AD, in an effort to reduce the risk of contamination. However, as previously stated, the addition of biochar to aqueous solutions considerably affected their pH, causing them to fluctuate in the neutral to slightly basic range, implying a potential variable in each experiment. As a result, future investigations might establish a consistent baseline pH for the reactions performed, allowing changes in reaction efficiency to better represent the chemical characteristics of the biochar. Furthermore, in order to reduce the effect of biochar particle size and volume on experimental results, the size of biochar could be standardised in future studies so that differences in reactor performance can be more accurately attributed to biochar's surface functionality. To gain a better understanding of biochar’s effects on the AD potential from different wastes and their functions, both the biogas productivity from animal wastes and the chemical changes are analysed in chapter 4.

3.3. Conclusions

According to the findings of this study, tested biochar improved anaerobic digestion under little or high ammonia stress. Because biochars' ammonium adsorption capabilities varied, it is likely that the favoured methane production was based on other mechanisms. In addition, chemisorption was found to be the major process in the sorption of ammonium ion on biochar. Furthermore, biogas generation reduced with increasing biochar dosage. Taking consideration of the biochar production cost, it would be beneficial that small amount of biochar ensures positive effects on the AD potential. It should also be important to consider the limitation of these experiments. Biological analysis were not done and therefore the functions of these biochar in microbial communities needs further investigation.

Table 3- 6. Main findings from Chapter 3.

Biomass	**Pyrolysis Temperature (°C)**	**pH_{pzc}**	**Initial ammonium concentration (g/L)**	**Maximum biogas production rate (mL/g/d) (biochar dose 0.1;1.0)**	**Cumulative gas production (mL/g) (biochar dose 0.1;1.0)**	**Maximum methane content (%) (biochar dose 0.1; 1.0)**
Rice husk	550	9.34	1	0.09;0.13	2.87;2.85	75.0;70.3 (at one time point)
			3	0.18;0.17	5.35;5.41	63.2;63.3
			6	0.15;0.16	4.74;5.26	63.7;61.7
Wheat straw pellets	550	10.89	1	0.14;0.20	3.0;3.02	73.8;75.8 (at one time point)
			3	0.15;0.17	4.71;5.33	64.6;63.6
			6	0.15;0.12	4.81;3.76	64.1;62.3

4. Effects of biochars derived from lignocellulosic residues/wastes on methane production from co-digestion of animal waste and maize silage

4.1. Introduction

The high livestock intensity not only has a significant impact on the global economy, but also potentially stresses the environment. A recent study discovered that adult animals may produce manure at a rate of about 8% of their body weight per day, corresponding to a dry mass of about 7.3 kg per cow per day (Font-Palma, 2019). The EU produces 1.4 billion tonnes of dairy manure per year (Foged *et al*., 2011), while the UK produces 31.3 million tonnes of dairy and beef cow dung per year (Smith & Williams, 2016). Accordingly, nearly 1.5 billion tons of manure are produced per year in China (Qian *et al*., 2018). The increased production of livestock manure, combined with environmental concerns, has increased the demand for its proper treatment.

Animal manure has been commonly applied directly onto lands as an organic fertilizer (Chambers *et al.*, 2001; Font-Palma, 2019), due to its richness in biodegradable organic matters. However, the inappropriate management and disposal of animal manure lead to global environmental and sanitation challenges. Large manure generation can result in higher local emissions of pollutants, including accumulation of metals and phosphorous in soils, spreading of pathogens, as well as odour issues (Petersen et al., 2007). Furthermore, excess nitrogen and phosphorus in animal manure can be flushed off by surface run-off or seepage, resulting in eutrophication of surface waters and nitrate pollution of groundwater (Velthof *et al.*, 2014; Dijk, 2016; Qian *et al.*, 2018). It was also reported that the handling and use of manure on

livestock farms are responsible for around 3 to 5% of total greenhouse gas (GHG) emissions globally, especially with liquid manure management (Søren, 2018). As a consequence, the management of animal manure has become a critical issue, with increasing negative environmental impacts.

Currently in Europe, there are a wide variety of manure treatments in the market. There are several commercial technologies to treat manure and slurries such as mechanical separation, composting and thermochemical conversion (Font-Palma, 2019). They are classified on the basis of their objectives such as energy production, phase separation, nutrients recovery and nitrogen removal. However, applications of conventional treatment technologies such as incineration and composting may be limited at the EU-27 level due to the EU environmental regulations (Edwards, 2015; Hou *et al.*, 2017). In China, a series of policies and regulations such as the "Sustainable Manure Treatment" program and "Prevention and Treatment on Pollution from Livestock Cultivation" regulations have also been enforced by the Chinese government since 2014 (Cai *et al*., 2019). In contrast, up to 40% of manure in China is not effectively treated and of 20% is still being directly discarded onto land (Chadwick *et al*., 2015). As such, a sustainable technology for livestock manure treatment is needed to achieve higher efficiency, lower pollution risk and easier operation.

Among the several manure treatment methods, anaerobic digestion (AD) stands out as a promising technology to achieve high efficiency and energy recovery. However, around 25% of total commercial AD facilities use sewage sludge, and AD of animal manures still faces numerous obstacles, including operational instability and biogas

quality (Fagbohungbe *et al.*, 2017b; Grando, 2017; Chiappero *et al.*, 2020). Livestock manure and slurry contain high content of nitrogen, which may present a potential inhibition risk as the result of ammonia accumulation in the digester when manure is digested individually (Cuetos *et al.*, 2011). The reported ammonia-mediated inhibition to methanogenesis occur at initial concentration of 100-1100 mg/NL unionized ammonia (Angalidaki, 1993; Molinuevo-Salces, 2010). To address this issue, the carbon content of animal manure needs to be increased before proceeding to the anaerobic digestion process. Lignocellulosic biomass such as agricultural residues are promising candidates to compensate the carbon deficiency of animal manure. Co-digestion of animal manure and lignocellulosic biomass provides an opportunity to balance the carbon-to-nitrogen ratio of feedstock for anaerobic digestion (Hashimoto, 1983; Hills, 1981; Ebner, 2016; Neshat, 2017). Wang *et al.* (2012) reported that co-digestion of cattle and chicken manures and wheat straw can improve the biogas yield by 10% and the synergic effect of these materials was responsible for improvement of anaerobic digestion. Similarly, Li *et al.* (2015) compared the digestion of cow manure and rice straw, and found methane production yield in co-digestion of these two materials was higher than that of mono-digestion of cow manure. In addition to that, high water content of animal manures may dilute the concentrated organic compounds existing in lignocellulosic biomass which may cause inhibitory effect on the process. Risberg *et al.* (2013) reported that co-digestion of manure and wheat straw did not improve the methane production yield as compared to that of mono-digestion of cow manure or wheat straw.

The use of additives such as activated carbon, zeolites, and biochar in AD has also been identified as a promising strategy for reducing inhibitor bioavailability without

negatively affecting the AD process (Rajagopal, 2013). Biochar is an example of adsorbents made from agricultural residues and/or other lignocellulosic biomass (Mašek *et al.*, 2019). Recent research has found that adding biochar to AD improves biogas output by lowering acid and ammonia inhibitions or boosting direct interspecies electron transfer (DIET) in syntrophic metabolisms (Barua & Dhar, 2017; Fagbohungbe *et al*., 2017b; Luo, *et al.*, 2015; Mumme *et al*., 2014; Torri & Fabbri, 2014). Gómez (2018) investigated the performance of batch AD of swine manure with the addition of almond shell biochar and discovered that biochar can increase biomethane generation by 30%. However, little is known about the effects of biochar on the process of semi-continuous co-digestion of cow slurry and agricultural residues.

Co-pyrolysis, in particular, has recently been identified as a new upgrading strategy for improving the quality of biochar (Sanahuja-Parejo et al., 2019). Two or more types of waste can be processed jointly in the co-pyrolysis process to maximise waste utilisation and reduce reaction time and energy consumption required to pyrolyze single waste material. For example, Liu *et al.* (2019) discovered a synergistic impact of combining sludge and water hyacinth as feedstocks in a co-pyrolysis process. Similar results were also reported by Bi *et al.* (2021) which biochar derived from sludge and peanut shell has well-developed surface functional groups and a greater activation energy. Furthermore, because there has been little research on the co-pyrolysis experiments of woody biomass and digestate, research on the features of the resulting biochar would provide insight into the resource utilisation of the two components.

The effect of biochar and co-pyrolytic biochar additions on the process performance and system stability of co-digestion of cow slurry and maize silage employing continuous stirred tank reactor with increasing input of external ammonia to stimulate ammonia inhibition conditions was explored in this study. The degradation of substrates was also assessed to evaluate the efficiency of mass transitions. The work described in this study aimed at investigating the mechanisms underlying the observed higher methane yields and AD process stability.

4.2. Methodology

Biochars used in this study were produced from four feedstocks: rice husk, wheat straw pellets, mixture of hardwood chips and digestate (50:50 w/w). Rice husk and wheat straw pellets biochars were produced by the UK Biochar Research Centre (UKBRC) at 550^{o}C in a pilot-scale pyrolysis facility (Mašek *et al*., 2018). The standardized production procedure and resulting biochar physicochemical properties can be found on the website of UKBRC (Mašek, 2018). The production of biochar from the mixture of hardwood pellets and digestate was manufactured by the firm Swiss Biochar© (Riedlingsdorf, Austria) as followed Mumme (2014). A 1:1 (w/w) mixture of hardwood pellets and digestate was used as feedstock and pyrolyzed in a 500-III pyrolysis screw reactor (PYREG GmbH, Dörth, Germany) for 20 min with a constant temperature raise in the reactor until a peak pyrolysis temperature of 500^{o}C was reached. The biochar was consecutively stored open with no covering for several days, packed in 1.5 m^{3} plastic bag, homogenized and stored at -20^{o}C until used for the experiment.

Figure 4-1. Schematic figure of PYREG pyrolysis unit.

Semi-continuous AD experiments were conducted in CSTR reactor with working capacity of 8 L that were seeded with inoculum collected from a local farm. Prior to continuous feeding operation the reactors were operated without feeding for 7 days.

In the adapting period, no substrates were added in order to enrich the biomass in methane producing microorganisms and to prevent foaming, a method that has been widely adopted (Dareioti & Kornaros, 2014). The operation was subsequently switched to continuous mode to deliver the hydraulic retention time (HRT) of 14 days. Generally, relatively long HRT is required in anaerobic digestion of lignocellulosic biomass due to these type of substrates is persistent to anaerobic microbes (Yadvika, 2004). 60-90 days have proven as the optimum duration to achieve complete digestion of polymeric substrates (Rivard, 1988). While Bank (2004) reported that HRT of 20 days in anaerobic digestion of maize was sufficient to generate high methane yield. Hence, shorter HRT is desirable because of its economic feasibility and increase of process efficiency (Parajuli, 2022; Dareioti, 2014). At the same time, biochar was introduced into three of the four CSTRs at a ratio of 6% w/w. The reactor without biochar supplementation was used as a control. The starting organic loading rate (OLR) was initially 3 gVS L^{-1} per day. For the biochar-treated reactors, biochar was added five times a week to maintain consistent biochar concentrations. At the same time of each day, the reactors were opened to discharge digestate and fed fresh substrate. The CSTRs were maintained under mesophilic conditions (37±1^{o}C) by heating using a water batch.

4.3. Results and discussions

4.3.1. Characteristics of biochar

The results revealed that moisture content (MC), volatile matter (VM), fixed carbon (FC), and ash content (AC) varied greatly. It is clear that these properties were related to feedstock types and pyrolysis or co-pyrolysis conditions. The moisture content of co-pyrolyzed biochar was high with value of 30.86 $\pm$ 2.56 wt% than other biochars RH and WSP at 7.14 $\pm$ 1.56 % and 12.07 $\pm$ 1.41 % (dry basis), respectively. It was evidenced that the moisture content could partially influence biochar yield, while a higher moisture in the biomass was favourable the biochar yield from processing at a higher pressure (Nanda *et al*. 2016). The volatile matters in RH and WSP biochar were lower than that of HD biochar. Literature suggest that in the range of 4.32% to 14.40% volatile matter in biochar, its related pyrolysis was incomplete whereas complete decomposition would require a longer pyrolysis time or a higher temperature (Tomczyk, 2020). Furthermore, high fixed carbon content in biochar RH and WSP with values of 43.86 $\pm$ 4.48% and 67.48 $\pm$ 1.02% indicates the loss of volatile matter from biochar, implying improved stability of biochar during storage or use as a solid fuel. HD biochar has fixed carbon of 54.35 $\pm$ 2.05%, which was higher than the reported FC content in co-pyrolyzed biochar from sewage sludge and lignocellulosic biomass. Alvarez (2015) investigated co-pyrolysis of sewage sludge and pinewood at a mixture ratio of 1:1 (wt/wt) using conical spouted bed pyrolysis unit, and found that the fixed carbon content of the resultant biochar was 29.6%. Meanwhile, these results are in line with previous findings using pilot pyrolysis unit. This might be attributed to a prolong contact of vapor-phase pyrolysis species with the char was maintain in the fixed bed configuration, therefore led to a higher fixed caron content (Kwapinska, 2021)

The fixed carbon inversely related to ash content; with increased of ash content fixed the fixed carbon decreased. Also the ash contents in both raw biomass and biochar are commonly correlated with non-volatile and non-combustible components. It is clear that biochar RH has the highest ash content of 47.93 %, which could be attributed to the high silica content in its raw material (Singh *et al.*, 2021). Meanwhile, higher ash content and fixed carbon can contribute to a high oxygen-to-carbon (O/C) ratio due to the structural rearrangement of aromatic rings and the formation of crystal structures, such as graphite (Spokas, 2010). While in this study, with increasing ash content of biochar, the O/C ratio followed an order of HD>WSP>RH. This implying the carbonization of rice husk with O/C ratio of 0.01 was higher than other tested biochar. Moreover, HD biochar was enriched in oxygen content with a higher atomic O/C ratio of 0.27. The hydrogen-to-carbon (H/C) ratio has been proposed as an index of aromaticity and resistance of biochar to microbial and chemical degradation (Crombie, 2013). The H/C ratio of all tested biochars were low ranging from 0.2 to 0.4, which were in line with biochars produced from similar conditions (Li & Yu, 2020). This can be attributed to higher degree of carbonization, leading to high aromaticity produced (Han, 2016). According to the IBI and EBC guidelines, char materials can be categorized as “biochar” when atomic O/C and H/C ratios are lower than 0.4 and 0.7, respectively (Schmidt, 2012). All the tested biochars fulfilled these criteria, implying in increased stability of the biochars compared to their feedstock materials.

The surface area and average pore diameter of three tested biochars were determined by gas adsorption analyser as shown in Table 4-1. The surface area and average pore diameter of tested biochars varied dramatically. Biochar WSP has the lowest pore volume (0.001 mL/g) and pore diameter (nm) than other biochars. The specific surface

area of RH biochar was higher than for other biochar at value of 68.55 m^2 g^{-1}. The possible reason for increased porosity of RH biochar is that ash content could act as a passivator during pyrolysis and be embedded in the porous of biochar resulting in an increase of total pore volume (Meng, 2021). In addition, the surface area and pore volume of tested biochars were in the range of previous literature. It has been reported that the surface area of pyrolytic biochar ranged from 23.33 to 230.91 m^2 g^{-1} when the pyrolysis temperature was 350 – 500^{o}C (Singh *et al*., 2021).

Table 4-1. Physiochemical properties of biochars.

Biochar	Rice Husk (RH)	Wheat straw pellets (WSP)	Hardwood/digestate briquette (HD)
pH	9.71	9.94	9.53
Ctot (wt%)	48.69	68.26	67.28
N(wt%)	1.04	1.39	1.32
H(wt%)	1.24	2.1	3.32
O(wt%)	2.47	6.92	27.79
C/N	46.82	49.11	50.97
H/C atomic ratio	0.02	0.02	0.04
O/C atomic ratio	0.01	0.07	0.21
Electrical conductivity (dS/m)	0.48	1.7	26.97
Moisture (wt%)	7.14	12.07	30.86
Fixed carbon (wt%)	43.86	67.48	54.35
Total ash (wt%)	47.93	21.25	14.79
Pore volume (mL/g)	0.057	0.001	0.002
Pore width (nm)	2.65	1.43	7.48
Surface area (m^2/g)	68.55	1.75	6.78

Figure 4-2 presents the FTIR spectra for tested biochar. It can be seen that the FTIR results were confirmed with ultimate analysis and proximate analysis as aforementioned. Noticeable, spectra of biochar WSP and HD showed different patterns, which could be attributed to their different elemental compositions. The peaks are assigned to O-H stretching band at 3404-3410 cm^{-1}, C-H stretching vibrations in aliphatic and aromatics structures at 2851-2873 cm^{-1}, carbonyl and carboxyl groups in carbohydrates at 1605 cm^{-1}, aromatic ring stretching vibrations of C = C at 1559-1566 cm^{-1}. The C = C band was only observed in biochar WSP, which

could be attributed to its higher degree of carbonization. Also the peak at 1428-1439 cm^{-1} was assigned to stretching vibrations of C-H and CH_n in aliphatic and biochar. The phenolic OH and aromatics C-O bonds were identified at 1088-1120 cm^{-1} in biochar WSP. The peaks at 603-876 cm^{-1} were for the weak vibration of C-H bonds in heteroaromatics and aromatic compounds showing in the spectra of biochar WSP. In general, it is clear that biochar WSP has higher peak intensities than co-pyrolytic biochar HD. The possible reason is that enhanced dehydration and decarboxylation promoting formations of C=O and carboxylic acid O-H bands under higher pyrolysis temperature (Axel Funke & Felix Ziegler, 2010).

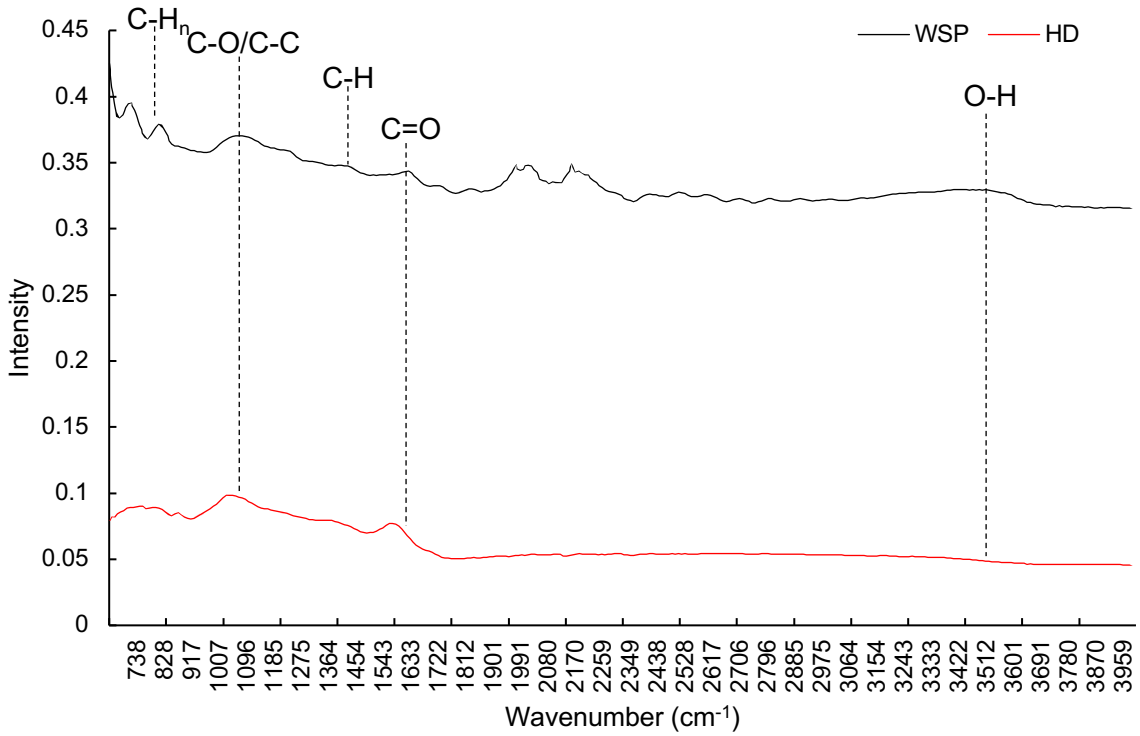

Figure 4- 2. FTIR spectra of biochar WSP and HD.

4.3.2. Biogas and biomethane productions from co-digestion

4.3.2.1. Batch AD tests

The AD performance of cow manure and maize silage was investigated in two different tests using a batch AD system. Throughout the experiment, the volume of biogas was measured on a daily basis. The composition of the biogas from the 1st experiment was measured every other day. All treatments were carried out in quintuplicate. To promote ammonia stress in the co-digestion of cow slurry and maize silage, ammonium carbonate was introduced to certain groups at the start of the experiment.

In the 1st batch experiment, levels of total ammonia remained constant throughout the experiment, around 3000 mg kg^{-1}. After 28 days of anaerobic digestion, the cumulative biogas yield from controls, RH, WSP, and HD reactors was 166.38, 226.32, 107.88, and 10.80 mL g^{-1}, respectively, with a 0 g ammonia carbonate dose. It can be seen that the control reactors started producing biogas on the second day of the test (Figure 4-3). Biogas production increased (36.0%) in reactors treated with biochar RH, but was inhibited in those supplied with biochar WSP and HD. It is worth noting that the pattern of inhibition in biochar HD supplemented reactors differed from that in biochar WSP-treated reactors, resulted in a 5-days delay in biogas production. The higher gas yield from RH biochar-amended reactor was attributed to greater pore volumes and larger surface area. The improved porous structure of biochar could provide micro spaces for the growth of microorganisms in anaerobic reactors while at the same time avoiding direct exposure to acids or potential metabolic inhibitors (Jiang, 2020). Our results are in line with other study that biochars derived from sewage sludge, rice husk and hardwood pellets at 550°C have different impacts on methane yields ranging 0.16-0.219 Nm^3/kg from anaerobic digestion (Chiappero, 2021). Meanwhile, with increasing

ammonium concentration of 3 g/kg, biogas production of the control group increased by 6.77%. The higher tolerance of the co-digestion to high ammonia levels can be attributed to a certain level of adaptation of the microbial community, which is in line with previous studies (Vrieze, 2015). While biochar supplement led to inhibitions in gas production from ammonium-stressed AD.

The methane content of these reactors is shown in Figure 4-4. Methane concentrations in the control groups exhibit similar patterns between the two sets of data, with non-ammonium-induced reactors producing biogas with an average of 55.08 $\pm$ 1.71% methane at day 60, and ammonia-stressed reactors producing biogas with an average of 54.37 $\pm$ 1.72% at the same time point. Furthermore, the methane content for control reactor without additions of ammonia bicarbonate increased by 77.68% at day 6. While, the highest methane content for ammonium stress reactor has lower with a value of 69.83%. Meanwhile, the addition of biochar to non-ammonium-stressed reactors resulted in an increase in methane concentration from reactors with an average value of 97.16 $\pm$ 1.81% by day 10, and maintained the average value of 57.08 $\pm$ 2.47% by the end of the test. The methane content in biogas from ammonia-stressed reactors appeared to rise over time, reaching 106.76 $\pm$ 2.09% by day 10 and 55.08 $\pm$ 1.71% by the end of the test. It should be highlighted that the type of biochar has no discernible effect on methane concentration. The enhanced methane content may be attributed to the capture of CO_2 from biogas via an in-situ biogas upgrading by sequestering CO_2 with biochar during AD (Shen, 2015). In addition, both mono-pyrolyzed biochar showed lower H/C and O/C atomic ratios than HD biochar, suggesting significant hydrophobicity and aromatization, therefore non-

polarity and high hydrophobicity of biochar can effectively improve CO_2 adsorption in presence of water (Chiappero, 2021).

Of note is that although the biochar and substrates (maize silage and cow manure) used in these experiments were from the same sources, the substrates had been stored at 4 ± 2 °C for ~40 days. As such, it is possible that the compounds or microbial community in the cow manure, or the organic matters in maize silage, had changed significantly between tests. It is essential to mention that, while each treatment had a distinct biogas production profile, the tests had several limitations. Moreover, the large value of standard deviation in determination of methane concentration between the two set of data highlights a weakness of the experiment design and an uncontrolled variable in each experiment. Furthermore, litter pre-treatment of cow manure and maize silage was performed prior to their use in AD. The increased biogas productivity from the second test is most likely attributable to a decrease in the amount of nitrogen compounds as a result of storage at 4°C. It is also the reason why we observe positive effects of biochar addition in the AD potential. Ageing of the digestate and cow manure was also not quantified as the organic matter of the solid fraction was not measured, and it is considered that hydrolysis may occur and lead to the depletion of nitrogen compounds. Furthermore, despite the expectation of ceased metabolic processes at 4°C, however an occasional degassing the digestate and cow manure containment vessels was required due to the accumulation of biogas. As such, it is assumed that a portion of nitrogen compounds and other organic material might naturally lose via this storage method, causing by the slowed and continued microbial activity as witnessed by the impacts on the eventual biogas production and methane content in tests. Ideally,

the materials acquired for AD experiments should be from the same source and as fresh as practicable; any potential degradation should also be monitored.

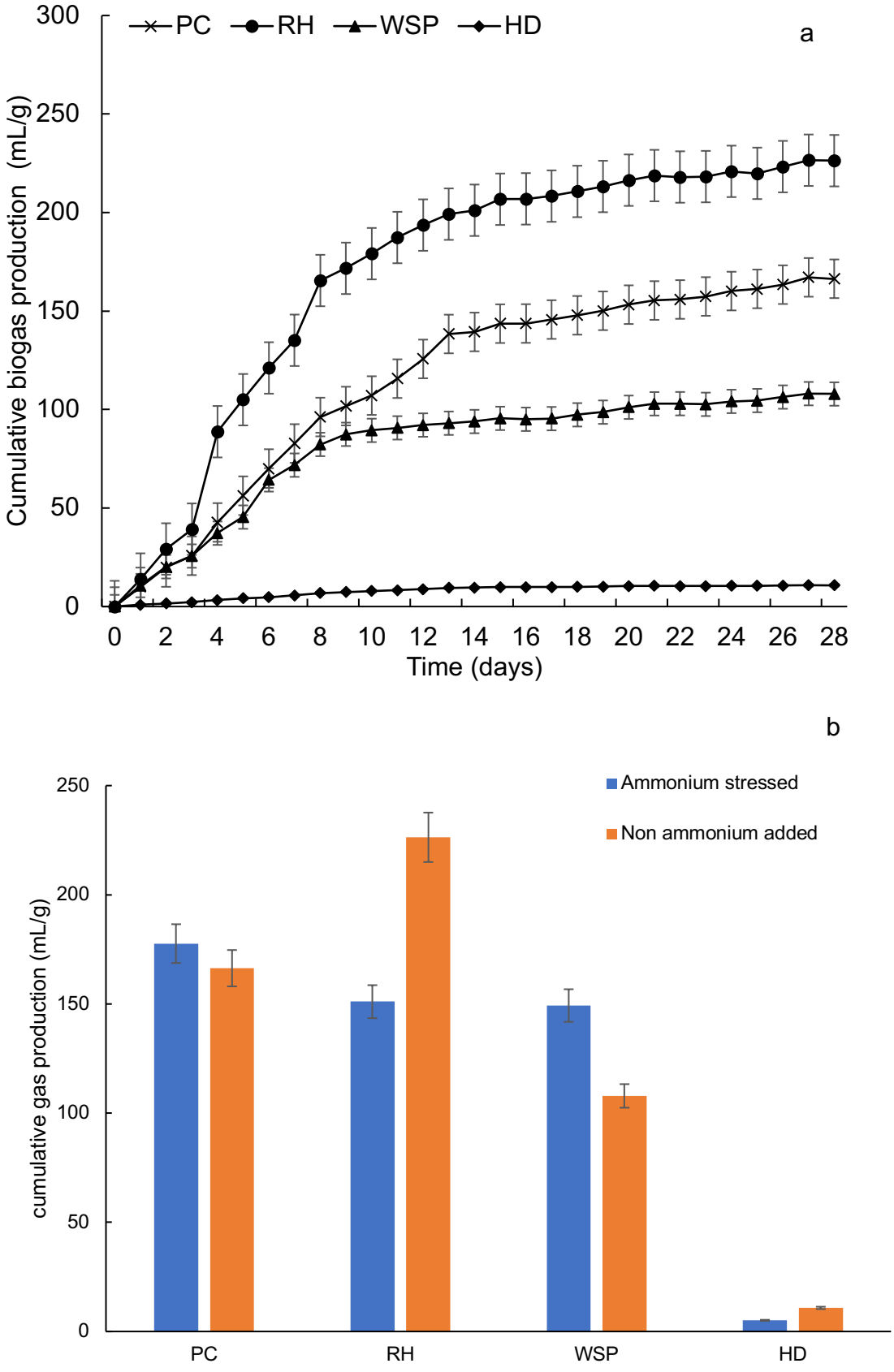

Figure 4-3. Cumulative biogas production (mL g-1VS) on (a) no ammonium stress and (b) ammonium stress of 3 g/kg.

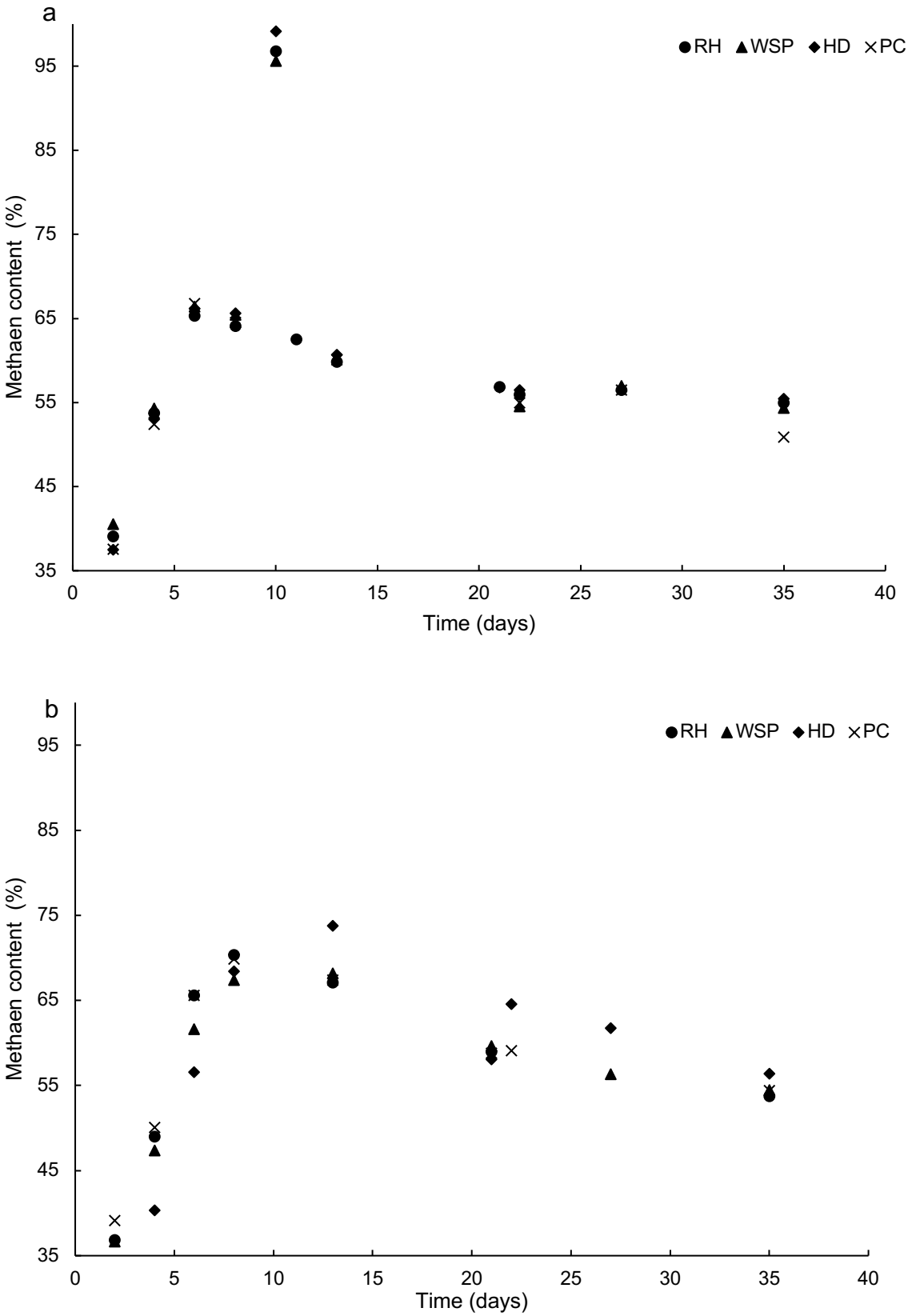

Figure 4-4. Methane content (%) in biogas under (a) no ammonium stress and (b) ammonium stress of 3 g/kg over course.

Previous tests had shown that biochar supplementation improved co-digestion of cow manure and maize silage by increasing methane content; yet, reactors were still inhibited at ammonium concentrations of 3 g kg^{-1}. As such it was unknown whether co-digestion could overcome ammonium inhibition at higher concentrations, and thus the ammonium concentration was increased for the test to 3, 4.5, and 6 g kg^{-1}. In addition, the AD potential of non-ammonia-induced reactor was conducted as positive control. Each treatment was conducted in triplicates. The digestate, cow manure and maize silage were all obtained from the same batch that was used in the 1st experiment. The methane concentration of the biogas was measured every other day from day 1 to day 10, and then monitored at day 15 and the end of the test. This AD test were designed for an internship biotechnology project undertaken by Natalie Steller who aided in monitoring of the experiment using the same reactors.

Figure 4-5 shows the cumulative biogas yield (mL g^{-1}) and methane content (%) from co-digestion of cow dung and maize silage with additions of RH, WSP, and HD biochars. Unlike in the previous study, all biochar-supplemented reactors show an enhancement in biogas production. The cumulative biogas productions in control group, biochar RH, WSP and HD reactors were 230.46, 392.48, 401.04 and 409.60 mL g^{-1} VS. Methane concentrations from the control groups and biochar-amended reactors shared similarity with an average of 62.4% and 62.13 $\pm$ 0.41%, respectively.

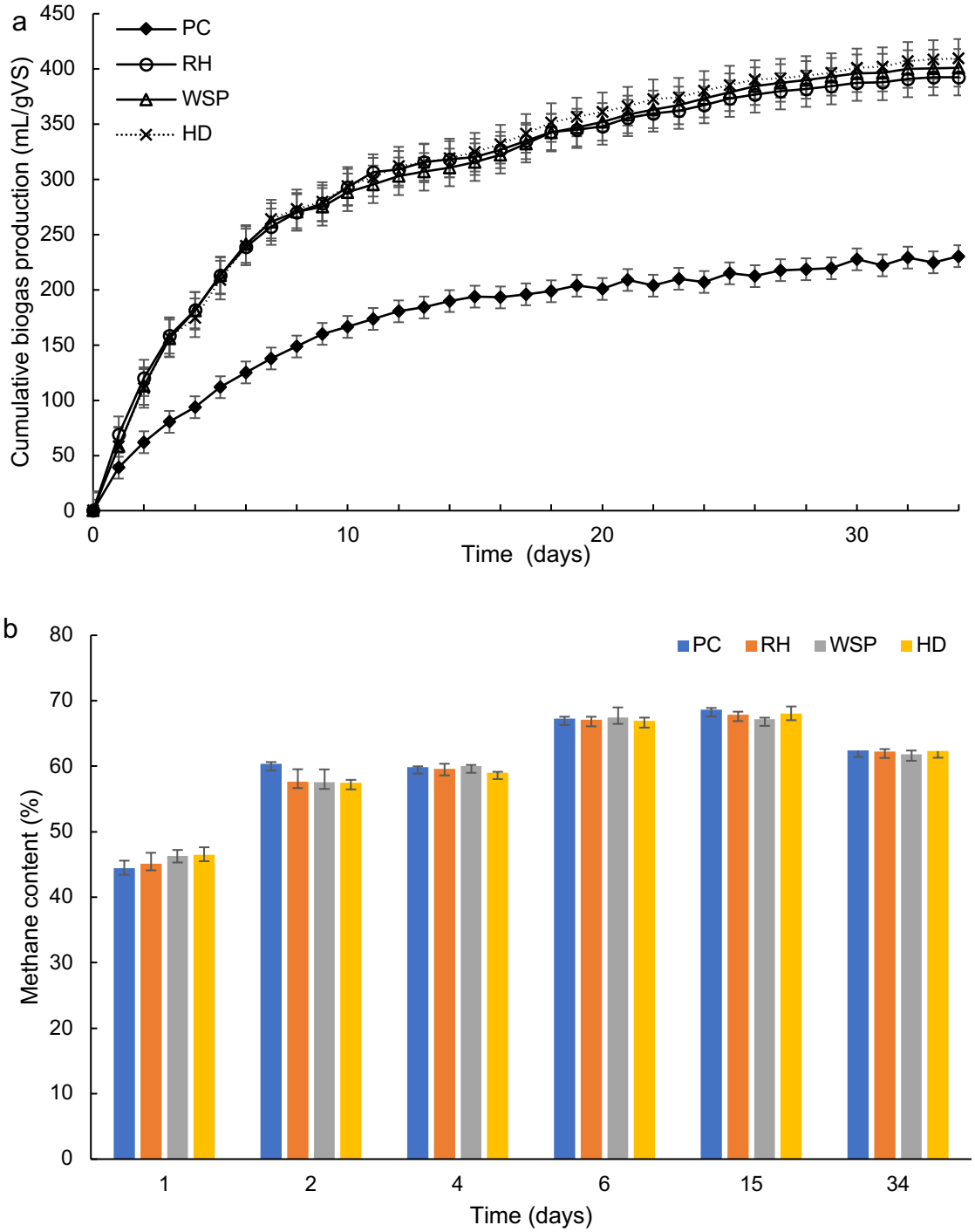

Figure 4-5. Cumulative biogas production (mL/g) (a) and methane content (%) (b) of digesters under no NH_4^+-N stress (in average and standard deviation).

Similarly to the last test, all reactors began producing biogas immediately and then began to plateau on day 18 (Figure 4-6). The increased ammonia content (3 gNH_4^+-N kg^{-1}) in the digestate led to a 54.29% increase in biogas production from control group

at the end of the test; however, biochar-supplemented reactors retained at the same level of biogas production from the previous test over 35 days. Moreover, biochar RH-supplemented reactors managed to produce slightly greater biogas production with an average value of 415.48 mL g^{-1} at the end of the test. The increased biogas production is likely due to the promoted metabolism with supplement of RH biochar with considerably higher content of bioavailable sulphur as compared to most other types of biochar (Dunnigan *et al*.,, 2018). Sulfur has proven as a predominant electron acceptor in the metabolism of glucose to acetate and carbon dioxide by reducing bacteria such as *Sporanaerobacter* on the surface of carbonous material (Dang *et al.*, 2016; Hernandez-Eugenio *et al.*, 2002). Despite the expected effect of biochar, no significant changes in cumulative biogas generation were identified in relation to biochar type. In contrast to the 1st experiment, the methane content of the biogas from these reactors was similar with an average of 61.23% from the control group and 60.27 $\pm$ 0.41% from biochar-supplemented reactors (Figure 4-6). The lower standard deviation in these reactor methane content is attributed to increased manual agitation from once per day to twice per day.

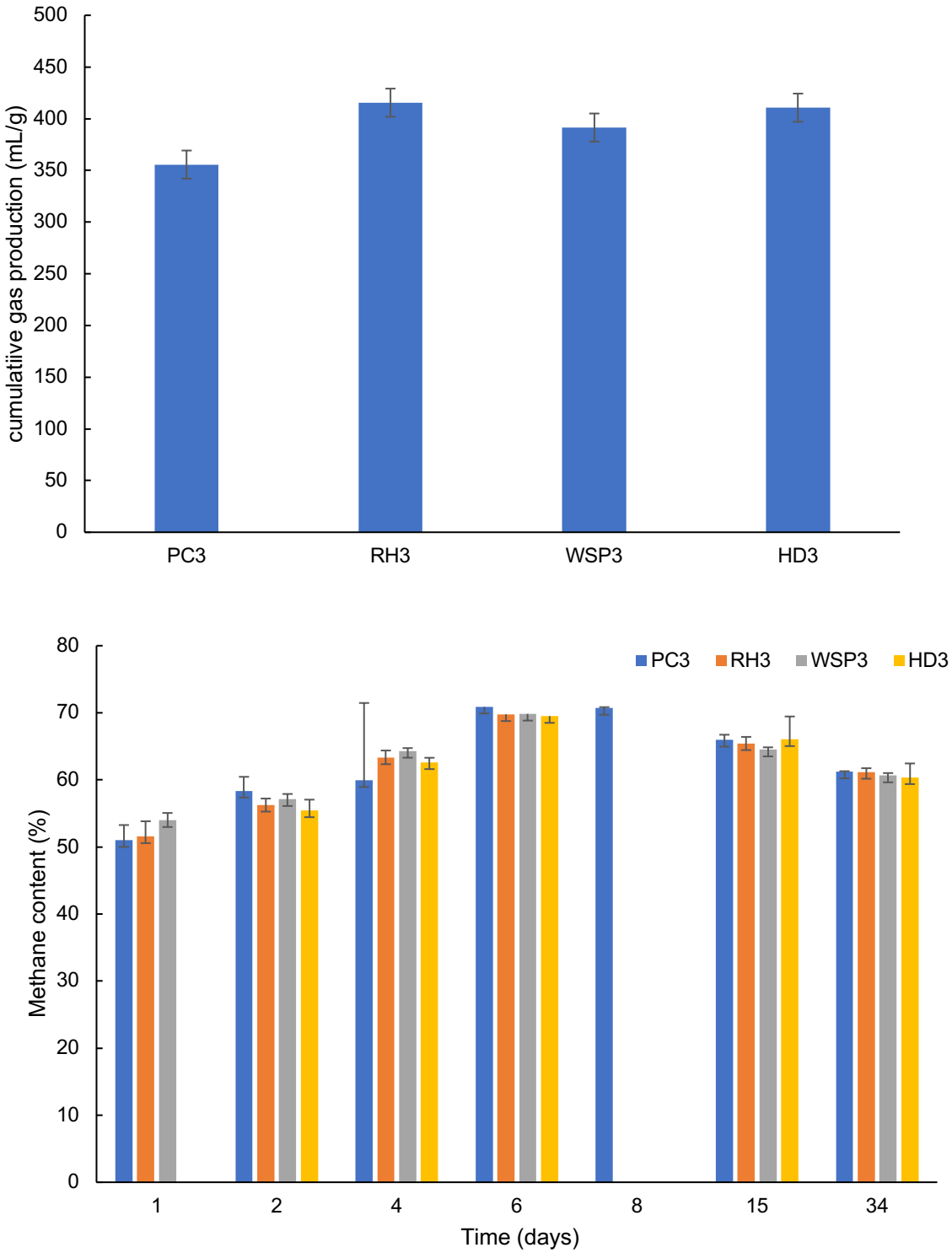

Figure 4-6. Cumulative biogas production and methane content of digesters on ammonia stress of 3 g/kg in the 2nd BMP test.

Biogas production and methane content of the reactors under ammonia concentration of 4.5 g NH_4^+-N kg^{-1} were shown in Figure 4-7. It is important to note that all biochar-

supplemented reactors were significantly inhibited. The cumulative biogas productions for these reactors were 387.14, 371.09, and 398.90 mL g^{-1}VS. Whilst the control group produced 464.14 mL g^{-1} of biogas over 35 days of AD higher than that from AD with ammonia concentration of 3 mg kg^{-1} (355.59 mL g^{-1}) and from AD without addition of ammonia bicarbonate (230.46 mL g^{-1}). The lower gas production from biochar-amended reactors implied biochar addition retained the co-AD process efficiency.

Although biochar-supplemented reactors inhibited biogas production, we saw no such impacts on methane generation in that experiment. The methane content of the biogas from these reactors was similar to previous tests. Moreover, the methane content in biogas from biochar-amended reactors was 69.88 $\pm$ 2.95%, while biogas from control group had an average methane concentration of 64.37 $\pm$ 2.06%. The increased methane content and the reduced biogas yield may be due to the conversion of CO_2 to CH_4 by aceticlastic methanogens through direct interspecies electron transfer (DIET) (Zhou, 2020). Another possibility for the enhanced methane content may be the improved ammonia tolerance by adsorbing free ammonia and ammonium ions onto biochar. Tu *et al.* (2020) reported that biochar was capable to adsorb the available ammonia and reduced ammonia toxicity by converting a little amount of ammonia to bioavailable nitrogen.

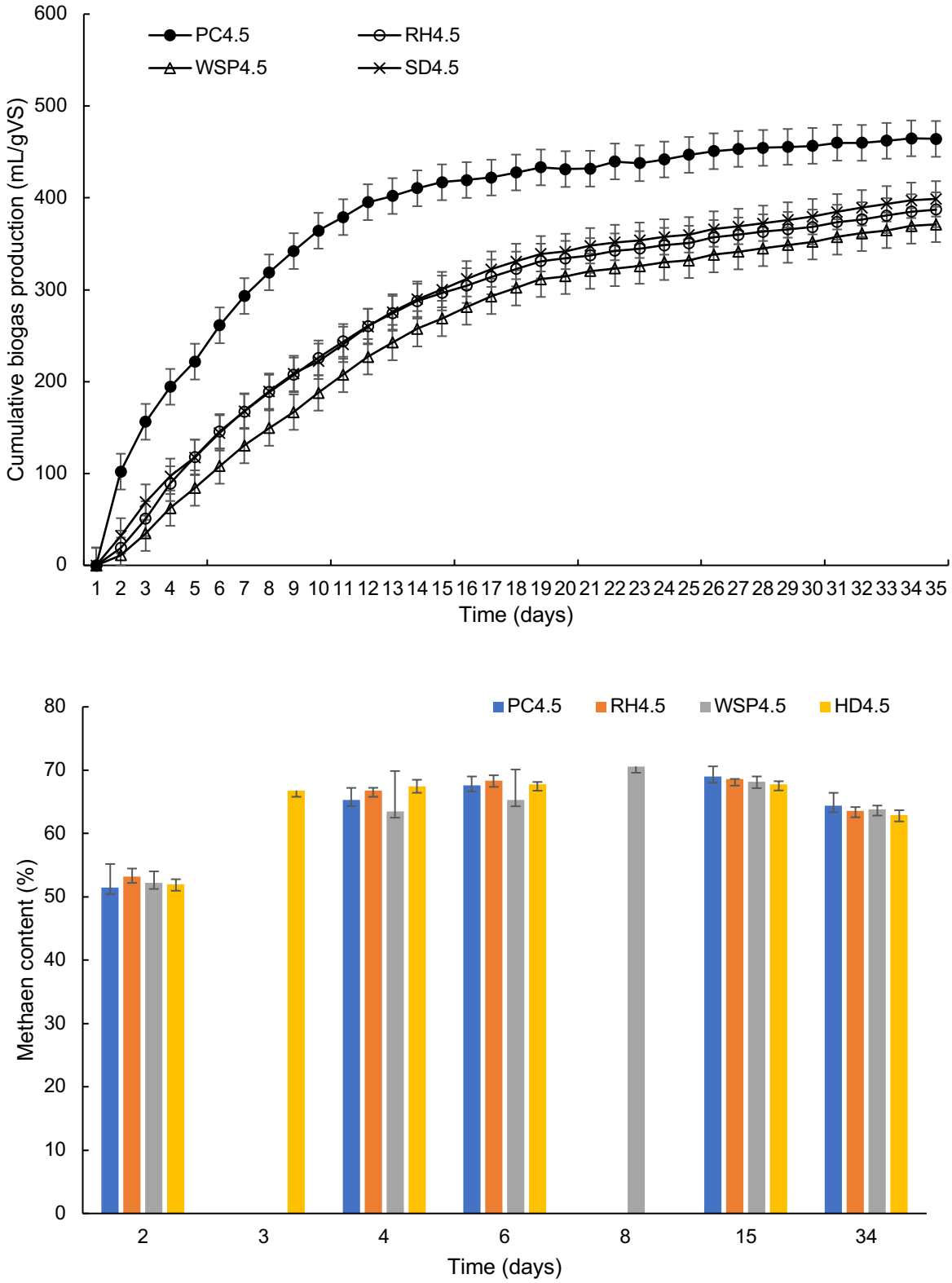

Figure 4-7. Cumulative biogas production and methane content of digesters on ammonia stress of 4.5 g/kg in the 2nd BMP test.

Figure 4-8 shows a distinct difference in biogas production between the control reactors and biochar-amended groups when the NH_4^+-N concentration increased to 6 g/kg. Unlike the last test, the controls in this test managed to increase biogas produce than the last digestate-only controls at 418.15 mL g^{-1} over 230.46 mL g^{-1}VS. Whilst as compared to the last test (4.5 g NH_4^+-N kg^{-1}), the increased level of ammonia resulted in mild inhibition and a 9.9% decrease in the biogas production from the controls. Biochar-supplemented reactors were capable of degrading increased ammonium and generating a larger amount of biogas. This was not seen in previously, as biochar WSP and HD reactors produced greater biogas, with values of 471.62 and 485.52 mL g^{-1}, respectively. Cheng *et al*. (2020) investigated anaerobic digestion of piggery wastewater with addition of biochar derived from rice straw. They found that the biogas yield was increased by 4.9-folds with addition of rice husk biochar at a dose of 15g under high ammonium stress level. The enhanced biogas production with addition of HD and WSP biochar might be due to their higher electrical conductivity with values of 26.97 and 1.7 dS/m. Biochar has been demonstrated to promote DIET between methanogenic archaea and their syntrophic partners, leading to enhanced gas generation (Barua, 2017). Luo *et al*. (2015) investigated biochar derived from fruitwood at 800^{o}C and found that Methanosarcina resided deep within the pore channel of the coarse biochar and aided in establishing methanogenic zones in anaerobic digestor. On the other hand, the addition of RH biochar had no effects on gas production compared to the control group, which is in agreement with previous studies (Chiappero, 2021). Moreover, with the increased NH_4^+-N concentration, biogas production for biochar RH-treated reactors increased by 1.08-fold (419.22 mL g^{-1}) compared to 387.14 mL g^{-1} from the last test under 4.5 g NH_4^+-N kg^{-1} at the same time point. Wang *et al.* (2022) investigated biochar derived from lignocellulosic biomass at different

temperatures and their effects on anaerobic digestion of hydrothermal liquefaction wastes. They found that a pore volume that is too large may be detrimental to digestion process. RH biochar has relatively higher pore volume of 0.057 mL/g than other used biochar which might be partially responsible for the low biogas yield.

The methane concentration of these reactors was increased with increased ammonia concentration. All of these reactors exhibited a minor suppression of methane production until day 8 (43.38 $\pm$ 6.46%) and gradually climbed back to the level of earlier tests, which subsequently managed to increase by the end of the test. Of note is that the methane concentration was considerably higher in biochar WSP and HD-treated reactors than for other treatment conditions at 71.93 $\pm$ 1.23% and 71.2 $\pm$ 0.69% over 66.5 $\pm$ 5.94% by day 35. Westerholm *et al*. (2012) found that addition of biochar in the high ammonia nitrogen system can increase the abundance of *Syntrophaceticus schinkii* by 9-fold, and increase the proportion of the *Methanothermobacter thermautotrophicus*, thereby leading to a rapid recovery of the digestion performance of ammonia inhibited system. Similar findings have also reported by Luo *et al*. (2015). Hence, these methanogenic zones might be constructed easier with supplementation of WSP and HD biochar, which have the higher surface area and greater diversity of oxygen-containing groups, resulting in a higher methane yield.

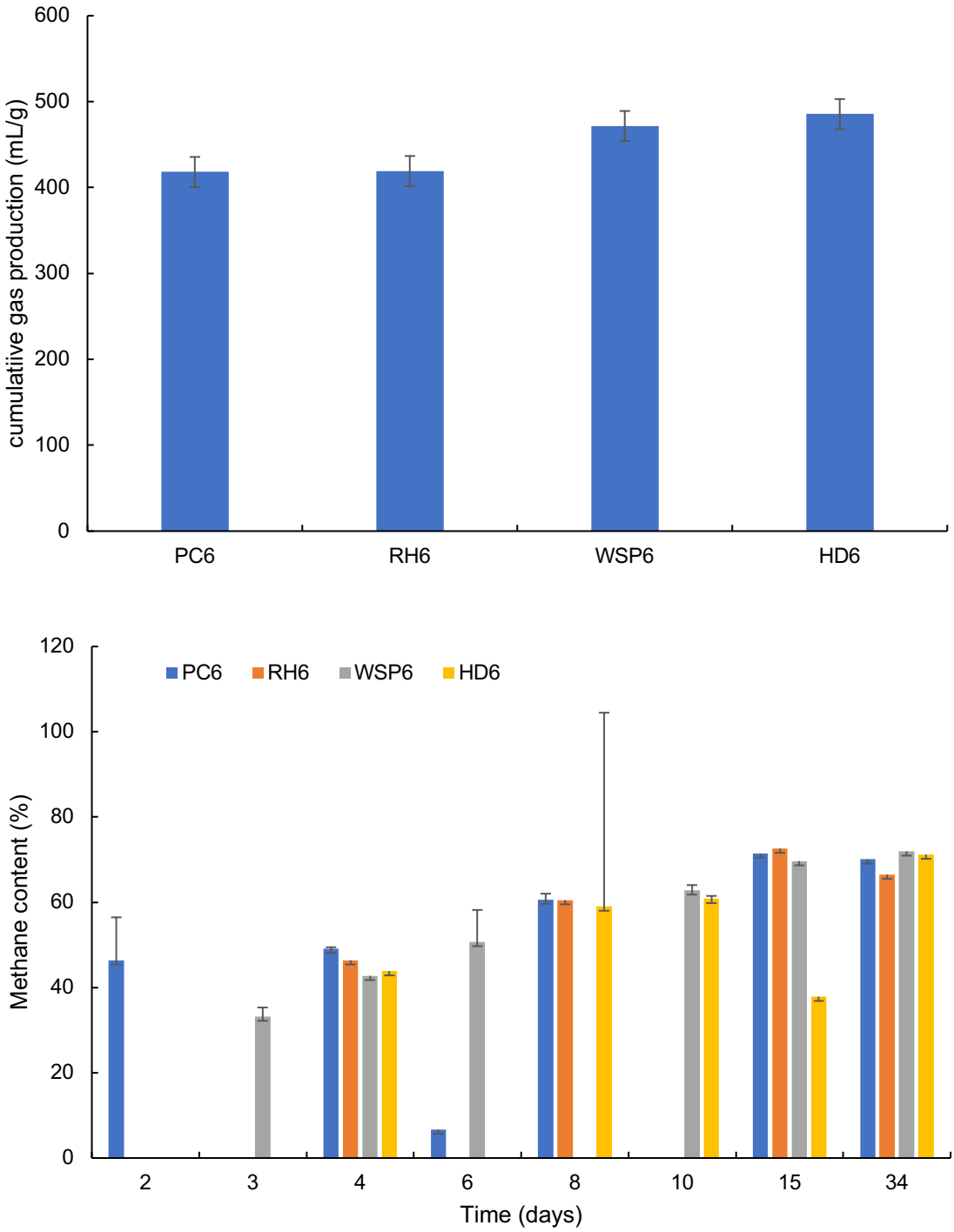

Figure 4-8. Cumulative biogas production and methane content of digesters on ammonia stress of 6 g/kg.

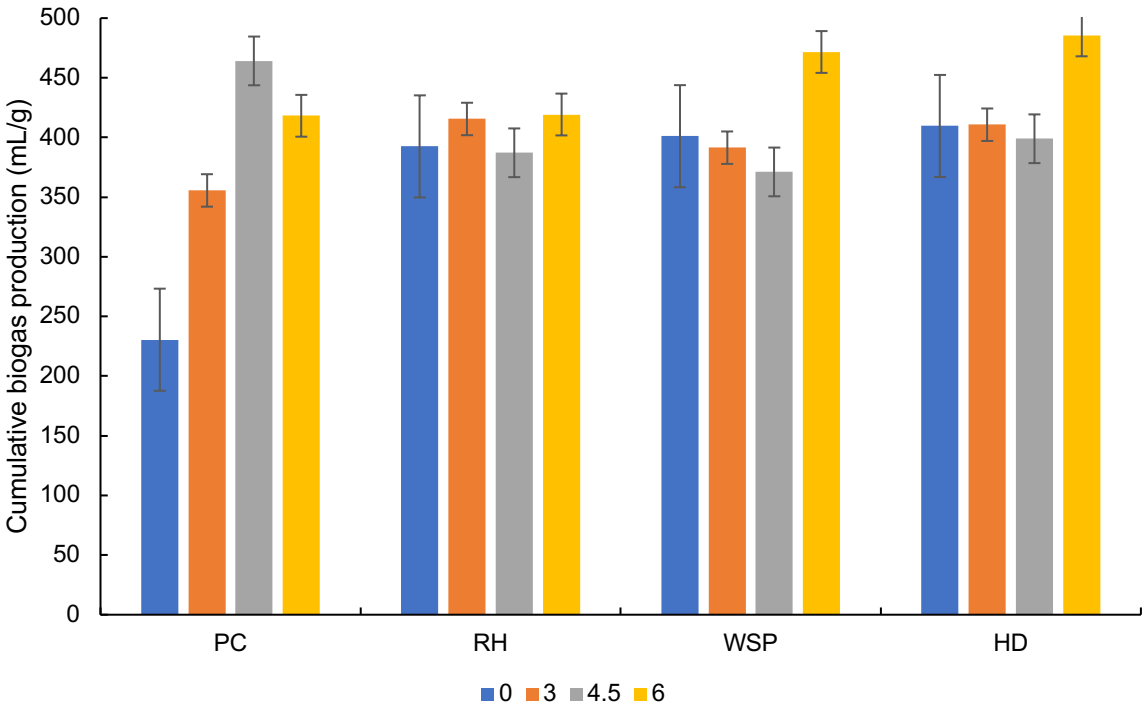

Figure 4-9. Cumulative biogas production from 2nd batch AD study. "0, 3, 4.5, 6" stands for external ammonium addition with concentrations of 0, 3.0, 4.5, 6.0 g/kg.

4.3.2.2. Semi-continuous AD tests

When compared to batch syringe reactors, it was assumed that CSTRs reflect an idealised flow reactor in that all of the microbial cultures in a CSTR are evenly suspended in the liquor, allowing for equivalent organic load in the effluent and greater inoculum substrate contact. However, it is important to note that CSTRs which cannot be used to uphold large quantity of fermenting microbes, has been shown nonlinear behaviour in literature including limit cycles and multiplicity of steady states due to biomass washout at low hydraulic retention time (Saratale et al., 2019; Show *et al*., 2019). It is expected that the use of biochar in CSTRs might improve microbial immobilisation for improved biogas generation and lower sensitivities to environmental factors such as pH shifts and other inhibitors. The experiment was conducted for 60 days in total and was divided into two stage based on the changes of NH_4^+-N concentrations. On the first day, foam was witnessed forming on the top of stirring

tube. It is estimated that foam took up more than expected working volumes inside the CSTR reactors with parts of the headspace during the gas generation process, which can be minimised by raising the gas flow rate and modifying the impeller types (Nges & Liu, 2010; Routledge *et al*., 2011). As such, the agitation speed was increased from 80 RPM to 120 RPM; however the control and reactor with supplemented of biochar WSP were continuing to form foam by day 3. It is possible that the process of defoaming naturally requires a greater period of time. These reactors stopped generating foam from day 4 and a layer of floating 'cake' (a mixture of maize silage and biochar) was spotted on top of the digestate on day 22. To improve homogeneity, the stirring speed was set to 200 rpm. The reactors were operated under batch feeding condition for 7 days to adapt and enrich the entire consortia of microorganisms. Biochar (6 %w/w) was introduced to the AD system since day 7 and substrates (a mixture of cow manure and maize) were fed to these reactors five times a week.

The biogas yields of HD, WSP and RH were 129.61, 164.16 and 115.02 mL g^{-1} by day 7 which were 42.1-102.8% higher than that of the control group (80.92 mL g^{-1}). This is consistent with the 2nd BMP experiment on no NH_4^+-N stress. The preliminary findings indicated that biochar additions could improve the efficiency of co-digestion of cow manure and maize silage. However, methane levels in the biogas produced by such reactors were below the detection limits. Similar results have been reported in previous studies (Petropoulos *et al.*, 2021). The low methane content of the biogas is attributed to accumulation of un-hydrolysed matter, which is challenging to methane production. Likewise, a similar study found that hydrolysis of substrates containing higher concentrations of protein and lipid was inhibited due to the presence of unhydrolyzed lipids (Lü, *et al*., 2007). Magdalena *et al.* (2018) also investigated the efficiency of

hydrolysis on the digestion of high protein substrate, and recorded low content of bioavailable organic matter to anaerobic microorganisms. Furthermore, manure contains a high concentration of nitrogen, which can greatly suppress methanogenesis during the digestion process (Aboudi *et al.*, 2020). Hence, this implies the importance of optimal fermentation for cow manure with addition of other carbon-rich materials.

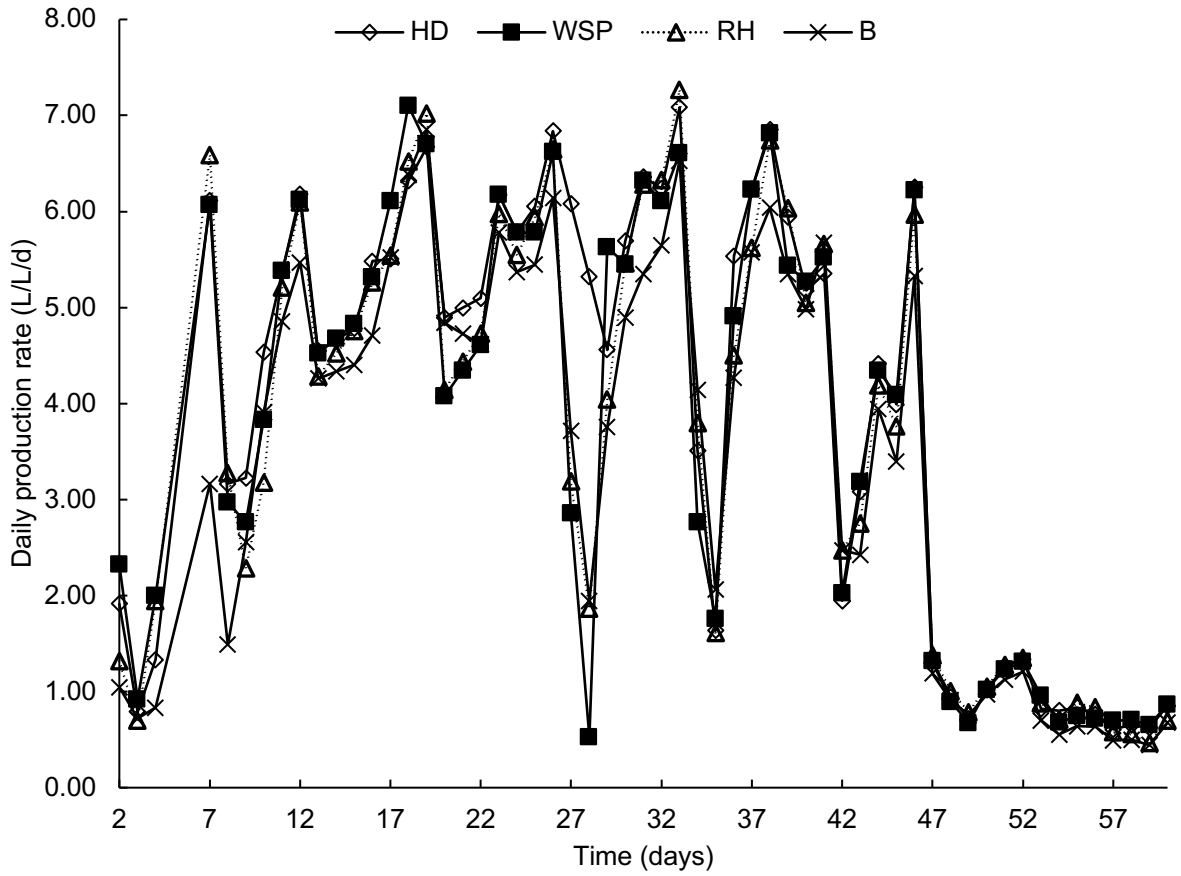

Figure 4-10. Biogas production rate of the CSTR digester over the course of experiment. 'B' = the control, 'L/L/d' = daily gas production (L)/working volume (L)/day (d).

After the initial adapting period, the CSTR reactors were continuously fed and operated for 53 days. Operational consistency in the parameters such as VFAs, ammonium and TSS/VSS was monitored once per week. To simulate ammonia inhibition, the nitrogen concentration of the inoculum was increased in steps from day 38 by introducing external ammonium carbonate ($CH_6N_2O_2 \cdot CH_5NO_3$, Carl Roth GmbH

& Co KG). The fluctuations in the volumetric biogas production rate along with the AD reactors operation time are shown in Figure 4-10.

In the first stage, biogas production rate in biochar-supplemented reactors immediately increased with the increase of stirring speed by day 7. The biogas production rate in the control was 3.16 L $L^{-1}d^{-1}$, which was lower than that for biochar-amended reactors with an average 6.26 $\pm$ 0.29 L $L^{-1}d^{-1}$ biogas production rate. Then maize silage was introduced to the system at day 8 which led to a significant reduction in biogas productivity. Also noticeable in the biogas curves is that all the reactors can be naturally recovered which requires around 5 days until increased biogas production observed. Similar patterns were found out in day 22 to 27, and these rectors recovered to produce biogas with rate of 6.56 $\pm$ 0.30 L $L^{-1}d^{-1}$ which were similar to the level of biogas production rate at day 18 with an average over 6.58 $\pm$ 0.36 L $L^{-1}d^{-1}$. Furthermore, WSP and RH biochar-supplemented reactors, as well as the control, saw a sudden drop of 56.0% biogas productivity by day 28. In contrast, HD biochar-amended reactor showed a mild inhibition by reducing biogas production by 13%. Over the course of next 5-days feeding operation, RH biochar amended reactor achieved the maximum biogas production rate (7.27 L $L^{-1}d^{-1}$) at day 33, which was considerably higher than that of the control (6.53 L $L^{-1}d^{-1}$). Although the rate of biogas production fluctuated greatly, the methane content remained consistent (around 48.6 $\pm$ 1.37%) during the first stage.

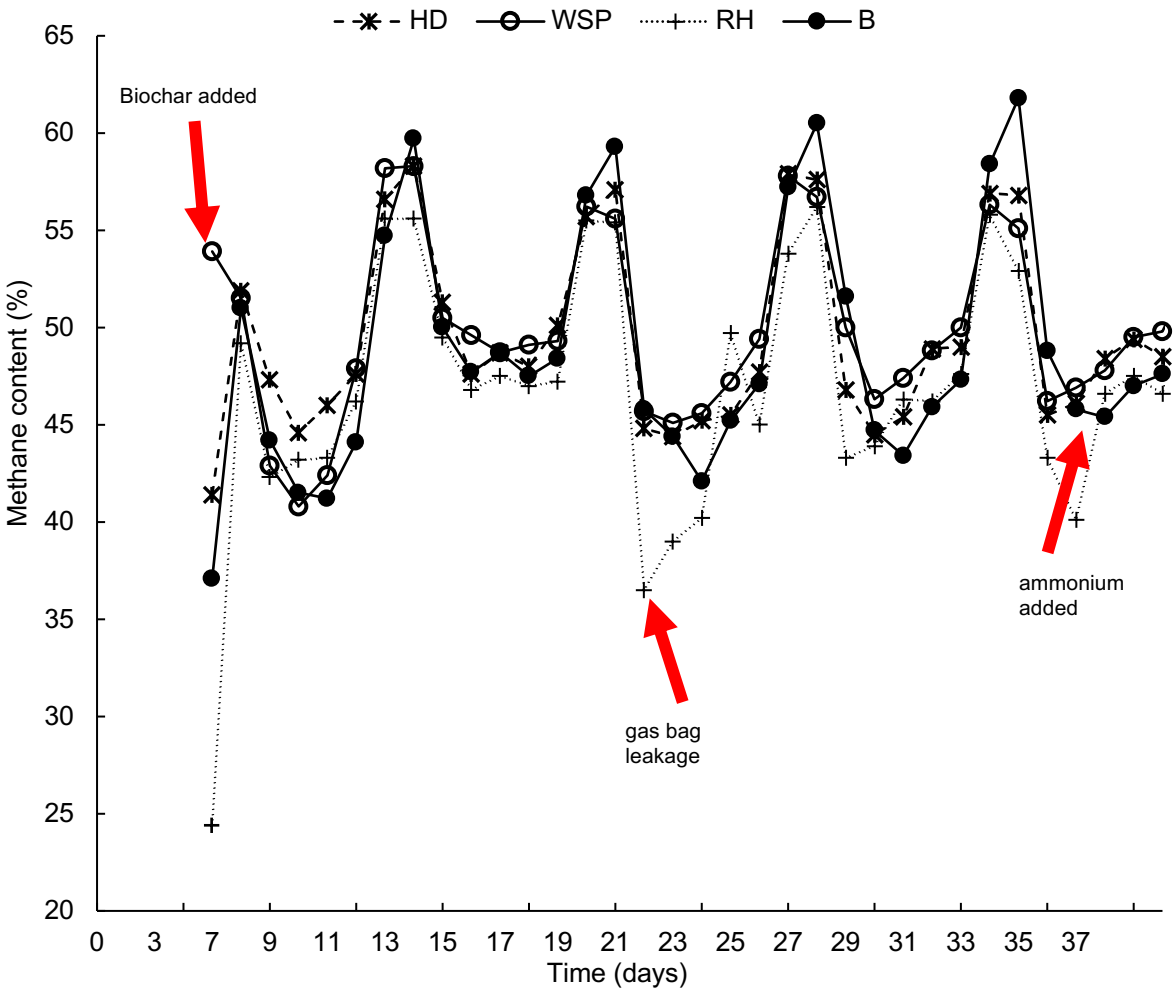

Figure 4-11. Daily methane content (%) in biogas from CSTR digesters. 'B' = the control.

In the second stage, feeding of maize silage and cow manure led to decreases in biogas production for these reactors. However, unlike the first stage, all of the reactors recovered from inhibitions in just three days. After the addition of ammonium bicarbonate, a mild inhibition was found out in all reactors and resulted in a 1.97-fold reduction in biogas production rate by day 42. The reason may be that excess FAN/TAN concentrations (150 to 1200 mg L^{-1}) is toxic to anaerobes and can suppress methane production (Chiappero *et al.*, 2020). Then, curves with an increasing trend were shown in these reactor by day 46 with a high rate of biogas production of 6.15 ± 0.16 L $L^{-1}d^{-1}$ and 5.33 L $L^{-1}d^{-1}$ for biochar-supplemented reactors and the control,

respectively. Furthermore, the addition of all tested biochars improved the ammonium tolerance by recovering 12-16.4% biogas production from day 46. Similar results were reported by Shen *et al.* (2016) that biochar derived from pinewood and white oak enhanced process stability of AD by alleviating free ammonia inhibition by up to 10.5%. It could be attributed to the improved NH_3 adsorption by biochar addition (Shen *et al.*, 2015), resulting in mitigated ammonia inhibition in favour of biogas production.

Meanwhile, both the biogas production rate and methane content decreased suddenly during the last stage when ammonia stress was continued to increase. The biogas production rates from biochar HD, WSP and RH-supplemented reactors were 0.74 $\pm$ 0.10, 0.75 $\pm$ 0.11 and 0.70 $\pm$ 0.16 L $L^{-1}d^{-1}$ respectively compared to the control at 0.58 $\pm$ 0.10 L $L^{-1}d^{-1}$ by the end of the test. The methane content in this stage was also diminished as a result of ammonia inhibition, although it remained relatively stable at around 43.4%. Accordingly, the methane content from a stable AD system using animal manure as the main feedstock was greater than 60% (Roubík *et al.*, 2018). Hence, the relatively low methane content in this stage shows that AD performance is unstable under high ammonia stress. Therefore, taking the biogas production rate and methane content into consideration, anaerobic reactor can run smoothly, or even less to ensure a stable methane content when the ammonium concentration is no more than 1.59 g NH_4^+-N kg^{-1}. An important note to make regarding the supplementation of biochar in AD reactors is that no distinct difference was exhibited influencing by biochar type during this stage. In addition, any conclusion derived as a result of no replications may be subject to a larger degree of uncertainty.

The fitting parameter of cumulative biogas data to a modified Gompertz model is shown in Table 4-2. The theoretical biogas production was 356.9, 358.9, 345.5 and 209.8 mL/g respectively for the reactors with addition of HD, WSP, RH biochar and the control group. These results were consistent with experimental results of biogas generation (R^2>0.99). Further, lag phase for biochar treatment groups (0.049-0.050 d) was considerably shorter than for the control group (0.054 d). Hence, kinetic study shows that biochar addition has the potential to promote efficiency of biogas production from co-AD of cow manure and maize silage.

Table 4-2. Fitting parameters by the modified Gompertz.

Biochar	P_0 (mL/g)	R_{max} (mL/g/d)	t_0	R^2
HD	24371	356.9	0.05004	0.9979
WSP	23907	358.9	0.04947	0.9974
RH	24118	345.5	0.0493	0.9978
B	21264	209.8	0.05404	0.9976

Methane yield and daily production rate were evaluated to investigate the effects of those biochar on AD performance. During the whole AD period (Figure 4-12), the trend of methane production is consistent with the biogas production in all treatments. Methane production rate started increasing from day 7 onwards, without significant lag, and gradually decreased until the end of the test. The maximum daily methane production was observed at day 12 which was 19.76, 19.68, 18.41 and 16.20 mL $g^{-1}d^{-1}$ for reactors with addition of HD, WSP, RH biochar and the control, respectively. Similar results were reported by Yu *et al*. (2021) observing a 13% increase in methane production with biochar supplementation at 10 g/L during AD of corn stover and chicken manure. Likewise, Cheng *et al*. (2020) reported up to a 26% increase in

biogas yield from piggery wastewater by supplementing 15 g rice straw biochar. Therefore, these observation indicated that biochar has the potential to promote methane fermentation in co-digestion of cow manure and maize silage.

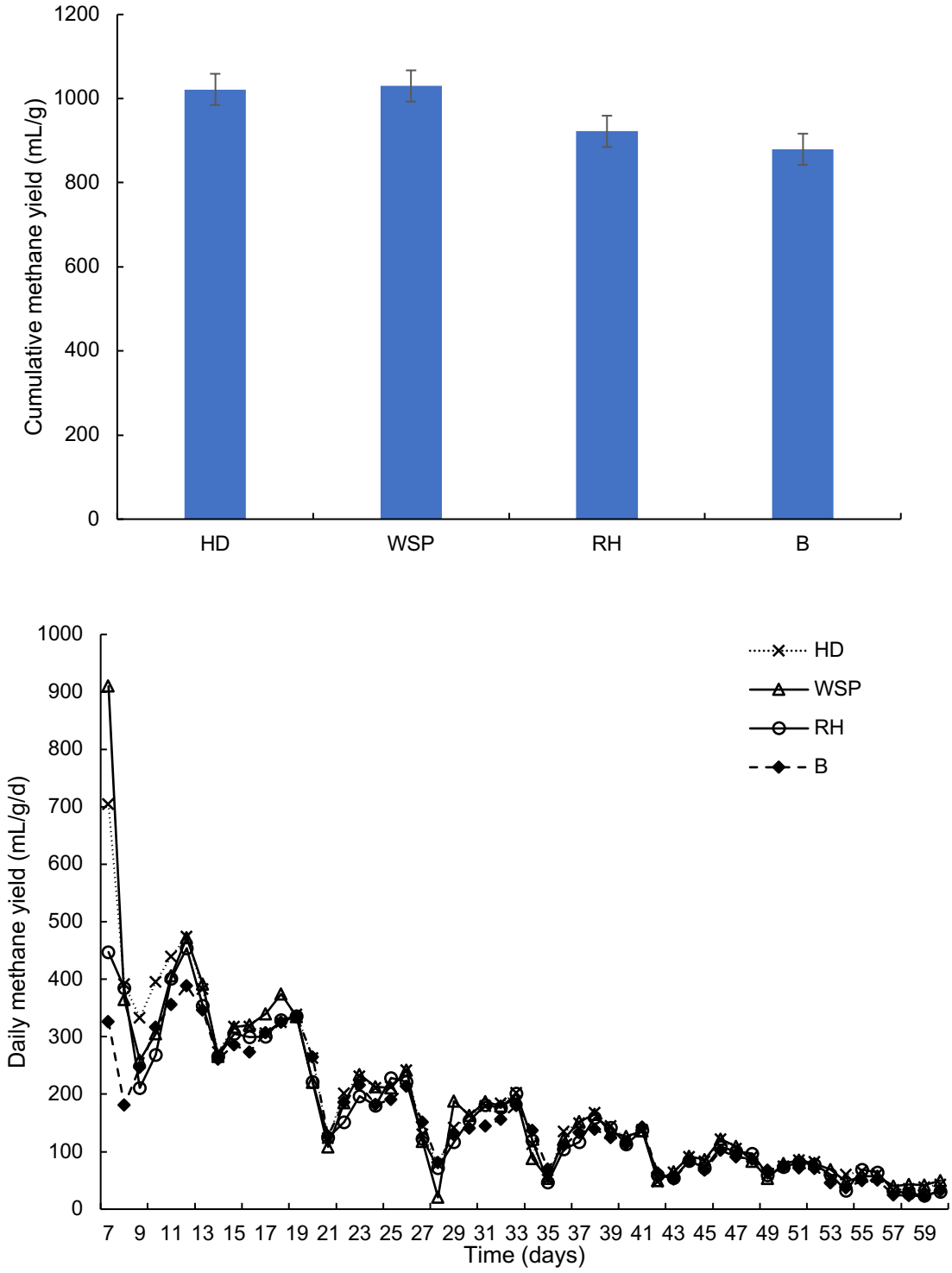

Figure 4-12. Cumulative methane yield (mL/d) and daily methane production rate (mL/g/d) of the CSTR digesters. 'B' = the control.

When ammonium concentration increased from day 38 onwards, all treatments saw a decrease in daily methane generation (54.8-71.4%). Then, the methane production recovered after 8 days and increased to 5.06, 5.08 and 4.52 mL/g/d for the HD, WSP and RH biochar amended reactor, respectively. The ultimate methane yields were 9588.84, 9495.05, 8815.29 mL g^{-1} for the reactor with addition of HD, WSP and RH biochar, which were 3-12.9% higher than for the control (8494.17 mL g^{-1}VS). The increased methane production with addition of biochar might be contributed from the unique physical and chemical characteristics of biochar. Previous studies observed that methanogens are concentrated around biochar when using ammonia as the sole source of nitrogen and CO, H_2, formate and glycol as electron donors (Luo et al., 2015; Zhao *et al.*, 2015). Therefore, the addition of biochar to the conductive AD system might improve direct interspecies electron transfer (DIET) and increase methane production.

4.3.3. Changes in intermediate contents during co-digestion process

To investigate the AD performance of co-digestion on different ammonia stresses, changes in the effluent pH, TSS, and TAN concentrations were analysed over the course of the experiment. The pH of AD reactor is an important parameter for monitoring the stability of AD process, and influencing the activity of methanogens and metabolic pathways (Li *et al.*, 2018; Zhang *et al.*, 2019). It can be affected by the following factors: formation of ammonium carbonate, the removal of CO_2, and the removal of fatty acids (Möller & Müller, 2012). Figure 4-13 shows pH changes in the digestate from the CSTRs reactors. The initial pH in these reactors stayed constant at 7.7 ± 0.1, while the addition of cow manure has a significant influence on the pH of the control from day 7 to 15, leading to a 13.9% increment. The reactors with

supplementation of all biochars had similar pH and maintained stably. The pH of these reactors varied from 7.44 to 7.65 by day 14. This is mostly due to the alkali and alkaline earth metals released from biochar during AD, which can generate an HCO_3^-/CO_3^{2-} buffer via CO_2 consumption (Lehmann *et al.*, 2011; Zhang *et al.*, 2019). On the other hand, pH of the control group increased from 7.81 to 8.69, which might be due to ammonification of protein produced by the addition of cow manure (Zhang *et al.*, 2016), resulted in low biomethane production rate. Until day 37, pHs in all groups ranged in a slightly alkaline range close to the literature level (Zhang *et al.*, 2019). Then pHs of these reactors gradually increased to 7.65 from day 38 to 46 due to the increasing concentrations of ammonium carbonate. Furthermore, the pHs rose rapidly on day 56 and then settled to a plateau by the end of the test. In the last stage, we did not see significant impacts of biochar on altering the pH variation under high level of ammonia stress. Nevertheless, it can be seen that biochar-treated reactors show a mild buffering capacity compared to the control.

It was assumed that external ammonium addition might aggravate ammonia inhibition in the form of higher pH and decreased methane production (Shen et al., 2015). These experimental results, however, revealed that pH variation was positively correlated to biochar addition, showing that biochar can improve buffering capacity during AD. In addition, the improved buffering capacity can be attributed to the accelerated carbonation reaction, which is dependent on the syntrophic metabolism between organic acid-oxidizing acetogenic bacteria and CO_2-reducing methanogenic archaea (Stams & Plugge, 2009). It should be noted that this reaction also relies on the efficiency of interspecies electron transfer, which can be stimulated by the addition of electrically-conductive materials such as activated carbon and biochar (Viggi *et al.*,

2014; Zhao *et al.*, 2016). Therefore, further research is required to elucidate the role of biochar on electron transfer mechanism in the co-digestion of cow manure and agricultural residue.

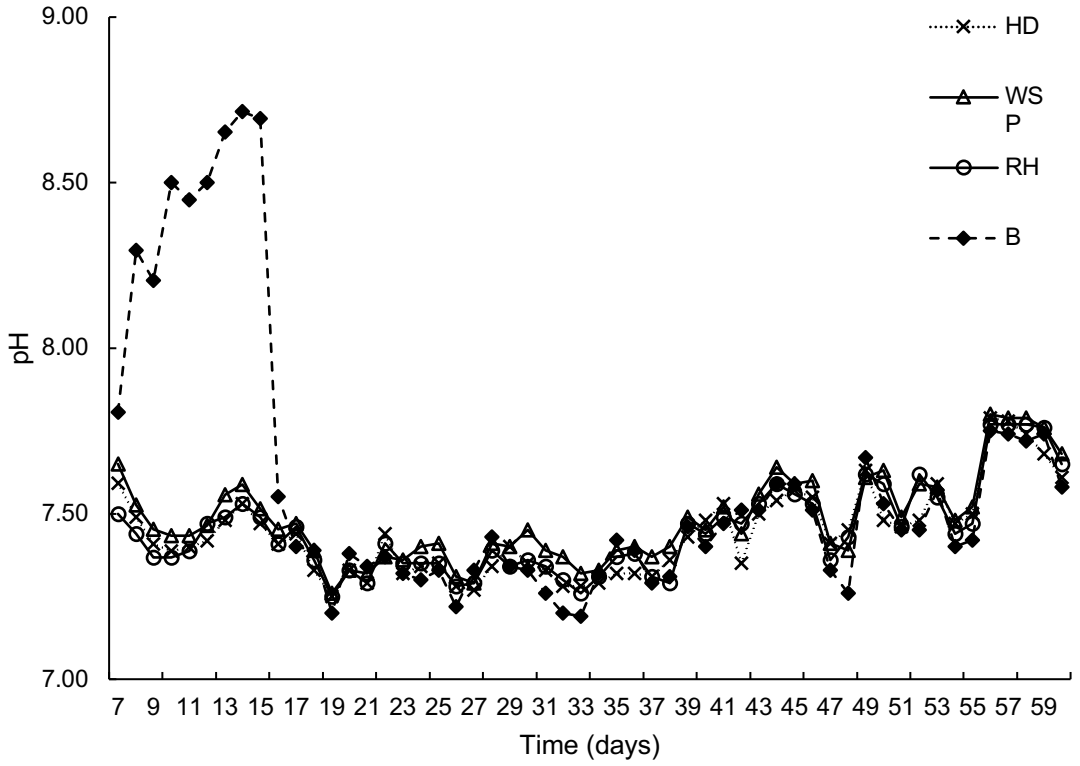

Figure 4-13. The changes in pH of the digesters over the course of experiment.

4.3.3.1. Changes in concentrations of volatile fatty acids (VFAs)

VFAs are another major factors affecting AD process stability and methane generation. Monitoring changes in VFA concentration is crucial to signal the metabolic status during AD (Lu *et al.*, 2017). Figure 4-14 shows weekly changes in VFAs for these reactors. The concentration of acetic acid from biochar-supplemented reactors and the control at day 9 were an average 1.25 $\pm$ 0.08 g L^{-1} and 1.38 g L^{-1}, respectively. Then, the concentration of acetic acid from all the digesters decreased by 60% by day 16. All reactors continued the decreasing trend that the concentrations of acetic acid from reactors with supplementation of biochar HD, WSP and RH were reduced by

57%, 53.8% and 55.3%, higher than that of the control (31.5%) from day 16 to day 23. The addition of HD biochar resulted in a slightly decrease in acetic acid concentration by 2.8% from day 30 to 38, whereas increased acetic acid concentrations were observed from other treatment groups with an average of 27.9±0.14%. It implied a considerably better degradation in HD biochar-amended digester, might result in a higher methane production at that stage. After the introduction of additional ammonium carbonate at day 38, methane production from these reactors started dropping by 54.8-71.4%, displaying complete inhibition of methane production. On the other hand, acetate contents for all digesters increased by 44.4-67%, subsequently led to a significant fluctuation in the digestate pH. This finding is in line with the results of Zhang *et al*. (2019) reported a reduction of acetate in the range of 80.62-86.98% in the digestion of municipal wastewater with supplement of corn straw biochar. Over the course of these two stages, the concentration of acetic acid from reactors with supplementation of biochars were average 0.69 ± 0.36 g L^{-1}, which was considerably lower than that of the control group (0.93 ± 0.38 g L^{-1}). It implies that biochar supplementation has the potential to improve acetate degradation during co-AD and promote rapid utilization of acetate to biogas.

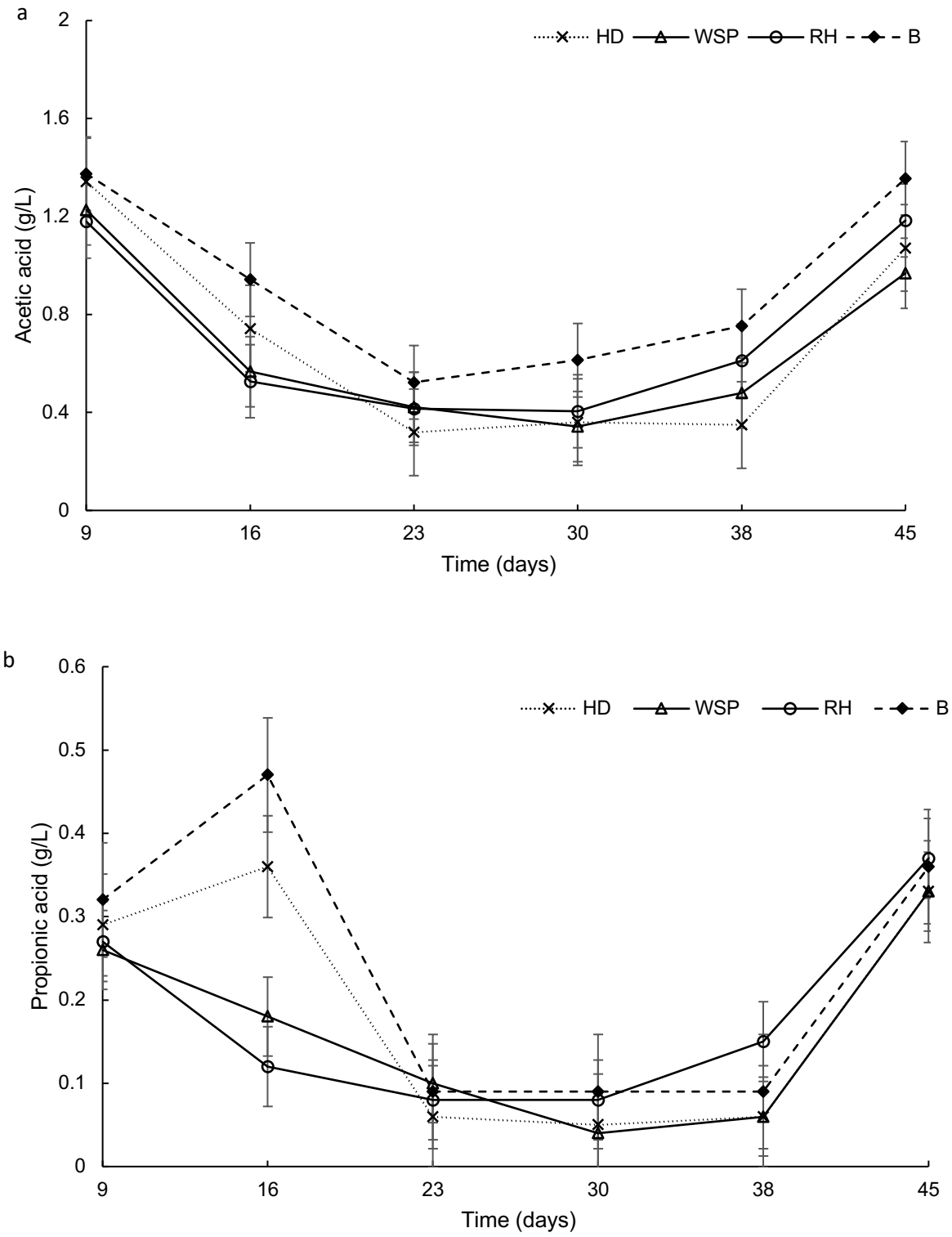

Figure 4-14. Variations in the VFAs concentrations (a) acetic acid and (b) propionic acid.

Propionic acid is also an important intermediate for methanogenesis. When excess propionate accumulates in the digesters, the conversion of propionate to acetate and hydrogen becomes thermodynamically unfavourable, affecting syntrophic metabolism

(Dang *et al.*, 2017; Zhang *et al.*, 2019). Changes in the concentration of propionic acid of the aqueous phase of the digestate are shown in Figure 4-14 for the control and biochar-supplemented reactors. The initial concentration of propionic acid from these reactors were similar with an average of 0.29 $\pm$ 0.03 g L^{-1} by day 9. The concentration of propionic acid for the control rose by 46.95% by day 16. We saw a similar pattern in HD biochar treatment group with a little increase of 24.1 %. These values from these digesters followed by a sharp decline of 82.1 $\pm$ 0.02 % by day 23. In addition, the average propionate concentration of the control during the AD process was 0.237 g/L, which was still 19-31.7% higher than that of all biochar amended reactors. In RH and WSP-supplemented reactors, the propionic acid concentration was gradually reduced by 44.4 and 76.9% with an increasing trend in biomethane production between day 9 and day 30, indicating an improved degradation of propionate with the addition of biochar. Furthermore, reactor with supplementation of biochar HD maintained at a concentration of 0.06 $\pm$ 0.01 g L^{-1} propionic acid for 15 days until day 38. Whereas RH and WSP-supplemented conditions, propionic acid concentrations showed an increase of 87.5% and 50% from day 30 to day 38. After the ammonia concentration lifted, a sharp increase in propionic acid concentration was observed for all the reactors with an average of 0.34 $\pm$ 0.02 g L^{-1} similar to the control of 0.36 g L^{-1}, suggesting a strong inhibition in the AD system.

Throughout the experiment, we saw an improvement in degradation of propionic acid in reactors with supplementation of biochars. Likewise, Luo *et al*.(2015) reported 11.4 to 30.3% enhancement in methanogenic log with a faster degradation of propionate for AD of pulp sludge with supplementation of fruitwood biochar. In contrast, a recent study reported that total VFAs concentration of digestate was maintained at a relatively

low level (4.92-7.10 g L^{-1}) during digestion of piggery wastewater with addition of rice straw biochar at 2-10 g L^{-1} (Cheng *et al.*, 2020). The improved degradation of VFAs with addition of biochar can be attributed to the electron-donating and electron-accepting capacity of biochar, resulting in the faster metabolism of propionate via biochar-mediated direct interspecies electron transfer (DIET) between propionate/acetate oxidation bacteria (Zhao *et al.*, 2016; Zhang *et al.*, 2019). As a result, employing biochar in co-AD enhanced methanogenic activity and syntrophic pathways. It is important to note that biochar types had no significant effect on the amount of VFAs degraded, however biochar-treated reactors showed a potential to change the degradation rate and attain a stable condition when compared to the control.

4.3.3.2. Changes in ammonium concentrations

Ammonia inhibition is seen as the primary reason of reduced methanogenesis and system failure during the high-solid AD process (>3 % TSS) (Chiappero *et al.*, 2020). The concentration of ammonia is proportional to the ammonium concentration, pH value, and temperature. An optimal ammonium concentration might ensure AD stability and methanogenic activity by neutralizing the organic acids and providing methanogens nitrogen source (Rajagopal *et al.*, 2013; Jiang *et al.*, 2019; Yu *et al.*, 2021). However, excess ammonia concentration (>4.2 g/L) has the potential to cease biogas production due to hydrophobic ammonia's ability to passively cross the cell membrane and provoke proton imbalance (Rajagopal *et al.*, 2013; Li *et al.*, 2018; Jahn *et al.*, 2020).

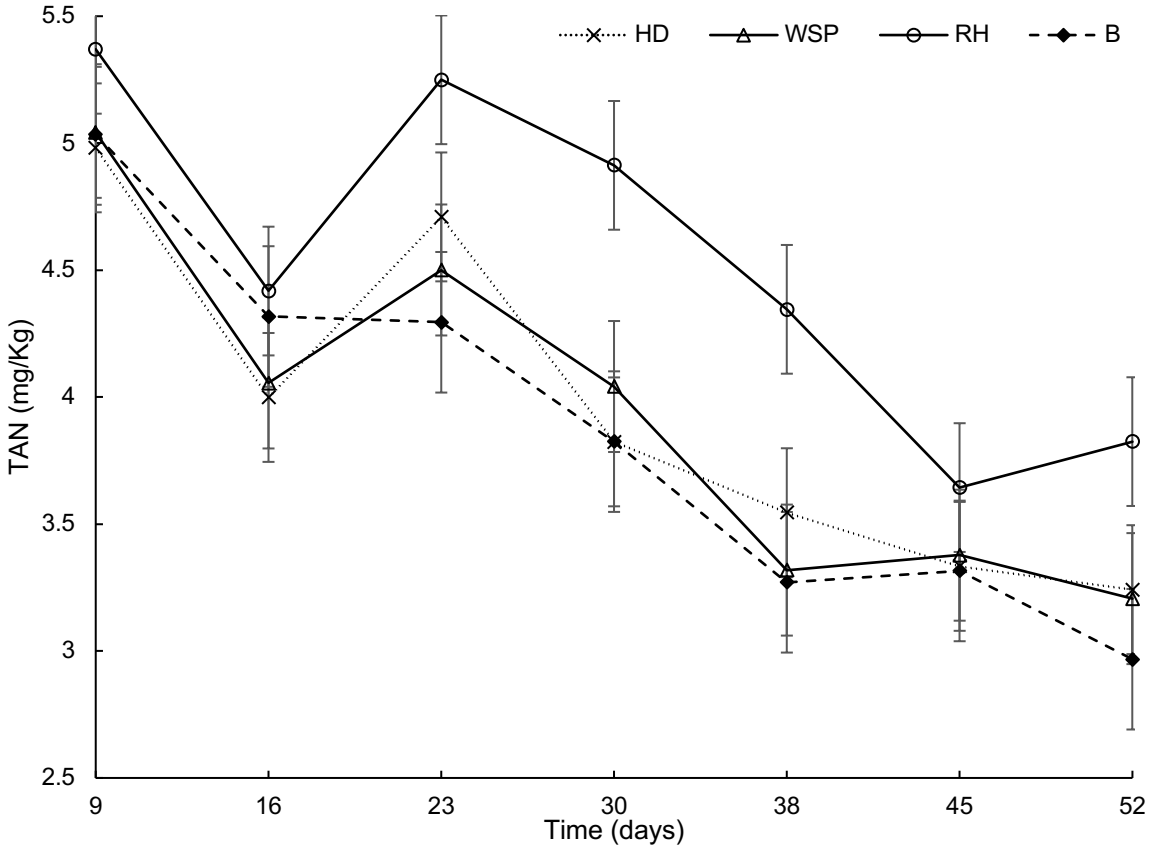

Figure 4-15. TAN concentrations of the CSTR digesters over the course of experiment.

Figure 4-15 shows changes in the TAN concentration of the digestate for these reactors, and immediately noticeable is that the ammonia concentration in all reactors present a decrease of an average 17.8 $\pm$ 0.03% by day 16. Of note is that biochar RH-supplemented reactors had ammonia concentration with value of 5.37 g L^{-1} by day 9 compared to 5.04 g L^{-1} for biochar WSP-treated reactor, 4.98 g L^{-1} for reactor with supplementation of biochar HD and 5.03 g L^{-1} for the control by the same time point. The shape of the curves for biochar-treated reactors differs noticeably, with an increase of 15.9 $\pm$ 0.04% in TAN concentration by day 23. This was not seen in the control, as the curve retained at the same level with ammonia concentration of 4.29 g L^{-1} by day 23. Biochar RH-treated reactor had a greater ammonia concentration (4.35 g L^{-1}) than the other treatment conditions, presenting a 17.2% decrement in TAN

concentration. WSP and HD biochar supplemented reactors reduced concentrations of their TAN with a 25.5 $\pm$ 0.01% reduction to a value similar to that of the control (23.8%). Under high ammonia stress from day 38, biochar RH-treated reactor's TAN were continued to reduce by 16.2%. Similar pattern was also shown in reduced TAN concentration (by 5.96%) of biochar HD-supplemented reactor. On the other hand, the control and biochar WSP-treated reactor showed a little increase by 1.77% and 1.37%, respectively at the same time point. Then, a reduction was observed in TAN concentration of the WSP and HD-supplemented reactors (a decrease in TAN concentration of an average 3.90 $\pm$ 0.02%) compared to the control with a reduction of 10.5%. In contrast, the addition of biochar RH causes a 4.97% increase in the TAN concentration of the digestate in reactor by the end of the experiment.

The absolute TKN content is an index for the amount of nitrogen that is present as both organic nitrogen and TAN. Changes in the TKN concentration of the reactors were also monitored over the course of the experiment, showing in Figure 4-16. The initial TKN concentration of biochar-treated reactor was an average of 7.71 $\pm$ 0.2 g L^{-1} to a similar value of the control (7.85 g L^{-1}). The presence of biochar RH had a positive impact on the TKN removal in the reactor, resulted in a reduction of 4.35%. The same finding was reported by Sánchez *et al*. (2021) that investigated mesophilic semi-continuous anaerobic digestion of swine manure with supplementation of biochar derived from wheat straw and corn straw at 500^{o}C, and found a 13% decrease in TKN concentration in the reactors with biochar addition. Whilst, WSP and HD biochar-treated reactors saw little increase in TKN concentration (0.76% and 2.0% increase, respectively). These trends are mirrored by the change observed in TAN concentrations under the same conditions. Furthermore, fluctuations of TKN

concentration for biochar WSP and HD-supplemented digesters between day 23 to day 38 are likely due to the altered nitrification transition by the addition of biochar (Taghizadeh-Toosi *et al.*, 2012). The other treatment conditions, on the other hand, were able to return to the baseline TKN concentration by day 52. The addition of biochar RH improved the TKN removal by 1.06%, led to a higher production of biogas at the same time point (~day 46).

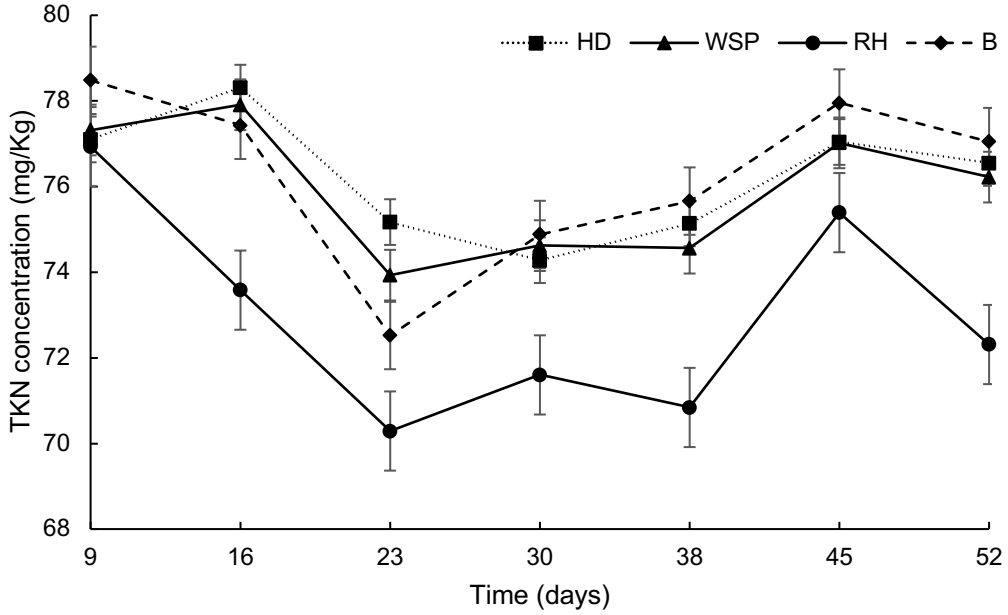

Figure 4-16. TKN concentrations of the CSTR digesters over the course of experiment.

Furthermore, the average ammonium concentration (3.9-4.5 mg NH_4^+-N kg^{-1}) in all of the treatment with biochar was slightly higher than that of the control group (3.82 mg NH_4^+-N Kg^{-1}) . The highest mean ammonium concentration (4.5 mg NH_4^+-N kg^{-1}) was observed in the treatment with supplementation of RH biochar. Biochar supplemented digesters increased cumulative methane production significantly under higher ammonium concentration conditions. These difference could be explained by an enhanced disintegration of inoculum and the consequent availability of more biodegradable organic compounds with biochar addition (Jahn *et al.*, 2020). These

observations were in line with the study of Jiang *et al*. (2019) that revealed a stable digestion of cattle manure at up to 6 g/L of ammonia concentration after 6 months of operation. Similarly, Yu *et al*. (2021) recorded an enhanced AD process by improving the degradation of lignocellulose biomass using corn stover biochar under high ammonium concentration. Meanwhile, previous studies suggested that biochar addition was negatively correlated to ammonia, but mitigated ammonia inhibition by promoting ammonia inhibition on the surface of biochar (Shen *et al*., 2015; Taghizadeh-Toosi *et al*., 2012). Furthermore, biochar can be used to adsorb the available ammonia and reduce its toxicity by converting few ammonia to bioavailable nitrogen (Tu *et al.*, 2020). Because of the limited ability of adsorbing ammonium ion on increasing ammonia stress in the second stage, it is important to consider that the alleviation of ammonia inhibition in the first stage by biochars is likely dependent on biochemical rather than physiochemical causes.

Meanwhile, the available research related to the ability of biochar to reduce the toxicity of ammonia inhibition on an AD digester is still to a high degree of uncertainty. Cai *et al.* (2016) suggested that the addition of biochar did not affect the degradation of proteins nor adsorb significant amounts of ammonium due to the similar nitrogen level between biochar-treated reactor and the control. In contrast, a study showed that biochar with higher adsorption capacities is based on the physiochemical reasons, and the use of biochar under high ammonia stress can enrich methanogens (Lü *et al*., 2016). Additionally, our study found out that with increased ammonia concentration (6 g kg^{-1}), the addition of biochar resulted in an apparent increase in methane production and biogas productivity from co-digestion in the BMP test. Therefore, it can be expected that the ability of biochar in increasing the methane production in the

anaerobic digestion of nitrogen-rich feedstock are not solely based on its adsorption capacity, whereas biochars could stabilize the ammonium level under higher ammonia stress.

4.3.3.3. Organic removal efficiency

Take the consideration of converting the organic parts of biowastes into biogas, it is important to determine the removal efficiency of organic wastes. It has also been considered as the main indicator for evaluating the AD performance. As such, the AD efficiency in this study was examined by the TSS and VSS removal efficiencies (Figure 4-17). A 19.1 $\pm$ 0.01% increment in the TSS removal efficiency in biochar-amended digester was observed, which was higher than that of the control group (a 12.73% reduction). Then, all the reactors exhibited gradually decreases in TSS content, with an average of 3.39 $\pm$ 0.16 TSS (% FM) at day 45. Among them, bioreactors with addition of RH biochar has great TSS removal efficiency by reducing 40.15 $\pm$ 0.05%. Our findings are in agreement with study by Sánchez *et al.* (2021) that an average TSS removal efficiency was 47.7$\pm$6.7% in the semi-continuous anaerobic co-digestion at a organic loading rate of 3 g/L. Martinez *et al.* (2018) also found that the use of biochar (30 g/L) derived from vineyard purnings in co-digestion of sewage sludge and orange peels resulted in 62-67% removal efficiency.

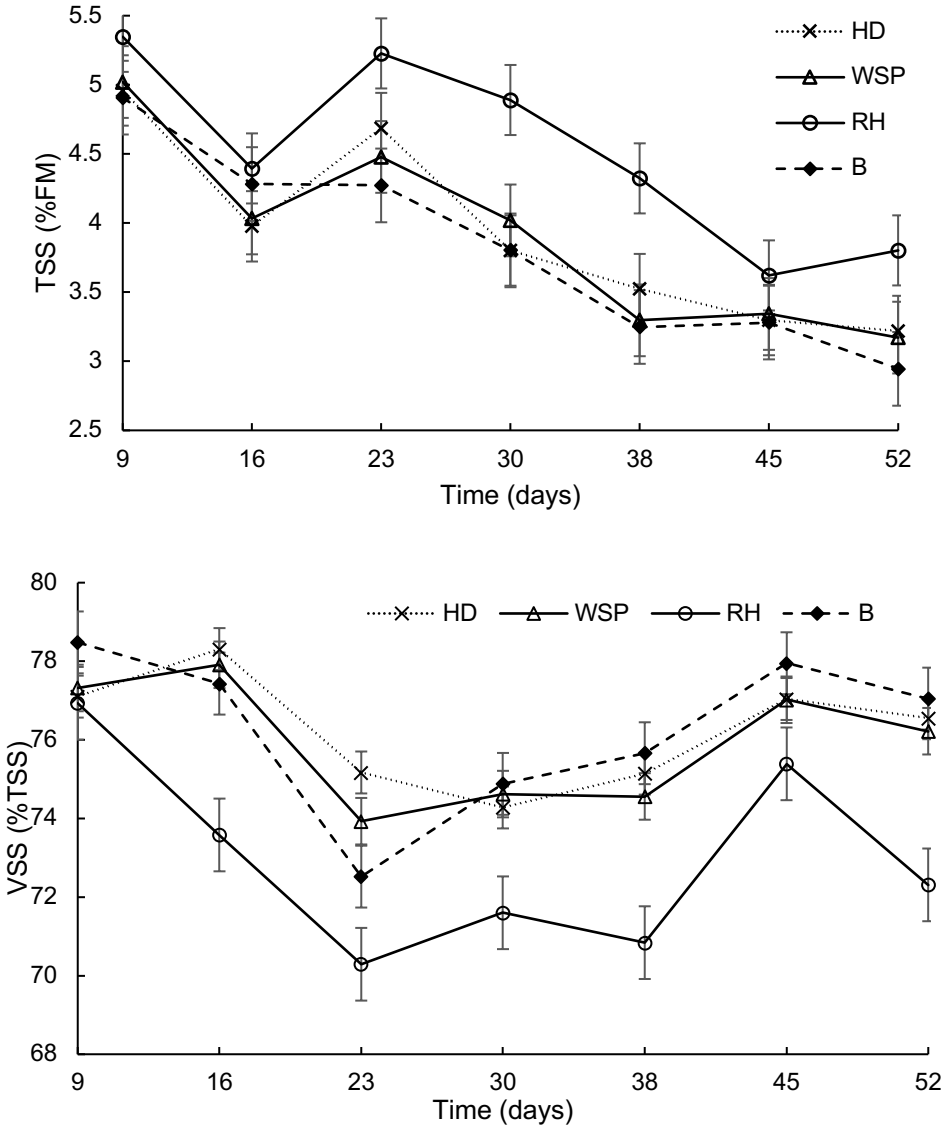

Figure 4-17. Changes in TSS and VSS content of digestate of the CSTRs reactors.

Figure 4-17 shows changes in the VSS content across all the reactors. The addition of RH biochar enhanced VSS removal efficiency by 8.63% by day 23, implying that RH biochar can stimulate organic removal efficiency at a lower range of TAN concentration and facilitate the transformation of free ammonia to bio-available ammonia (Martinez, 2018; Sánchez, 2021). Meanwhile, biochar RH-treated reactor showed a lower level of VSS content at 70.91 $\pm$ 0.66 VSS (%TSS) than that of other biochars with an average 74.85 $\pm$ 0.41 VSS (%TSS). Wambugu *et al*. (2019) suggests

that the presence of trace elements such as Fe, Co, Ni and Mn (in quantities less than 10 mg/kg) in biochar can stimulate the anaerobic process by enhancing degradation efficiency. These elements are essential for methanogenesis, involving the action of acetyl-CoA synthase and methyl coenzyme reductase to catalyse crucial metabolic steps. Another possibility is that biochar addition can enrich electroactive bacteria such as acetoclastic methanogens that is capable of participating in DIET, therefore accelerating substrate degradation (Zhang, 2020). Whereas, we did not see a strong influence of biochar WSP and HD on the VSS removal efficiency. Moreover, at end the test, the average VSS removal efficiency of all treatment was 2.5±2.4%, which was much lower than the reported level (Martinez, 2018). Wang *et al*. (2021) reported that biochar with high electrical conductance but less redox potential did not enhance the degradation efficiency of anaerobic digestion of kitchen wastes. In addition to that, most of the results reported in the literature corresponded to studies carried out in batch mode and not in continuous mode where the stimulatory effect of the biochar decreases with the course of the process (Wambugu, 2019; Indren, 2020; De Vrieze, 2016).

4.4. Conclusions

Table 4-3. Main findings from Chapter 4.

Biomass	Pyrolysis Temperature (°C)	pH	Electrical conductivity (dS/m)	Biochar dosage (batch; CSTR)	Maximum biogas production rate (mL/g/d)		Cumulative gas production (mL/g)		Maximum methane content (%)	
					Batch	CSTR	Batch	CSTR	Batch	CSTR
Rice husk	550	9.71	0.48	2 g/L; 6%	68.9 (no external ammonium added)	76.4	419.2 (TAN_0=6 mg/kg)	1940	64.1	55.6
Wheat straw pellets	550	9.94	1.7	2 g/L; 6%	92 (TAN_0 =6 mg/kg)	70.3	471.6 (TAN_0=6 mg/kg)	1950	63.9	58.3
Hardwood chips and digestate	500	9.53	26.97	2 g/L; 6%	95.2 (TAN_0 =6 mg/kg)	70.9	485.5 (TAN_0=6 mg/kg)	2000	64.1	58.3

In this study, the addition of biochar on anaerobic digestion under different ammonium nitrogen stress was investigated and the effectiveness of digester design aimed at biogas and biomethane productivities were assessed. It was shown that the addition of RH biochar improved biogas productivity at a low level of ammonia stress. Biochar WSP and HD increased the biogas and methane yields under no and/or higher ammonium stress. The ammonia adsorption capabilities of these biochars were insufficient based on the analysis of TAN and TKN removal efficiency for biochar-treated reactors and the control reported in this work. As previously demonstrated in Chapter 3, the role of biochar on anaerobic digestion was proven to be due to biochemical reasons. However, the limits of these investigations should be carefully addressed. Because no biological tests were performed, the data must be interpreted with extreme caution. It was also demonstrated that the physicochemical properties of biochars were correlated to the feedstock type and manufacturing method. Although these biochars possess limited ammonia adsorption capacities in this study, studies

have proved the potential of maximizing biochars' adsorption abilities by optimizing feedstocks selection and other post-treatments. In addition, the use of biochar has been shown to increase the VFAs degradation and promote the organic removal efficiency.

5. Application of hydrochar derived from agricultural residues in anaerobic digestion of sewage sludge

5.1. Introduction

Agricultural wastes and residues are by-products from human activities related to food production. Agricultural waste, or biomass, has the potential to be a valuable feedstock for the production of fuel, enzymes, and chemicals (Tripathi et al., 2019). In Europe alone, 660,000 tons of agricultural wastes are produced annually (de Diego-Díaz *et al*.,2018). In 2016, 53.7 % of this was recycled, 23.5 % was landfilled, and 20.5 % was burned (István, 2020). China generated approximately 476.8 million tonnes of straw and animal manure waste in 2017 (Wei *et al.*, 2020). Of this, 35% was disposed through landfill dumping and simple incineration (Wei *et al.*, 2020). In 2019, over 500 million tonnes of crop residue were produced in India (Bhuvaneshwari, 2019). Instead of utilizing energy, over 90 million tons of agricultural residue was burnt by local farmers (Bhuvaneshwari, 2019; Kapoor *et al.*, 2020). Improper treatment of agricultural wastes such as landfills and open burning leads to greenhouse gas emissions, odours, and surface water as well as underground water contamination (Millati *et al*., 2019). Open burning of crop residues can also cause severe air pollution. Jain (2014) determined that cumulative CO and CO_2 emissions from the burning of 98.4 million tons of crop residue are 8.57 and 141.15 million tons respectively. Thus, landfill and incineration are not only adversely impacting on environments, but also be considered unsustainable solutions with high costs.

Hydrothermal Carbonization (HTC) has emerged as a particularly suitable method for conversion of agricultural biomass with high moisture content, as it does not require energy-intensive drying of biomass before processing. The main product of HTC is a solid carbonaceous material referred to as hydrochar. Because of high degree of aromatization, hydrochar contains a considerable number of oxygen-containing functional groups (Kang *et al.*, 2012b). Hydrochar has low ash content and a large surface area, making it a low-cost adsorbent for contaminants in aqueous solutions (Takaya *et al.*, 2016; Li *et al.*, 2016; Fang *et al.*, 2018).

Microbial degradation of agricultural waste is effective alternative for mitigation of environmental contaminants and utilization of bioenergy (Bhuvaneshwari, 2019). Complex substance in biomass can be degraded by microbial consortia to polymers such as ethanol (Sharma *et al*., 2020). The microbial degradation possess an inherent ability to adapt to wide environment without adversely impacts (Sharma *et al*., 2020). Current microbial degradation techniques include hydrolysis, aerobic and anaerobic digestion, and dark fermentation (Pathak & Navneet, 2017). Anaerobic digestion (AD) is a well-established technology that is frequently used to convert organic residues into biogas, which can then be utilised to generate power or refined to synthetic natural gas (Caposciutti *et al*., 2020). The digestate from anaerobic bioreactors can be used dewatered and applied as an agricultural fertilizer (Hosseini *et al.*, 2019). AD is widely used for the treatment of organic materials with a high moisture content, including agricultural residues, wastewater treatment sludges, food waste, and other organic materials. Previous studies found that anaerobic fermentation of protein-rich material led to accumulation of free ammonia and was potentially toxic to methanogenic activity when free ammonia content was higher than 600 mg/L (Dai *et al.*, 2013; Rajagopal *et*

al., 2013; Rasapoor *et al*., 2020). In order to mitigate inhibitions in AD, addition of carbon material in AD can potentially reduce ammonia inhibition by balancing macro-elements such as carbon-to-nitrogen-to-phosphorus (C/N/P) ratio.

The use of hydrochar in anaerobic digestion has also attracted growing interest (Mumme *et al.*, 2011; Reza *et al.*, 2015; Wang *et al.*, 2017; Tradler *et al.*, 2018). Hydrochar has shown capacities of alleviating inhibition, providing additional carbon source and increasing biomethane generations. Arenas (2020) assessed the digestion of pork dead carcasses using hydrochar from pine trimming to favour microbial degradation. They observed a 24% biomethane production with the addition of hydrochar, resulting in methane yields of around 470 L CH_4 kg^{-1} VSS added. Mumme *et al.* (2014) also studied biogas production from AD of agricultural waste with supplement of hydrochar obtained from wheat straw, and found that the addition of hydrochar led to a 21% increase in biomethane yield. They also observed that hydrochar intensified ammonia inhibition and was partially biodegradable in the AD environment. However, there has been little research into the particular processes of hydrochar's roles in anaerobic digestion, such as the importance of surface functionality of hydrochar and its relationships to biomass composition.

Therefore, the goals of this study were to: (i) explore the physicochemical characteristics of hydrochars derived from a range of different biomass (rice husk, wheat straw pellets, oil seed rape and alkali lignin); (ii) investigate the influence of lignin content on hydrochar yield and surface functionality; (iii) determine the effect of hydrochars on the performance of mesophilic anaerobic digestion and the potential of hydrochar to promote methane generation and biogas production. Overall, this work

was aimed at developing a better understanding of the hydrochars' physicochemical properties and how this may impact their functions in anaerobic digestion.

5.2. Results and discussion

5.2.1. Physiochemical properties of hydrochar

5.2.1.1. Yields of hydrochar derived from agricultural residues

It is well known that feedstock type are key component of influencing the HTC process, the products yield and properties of the resultant products. This study aimed to understand the effects of biomass type on the HTC performance. Three lignocellulosic biomass were used in this study (Table 5-1) and converted into hydrochar under same process conditions. Lignin, the largest non-carbohydrates component (15-40%) in lignocellulose biomass (Yoo, 2020), was also used to determine the effects of lignin on hydrothermal conversion process. It is hypothesized that the carbonization degree of the hydrochar depends on the composition of the raw materials, and the hydrochar derived from lignin biomass has higher aromatic structure content.

The feedstock type had a remarkable influence on the hydrochar yield. Hydrothermal treatment of used lignocellulosic biomass yielded 45.1-61%, while HTC of lignin achieved to a hydrochar yield of 85.6% (Table 5-2). With the increase of lignin content, the hydrochar yield of these lignocellulosic biomass increased, followed a trend as: OSR<WSP<RH. This agrees with previous report of the HTC of lignin, woodmeal and cellulose, revealing that the char yield from lignin HTC was the highest one (Kang *et al*., 2012a). Lignin has a stable phenolic structure, which is favourable to char formation via a condensation reaction, resulting in higher hydrochar yield (Kang *et al*., 2012a). Meanwhile, lignocellulosic biomass consists of cellulose and hemicellulose, small portions of lipids and proteins. The thermal decomposition of biomass is related to the biomass composition such as hemicellulose (150~300^{o}C), cellulose (315~400^{o}C), and lignin (160-900^{o}C) (Lester, 2007; Carrier, 2016). The major portion

of lignocellulosic biomass is made up of cellulose, and their chains are individually arranged as cellulose fibres and are attached via hydrogen bonding (Khan, 2021). Lower solubility of cellulose resulted to lower hydrochar yields from RH, WSP and OSR biomass than lignin under current temperature condition (250^{o}C) (Liu & Zhang, 2009). Previous studies suggest that completed hydrolysis of cellulose requires higher temperature, ranging from 280-320^{o}C and longer reaction time (20 h) by hydrothermal conversion (Hashaikeh *et al.*, 2007; Kang et al., 2012a). Another possibility is that secondary decomposition and further conversion of condensable to incondensable gaseous products occurred during the HTC process. Reductions in the solid product of cellulose have been seen due to better degradation by fragmentation of larger molecules into liquids or incondensable lower molecular gas at temperature above 200^{o}C. Dong (2019) reported an increase of methane from HTC of pea pod was seen as the temperature increased from 250^{o}C to 350^{o}C. Similarly, Basso (2016) tested hydrothermal treatment on grape marc at 180, 220, and 250^{o}C, and found gaseous phase is preferred to the solid product thereby reducing the solid yield at increased temperatures.

Table 5-1. Yield of hydrochar and fuel characteristics.

Material	Biomass	Solid yield (wt.%)	C recovery (%)	HHV (MJ/Kg)
RH	Rice husk	61	78.21	17.68
WSP	Wheat straw pellets	53.9	76	25.19
OSR	Oilseed rape pellets	45.1	68.22	28.96
AL	Alkali lignin	85.6	79.78	22.08

In addition to that, cellulose is a polysaccharide linked by hydrogen bonds between D-glucopyranose units forming chains which resulting in various degree of crystallinity (Paksung *et al.*, 2020). The hydrolysis of crystalline cellulose is supposed to be slower due to thesis inter- and intra-molecular forces (Dinjus, 2011; Takada, 2018). The crystalline-to-amorphous transformation has to been taken before hydrolysis when supercritical water destroyed the crystal structure at an sufficient reaction temperature (Deguchi, 2008; Takada, 2018). In the case of lignin, as a phenolic polymer, the majority of lignin fragments are hardly changed, and may reduce the hydrolysis rate when the temperature of hydrothermal carbonization is not high enough (less than 377^{o}C) (Fang *et al*., 2008; Kang *et al*., 2012b). Only a small fraction of lignin can be dissolved in water with the temperature under 200^{o}C (Hashaikeh *et al*., 2007). While the process temperature in this experiment is 250^{o}C, and thus it can be expected that the water-solubility homogeneous reaction may not be the predominant pathway of producing hydrogen from lignin. Literature suggested that solid-to-solid conversion is the preferential alternative to produce polyaromatic char from the non-dissolved lignin (Fang *et al.*, 2008; Dinjus, 2011). Furthermore, hemicellulose is a pentose polymer linked by hydrogen bonds between celluloses and associated lignin with covalent bonds, consequently forming the plant cell walls (Sun, 2010; Wang *et al.*, 2018). As compared with lignin, hemicellulose is easier to degrade into monomers at lower temperature. It has been reported that hemicellulose can be dissolved at 180^{o}C, and the resultant monomers undergo polymerization reactions to form hydrogen (Fengel & Wegener, 2011; Kang *et al.*, 2012b).

Table 5-2. Hydrochar yields from different feedstocks.

Biomass	Biomass category	HTC temperature (ºC)	Char yield	Reference
Acacia HC	Woody biomass	200	70	(Magdziarz, 2019)
Agave pulp	Agricultural biomass	180	54.2	(Merzari, 2018)
		220	50.9	
		250	34.8	
Arecanut husk	Agricultural biomass	200	58.72	(Ramesh, 2019)
Dry straw	Agricultural biomass	220	49.5	(Oliveira, 2013)
Poultry manure	Organic municipal wastes	220	52.5	(Oliveira, 2013)
Rice husk	Agricultural biomass	180	7.4	(Nizamuddin, 2018)
		200	73.42	
		220	65.6	
		250	55.19	

5.2.1.2. Proximate and ultimate analysis

As shown in Table 5-3, the carbon content, hydrogen-to-carbon (H/C) ratio, and oxygen-to-carbon (O/C) ratio in all of these hydrochars are among 35-42%, 16-20 and 0.57-0.79, respectively. The carbon (C) recovery (%) in the produced hydrochars ranges from 68.2-79.8%, which is lower than the reported value of C recovery from pyrolysis (80-94.5%) (Arauzo et al., 2020; Kang et al., 2012b). It might be explained by improved polymerization reactions during high-temperature pyrolysis resulting in increased formation of aromatic structures (Yuan *et al.*, 2015). Meanwhile, hydrochar derived from alkali lignin has higher carbon recovery as compared to other feedstocks. This agrees with the value of Table 6-2, showing that the C content in alkali lignin hydrochar is higher than in other hydrochars. Furthermore, the higher heating value (HHV, MJ kg^{-1}) is another characteristic parameter to evaluate fuel properties of

hydrochar. The HHV values of these hydrochars are between 17.67-28.96 MJ kg^{-1}, which are in the same range of reported levels. Arauzo (2020) conducted hydrothermal carbonization for sewage sludge granules at 260°C, and obtained hydrochar with a HHV between 12.4 and 31.1 MJ kg^{-1}. Meanwhile, hydrochar with HHV among 24-30 MJ kg^{-1} can be considered as the equivalent to the medium-rank and high-rank coals (Kang *et al*., 2012b). Furthermore, carbonization degree relates to the aromaticity and polymerization during the HTC process. The aromaticity increased as the carbonization degree increased. Noticeably, both the C content and HHV value of RH hydrochar were considerably lower than that for the other hydrochars, which might be attributed to the higher content of silica in the original feedstock. Our findings were also in agreement with the study by Kalderis *et al*. (2014) that hydrochar rice husk produced at 300°C and 6 h residence time had a heating value of 17.8 MJ/kg and a fixed carbon recovery of 113%. Previous studies suggested hydrothermal carbonization of biomass with higher silica contents has lower carbonization degree due to that exceed silica inhibited the HTC process by shielding carbon from biomass to the char products, resulting in incomplete carbonization (Fagbohungbe *et al*., 2017a; Kang *et al*., 2012a).

Table 5-3. Proximate and ultimate analysis of hydrochars.

Biochar	Volatile matter (%)	Volatile matter (%)	Total ash (%)	C (wt.%)	H/C	O/C
RH	3	41	27	4.59	0.59	0.56
WSP	3	52	10	5.68	0.64	0.30
OSR	3	57	5	6.14	0.75	0.20
AL	7	38	21	4.97	0.74	0.42

The degree of coalification and reaction pathway is represented in the van Krevelen diagram (Figure 5-1), where the O/C and H/C atomic ratios of biomass feedstock are

compared with the produced hydrochar and typical coals including peat, lignite, bituminous and anthracite. As expected, biomass feedstocks have higher O/C and H/C ratios compared to hydrochars. During the HTC process, the initial carbohydrates undergoes dehydration and deoxygenation reactions, and further forms carbon-rich materials (Diebold, 1994). Meanwhile, these reactions associate with elimination of water and carbon dioxide (Paksung *et al*., 2020), attributing to differences in chemical composition of the resultant hydrochar. Dehydration can lead to an increased carbon content in hydrochar by 65% (Jung, 2018). In this study, dehydration occurred during the HTC process for all used feedstocks. The H/C ratio before and after the HTC of rice husk dropped from 0.11 to 0.05, resulted in a 55% decrease. Hydrothermal treatment of Oilseed rape pellets also led to decrease of H/C ratio by 42%. The H/C atomic ratio of these hydrochar are in a range of value similar to those reported in the literature (Sharma, 2019; Arauzo *et al.*, 2020). In addition to that, decreasing trend was also observed in the O/C ratio with a 20% (from 2.20 to 1.75) decrement after hydrothermal treatment of rice husk. Hydrothermal treatment also caused a reduction in the O/C ratio by 70% (from 0.69-0.2) for hydrothermal conversion of oilseed rape pellets. These results show an efficient dehydration and deoxygenation occurred during the HTC process. Meanwhile, a higher atomic O/C ratio can reflect a low carbonization grade with presence of polar functional group (Wiedner *et al*., 2013). The O/C ratios of these hydrochar range from 1.27 to 1.75, which implies that those hydrochar are close to lignite with similar atomic ratios. Differences of O/C ratio between RH hydrochar and other chars can be attributed to higher lignin content of rice husk (Wiedemeier *et al*., 2015). Furthermore, higher ash content in feedstock can be attributed to the retard aromatization, consequently resulting in a higher O/C ratio (Mukome *et al.*, 2013). Previous studies reported that a high condensation of aromatic

ring system with H/C ratio less than 0.3, whereas poor aromatic condensation occurs with H/C ratio more than 0.7 (Hammes *et al*., 2006; Wiedemeier *et al*., 2015; Wiedner *et al.*, 2013). In this study, the H/C ratio of all hydrochars are higher than 0.6, while only RH and AL hydrochar have an O/C ratio over 0.4. Then, as expected, hydrothermal carbonization of rice husk and alkali lignin tends to form mainly aliphatic compounds in the resultant products (Méndez *et al.*, 2019). It can also be assumed that hydrochars derived from wheat straw pellets and oilseed rape pellets have higher contents of aromatic compounds. Meanwhile, molecular structure and size of the aromatic cluster in hydrochar could be stimulated by a prediction model on the basis of the H/C ratio (Xiao, 2016). It is supposed that the distribution of aromatic rings would form a rectangle-like shape, and the corresponding structure of char follows the same pattern. In this structure, hydrogen atoms are linked to the marginal carbon and theoretically expressed as C_mH_n (where m is the row number and n is the column number). Correspondingly, these hydrochars with H/C ratios of 0.05-0.06 are assumed a 50x50 rectangle with a turbostratic aromatic cluster structure. This finding is also confirmed by Zhang *et al.* (2020) that the char product transited from amorphous to a composite with a graphene-like structure during the carbonization process. Meanwhile, this model limits to considering hydrochar as a whole as the integrated skeletal structure. Further research may be needed to confirm the formation and transition mechanisms during the HTC process.

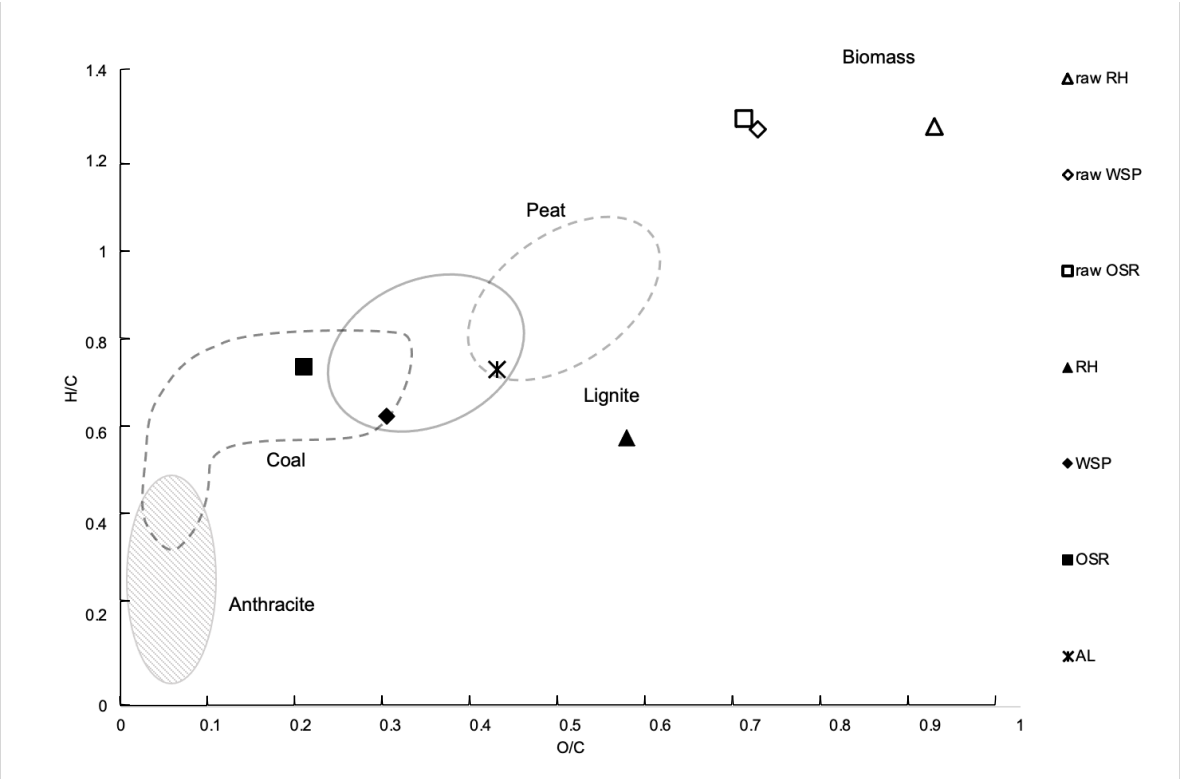

Figure 5-1. The Van Krevelen of applied hydrochars and their raw biomasses. The O/C and H/C atomic ratios of typical coals including peat, lignite, bituminous and anthracite are also shown. Mean of results, n=3.

The volatile matter (VM) of these hydrochars ranged from 38 to 57%, and of which that OSR hydrochar has the highest VM content of 57% (Table 5-3). The fixed carbon (FC) content of these hydrochar were among 13-52%. According to the principle of mass conservation, the FC content is associated with the volatile matter which serves as a raw material for its production during the carbonization process (Gao *et al*., 2019; Wüst *et al*., 2019). As aforementioned, high ash content in rice husk may restrain the polymerisation and consequently lead to a reduction of C content in the resultant hydrochar. Another possibility for the lower FC content of RH hydrochar is associated with its structure and chemical properties. In addition, the degradation of complex lignin in rice husk may only occur at higher temperature. Furthermore, the ash content of these hydrochars varies from 5 to 27%. The highest ash content was found in RH

hydrochar, which might be attributed to the destruction of volatile matters and no degradation of the mineral compounds at these conditions (Syed-Hassan *et al.*, 2017).

5.2.1.3. The pH and EC of hydrochars

Hydrochars produced from llignocellulosic biomass showed a pH ranging from 4.01 to 5.23, which are close to reported pH level (5.0-7.5) . The acidic pH of hydrochar is due to acid-catalysed dehydration of monosaccharides dominated the HTC process, resulting in the formation of acidic functional groups on hydrochar surface (Jain, 2016). In contrast, hydrochar derived from lignin showed an alkaline pH of 9.52. It has reported that dissolvable lignin is decomposed into phenolic products such as syngas and phenols by hydrolysis and dealkylation; these intermediates are further formed phenolic char (Fang *et al*., 2008). While the non-dissolved lignin tends to form highly condensed char with polyaromatics at low temperatures via solid-solid reaction pathway (Saha, 2019). Therefore, base-catalysed dehydration of carbohydrate is suggested to be undergoing during the HTC of alkali lignin.

Table 5-4. pH and water-soluble EC of hydrochars.

Biochar	**pH**	**EC (µS/cm)**	**pH**	**EC (µS/cm)**
	1 hr		24 hr	
RH	3.92	62.1	4.81	56.4
WSP	4.10	108.75	3.96	143.15
OSR	5.17	1345	8.93	1401
AL	9.53	145.85	5.09	218.45

Water-soluble electrical conductivity (EC) for these hydrochars is presented in Table 5-4. The EC value of all these hydrochars is among 56.4 to 1401 µS cm^{-1}. Hydrochars derived from lignocellulosic biomass showed relatively low values, which might be

attributed to the decomposition or valorisation of the most dissolved salts in the process water during the HTC process (Yuan *et al.*, 2015). Meanwhile, the majority of hydrochar shows an increasing EC value after the 24-hours incubation, whilst the EC of RH hydrochar decreased by 9%. This could explained by adsorption of dissociated salts from process water to hydrochar during the HTC process (Chen *et al.*, 2017), and further desorption from hydrochar to the analytical solution. Another possibility for the decrement in EC of RH hydrochar is that this hydrochar has lower pH than all other hydrochars. Ren (2017) suggested that EC serves as an indicator of salinity, and decrease in salinity of hydrochar's applied environment is depended on the decreasing electrical conductivity of hydrochar. On the other hand, OSR hydrochar shows a highly-conductive behaviour, with a EC value of 1401 μS cm^{-1}. The high electrical conductivity is associated with the redox groups on the surface of hydrochar and its chemical properties.

The electrical properties are also associated with microscopic parameters (such as the molecular structure and intrinsic EC of the solids) and macroscopic parameters (applied pressure and compression ratio, etc). In this study, electrical conductivities of these hydrochars were analysed in the function of resistance (Figure 5-2). All hydrochars show semi-to-high conductive properties (Hoffmann *et al*., 2019), with the value of around 10^4 S m^{-1}. Furthermore, the increment in EC values is observed for all hydrochars, which is proportionally attributed to the applied pressure. The greater increase in electrical conductivity of all tested hydrochars was observed at the applied pressures from 100 to 1000 bar. The highest increment (93%) was found in RH hydrochar with a EC value of 258.45 S m^{-1}. Then, the electrical conductivity for RH and OSR hydrochar mildly decreased by 22.2±0.11% with increasing applied pressure

from 1000 to 2500 bar. In the meantime, AL hydrochar maintained the same level of electrical conductivity (265.6±0.007 S m^{-1}) with increasing compression pressure from 1000 to 2500 bar. Whereas electrical conductivity for WSP hydrochar increased by 2-fold under the same compression level. The increment of EC for WSP hydrochar can be due to that compression eliminates the empty space in the internal structure of the hydrochar through collapse and flattening of porous structure, resulted in an internal fracture (Gabhi, 2017). Therefore, better contacts between individual carbon particles leads to higher electrical conductivity. Meanwhile, a great fluctuation in electrical conductivities for WSP and OSR hydrochars was observed when the applied pressure increased to 4500 bar, and followed by an sharp increase. The fluctuation may be due to the elastic properties of EC and contact resistance (Gabhi, 2017). Whereas EC for RH and AL hydrochars continued to increase by 52.2±0.02% from 4000 to 5000 bar. The highest electrical conductivity was observed for AL hydrochar, with value of 354.6±0.01 S/m. Among the lignocellulosic biomass derived hydrochars, RH hydrochar with higher ash content (27%) has an EC of 252.6±0.13 S/m, which was 1.5±0.41 times higher than that of WSP and OSR hydrochar with lower ash content (7.5±3.53%) These results also showed that the electrical conductivity was proportional to the ash content.

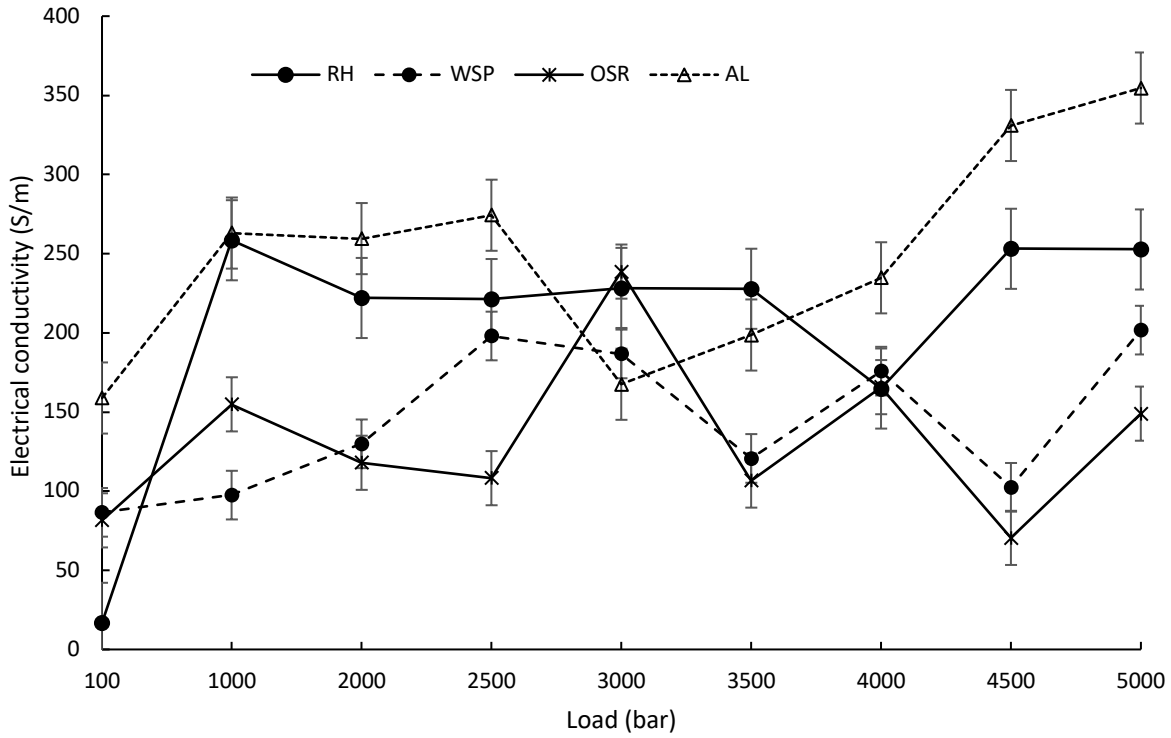

Figure 5-2. Electrical conductivity (S/m) of hydrochars under compressions.

In theory, the behaviour of hydrochar during the compression movement might be explained by two pathways (Figure 5-3): (1) the formation of carbon agglomerate during compression and consequently the void among particles compacts and/or collapsed; (2) the fragmentation during the extrusion process where the polymer chain flatted creating spaces for carbon particles. Accordingly, the positive influence of applied pressure on the conductivity value in the first compression movement could be due to the dispersion of carbon particles inside the hydrochar matrix. The differences in the increment ratio during the first stage are reasonably attributed to the initial feedstock structure and chemical properties. Wheat straw and oilseed rape were pelleted before the HTC process, while no pre-treatment was applied to the other feedstocks. It has been reported that pelleting process can result in partial deconstruction of plant biomass attributing to high shearing and mixing force coupled with heat development (Guragain *et al*., 2013; Theerarattananoon *et al*., 2012).

Notably, the effect of pelleting may vary wildly from biomass to biomass. Furthermore, as the high pressure applied, the decrement of conductivity indicates the collapse of carbon particles led to the low π-π interactions (Noori *et al.*, 2020). At the final stage, the increased conductivity of OSR and AL hydrochars shows a reversible plastic formation during the extrusion. Another possibility for the increment is that the large carbon particles in these two biomass were disrupted during the HTC process forming a smaller sized well-dispersed particles which can prevent the formation of conglomerate under high pressures (Giorcelli & Bartoli, 2019).

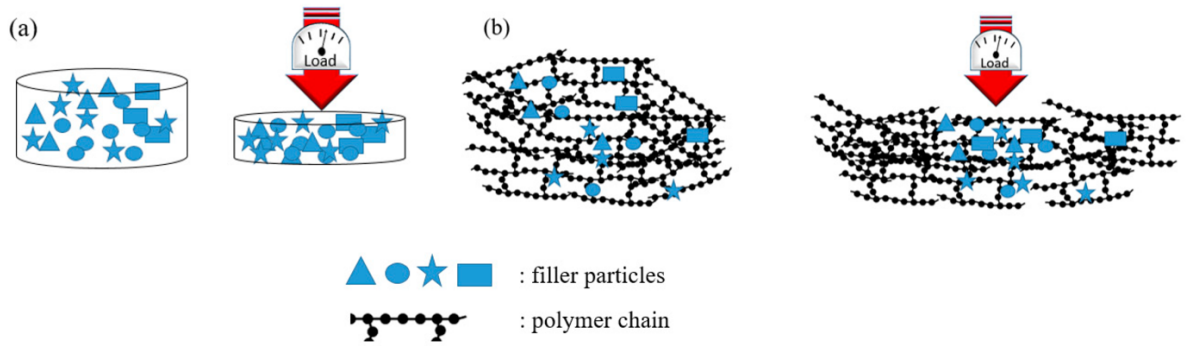

Figure 5-3. Potential pathways of hydrochars under compression movement (Giorcelli and Bartoli, 2019).

5.2.1.4. Water-extractable DOC of hydrochars

Dissolved organic carbon (DOC) is an important fraction of hydrochar, which can be used for regulating nutrients transportation (Lei *et al.*, 2018; Liu *et al.*, 2019). DOC also plays an important role in nitrogen circle under nitrogen-saturated conditions in aquatic environment (Fang *et al.*, 2009). Furthermore, DOC can influence the biochemical transformation during =anaerobic digestion process because microbial metabolism occurs in the water-soluble environment (Yekta *et al.*, 2012; Xing *et al.*, 2012). However, exceed DOC may cause eutrophication and acidity of aquatic environment (Dolling & Porter, 1994; Mukherjee & Zimmerman, 2013). In this study, the DOC of all

hydrochars ranges from 18.82 to 137.76 mg L^{-1} (Table 5-5). AL hydrochar has higher DOC concentration of 137.76 mg L^{-1}, which might be due to higher solubility of larger molecular (Chen *et al.*, 2015a). Another possibility is attributed to higher extraction rate of light-adsorbing organic compounds under strong alkaline conditions, subsequently promoting the dissociation of carboxyl and phenyl groups (Liu *et al*., 2019). AL hydrochar also has higher pH value than that of other hydrochars, which may result in increased alkalinity of extraction solution. This finding is in agreement with a study by Liu *et al.* (2019) that the alkaline ash content of the char products contributed to the pH increased and further enhanced the dissociation of organic materials in the surrounding environment.

Table 5-5. DOC and UV-vis analysis of hydrochars. Mean of results, n=3.

Biochar	DOC (mg/L)	E2:E3	S275-295
RH	25.41	12.34	3.07
WSP	18.82	8.49	2.46
OSR	40.20	3.34	2.86
AL	137.76	3.16	2.82

Meanwhile, visual appearance of the extracted DOC solutions was further verified by the UV-spectra. In general, the UV-vis absorption spectra of extracted hydrochar-DOC samples were presented in bulk and featureless. It has been reported that the multiple chromophores cause the occurrence of overlapping absorption bands (He *et al.*, 2009; Minor *et al.*, 2014; Qu *et al*., 2016). In order to extract information from these UV-vis spectra, several spectra ratios such as E_2:E_3 and $S_{275\text{-}295}$ have been determined in this study. The ratio of spectra at 254 to 365 nm (called E2:E3) has been used for regulating changes in the relative size of dissolved organics molecular (Helms *et al*., 2008). They suggested that E2:E3 ratio decreased as molecular size increased due

to the accumulation of high-molecular-weight DOC which can enhance light absorption at longer wavelength. The slope coefficients of 275-295 nm to 350-400 nm have also been used to compare DOC and the photochemically shift in molecular weight (Chen *et al.*, 2015b). In this study, E2:E3 ratios of all hydrochars were 12.34, 8.49, 3.34 and 3.16. Accordingly, the aromaticity increased as the E2:E3 ratio decreased (Helms *et al.*, 2008; Minor *et al*., 2014). It can be seen that the aromaticity increased in the order of RH > WSP > OSR > AL, which has been confirmed by the ultimate analysis discussed in previous section. As such, it is expected that higher aromaticity of hydrochar is responsible for higher water solubility and its off-site transportation. The difference in extracted DOC also relates to the biochar stability. This study determined that all the hydrochars have relatively high solubility of dissolved organic carbon, following in an order of AL > OSR > RH > WSP. This indicates that higher degree of aromatization enhanced the accumulation of light-adsorbing organic compounds, which may gradually release into the surrounding environment. While in the case of RH hydrochar, it is assumed that a small fraction of organic matters from the raw material remained and uncarbonized from the HTC, then leaching out to the aquatic environment. It should be noted that this study examined water-extractable DOC of hydrochar obtained from different pre-treated biomass. The hydrochar made from unpelleted biomass has lower aromaticity and lower DOC concentration, suggesting the potential relationship between particle size and DOC. Therefore, future works could be directed to quantify and characterize DOC in hydrochars with various particle sizes from micron to cm.

5.2.1.5. Surface functionality analysis of hydrochars

Oxygen-containing functional groups play an important role in the redox-properties of hydrochar (Ren *et al.*, 2020). It is known that biochar can facilitate electron transfer for microbial metabolism due to its redox-active properties (Wu *et al*., 2017; Yuan *et al*., 2018). Therefore, it was hypotheses that hydrochar may have similar redox properties which can also promote methanogenesis during the AD process. Furthermore, the oxygen-containing functional groups are recognized as the main ion-exchange sites (Saha, 2019).

The ATR-FTIR analysis was applied for all hydrochars to identify surface functional groups. The predominant functional groups on the hydrochars' surface were presented in Figure 5-4. Peak assignment and identification have been determined by following previous literatures (Schwanninger *et al.*, 2004; Uddin *et al.*, 2014; Jain, 2016). A noticeable broad peak at 3280-3350 cm^{-1} was found in all hydrochars, assigned to the O-H bonding from water. In addition to that, RH hydrochar has lower hydroxyl content which might lead to an increase in hydrophobicity (Liu *et al*., 2013). In addition, carboxylic acid group was more defined in OSR hydrochar which was likely due to dehydration and decarboxylation of hemicellulose (Kambo & Dutta, 2015). In addition to that, AL, WSP and OSR hydrochars shared similar functional groups such as aliphatic C-H bonds at 2880 cm^{-1} which assigned to alkyl groups, and the presence of H_2O at 1660 cm^{-1}. Peak at 1020 cm^{-1} for aliphatic ether C-O stretching bond was also observed in all hydrochars. While, The C=O groups appeared at peaks of 1690 cm^{-1} was only identical in WSP and AL hydrochars. Meanwhile, WSP hydrochar shared similar peak intensities with AL hydrochar. Whereas, peaks from OSR hydrochar have higher intensity which might be attributed to enhanced dehydration

and decarboxylation promoting formations of C=O and carboxylic acid O-H bands (Funke and Ziegler, 2010). The presences of peaks at 1590 cm^{-1} for alkene C=C and 780 cm^{-1} for aromatic C-H bonding in most hydrochars were due to decomposition of polymeric substances and the secondary reaction between hydrochar and processing water after HTC that consequently forming hydroaromatic structures (Wang *et al.*, 2018).

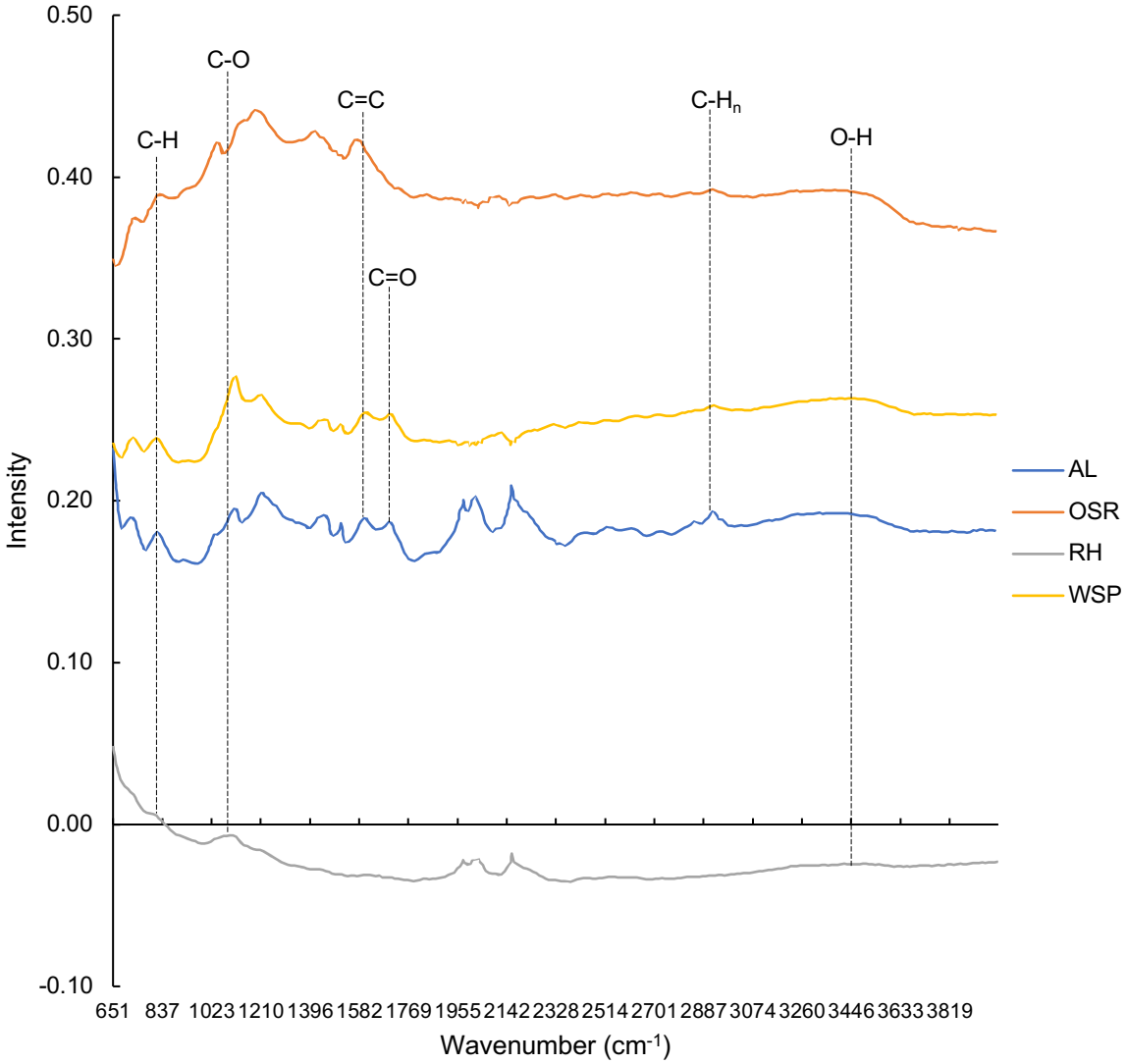

Figure 5-4. FTIR spectra of tested hydrochars

Meanwhile, the presence of C=O stretching vibrations irreversibly relates to the decarboxylation process. It has been reported that the stretching of C=O bonding in hydrochar decreased in the HTC process and nearly disappeared due to the

degradation of carboxyl and acetyl group (Sevilla *et al*., 2011). Similar results were found during the HTC of corn cob and miscanthus; C=O vibrations were completely disappeared after the HTC (Calucci *et al.*, 2013). However, they reported that dehydration of hydroxyl groups in the monomers derived from cellulose can contribute to the formation of C=O bonding for quinone, ester or carboxyl groups. Thus, the presence of C=O bonding in oilseed rape straw and alkali lignin hydrochars may be due to above reasons.

5.2.2. Biogas and biomethane productions

The AD experiments were conducted in mesophilic conditions for 60 days, until the biogas production was negligible. Figure 5-5 presents biogas production from sewage sludge with the supplement of hydrochar. In the first 30 days, the biogas production from the control achieved 55.58 mL g^{-1}, which was considerably lower than the average biogas yield of 478 mL g^{-1} produced from co-digestion of WAS and nitrogen-rich substrate (Hagos *et al*., 2017). The low biogas production from the control group might be attributed to serious inhibition occurred in anaerobic digestion of mono-substrate (activated sludge). Another possibility is that sewage sludge has a lower content of carbon and nitrogen, requiring longer degradation time and/or other pre-treatments to facilitate hydrolysis.

The biogas productions from bioreactors with hydrochar additions ranged from 28.32 to 53.66 mg g^{-1}. It followed the order of RH < WSP < OSR < AL. In addition, the type of hydrochar used had a significant effect on cumulative biogas production. However, the lowest biogas production (47.3 mL/g, 1.6 times lesser than the control group) was observed in bioreactor with addition of RH hydrochar, indicating serious inhibition

occurred during the AD process. The addition of RH also caused a four-days lag phase in biogas production. On the other hand, the maximum daily gas production for these tested groups were similar with an average value of 1.82±0.5 mL/g/d.

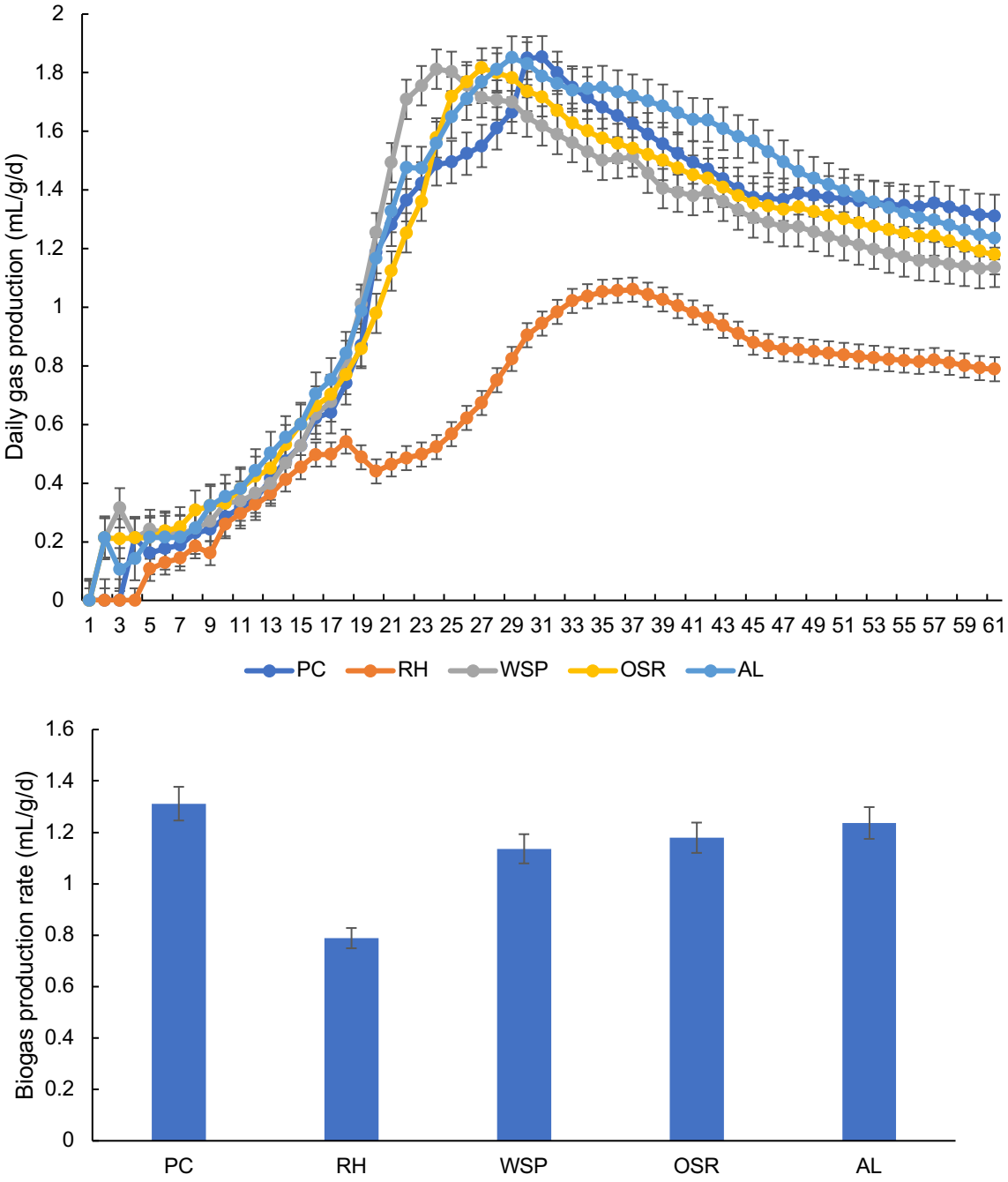

Figure 5- 5. Daily gas production (mL/g/d) over the course and final-day gas production rate from AD with additions of different hydrochars. Data were presented as Mean±Standard Deviation.

The enhanced biogas production can be due to the alkaline properties of AL hydrochar with pH of 9. 52 acted as a pH buffer alleviating acid accumulations. This is in line with a study by Ren (2020) investigated effects of hydrochars derived from corn straw, Enteromorpha algae and poplar wood on AD of cassava stillage. They found that the hydrochar addition facilitated acetate degradation and further promoted biogas production. Similar observations were reported by Wambugu (2019) about the role of hydrochar produced from brewery residue in the AD of food waste. They suggested that hydrochar could provide sufficient buffering to counter the acids accumulation at moderate volatile fatty acids (VFAs) concentrations. Another possibility can be the dissociation of DOC from AL hydrochar served as an additional substrate during the AD process. This finding has been confirmed by previous studies which investigated the possibility of hydrochar leaching out dissolved organic materials and nutrients in the bioreactors (Kambo & Dutta, 2015; Wambugu *et al.*, 2019).

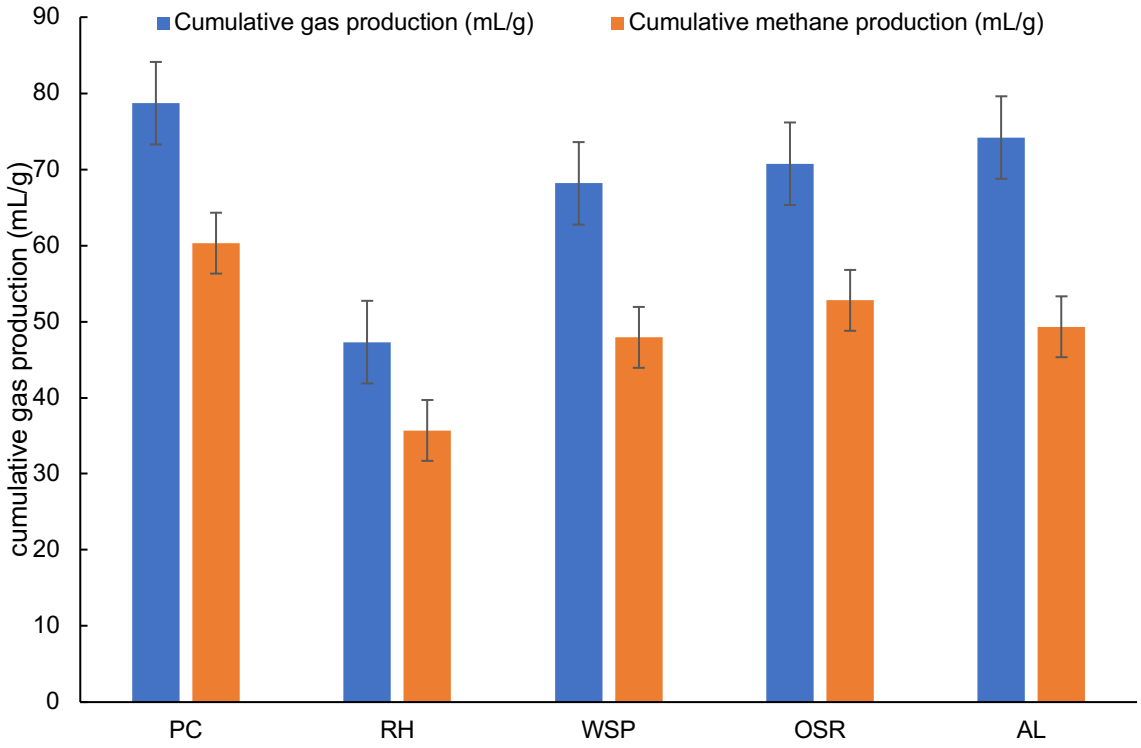

Figure 5-6. Cumulative biogas and biomethane productions (mL/g) from AD of sewage sludge with hydrochar addition.

Meanwhile, biogas production from all treatment groups gradually reduced until the end of experiment, except from the control group spotting a slight increase from day 56. Meanwhile, cumulative biogas yields from all lignocellulosic biomass-based hydrochar (with average of 65.1±12.1 mL/g) were lower than the control group (78.7 mL/g). The negative effect of hydrochar addition on the gas yield can be due to the presence of aromatic component in hydrochar (Xiao *et al.*, 2018). Furthermore, hydrochar might exacerbate the ammonia inhibition. Mumme *et al.* (2014) found that methane production from hydrochar added bioreactor was decreased and the presence of hydrochar led to an ammonia inhibition with total ammonium nitrogen (TAN) levels of 2.5-5.0 kg kg^{-1}. The reason is that nitrogen compounds contained in hydrochar such as NH_2 can be protonated into NH_3 or NH_4^+ (Yu & Dai, 2010; Zhou *et*

al., 2020). It is known that NH_4^+ has a negative effect on methane generation (Hadj *et al.*, 2009), and NH_3 may also have the similar inhibition effect in the AD system (Hameed *et al.*, 2019; Pastor-Poquet *et al*., 2018). In addition, the protonation transfer from NH_2 to NH_4^+ acquiring H^+, which is negatively influence the direct interspecies electron transfer for methanogen during the methanogenesis process (Wang *et al.*, 2019).

Average methane contents and cumulative methane yields during 60 days AD of sewage sludge with hydrochar and control were shown in Figure 5-6,7. The average methane content was ranged between 73.3-76.8% for biochar-amended group and 74.8% for the control, within the normal methane range yielded from anaerobic digestion (Campuzano, 2016). The highest methane content, 76.8% was observed from OSR hydrochar amended reactor. The enhanced methane production with addition of OSR hydrochar could be attributed to surface structure of OSR hydrochar with increased functional group density. Xu *et al.* (2018) reported that the highest methane generation was obtained by adding 4g/L of hydrochar to AD of pig carcasses, and found that the addition of hydrochar facilitated volatile fatty acids (VFAs) transformation to biogas by increasing functional group density and microbial biomass stability. Choe *et al*. (2019) stated that co-digestion of fish processing wastes with bamboo hydrochar produced at 200^{o}C increased methane yield by 127% over the mono-digestion of fish processing wastes. While, among all the treatment groups, hydrochar RH-treated reactor had lower methane content at 73.3%. This results of this study agreed with Choe *et al.* (2021), which was found the addition of hydrochar derived from tofu residue at 180^{o}C resulted in a decreased gas production with the lowest methane content of 47.5%. They suggested that the lower methane content

was due to the Mailard reaction's produced components such as furans, pyrroles and pyridines at hydrothermal temperature of 180 and 200°C. The mildly negative effect of adding RH hydrochar on the methane content might also be attributed to the formation of phenol compounds in hydrothermal liquids, which are toxic to anaerobic bacteria and could inhibit methanogenesis (Libra, 2011).

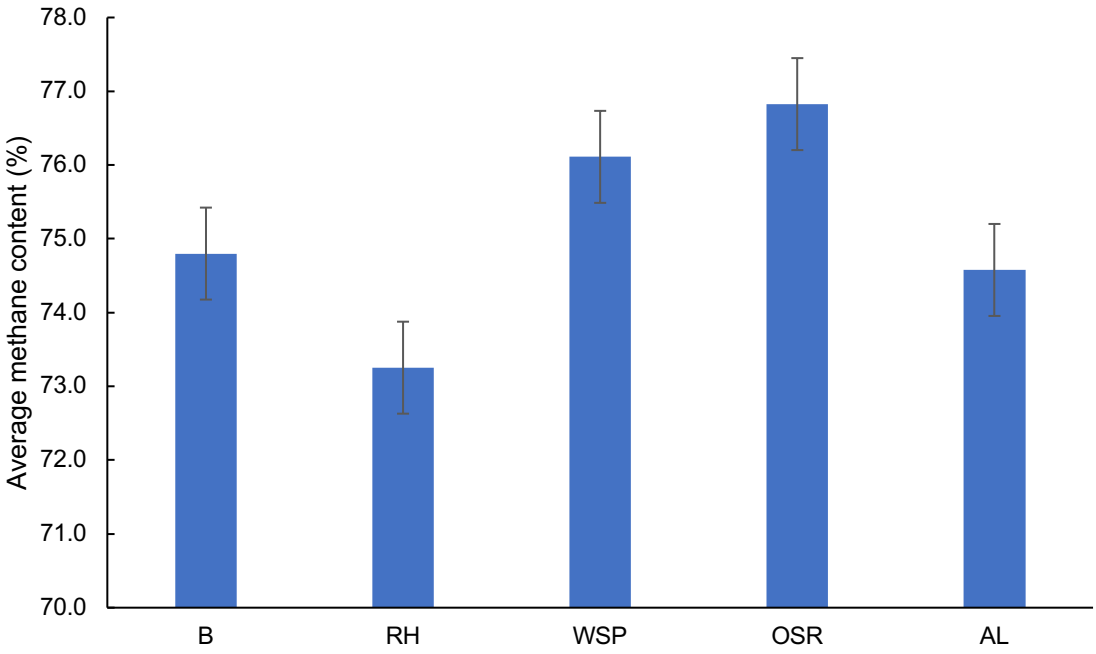

Figure 5-7. Average methane content (%) in biogas from reactors. "B" stands for the control group.

The potential mechanisms of hydrochar on enhanced methane generation are discussed here focusing on its chemical properties. One possibility for enhanced methane generation is the decomposition of hydrochar, leading to the leakage of soluble organic materials during the AD process and provide extra carbon sources contributing to the overall methane yield (Mumme *et al*., 2014). In the present study, an increment in water-extractable DOC was observed in all the hydrochars. However, typical soluble organic matters in hydrochar have the humic acid-like and protein-like structures such as tyrosine and tryptophan (Xu *et al*., 2020), which are resistant to

biodegradation. Therefore, the contribution from dissolved organic carbon to methane production may be limited and its role on facilitated hydrolysis of substrate should be focused (Wei *et al.*, 2020). Nevertheless, previous study reported that the presence of aliphatic compounds in DOC and the hydrochar matrix might promote the microbial growth and metabolisms (Freeman, 2001). Ji *et al.* (2020) also confirmed that hydrochar can adsorb high molecular weight organic compounds and release refractory organic matter into the applied environment. They found that the type of dissolved organic matters was dominated by substances with lignin and carboxylic rich alicyclic molecular-like structures. Another possibility for the enhanced methane content is due to the alkaline nature of hydrochar (Fidel *et al.*, 2017). Gao *et al.* (2015) reported that the buffering system in the AD of kitchen waste was enhanced by the addition of hydrochar. The potential mechanism can be explained by the following equation:

$$C_xH_yCOOH + NH_3 \cdot H_2O \rightarrow C_xH_yCOO^- + NH_4{}^+ + H_2O$$

In the present study, this hypothesis was confirmed by the highest biogas production from alkali lignin hydrochar amended bioreactor, which was attributed to its alkaline nature with a pH value of 9.52. Furthermore, the promoting effects should be associated with functional groups on the surface of hydrochar. In the present study, the results showed that the less oxygen-containing functional groups were exhibited in RH hydrochar. The absorbance peaks of OSR hydrochar were more abundant and that of AL hydrochar were more sharper than other hydrochars. It is known that the peaks of 874, 1610 and 2921 cm^{-1} are assigned to the bonding with aromatic structure in hydrochar (Xu *et al.*, 2020). Meanwhile, other oxygen-containing functional groups such as the C-H bond in alkanes and O-H bonding in phenols, esters and alcohols were appeared in these two hydrochars. Functional groups such as phenolic hydroxyl

and benzo-quinolyl have proven as the major redox moieties, which can act as electron donor or acceptor of carbonaceous matters (Ratasuk and Nanny, 2007; Klüpfel *et al.*, 2014). Hence, presences of redox moieties can promote methanogenesis process (Zhou *et al*., 2020). The aromatic structure (π-electron) in hydrochar is also recognised as the active moieties for electron transfer (Mai *et al.*, 2017). As aforementioned, all the hydrochars have relatively high electrical conductivity. Therefore, the more abundance oxygen-containing functional groups on the surface of hydrochar and its high electrical conductivity can favour microbial growth and metabolism by promoting the electron transfer, consequently achieving the purpose of enhancing methane production (Wang *et al.*, 2020; Xu *et al.*, 2020).

It should be noted that most of the hydrochar used in this study were produced from agricultural residues. The chemical properties and catalytic moieties of hydrochar can be tailored by the HTC temperature and retention time. Hydrochar can also remain in the digestate after fermentation, which could potentially add the value to digestate. Therefore, this study showed that hydrochars produced from agricultural residues and can be used back into the waste treatment system by applying to the AD system to stimulate the sustainable energy production process. The present study was conducted in lab-scale batch experiment. Larger-scale experiments using continuous stirred tank reactor (CSTR) and field-level digesters should be considered in the future work. Although hydrochar can considerably promote methane generation, a small fraction of substance with aromatic structure or lignin was released from hydrochar (Uchimiya, 2015; Ghidotti *et al.*, 2017). The potential toxicity from these compounds on microbial growth and metabolism should also be investigated. In addition, hydrochars derived from oilseed rape and alkali lignin have higher aromatization

degree and more abundance of oxygen-containing functional group, indicating that the chemical properties of hydrochar can be tailored during the HTC process. Further studies need to focus on the application of hydrochar in the digestion under inhibition conditions to achieve more reliable support in engineering hydrochar production and its application to the commercial industry.

5.2.3. Changes in degradability of sewage sludge-based digestion

It is known that a charred biomass has less decomposition capacity as compared to organic substances. A small amount of volatile organic matters are still possibly dissolved during the AD process. Previous studies reported that hydrochar has lower carbonization grade, but contains more water-extractable organic carbon and alkyl moieties (Kambo & Dutta, 2015; Reibe *et al.*, 2015; Yue *et al.*, 2017). The decomposition rate can vary wildly, depending on the feedstock and thermal conversion conditions (Yue *et al*., 2017). The degradation capacity in functions of methane productions during the AD process was further analysed by a two-pool carbon model according to a previous study by Mumme *et al.* (2014). The highest degradation constant k was observed in all the treatments by day 14, where the maximum degradation was found in RH hydrochar-added bioreactor with a k value of 0.19. This might be attributed to humic acids presented in hydrochar, which retard methanogenesis by limiting electrons and inhibiting the reaction of acetyl-CoA → 5-methyl-THMPT, causing less short-chain fatty acid being consumed (Liu *et al*., 2015). In addition, bio-availabilities of those hydrochars were decreased by 64.5 – 81% from day 28 onwards. This could be explained that hydrochar may not be fully decomposable, which was in line with the study by Yue *et al.* (2017). They reported that only a small fraction of dissolved organic matters decomposed during the AD

process, while nutrients such as heavy metals remained in the hydrochar particle. Furthermore, the presence of aromatic compounds such as lignin and phenols in hydrochar, are highly resistant to microbial decomposition (Libra *et al*., 2011; Usman *et al*., 2020). However, this study observed that dissociation of soluble organic matters from hydrochar may occur, and may increase the total carbon sources in the digestate, sequentially leading to exceed accumulation and causing the loss of biogas productions.

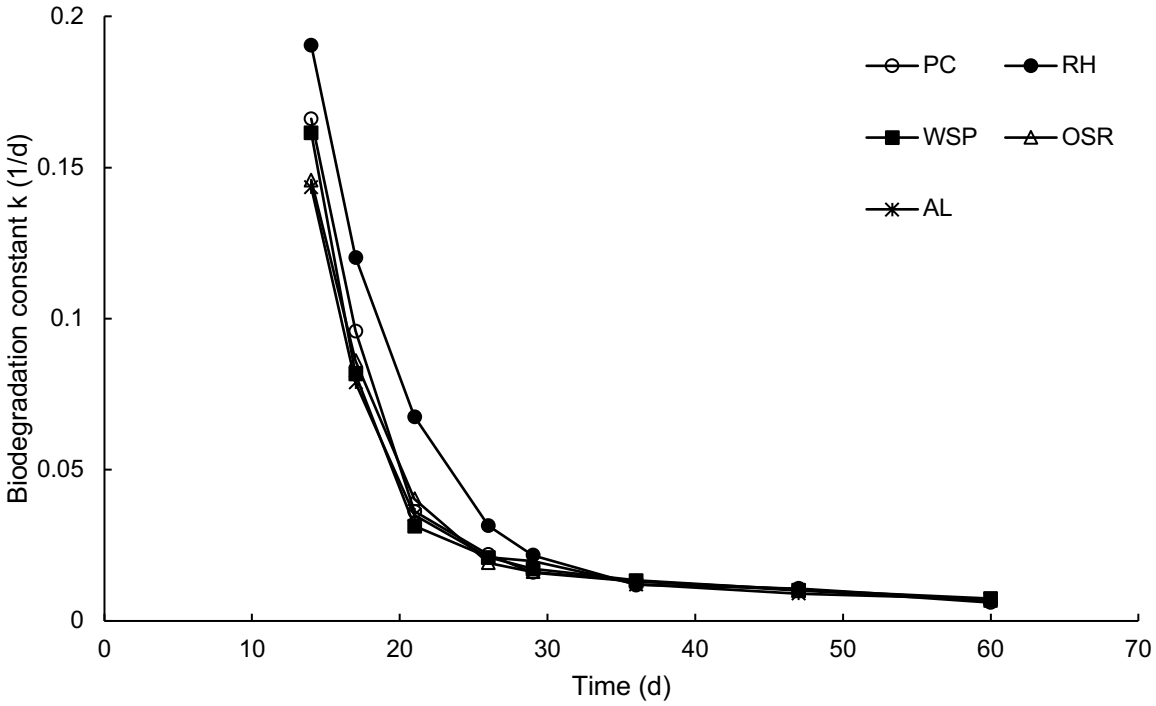

Figure 5-8. The degradation capacity in functions of methane productions during the AD process.

5.3. Conclusions

Table 5- 6. Main findings from Chapter 5.

Biomass	HTC Temperature (oC)	Hydrochar yield (%wt)	C recovery (%)	equilibrium pH	Electrical conductivity (μS/cm)	Maximum biogas production rate (mL/g/d)	Cumulative gas production (mL/g)	Average methane content (%)
Rice Husk	250	61	78.21	4.81	56.4	1.06	47.3	73.3
Wheat straw pellets	250	53.9	76	3.96	143.15	1.81	68.2	76.1
Oilseed rape pellets	250	45.1	68.22	8.93	1401	1.8	70.7	76.8
Alkali lignin	250	85.6	79.78	5.09	218.45	1.85	74.2	74.6

In this study, three agricultural residues and a component of lignocellulose were investigated their suitability for the hydrothermal carbonization and the role of resultant hydrochar on anaerobic digestion of sewage sludge. Our study found that chemical properties and structure of hydrochar were attributed to the original biomass. The solid yield increased as the lignin content of biomass increased. All the hydrochars have relatively high heating value. Hydrochar derived from biomass with high silica content has lower carbonization degree and the presence of silica inhibited the HTC process by shielding carbon from biomass to hydrochar. This study also found that all the hydrochars have considerately high electrical conductivities. Meanwhile, it was shown that the aromatization degree of these hydrochars has a positive effect on solubility of organic carbon in hydrochar and its off-site transportation. Overall, hydrothermal carbonization is a sustainable pathway to obtain clean energy in form of hydrochar from agricultural residues. The digestion of sewage sludge was improved by the addition of hydrochar with upgraded methane content up to 76.8%. In addition, the presence of surface functional groups such as phenol and bonding with aromatic structure was contributed to the increment in biogas production. Some surface functional groups can also serve as redox moieties to enhance methane generation by promoting the electron transfer between microorganisms. Yet, from this study it

remains uncertain that the decrement in biogas production after 30 days. Substances such as amine (NH_2) and -OH group might play an important role in regulating methanogenesis process. Pre-treatment and/or activation of the char product is investigated in the next chapter.

6. Effects of activated biochar in biogas production from anaerobic digestion of sewage sludge

6.1. Introduction

Previous sections found that applying biochar to AD under a moderate to high intensity of inhibition may have little effect on methanogenesis. Mumme (2014) found no significant effects of biochar produced from a mixture of paper sludge and wheat husks on methane production at ammonia concentrations ranging from 500 to 5000 mg/Kg. Furthermore, comparatively low density of biochar may result in uneven homogenization with digestate sludge, particularly in a continuous digestion system with a large reaction volume, which might induce foaming and clogging. Metal doping on biochar could be a viable technique for addressing this challenge. In addition to that, application of biochar in real systems has proven time-consuming and increased processing cost due to separation costs, especially for powdered grades (Sewu, 2020). Hence, the production of magnetic biochar has gained much attentions as the solution as it offers a simpler and easier separation route than other traditional approaches such as filtration. In the meantime, iron oxides have found to improve AD efficiency in terms of lag phase and production rate by mitigating the inhibitory effects of excess H_2S and related harmful chemicals (Li *et al.*, 2007; Su, 2013; Rana *et al.*, 2020). Ambuchi (2018) found that iron oxide nanoparticle supplementation increased biomethane generation by up to 45% during AD of beet sugar industrial wastewater. Similarly, Qin (2017) demonstrated that iron-doped rice straw biochar can increase biomethane production by 11% during AD of municipal solid waste. In general, magnetic biochar is produced by pre- or post-biochar production (Sewu, 2020). The metal ions may attach onto the surface or get into the interior of biomass, and transform into metal hydroxide or nano-metal oxide through pre-treatment. Magnetic

biochar can also be synthesized after the pyrolysis of biomass by evaporative method, heat treatment, conventional wet impregnation method, and directly hydrolyzes (Tan, 2016). In addition to that, the physiochemical properties including Fe_3O_4 loading content, saturation magnetization and thermal stability of the biochars prepared from post-treatment were higher than biochars prepared from chemical co-precipitation of iron oxides onto biomass before pyrolysis (Baig, 2014). To the best of the authors' knowledge, there are limited reports available on biomethane production with different magnetic biochars additions during sewage sludge digestion. Furthermore, there is a lack of understanding of how iron-doped biochar affects alterations and distribution of both organic degradation and metal distribution in AD.

The effect of iron-doped biochar supplementation on sewage sludge digestion was investigated in this study using two types of biochar feedstocks at three loading levels. The influences of magnetic biochar on mobility of heavy metals in digestate of AD and \degradation of organic material during the process were also investigated. Experiments with no additives were also carried out for comparison. This work is expected to reveal new insights into the mechanism of digestion of sewage sludge with magnetic biochar addition and to target an alternate method to sludge treatment.

6.2. Synthesis and characterization of activated biochar

The elemental composition of the magnetic biochars was identified by ultimate analysis (Table 6-1). It is shown that major elements such as nitrogen and carbon in the resultant biochar were decreased. Activation caused a reduction carbon contents of magnetic biochar by 52.3-61.1%. This may be attributed to improved polymerization occurred during activation process, resulting in a reduction of carbon matter in the biochar bulk (Yuan, 2018). Furthermore, the carbon content (23.2%) in the magnetic rice husk biochar is significantly higher than that of magnetic sewage sludge biochar (11.5%). It may be attributed to that lower carbon content in the pristine biochar and its feedstock (Qambrani, 2017; Souza, 2021).Meanwhile, the carbon to nitrogen ratio is characterised as one of the most important parameters to predict mineralization and nitrogen release in the applied environment (Racek, 2020). A higher level of C:N ratio can contribute to higher immobilization by microbes and enhance nitrogen availability (Racek, 2020). In the present study, the C/N ratio of magnetic sewage sludge biochar (8:1) is higher than that of magnetic rice husk biochar (65:1), indicating a higher available nitrogen in the former biochar. Moreover, the oxygen content of both magnetic biochars increased considerably by 46.7-74.3%, and the highest oxygen content was 12.3%$_{wt}$ for magnetic sewage sludge biochar. The high oxygen content in magnetic biochar is attributed to increasing O-containing groups on the surface of the resultant Char (Hao, 2017; Li, 2020). Furthermore, our results showed that the hydrogen content of the pristine biochars and both magnetic biochars remained at similar levels, ranged from 1.24% to 1.57%.

The oxygen to carbon (O/C) ratio is an indicator for biochar's stability. This study observed higher O/C ratios for both magnetic biochars (1.07 for MSW and 0.41 for

MRH) than the pristine biochars (0.22 for SS and 0.05 for RH), indicating improved stabilities by post-treatment. Meanwhile, the hydrogen to carbon (H/C) ratio of biochar over 0.7 is recognized as non-pyrolytic chars or pyrolysis deficiencies (Racek, 2020). In the present study, MSS biochar has the highest H/C ratio of 0.13, indicating that this activation method led to a high degree of mineralization and formation of non-pyrolytic chars from sewage sludge granule (Özçimen & Ersoy-Meriçboyu, 2010). Furthermore, impregnation can introduce external hydrogen atoms to biochar through the associated interaction of activate hydrogen atoms in functional group, and further transform into intra- and inter-molecular hydrogen bonds (Sun, 2013; Xiao, 2018).

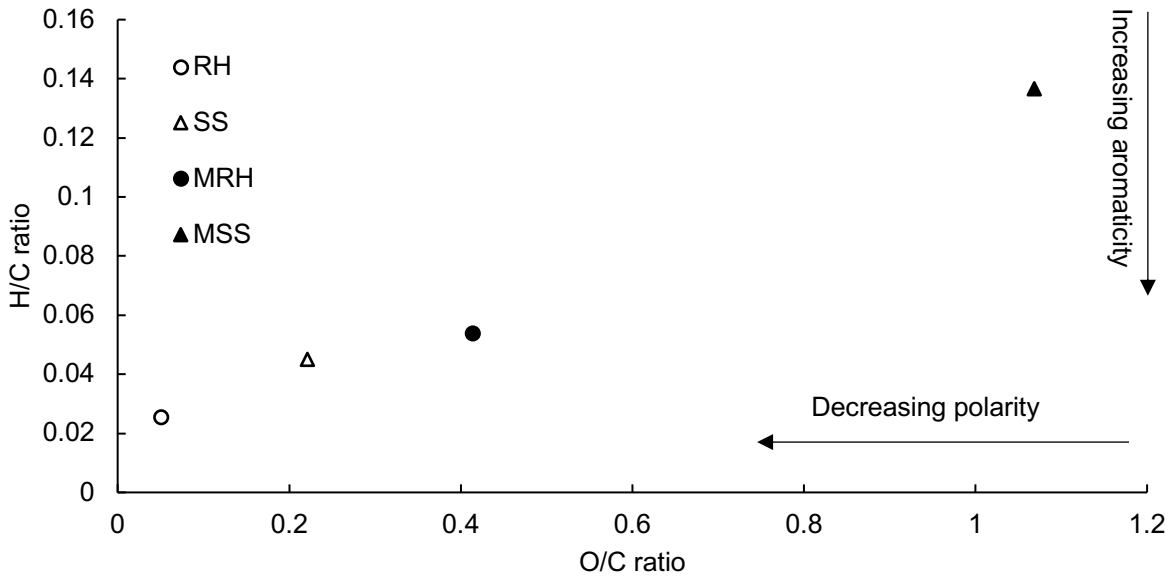

Figure 6-1. Van Krevelen diagram of activated biochars and the pristine biochars.

The molecular structure of biochar and size of aromatic cluster in biochar can be estimated on the basis of their H/C ratios (Xiao, 2016). According to that, the size of aromatic clusters in RH and SS biochar were calculated to be approximately 100x100 and 50x50 benzene rings in a rectangular arrays, which MSS and MRH biochars have smaller aromatic clusters (a 13x13 rectangle with a composite and stratified

microcrystalline structure for MSS biochar, and a 40x40 turbostratic rectangle aromatic cluster structures for MRH biochar). The corresponding calculated aromatic cluster size of these magnetic chars is 3.20 and 9.84 nm, respectively. These results suggest that impregnation-pyrolysis process can cause shrink of the aromatic cluster, which may be the result of Stone-Wales transformations. The Stone-Wales transformation can lead to the breakage of the rotated bond and the uniform deformation of atoms, resulting in changes of cylinder-like pattern (Song, 2006).

The metallic components of all biochar samples were analysed by ICP-OES, and presented in Table 6-1. RH biochar has a negligible Fe content, whereas MRH biochar has the highest Fe content of 14.54 mg/Kg. Similar results have also observed for SS and MSS biochars. On the other hand, potassium (K) content in MRH and MSS biochars was increased by 71% and 60%, respectively. This may be attributed to a small amount of organic carbon remained in the pristine biochar undergone secondary-pyrolysis, resulting in accumulation of ash during activation process. Similar trends were observed from phosphorus content in both magnetic biochars with values of 0.53 and 5.40 mg Kg^{-1} for MRH and MSS biochar, respectively. Therefore, our results implied that magnetic biochar derived from rice husk and sewage sludge suppressed potassium and phosphorus releases, which can potentially enhance ion exchange capacities.

Apart from this, zinc (Zn) and copper (Cu) contents were dramatically decreased after activation, where null or little (0-0.48 mg Kg^{-1}) was detected in both magnetic biochars. Similarly, MSS biochar has lower lead (Pb) concentration than SS biochar. While, the lead, zinc and copper concentrations in SS biochar reached to 201, 835.7 and 255.2

mg Kg^{-1}, which exceed the WHO recommended safe limits for soil, plants and microorganisms (Kinuthia, 2020). The decrement of heavy metals in magnetic biochar from activation indicated that the impregnation-pyrolysis can significantly reduce potential toxicity of heavy metals and ensure the safety of magnetic biochar for its further application. The aforementioned results also suggested that using iron hydrochloride as magnetic precursor is a commendably green approach to generate magnetic biochar and alleviate toxic tendencies, therefore prevent secondary pollution when employed in aqueous environments or anaerobic digestion applications.

Table 6-1. Elemental compositions and ion concentrations of the pristine biochars and the resulting biochars.

	Elemental composition (wt%)					Ion concentration (mg/Kg)						magnetic susceptibility ($x10^{-6}$ m^3/kg)
	N	C	H	O	S	P	K	Pb	Zn	Fe	Cu	
RH	1.04	48.69	1.24	2.47	-	0.1	0.39	-	23.58	-	5.4	0.90
SS	3.75	29.58	1.33	6.55	-	2.29	0.34	201	835.69	-	255.22	2.55
MRH	0.36	23.22	1.25	9.61	-	0.53	1.35	0.00	0.00	14.54	0.0001	38.42
MSS	1.41	11.5	1.57	12.29	0.18	5.40	0.85	0.02	0.04	10.29	0.482	1.98

*Modified dry ashing followed by ICP-OES. Results are based on the mean of duplicates of each case.

The ability to remove magnetic biochar from the liquid phase was investigated using mass specific magnetic susceptibility analysis (Table 6-1). In particular, magnetic susceptibility is characterised as the indicator of the extent of a magnetized substance when in an external magnetic field (Sewu, 2020). It should be noted that ferromagnetic materials exhibit strong magnetic properties when the externally applied magnetic field is reduced, whilst paramagnetic materials may lose their magnetic properties (Morrish, 2001; Skomski, 2010). In the present study, the mass magnetic susceptibility of MRH

biochar was significantly increased from 0.89x10^{-6} m^3 Kg^{-1} to 38.42 x10^{-6} m^3 Kg^{-1}. The increased magnetic susceptibility can be explained by the formation of magnetite during the iron doping process (Han, 2015). This results are in line with a study by Zhao (2019) that the total magnetic susceptibility of magnetic wheat straw biochar produced at 500^{o}C was 26.5 x10^{-6} m^3 Kg^{-1}. On the other hand, the magnetic susceptibility experiences a contrary variation with a change in feedstock type. Sewage sludge biochar exhibit paramagnetic behaviours with a magnetic susceptibility of 2.55 x10^{-6} m^3 Kg^{-1}. While MSS biochar showed a 29.1% decrease in mass magnetic susceptibility. As aforementioned, SS biochar is characterised by higher metal contents, and can favour Fenton-like reaction or ozonation by leaching metal ion especially iron to the solution during impregnation process, thereby resulting in reduced magnetic susceptibility.

Extensive studies have reported that surface functional groups of magnetic biochar can be served as active moieties during biodegradation process (Klüpfel, 2014; Yi, 2019). Functional groups on the surface of magnetic biochar are also important for magnetic biochar catalytic activity (Yaashikaa, 2020). The presence of carboxylate and phenolate functional groups on biochar surfaces may alter the redox potential via electron mediated transformation (Sun, 2017), influencing the cation exchange capacity (Mia, 2017). Thus, it is hypothesised that the impregnation-pyrolysis can alter the surface functionality and cause the appearance of new bands on the surface of the resultant biochar samples. The surface functional groups of all magnetic biochar samples were examined by the Fourier transform infrared (FTIR) spectra in the present study (Figure 6-2). Peaks identified to functional groups in the spectra: O-H (3200-3500 cm^{-1}), C-H$_n$ (2850-2918 cm^{-1}), C=O (1600 cm^{-1}), C=C (1455 cm^{-1}), C-O

(1030 cm^{-1}) and Fe-O (700-880 cm^{-1}) (Schwanninger *et al.*, 2004; Saha *et al.*, 2019; Wang *et al.*, 2021). Noticeably, the peak at 3415 cm^{-1} of the broad adsorption band O-H was strengthened in both magnetic biochars as compared to the pristine biochars, which may be associated with the addition of metal oxides (Liu, 2019). Furthermore, MSS biochar has more identical O-H functional groups than that of MRH biochar. The vibration of carbonyl C=O band at 1648 cm^{-1} were also observed in both magnetic biochars. The intensity of the C=O group was obviously increased in magnetic biochar derived from rice husk, associating with the transformation of O-containing groups during activation process (Zhang, 2019). In addition, bands for C-H at 1434 and 875 cm^{-1} disappeared after Fe impregnation, whereas an aromatic band of C=C at 1630 cm^{-1} appeared in MRH biochar. This can be explained that the pristine chars used in this study undergone a secondary pyrolysis, and resulted in a crack of aliphatic chains and the formation of char with condensate carbon structure. Our results are in line with a study by Devi and Saroha (2014) who investigated the surface functionality of zero-valent iron magnetic biochar derived from the paper mill sludge. They reported that polymerization and carbonization of biochar occurred during the synthesis of magnetic biochars, resulting in the decomposition of C-H bonds and formation of aromatic structure clusters.

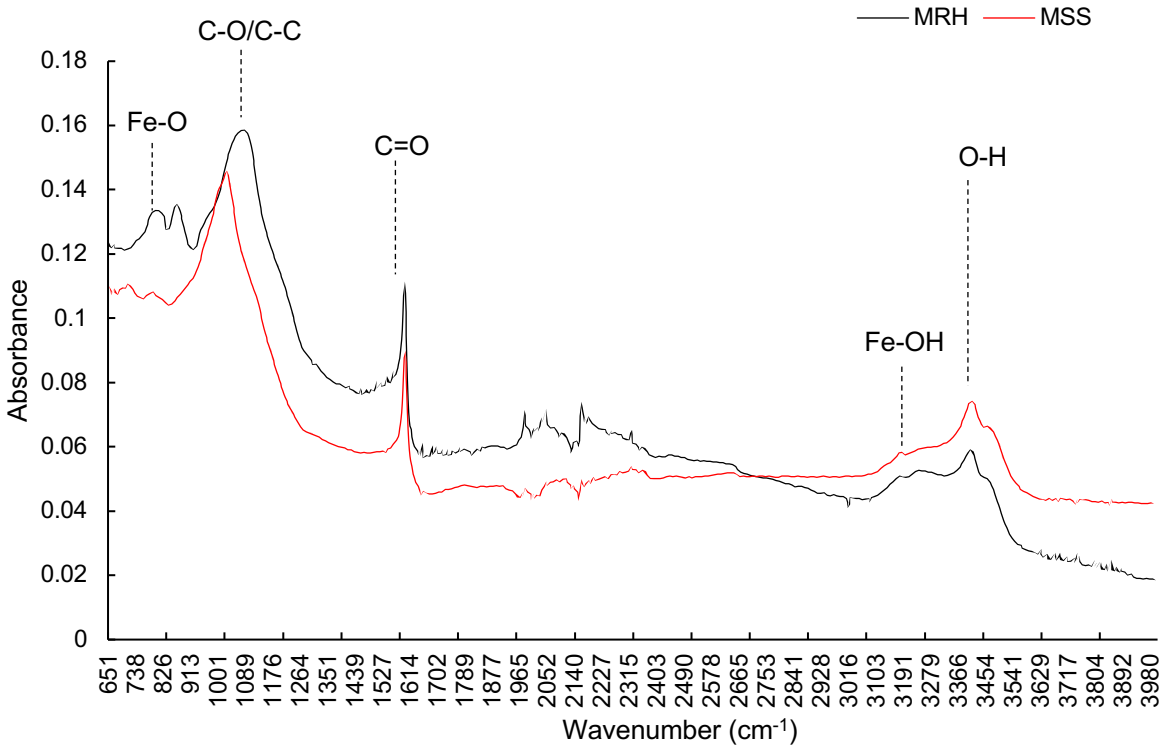

Figure 6-2. FTIR spectra of biochar MRH and MSS.

Meanwhile, the peak at 3308 cm^{-1} corresponds to the stretching frequencies of Fe-OH bonds (Kumar, 2017), which was found in both magnetic biochars. This may be attributed to the decomposition of hydroxyl group and its further reaction with iron ion, resulting in the formation of new chemical bonds (Zhou, 2021). However, peak at 750 cm^{-1} assigned to Fe-O groups was only detected on the spectra of MRH biochar. Fe-O stretching bond of Fe_3O_4 at 470 cm^{-1} was also observed in the spectra of MRH biochar (Devi & Saroha, 2015), which is compatible with its highest magnetic susceptibility of 38.5 cm^3/Kg. Furthermore, asymmetric and symmetric vibrations at 1536 and 1330 cm^{-1} were exhibited in MRH biochar, which may be due to the conjunction between iron oxides and nitro compounds (Godlewska *et al.*, 2020). Thus, these abovementioned difference between the spectra of MRH biochar and MSS biochar showed that MRH biochar contained more ferromagnetic properties than MSS

biochar. The current activation method could also lead to new appearance of Fe-O-C chemical bond between the iron species and carbon components of the bulk biochars (Wang *et al*., 2017). Meanwhile, the intensity and diversity of most surface functional groups in MRH biochar were more stronger than that of MSS biochar. Iron species can conjunct with carbon in a small area during the impregnation phase, and be carbonized as small nanosheet (Wang, 2017). The iron oxides were then formed and catalysed the bulk biochar into a graphene-like structure. The functional groups such as -OH, -COOH, -NH2 and -C=O were conjoined with iron oxides on the surface of biochar through condensation reactions (Peng, 2014; Wang, 2017).

To further confirm the iron chemical state and the phase structure on the surface of biochar after Fe impregnation-pyrolysis, X-ray diffractometry (XRD) analysis was conducted for magnetic biochar and the pristine biochars. According to XRD patterns (Figure 6-3), strong and sharp peaks were observed for both magnetic biochar, implying the iron oxides were well crystallized on the biochar matrix (Zhang *et al.*, 2013). While negligible crystalline peak was presented from the diffraction pattern of the pristine biochar, indicating the amorphous nature of the bulk biochar. Except from, silica peak was marked on the pristine biochar. It can be explained that silica is a key component of the mineral portion of lignocellulose materials and would remained in the biochar matrix during pyrolysis process (Mullen, 2010). The peaks which corresponded to the planes of Si-O-Si were also exhibited for MRH biochar, which may be attributed to the presence of iron oxide promoted the formation of Si-O-Si crystalline phase during pyrolysis process. These results are in line with previous study reported that SiO_2 is the dominating crystalline phase in magnetic biochar through similar magnetic modification process (Yang, 2019).

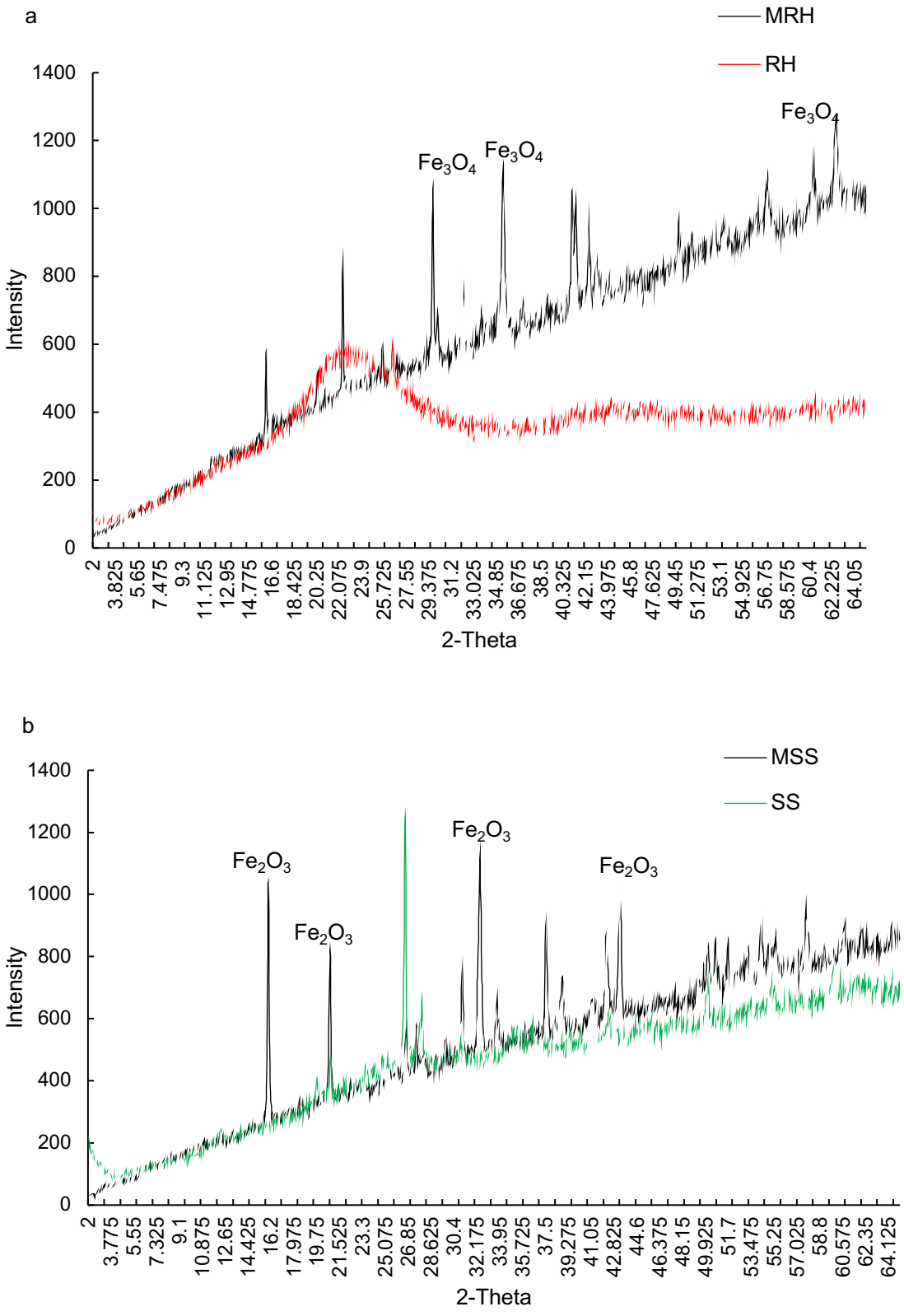

Figure 6-3. XRD patterns of (a) biochars RH and MRH and (b) biochars SS and MSS.

In addition, the primary peaks in MRH biochar were identified to be magnetite (Fe_3O_4) as the major crystalline phase at 35.25°, 42.9°, 56.9° and 62.4° (Dastgheib *et al.*, 2014). It has shown that these peaks were ascribed to the (220), (400), (422) and (440) planes and represented a face-cantered cubic inverse spinal structure of crystalline magnetite (Alam *et al*., 2020; Campos *et al*., 2019). Noticeably, a deviation from plane 400 to 440 was exhibited, which may be attributed to a partial transformation of magnetite to maghemite (γ-Fe_2O_3) (MacHala, 2011). Supposedly, the maghemite phase contains cations in two non-equivalent crystallographic sites, which should have few extra peaks at 23.77° (210) and 26.10° (211) as compared to crystalline Fe_3O_4 (Kim *et al.*, 2012; MacHala *et al.*, 2011). However, in the present work, these planes were not observed in MRH biochar. Similar phenomena were reported in previous literature (Alam *et al*., 2020; Kim *et al.*, 2012). Furthermore, these XRD results are in line with previous FTIR study. The absorbance of Fe-O bonds for magnetite or maghemite was observed in the FTIR spectrum of magnetic rice husk biochar. Therefore, transformation of $FeCl_3.6H_2O$ into iron oxides on the surface of RH biochar during impregnation-pyrolysis process can be explained by the following reactions.

$$FeCl_3 + 3H_2O \rightarrow Fe(OH)_3 + 3HCl$$

$$Fe(OH)_3 \rightarrow FeO(OH) + H_2O$$

$$6FeO(OH) + H_2 \rightarrow 2Fe_3O_4 + 4H_2O$$

$$6FeO(OH) + 4CO \rightarrow 2Fe_3O_4 + 4CO_2$$

$$6FeO(OH) + 4C \rightarrow 2Fe_3O_4 + 4CO$$

$$2FeCl_3 + H_2 \rightarrow 2FeCl_2 + 2H_2O$$

$$FeCl_2 + H_2O \rightarrow Fe(OH)_2 + HCl$$

In contrast, the diffraction peak at 2θ of, 21.12° in MSS biochar was corresponded to the (104) plane, which was also in good agreement with standard values for hematite (JCPDS No. 33-0664) (Chun *et al.*, 2010). It should be noted that hematite can have a weak ferromagnet or a canted antiferromagnet properties through the thermal treatment (MacHala *et al.*, 2011). Furthermore, hematite loses its magnetic ordering and behave as a paramagnet at temperature over 676.8°C (Zboril *et al.*, 2010). In our study, impregnation-pyrolysis was conducted at 550°C, which may result in the partial losses of magnetic properties for magnetic sewage sludge. Another possibility is that maghemite (γ-Fe_2O_3) cannot exist at a sintering temperature of 500°C, and convert to hematite (α-Fe_2O_3) when the pyrolysis temperature reached to 400°C (Zhang *et al.*, 2008). Meanwhile, lower intensity of these peaks was observed for MSS biochar, suggesting that as-prepared iron oxides with SS biochar were worse crystallized and had a lower hematite contents compared to the pristine biochar (Qin *et al.*, 2017). It can be explained by increased carbon burn-off caused by the use of highly active Fe during the iron doping procedure (Wurzer & Mašek, 2021). Meanwhile, non-magnetic iron oxides are identical on the diffraction pattern, but can reduce the magnetic saturation, thereby resulting its ferromagnet behaviours. Hence, theoretically, SS biochar magnetised with $FeCl_3$•$6H_2O$ would have less magnetic properties compared to other magnetic carbonaceous derived from lignocellulosic biomass. In addition, the peaks at 16.75°, 33.12° and 43.3° exhibited for MSS biochar are the characteristic peaks of FeOOH crystallite (JCPDS Card No. 29-0713) (Schwertmann, 1971; Wang *et al.*, 2013). The formation of FeOOH can be related to the hematite-to-goethite transition (Minyuk, 2011). It is well known that goethite can be formed by the hydrolysis of iron chloride via the following reaction (Wang *et al.*, 2013).

$$FeCl_3 + \frac{3}{2}H_2O \rightarrow \alpha - FeOOH + 3HCl$$

$$4Fe(OH)_2 + 2H_2O + O_2 \rightarrow 4Fe(OH)_3$$

$$Fe(OH)_3 \rightarrow \alpha - FeOOH + H_2O$$

Meanwhile, these XRD results for magnetic biochars correspond with findings by aforementioned FTIR analysis, implying that the magnetic biochar was successfully synthesized. The Fe-OH bond from goethite was presented in MSS biochar, but the Fe-O bond link from magnetite was presented in MRH biochar. These findings demonstrated that the formation of magnetite with high mass magnetic susceptibility worked well with rice husk biochar and ensured satisfactory separability from the digestate.

The pH of all biochar samples was measured in deionised water at two time points: 1 hour and 24 hours (Table 6-2). The pristine biochars showed a pH ranging from 7.42 to 9.86, indicating its alkalinity nature. RH biochar has the highest pHs of 9.54-9.86, attributed to presences of alkaline carbonates, alkali earth metals and organic anions in the ash of biochar (Li *et al*., 2016). The pHs of SS biochar ranged from 7.4 to 8.0. Whereas MRH and MSS biochars have lower pH of 2.25 and 2.4. Similar observation was reported by Mohubedu (2019) that magnetic biochar, from acorn cotyledon biomass by using similar iron precursor and modification treatment, has an acidic property with a pH of 4.3, indicating the magnetisation of biochar can change their pH by altering the surface charge.

Table 6-2. pHs and ECs of activated biochars and the pristine biochars.

Biochar	pH	EC (μS/cm)	pH	EC (μS/cm)
	1 hr		24 hr	
RH	9.82	118.7	9.49	145.4
MRH	2.255	2560	2.02	2975
SS	7.43	47.25	8.03	79.5
MSS	2.46	5465	2.3	3585

In this work, electrical conductivity (EC) were measured in two different approaches including water soluble EC and in proportions of compression. The electrical conductivity of the pristine biochar fluctuated widely from 47.25 to 145.4 μS cm^{-1}, indicating electrical conductivity was greatly associated with the raw material (Lehmann, 2007). This may be due to that the degree of carbonization of biochar can highly influence electrical conductivity of the bulk biochar. Gabhi (2017) reported that carbon content of biochar increased from 86.8 to 93.7 wt%, resulted in increased electrical conductivity from 2.5 $x10^{-4}$ to 399.7 S m^{-1}. It has also been reported that differences in the EC of biochar can be related to differences in their ash content (Singh *et al.*, 2017). In addition, electrical conductivity of biochar with high soluble salt content can be affected by the equilibration time. In theory, longer equilibration time lead to higher EC values (Singh *et al.*, 2010). This has been confirmed by increased electrical conductivity for both pristine biochar when the equilibration time increased from 1 hour to 24 hours.

Both magnetic biochars have significantly greater electrical conductivity with values of 2560 and 5465 μS cm^{-1}. It indicates that the formation of iron oxides on the surface of magnetic biochar may provide more active sites for the accessibility of pseudo-

capacitance to the electrolyte ions and improve the electrochemical reactions (Liu *et al.*, 2015). Meanwhile, MSS biochar presented higher conductive behaviour with a 54-fold increase in electrical conductivity from 47.25 to 5465 μS cm^{-1}, while the EC value of MRH biochar was 22-fold higher than the pristine biochar. It has been reported that enhanced EC of magnetic biochar is related to more oxygenated functional groups such as hydroxyl, carbonyl and carboxylate formed during magnetization modification process, leading to the enhancement of the negative charge density on the surface of magnetic biochar (Silva *et al.*, 2020). As aforementioned, magnetic biochar has more identical oxygen-containing groups than the pristine biochar, which are characterised as the redox-active moieties to enhance electron transfer. Furthermore, active moieties on the surface of magnetic biochar are dependent on pH. It has been reported that lower pH can reduce the dissociation and association of surface functional groups, resulting in the changes on the surface charge of the bulk biochar (Lu *et al.*, 2020). What is more, EC value measured in water is proportional to the quantity and nature of salts. Theoretically, higher salinity can improve the ability to conduct an electrical current. In our study, both magnetic biochar are acidic, implying the increment of electrical conductivity were mainly attributed to the active redox moieties on its surface. Electrical conductivity of biochar are also reported to associate with separation distances of carbon particles and their average size (Voet, 1964; Sánchez-González *et al.*, 2005). It has found that electrons were able to jump the gaps between spaced carbon aggregates via electron tunnelling (Sánchez-González *et al.*, 2005; Wendt, 1988). Therefore, the electrical conductivity of magnetic biochar samples were evaluated under a wide range of applied pressure values in the present study. Both biochars were exhibited an increasing trend of the EC value as the applied pressure

increased. EC of MRH biochar increased sharply at higher applied pressure from 3000 to 5000 bar owing to a closer contact of biochar particles (Hussain *et al.*, 2001).

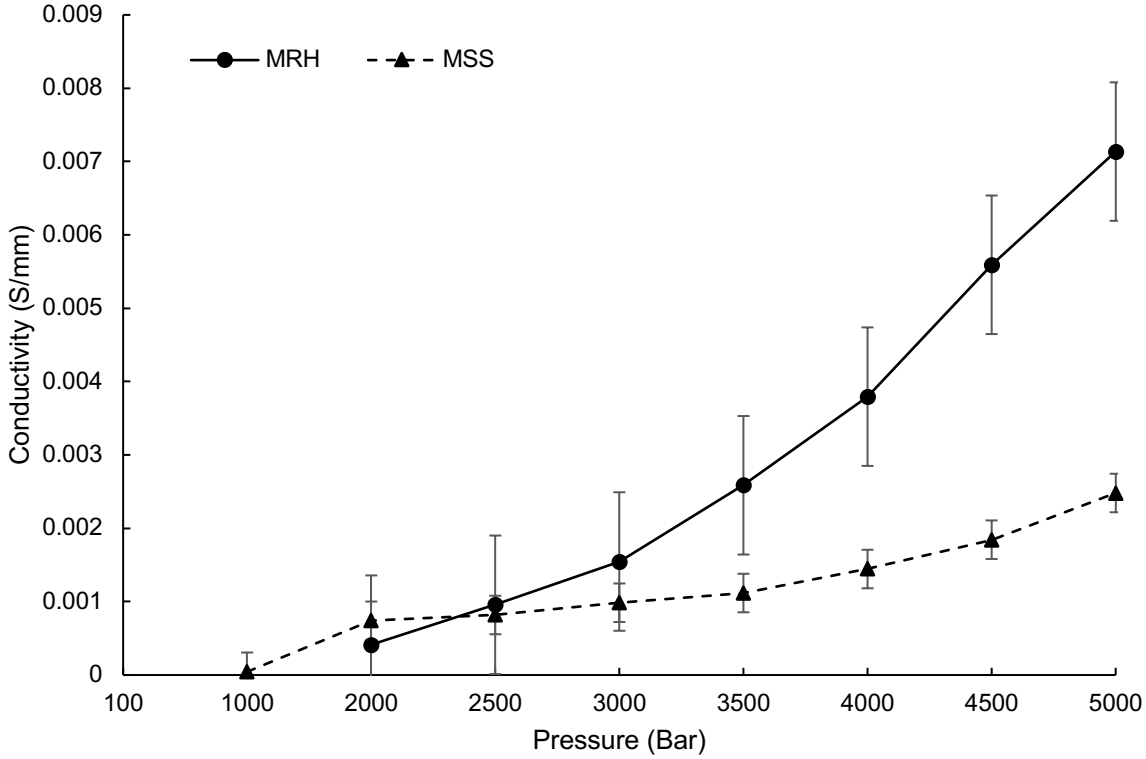

Figure 6-4. Electrical conductivity of biochar MRH and MSS in proportions of applied pressure. Results of mean (n=3).

6.3. Effects of activated biochar on gas production and biomethane yields

The biogas production rate (mL/d) and cumulative biogas yield (mL/g VS) from sewage sludge digestion with additions of 0.2-1.0% magnetic biochars and 0.2% pristine biochar are showed in Figure 6–5,6. All groups started producing biogas from the first day onwards, with no notable lag, which might be attributed to the presence of ruptured microbial-originated extracellular polymeric substances (EPS) in substrate (activated sludge) (Carrère *et al.*, 2010). Throughout the digestive process, two peaks can be observed in each group. The first peaks in the daily biogas profile appeared on day 2.

At this stages, most of magnetic biochar added reactors have greater daily gas productions ranging from 12.16 to 14.51 mL/d as compared to reactors with addition of SS and RH biochars. The improved gas production rate was attributed to facilitated utilization of organic matters by Fe(III)-reducing microorganisms with the presence of goethite on magnetic sewage sludge (Bird *et al.*, 2011; Haas & Dichristina, 2002). Meanwhile, soluble iron concentrations play important role on magnetic biochar's effect on AD. Many studies have reported that increasing iron concentration can enhance biogas production by nearly 50% (Qin *et al.*, 2017; Zhang *et al.*, 2012). MRH biochar has the highest Fe content among the used biochar, therefore, leading to an increase in daily gas production. In the meantime, our results showed that the addition of SS and RH biochar can cause inhibition in gas production at early stage of fermentation, resulting in 11.7% (RH biochar) and 34.6% (SS biochar) decreases as compared with the control group (12.53 mL/d). The addition of MSS biochar has also resulted in a mild decrease in daily gad production (10.30 mL/d) by 17.8% at the same stage. Then, a sharp drop in daily gas production by day 8 was observed in all treatment group. The abrupt drop in biogas generation can be due to acids acclimations, resulting in a drastic pH decrease and inhibiting microbial activities (Rana, 2020). After that, daily gas production of each group was able to rebound and followed a trend at this stage: magnetic biochar > pristine biochar ≅ the control. Following then, the daily biogas production of each group gradually reduced until no biogas was detected. These results indicated that the addition of magnetic biochar greatly enhanced daily gas production as compared with the pristine biochar and the control.

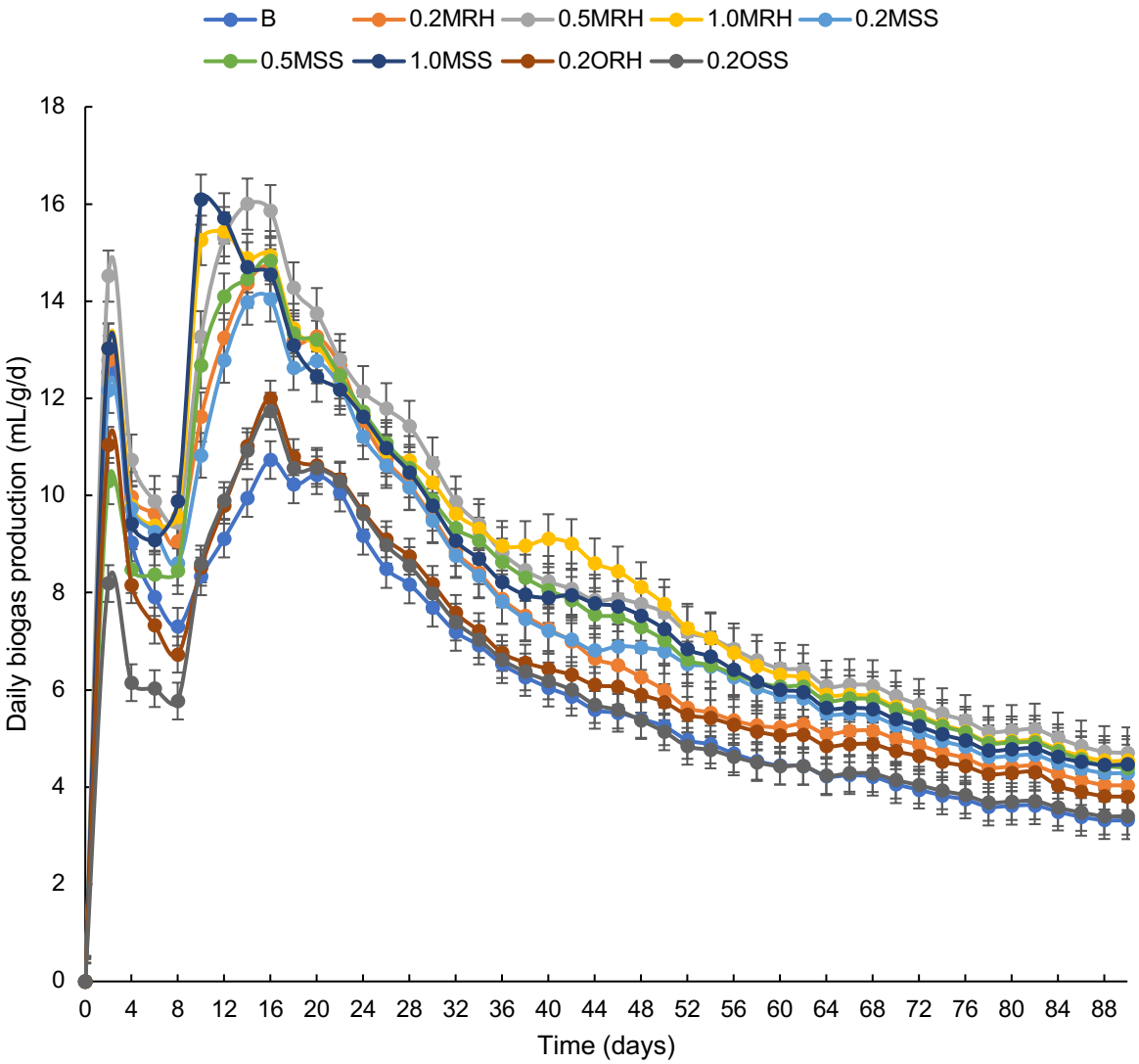

Figure 6-5. Biogas production rates of biochar-treated reactors and the control. “0.2, 0.5,1.0” stands for the biochar dose of 0.2, 0.5, 1.0%wt; “ORH,OSS” stands for the pristine biochar RH and SS.

The cumulative biogas production from all magnetic biochar treatments ranged from 1022 to 1192 mL/g, while the total gas yield from pristine biochar amended reactor were 964.15 and 862.07 mL/g for RH and SS biochar. Among them, the addition of MRH biochar at dose ratio of 0.5% resulted in greater total gas yield of 1192.29 mL/g. Several studies have shown that magnetite has lower redox potential (-0.314 V) and can be used as electron conduit to stimulate direct interspecies electron transfer (DIET)

between syntrophic bacteria and methanogens to enhance biogas production (Viggi *et al.*, 2014; Zhan *et al.*, 2021). As such, the increased gas yield of MRH biochar-amended group might be attributed to the presence of magnetite on biochar surface. While total gas yield increased as the dose ratio MSS biochar increase, with values of 1087.30, 1114.91, and 1133.08 mL/g for 0.2%, 0.5% and 1.0% MSS biochar, respectively. The difference in electrical conductivity and mineral content of magnetic biochar may provide a possible explanation as to why MSS biochar used in this study has different effect on gas production. It is known that redox potential and pH are major drivers of microbial systems (Husson, 2013). However, Saleem (2018) used acidic biochar (pH 4.8) which reduced methane fermentation. Biochar's electron-donating capacity has also been suggested to affect methanogenesis (Viggi, 2017). Therefore, this suggest that magnetic biochar hold a high redox potential, and is more effective at driving sludge-based biomethane fermentation toward a more efficient energy conversion spectrum by manipulating microbial activities. To confirm this, future studies should be directed at characterizing methanogens using of differing pH values, electron-donating capacities and mineral or carbon composition.

During the 90-day AD experiment, all treatments continuously produced biomethane. All magnetic biochar amended bioreactors showed higher biomethane yields (853.20-1020.61 mL/g for MRH biochar and 893.90-953.03 mL/g for MSS biochar) than reactors with RH (822.09 mL/g) and SS biochar (689.84 mL/g), and the control group (718.42 mL/g). The addition of MRH biochar at 0.5% tended to increase the cumulative methane production by 42%, followed by a MRH biochar dose at 1.0% (31.6%) and at 0.2% (18.8%). This suggests a possible dose-responsive relationship of an optimum of 0.5% of MRH biochar additive is efficient for optimal methane production. Similar

trend was also observed in MSS biochar amended groups that the optimum MSS biochar dose was 0.5%. Similar results have confirmed magnetic biochar can enhance AD performance by increasing methane production. For instance, Qin (2017) reported that applying 3.2% magnetic rice-straw biochar improved methane production by 11.69% during AD of municipal solid waste slurry. Wang (2021) reported up to 38.1% increase in methane yield from dairy wastewater digestion by supplementing 30mM of the Fenton sludge generated biochar. As previously noted, magnetic biochar can boost biogas and biomethane productions by interacting with iron oxides on the surface of the biochar, which may operate as a catalyst to stimulate the performance of anaerobic microflora (Krongthamchat, 2006; Qiang *et al.*, 2013; Rana, 2020). In addition, magnetite has proven to facilitate the secretion of extracellular polymeric substances (EPS) and serve as electron mediator to conduct electron exchange between syntrophic bacteria and methanogens to improve the CO_2 reduction for methane generation (Viggi *et al.*, 2014; Wang *et al*, 2019; Zhong *et al.*, 2020).

Noticeably, MSS biochar supplementation at 0.2% has yielded slightly higher methane production than MRH biochar additive at the same dose (6.12% increase). The difference in cumulative methane yield of these two magnetic biochar amended groups might be attributed to biochar with presence of different iron oxides. Goethite presented in MSS biochar can precipitate hydrolysis products of long chain fatty acids (LCFA) in digestion of lipid-rice wastes, therefore facilitating microbial growth and metabolisms (Lalman & Bagley, 2001). On the other hand, iron reduction process can compete with methanogenesis by using H_2 and acetate as substrates, which can lead to decreased methane production (Zhang *et al.*, 2012). Therefore, lower methane production with supplementation of magnetic biochar at 0.2% and 1.0% w/w than a biochar dose of 0.5% confirmed the hypothesis from the perspective of goethite, which could better reflect the selective pressure emphasized by forms of iron oxides. Overall, there are compelling reasons to believe that magnetic biochar has the capacity and applicability to improve the performance of sewage sludge AD.

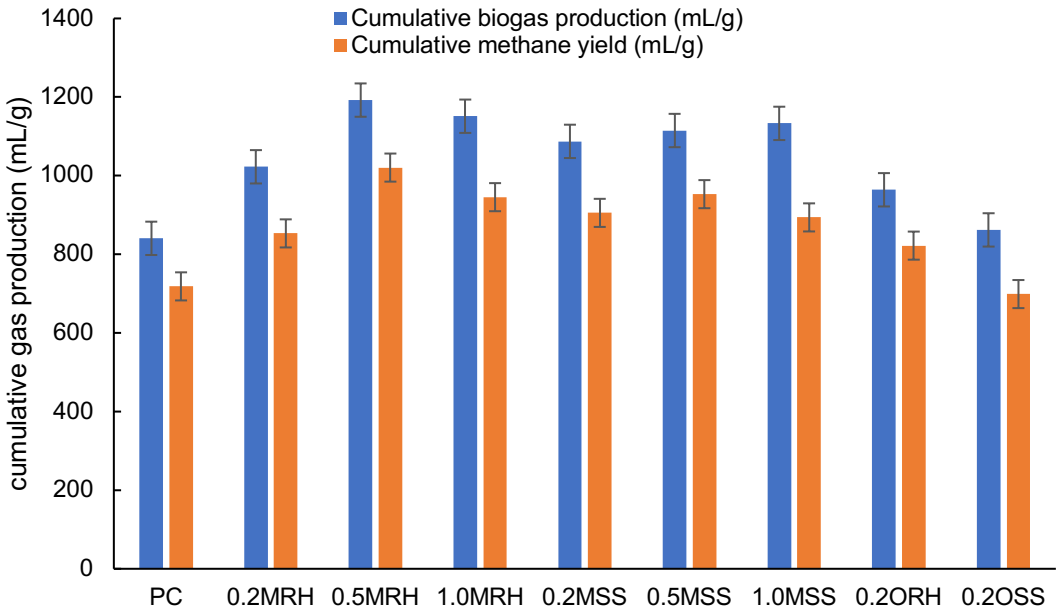

Figure 6-6. Cumulative biogas production (ml/g) and total biomethane yield of biochar-treated reactors and the control.

6.4. Changes in intermediates during AD process

6.4.1. Impacts of biochar on VFAs concentrations

Volatile fatty acids (VFAs) are critical indicators for determining the process stability and metabolic status during the AD process (Lu *et al.*, 2017). As shown in Figure 6-7, there were four major VFAs including acetate, butyrate, valerate, and propionate, with acetate being the most prevalent VFA. The acetic acid content in the control group was higher than treatment with magnetic biochar additives at 0.5%w/w. This may be attributed to the disintegration of the sludge particle and the solubilization of organic materials result in accumulation of acetic acid (Huang *et al.*, 2015). It has been reported that methanogens can use acetic intermediates and convert them to methane with supplementations of biochars (Li *et al.*, 2019), which is compatible with the increased methane in magnetic rice husk biochar and magnetic sewage sludge biochar at a dose of 0.5% w/w. Hence, our results showed that the use of magnetic biochar during sewage sludge digestion can increase the generation and consumption of acetic acid.

However, propionic acid concentrations in treatments with addition of magnetic biochar (11.41 g/L for MSS biochar and 12.45 g/L for MRH biochar) were slightly higher than that of the control group (10.71 g/L). By the end of the experiment, most VFAs were degraded in magnetic biochar amended groups. In contrast, higher contents of acetic acid (2.39 g/L) and isovaleric acid (4.66 g/L) were found in the control group, indicating inadequate VFAs conversion during sewage sludge digestion without supplementation of magnetic biochar. These findings were consistent with the study by Ambuchi (2018) that adding iron-oxide nanoparticles to the AD process

increased biogas and biomethane production rates, while facilitating acetate and propionate utilisation and suppressing hydrogen accumulation, therefore resulting in a higher biogas yield. Hence, our results indicate that the addition of magnetic biochar can alleviated the excessive acidification caused by the formation of VFAs in anaerobic fermentation system, can effectively enhance the buffer capacity of the fermentation system, making the environment suitable for the reproduction of anaerobic fermentative bacterial, and the fermentation process is accelerated.

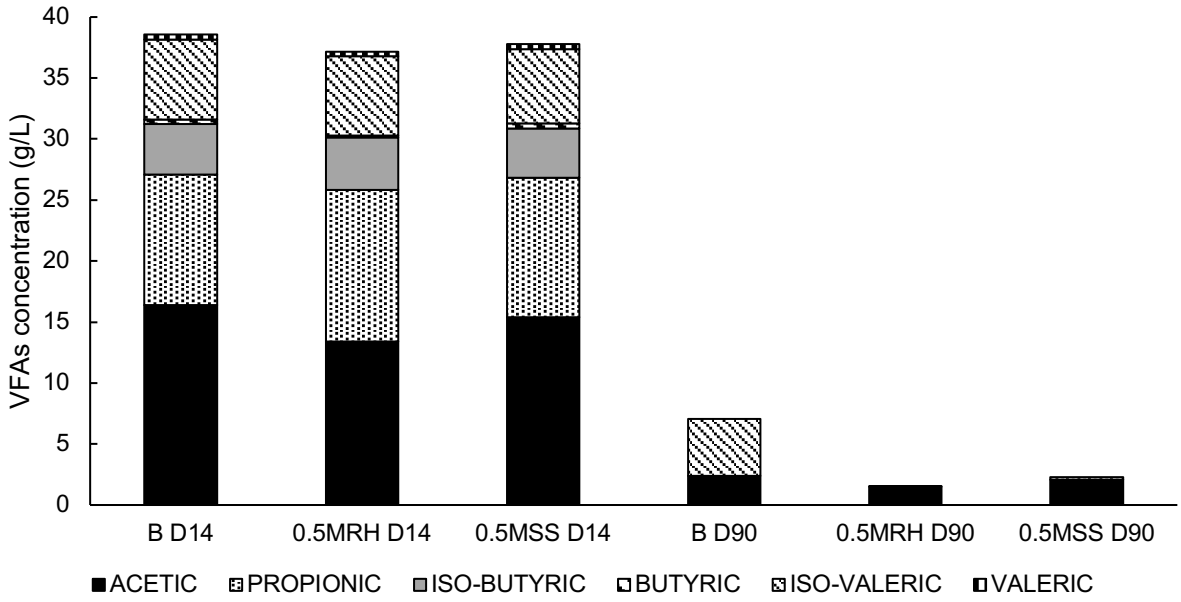

Figure 6-7. Volatile fatty acids (VFAs) degradation during sewage sludge AD.

6.4.2. Variations in ammonium concentrations

Ammonia (NH_3) and ammonium (NH_4^+) inhibition is recognized as a key issue in AD of active sludge, resulting in reduced methane production and reactor failure (Lü *et al*., 2016). This inhibition also has a synergetic effect with acids accumulation (Lü *et al.*, 2013). In this study, the ammonium concentration increased by 54% in the control group at the end of AD process, which can be attributed to the degradation of organic nitrogen to inorganic ammonia (Mutegoa *et al.*, 2020). Meanwhile, ammonium

concentrations in magnetic biochar amended reactors (Figure 6-8) ranged from 3.17±0.04 to 3.85±0.01 g/L, which were substantially greater than the control (2.04±0.02 g/L). Among them, MRH biochar additive at dose of 0.5% resulted in 21.8% increase in ammonium concentration than the control. This may be attributed to the high protonation of functional groups (C=O, C=C) on the surface of magnetic biochar, which conveys a partial positive charge repelling the polar attraction of NH_4^+ ions in AD of sludge (Kizito *et al*., 2015).

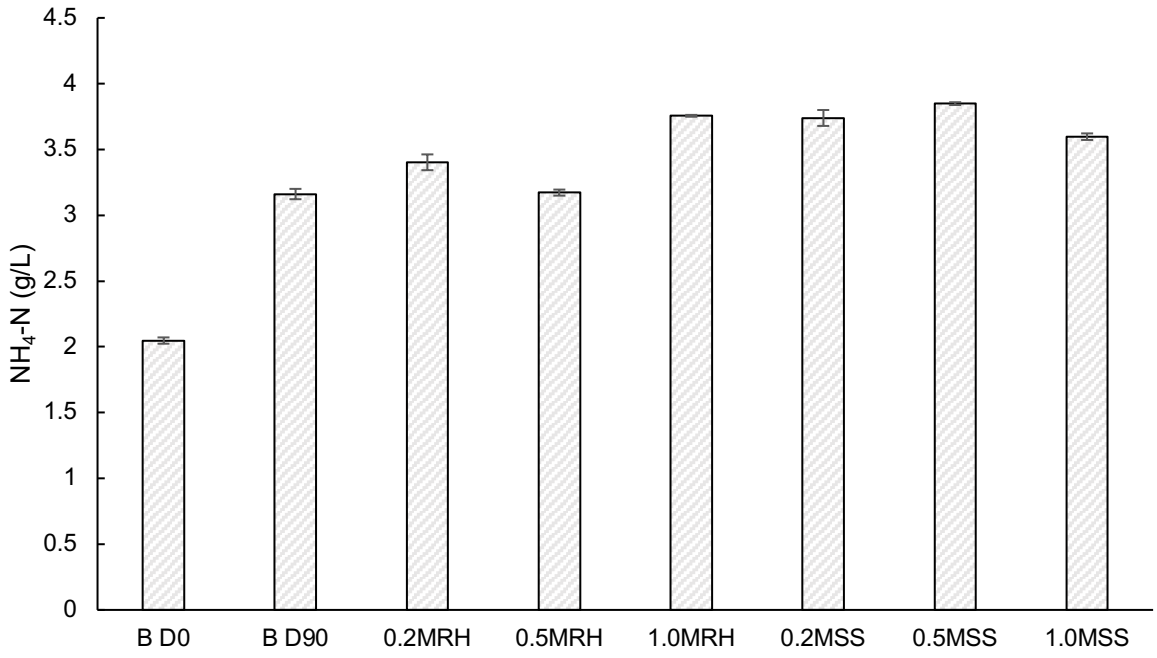

Figure 6-8. Changes in ammonium (g/L) concentrations from magnetic biochar-amended reactors.

Furthermore, it has been reported that biochar addition can improve inoculum degradation and provide more accessible organic nitrogen, hence favouring anaerobic digestion (Jahn *et al.*, 2020). This finding was evidenced by increased methane production in magnetic biochar amended groups in this study. Meanwhile, differences in surface chemistry between MRH and MSS biochar may explain these disparities in the variation of pH and ammonium ion concentration. In addition, magnetite on MRH

biochar has been shown to improve sludge hydrolysis via iron reduction by acting as an electron acceptor (Peng *et al.*, 2018; Weber *et al.*, 2006). In contrast, only hematite was observed on the surface of MSS biochar. The Fe(III) ion in hematite has been identified as a competing candidate for electrons during AD (Qin *et al.*, 2017), which could explain the exacerbated ammonium inhibition observed in this study. Further research is needed to confirm this mechanism.

6.4.3. Distribution of heavy metals during AD process

Heavy metals play critical roles in AD process, as they are required for the establishment and development of anaerobic microbes (Mudhoo & Kumar, 2013). However, relatively large concentrations of heavy metals may affect enzyme structure and have deleterious effects on process performance (Kavamura & Esposito, 2010; Şengör *et al*., 2009). The addition of magnetic biochar appeared to mobilize heavy metals during the AD process (Table 6-3). Total heavy metal concentrations of magnetic biochar amended groups were lower than that of the control group. The digester with MSS biochar addition at a dose of 0.5% resulted in lower total metal level in the fermentation liquor. Previous study found that biochar addition resulted in decreased metal concentration of digestate due to the increased surface area of magnetic biochar (Li *et al*., 2019). It has also been observed that magnetic biochar can adsorb and form compounds with heavy metals via negatively charged functional groups on its surface (Yu *et al.*, 2015). Another possibility is that iron oxides have a positively charged, which can decrease the leaching ability of these heavy metals and stabilize them via oxidation (Villalobos *et al.*, 2014; Ying *et al.*, 2012). Furthermore, MRH biochar at a dose of 0.5%w/w reduced the concentrations of Pb, Zn, Cu, and Fe

by 45, 53, 46, and 45%, respectively, as compared to the control. Noticeably, the capacity of MRH biochar on immobilization of heavy metals (particularly Pb, Zn and Cu) was higher than that of MSS biochar. It might due to the difference in surface complexation between MRH and MSS biochar. Wang (2021) reported that iron oxides with distinct crystal forms performs different functions during AD process. For instance, amorphous iron oxides such as $Fe(OH)_3$ are more efficient as an electron acceptor to cleave large molecules into small ones due to their higher redox potential than crystalline iron oxides (Wang *et al*., 2019). Therefore, above results suggest that the addition of magnetic biochar can mobilize heavy metals during AD process. The potential mechanism may include surface complexation, adsorption and precipitation (Fagbohungbe *et al*., 2017a; Pignatello, 2011; Tan *et al.*, 2015). It is believed that organic matter decomposed into small fraction and released soluble metals which can be adsorbed by magnetic biochar or accumulated in sewage sludge during AD process. In addition, reduced concentrations of soluble heavy metals could be attributed to increased stability of the AD process with supplementation of magnetic biochar (Shen *et al*., 2016). Overall, the results showed that a moderate dose of magnetic biochar during sewage sludge digestion has the ability to immobilize heavy metals and thus promote biogas production.

Table 6- 3. Concentrations of heavy metals in fermentation liquor after digestion and maximum permissible concentrations of potential toxic elements in soil after application of sewage sludge.

	Maximum permissible concentrations in soil (mg/Kg dry soil)*	**B**	**0.5MRH**	**0.5MSS**
Pb (mg/L)	200	0.04	0.04	0.02
Cu (mg/L)	200	0.06	0.05	0.03
Zn (mg/L)	300	0.20	0.18	0.11
Fe (mg/L)	ND	10.73	5.84	5.08

*The limit value were reported in the Sludge (Use in Agricultural) Regulations (Parliament, 1989). ND: none of determination.

6.4.4. Degradation of biomass during AD process

During the anaerobic stabilization process, large amounts of primary and secondary metabolic protein storage polymers were generated and stored in the digestate (Bustamante *et al.*, 2019). Thermogravimetry analysis of digestate provides insight into the transformation during the digestion as well as information on the characteristic variations in composition impacted by different biochar treatments. Gómez (2007) found TGA can be used to monitor the anaerobic stabilization process for municipal solid wastes and waste-activated sludge under mesophilic conditions. Likewise, other researchers reported the feasibility of using TGA to evaluated the organic component conversion of sewage sludge during the digestion process (Font *et al.*, 2001; Gómez-Rico *et al.*, 2005). In this work, proximate analysis for the digestate with different biochar treatments were conducted in triplicates, and its results were presented in Table 6-4. Several biochar amended groups such as 0.2MRH (9.42±0.02%) and 1.0MSS (9.99±0.07%) have higher moisture content than that of the control group (8.38±0.05%). This can be attributed to the increased fibrous structure of the digestate samples with biochar addition, as they tended to hold moisture for a longer period time (Ogwang *et al.*, 2021; Wu *et al.*, 2011). Additionally, the digestate's moisture content increased as the dosage of MSS biochar addition increased. In contrast, the digestate with addition of lower dosage of MRH biochar had greater moisture content. This implies that the capacity of moisture retention depends on the feedstock types of magnetic biochar. Furthermore, the fixed carbon content in magnetic biochar amended groups ranged from 81.81 to 85.63%, which was slightly lower than in the

control (87.25%). While the digestate with MRH biochar addition at dose of 0.5% has the highest content of fixed carbon (89.62 wt%) and the highest methane yield. Such findings can be attributed to the presence of structurally more complicated material, leading to increased vascularization (Bustamante *et al.*, 2019; Gómez *et al.*, 2007). It is also possible that a moderate dose of MRH biochar will improve the structural complexity of digestate, providing extra habitat for microorganism development. Correspondingly, the use of magnetic biochars increased the ash content in the digestate. Furthermore, the ash content increased as the dosage of magnetic biochar increased. The digestate from MRH biochar amended group at dose of 1.0% have higher ash content (9.33%). The observed difference in the ash content is most likely due to variations in the amount of inorganic minerals with a significant catalytic impact as a result of biochar treatment (Bridgwater, 2007). Overall, our results indicate that digestate structure could be affected by biochar in functions of feedstock types. These findings also imply that a moderate dose of magnetic biochar is sufficient to improve the digestate structure and composition during AD of sewage sludge, which may have implications for engineering practise for methane-rich biogas generation.

Table 6- 4. Proximate analysis of digestate obtained from the end of the test.

	Proximate analysis (wt%, db)		
	Volatiles	Fixed Carbon	Ash
B	8.38	87.25	4.36
0.2MRH	9.42	82.83	7.75
0.5MRH	8.45	89.62	1.93
1.0MRH	8.86	81.81	9.33
0.2MSS	8.48	85.64	5.88
0.5MSS	8.65	84.35	7.00
1.0MSS	9.99	81.88	8.13
0.2ORH	8.18	83.58	8.24
0.2OSS	8.24	84.02	7.74

Meanwhile, the big merit of magnetic biochar compared with unmodified biochar is the easily separable nature. This characteristic potentially endows magnetic biochar to be directly used in anaerobic digestion plant rather than worrying leaching of biochar particles that may lead to secondary pollution. It should be noted that during the synthesis process of magnetic biochar, toxic and harmful substances may be introduced or produced. Future works aiming at greener synthesis of magnetic biochar with higher redox activity should be attached with high importance.

6.5. Conclusions

Table 6-5. Main findings from Chapter 6.

Biomass	Modification	Equilibrium pH	Eletctrical conductivity (μS/cm)	Biochar dosage (%wt)	Maximum biogas production rate (mL/d)	Cumulative gas production (mL/g)	Cumulative methane production (mL/g)
Rice Husk	Fe-impregnated	2.02	2975	0.2	14.6	1022.6	853.2
				0.5	14.5	1192.3	1020.6
				1	15.43	1151.2	945.3
	Unmodified	9.45	145.4	0.2	12	964.1	822.1
Wheat straw pellets	Fe-impregnated	2.3	3585	0.2	14	1087.3	905.4
				0.5	14.8	1114.9	953
				1	16.1	1133.1	893.9
	Unmodified	8.03	79.5	0.2	10.9	862.1	698.8

In this work, a novel magnetic biochars with excellent mass magnetic susceptibility were successfully synthesized via chemothermal method. The iron-doping modification promoted the development of oxygen-rich functional groups and favoured the formation of iron oxides on the resultant biochar. Furthermore, effects of these biochars on anaerobic digestion of sewage sludge were evaluated. Both magnetic biochars improved biogas yield and biomethane production. The highest cumulative methane yield (1020.61 mL/g VS) was achieved from digestion with 0.5% w/w MRH biochar supplementation, which resulted in a 42% increase in methane generation. Magnetic biochar also improved AD performance by increasing VFAs degradation, improving heavy metal immobilisation, and promoting ammonium tolerance. Meanwhile, MSS biochar increased the moisture content of the digestate, whereas MRH biochar enhanced the digestate's fixed carbon concentration, indicating an

improvement in the digestate structure and composition. The role of magnetic biochars as electron donor-acceptor and providing more active sorption sites can be considered as the two main functions during AD process. The findings proposed that magnetic biochar can be served as a promising and low-cost additive on sewage sludge digestion. Although this study used sewage sludge from a local WWTP, future research should include tests done in continuous mode, which is more similar to a real-world scenario, to see if magnetic biochars' capacity to improve system stability and performance is maintained.

7. Conclusions

7.1. Overview

The aims of this thesis was to investigate effects of biochar and hydrochar on the AD potential and process stability, as well as the potential mechanisms of biochar on altering biogas and methane productivities. Feedstocks and production conditions most suitable for biochar/hydrochar application were assessed on the basis of volumetric biogas productions and experimental effects of biochars' ability on mitigating intermediates inhibition and buffering capacity. The results from this research are essential for practice use for adjusting digester design and choosing suitable feedstocks to produce biochar with optimal adsorption capacity and well developed surface functionalities. The use of biochar/hydrochar sourced from lignocellulosic biomass and other organic wastes were investigated. Activation by magnetic modification for lignocellulose derived biochar was also assessed.

7.2. Anaerobic digestion

Anaerobic digestion is one of the economically viable and environmentally friendly processes for converting bio-organic wastes to value-added products. AD processes involve complex dynamic systems including biochemical and physiochemical, and microbiological processes that can convert organic matter to methane and carbon dioxide by various groups of specific microorganisms (Forster-Carneiro *et al.*, 2008; Náthia-Neves *et al.*, 2018). However, due to its operation pattern and sensitivity to environmental variables, the AD process is unable to maintain high levels of biomass inventory and retain a greater quantity of fermenting microbes. As a result, economical difficulty of optimising biogas yield under fluctuating load in the field that makes it so potent, makes using carbon-based materials including biochar and hydrochar more

attractive, due to evidences showing accelerated and stabilized fermenting processes with addition of carbonous materials (Chiappero *et al.*, 2020; Gahlot *et al.*, 2020; Torri & Fabbri, 2014). However, as we have seen from this project, the AD process with the addition of biochar is still inhibited by intermediates such as VFAs and ammonia, and care must be taken to ensure that the use of biochar does not have an inverse effect on the AD potential. It is possible to pre/post-treat biochar, for example by co-pyrolyzing with different feedstocks or activating by chemical or thermal methods. It is also important to note that the modification must be interpreted with caution due to the potential additional expense and environmental concerns. Therefore, finding an optimized approach and a direct utilisation of biochar would be of enormous benefit as interest in pyrolysis increases.

7.3. Physiochemical properties of char

7.3.1. Carbon stability

The biochars used in this study were from four different feedstocks: rice husk, wheat straw pellets, and the mixture of hardwood and digestate, whereas hydrochars were derived from four feedstocks including oilseed rape pellets, sewage sludge, alkali lignin, rice husk and wheat straw pellets. For lignocellulosic biomass derived biochars, ultimate and proximate analysis revealed a high degree of carbonization in biochar WSP and RH. In addition, biochar HD produced from co-pyrolysis was characterised by a high proportion of hydrogen and low ash content. On the other hand hydrochars derived from feedstocks with high silica content may inhibit the HTC process by shielding carbon from feedstock to the resulting char. As expected, the HTC reaction associates with the elimination of water and carbon dioxide using D.I water as a

catalyst. Hydrochars pose a high level of the O/C ratio compared to biochars. In addition, hydrochars sourced from wheat straw pellets and oilseed rape pellets have higher contents of aromatic compounds, whilst rice husk and alkali lignin based hydrochars tend to form more aliphatic compounds. Furthermore, impregnation-pyrolysis in this study resulted in varied decrements in carbon content of the resulting biochar, which may due to the iron modification caused a greater loss of volatiles during the activation process. This implies that the adsorption ability of different feedstock to metal ions and its attributions on combing metal ions with surface functional groups. Biochar generated from sewage sludge had a higher nitrogen content than lignocellulosic biochars. Furthermore, an increase in oxygen content was seen in the resulting biochars via magnetic modification, suggesting that functionality was improved by increasing O-containing groups. Whereas these magnetic biochars have a low hydrogen content than the pristine biochar.

7.3.2. Surface functionality and structure

Over the chapters, FTIR analysis was used to characterise the surface functioning of chars. Similarity was shown in the peak intensity of lignocellulosic biochars; however, biochar WSP presents better functionated surface compare to biochar RH. In addition, similar patterns were seen in the FTIR spectra of biochar HD while the carboxylic O-H bond was strengthened in biochar HD, which may be associated with the co-pyrolysis of digestate. The FTIR analysis of hydrochar as seen in Chapter 5 reveals that the functional groups shared by WSP, OSR, and AL hydrochars included aliphatic and aromatic C-H bonds, alkene C=C bands, and C-O stretching bonds. While the C=O groups were only identical in hydrochar OSR and AL. All of these functional

groups, on the other hand, were poorly formed on the surface of hydrochar RH, which could be attributable to the low degree of decarboxylation or aromatization.

According to the FTIR spectra of magnetic biochars, impregnation-pyrolysis caused a recombination among oxygen containing groups including carboxyl, carbonyl, quinone, phenolic and ester ring bands. C=C bond appeared in magnetic biochar RH after activation, whereas the C-H band disappeared. It confirmed that RH biochar underwent a secondary pyrolysis and created an aliphatic chain crack with a condensate carbon structure. Additionally, stretching Fe-OH bonds were presented in both magnetic biochars, implying the successful formation of iron oxides on the resultant chars, which were in line with the finding by XRD analysis. It is also important to note that Fe-O groups were only identified in MRH biochar, implying that it has a greater number of ferromagnetic compounds than MSS biochar, which could be due to the presence of Fe^{3+} favouring the production of oxygen-containing functional groups (Wang *et al.*, 2017).

The gas adsorption analyzer determined a relatively close surface area value between biochar WSP and HD, but a greater surface area for biochar RH. The possible reason is that biochar RH poses a higher degree of carboniation at higher pyrolysis temperatures than biochar HD, suggesting that rice husk is an appropiate feedstock for utilisation of biochar with optimised specific surface area. In addition, biochar RH poses a little larger pore volume and better developed mesopares structures compared to the other two biochars, which is potentially beneficial for the uptake of AD inhibitor. Iron oxides were well crystallised on magnetic biochar matrix, whilst negligible crystalline peaks were observed from the diffraction patterns of the pristine

biochar, which were in agreements with the FTIR findings. In addition, the presence of a face-cantered cubic inverse spinal structured magnetite on the surface of MRH biochar was contributed from the partial transformation of magnetite to maghemite. On the other hand, different transformation was seen in MSS biochar with lower magnetic properties and the formation of hematite. The partial losses of magnetic properties were explained by the instability of maghemite at a sintering temperature of 500^{o}C. It is also important to note that the tested impregnation-pyrolysis would be less suitable for using sewage sludge as the feedstock compared to other lignocellulosic biomass.

7.3.3. Electrical conductivity

In this project, both water-soluble electrical conductivity of biochar and its electrical properties in proportions of compression was investigated to reveal the property relationship of biochar monoliths, with a focus on effects of feedstock type and manufacturing conditions. The main observation for lignocellulosic biochar was that water-soluble electrical conductivity was greatly related to the feedstock type. The degree of carbonization of biochar was found as the predominately factor. As such, biochar RH has higher EC compared to the other biochars. Furthermore, the ash content of biochar was also determined as one of factors influencing in the EC of biochar. Additionally, characterisation was assessed in the function of contacting time. It was showed that longer contact time led to higher EC values.

Magnetization modification has also proved to increase the EC of biochar, which is likely due to formation of iron oxides on biochar providing more active sites for the

accessibility of pseudo-capacitance to electrolyte ions and improving the electrochemical reactions. Meanwhile, this work found that the enhanced EC was attributed to increased oxygenated functional groups formed during the activation process, resulting the improvement of negative charge density of biochar. The surface redox-active moieties of biochars are also affected by their pHs (Yu *et al.*, 2015); however, due to the acidic nature of magnetic biochar, the reasons for increased EC values as functions of pHs and active redox moieties have not yet been determined.

The electrical properties of hydrochars produced from the HTC process showed a high degree of fluctuation, with particularly high EC values for OSR hydrochar. The fluctuation in EC values of biochars was attributed to the decomposition of dissolved salts from the HTC process and increasing contact time. However, with the increase of contact time, the electrical property of biochar RH reduced, yet, the underlying reasons could not be determined. Overall, the strongest effect on the electrical conductivity of biochar was attributed to the feedstock type, to weaknesses in the contact time and manufacturing parameters.

The electrical conductivity of hydrochars increased as the applied pressure increased. The most likely reason was that the dispersion of carbon particles inside the hydrochar monolith under high pressure compression. Whilst an inverse pattern was observed in the EC values of hydrochar RH, WSP and AL at a mild pressure range. The decrement in electrical properties of these hydrochars was attributed to the biochar structure and chemical properties. Biochar also showed an increasing EC value with increase of compression. However, magnetic biochars exhibited relatively lower EC at the same pressure range compared to the values of biochars. As previously stated,

increasing the acidic functional groups can result in a large reduction in pore volume and surface area in the biochar matrix. As such, it was assumed that magnetic biochar with well-developed surface functionality would have lower electron conducting behaviour. In addition, increased crystalline phases which resulted from the formation of iron oxides on magnetic biochar were contributed to the decreasing electrical conductivity. In conclusion, results about electrical characteristics of biochar in this thesis are highly encouraging; nevertheless, further research is needed to determine the influence of active redox moieties and pHs on the electron conducting behaviour of biochars.

7.3.4. Dissolved organic carbon

In general, the chemical processes during the HTC involving hydrolysis, dehydration and decarboxylation, can lead to formations of glucose, organic acids and phenol (Weiner *et al.*, 2014). By ongoing polymerization, these intermediates continued to form water-soluble polymeric substance and solids (as hydrochars). As such hydrochar is proved having high content of reactive carbon. However, it is found that DOC plays a key role in nitrogen cycle under nitrogen-saturated conditions and could affect the biochemical transformation in the aquatic environments (Fang *et al.*, 2009; Yekta *et al.*, 2012; Xing *et al.*, 2012). In this thesis, DOCs in hydrochars were examined and the UV-vis absorption spectra was used to regulate changes in the relative size of dissolved organics molecular. It was discovered that hydrochars with high alkalinity had increased DOC contents. In addition, differences in water-extracted DOC related to the stability and aromaticity of hydrochars. The hydrochar produced from untreated biomass has lower DOC concentration. Whilst, adverse results for

hydrochar AL and OSR were attributed to the high aromaticity. It should be noted that these tests were conducted with hydrochar without pre-treatment; however, it is unknown how the particle sizes of hydrochar were ranged and whether it would affect the solubility of larger organic molecular. From the limited sets of hydrochars tested here, it can be concluded that HTC resulting in high-DOC hydrochar are determined easily. As discussed for higher concentration of DOC, feedstock types need to be properly chose by avoiding biomass with poor structures which could result in exceed acidity in the applied environment.

7.4. AD with addition of char material

This thesis showed the successful use of biochar for enhancing the conversion of organic wastes to biogas. In brief, Chapter 3 showed that biochar has the potential to promote methane generation from sewage sludge under modest ammonia stress. Whilst methane content of the biogas for biochar-treated reactors in function of biochar dosage fluctuated greatly. Meanwhile, the 1st test exhibited that with increasing dosage of biochar WSP, the biogas yields and methane content in biogas increased; however this was not seen in biochar RH-treated reactors. When subjected to mild ammonia stress, increasing ammonia stress resulted in considerable inhibition in the control reactor; however, the addition of biochar boosted methane production by reducing ammonia inhibition. In addition, the third experiment in Chapter 3 demonstrated that increasing the concentration of ammonium in AD of sewage sludge can result in significant changes in biogas production and inhibition in the reactors with increasing dosage of WSP biochar. This shows that the application of biochar in sewage sludge based AD is limited, and that care must be taken when dosing a reactor with biochar that it does not cause negative impacts on the AD performance. This

leads to another finding of the project, in that increasing dosage of biochar led to the decrease of ammonium ion removal efficiency and biochar WSP proved to a better adsorption performance than biochar RH, which could be effectively used in removing ammonium in aqueous environment. This could also explain why, throughout the AD experiments in Chapter 3, there was a general decrease in the biogas productivity of the biochar RH-treated reactors.

The AD experiment in Chapter 5 was set up with hydrochars and sewage sludge that were acquired 60 days prior to the test and kept at 4^{o}C for the duration. It was seen that a lower volume of biogas was produced from the control group; however, the addition of hydrochar OSR and AL resulted in an increment in biogas productions compared to the control. Whereas, a reduced biogas yield was observed from reactor with the addition of hydrochar RH.

This thesis also assessed effects of biochars sourced from different feedstocks on the co-digestion of cow manure and maize silage. It can be seen that under no ammonium stress, the 1st BMP test in Chapter 4 showed a larger volume of biogas produced from biochar RH-treated reactor, which was not the case for tests in Chapter 3. Whereas reactors supplemented with biochar WSP and HD were inhibited showing a lower biogas productivity. The 2nd test was set at the same ammonium condition and saw an adverse result that all biochar-supplemented reactors were produced higher biogas production than the control. Although the methane concentration was similar between the control and biochar-amened reactors; the test saw a greater methane production rate from reactors with addition of biochar. The BMP test also showed that increased ammonium concentration was eventually boosted cumulative biogas production from

the control; however, a longer time was required for the control reactor to adapt higher level of ammonium concentration. Co-digestion of cow manure and maize silage with addition of these biochars were inhibited under modest ammonium stress. This was not seen in the BMP tests under higher ammonium stress, that biochar WSP and HD-treated reactors were capable of degrading exceed ammonium and generating larger volume of biogas than the control. Unlike the previous test in Chapter 3, digesters with biochar addition did not approach a plateau of biogas production at different ammoniumstresses, indicating the possibility of producing greater biogas and biomethane. Consequently, these biochar can be considered optimal to be used for digestion of nitrogen rich biowastes and agricultural residues in a small digester system.

It should be noted that the effects of biochar in different AD reactor units and conditions need further investigations to give recommendations for application of biochar with optimal AD performance. Therefore, a CSTR system was used, and it was hypothesised that the addition of biochar in CSTRs can enhance the immobilization of microbes for better biogas production and reduce sensitivities towards environmental factors such as pH and other inhibitors. Among the tests, it was seen that biochar supplementation facilitated the biogas production rate and shorten the adapting phase than the control. In the biochar-treated reactors, there were also minor changes in the digestate chemistry. In addition, it was evidenced that the biochar addition to co-digestion of cow manure and maize silage has limited benefits, with no significant difference in biogas generation from the biochar-treated reactor than the control under higher ammonium stress. Whereas biochar RH was able to improve TKN removal efficiency and increase methane yield at the same condition. It is likely that biochar

RH could not only adsorb more ammonium but also increase the digesters' tolerance toward to higher ammonium concentration. Although the priority should be to determine ammonium adsorption capacity of biochar, the use of biochar is a suitable approach that could be used for optimizing AD performance in practise.

Activated biochars were applied to AD syringe bioreactor to investigate their impacts on the performance of sludge digestion, and the dosing of biochar was also assessed. MRH biochar amended reactor was capable of generating higher cumulative biogas production compared to the other treatment conditions. Higher biomethane yield was exhibited in all biochar-treated reactors, which was attributed mostly to formation of iron oxides on magnetic biochar to serve as a catalyst stimulating the effectiveness of anaerobic microflora. Another observation was that the decrement in methane production with addition of MSS biochar at 0.2 %(w/w) and 1.0 %(w/w). It confirmed the hypothesis from the perspective of different crystalline phase of iron oxides, that goethite on MSS biochar could better reflect the selective pressure emphasized by forms of iron oxides and compete with methanogenesis by using hydrogen and acetate as substrate. Similar to previous tests, the use of biochar cause significantly changes in the digestate chemistry during the AD process. Similar to biochar RH's function, activated biochar increased ammonium concentration while decreased the pH, implied that its addition mitigated free ammonia inhibition by shifting the NH_3-NH_4^+ equilibrium towards NH_4^+ formation. Furthermore, as the dosage of activated biochar rose, the ash content of digestate increased, and it was discovered that a moderate amount of activated biochar is adequate to improve the digestate structure and mass transition on the AD of sewage sludge. In addition, the big merit of activated biochar compared to the untreated ones was the easily separable nature, which can endow biochar to

be directly used in industrial scale AD plant rather than worrying the leaching of biochar particles that may lead to secondary pollution. Yet, potential toxic and harmful substance which may be raised from the synthesis process of magnetic biochar were not determined. For the future work, greener synthesis of magnetic biochar with higher electron conductivity behaviour should be recommend attaching with high importance.

7.5. Conclusions

The use of biochar in anaerobic digestion for enhancing organic wastes to a value-added product as biogas is possible. However, future works are needed to investigate biochar associated biochemical mechanisms that could enhance the methane production and at what points biochars' addition that could cause process failure by inhibiting microorganisms activities. Meanwhile, physiochemical properties of biochars related to the feedstock type and manufacturing method. To improve surface functions and buffering capabilities, careful feedstock selection is required. Additionally, biochar from lignocellulosic biomass produced from pyrolysis has higher stability and could support the growth of anaerobic microorganisms in wastewater treatment digestate than hydrochar from similar feedstocks. The addition of biochar to co-digestion of animal waste and agricultural by-products reduced biomass washout from CSTRs digesters and increased inhibitor tolerance. Further investigation into biochars' application as a delivery mechanism for microbial communities is recommend. Meanwhile, activation of biochar by impregnation-pyrolysis method enhanced oxygen-containing functional groups and successfully fromed iron oxides on biochar. It also enabled biochar to be more easily separable and stive to become an environmentally friendly product, yet, due to weaknesses in the synthetic method design or operation, potential contamination through condensation could occur. The addition of activated

biochar to wastewater treatment digestate was successful in increasing biogas production by alleviating ammonium inhibition and improving mass transition in the AD process. Also, lower biochar does with optimal effects on methane production would be critical information in order to minimize the production costs. It is also important to take into consideration limitations of characterization techniques and reactors designs, and ensure that they are complemented with quantified analysis of known makers of process constitution.

Reference

Aboudi, K., Gómez-Quiroga, X., álvarez-Gallego, C. J., & Romero-García, L. I. (2020). Insights into anaerobic co-digestion of lignocellulosic biomass (sugar beet by-products) and animal manure in long-term semi-continuous assays. *Applied Sciences (Switzerland)*, *10*(15). https://doi.org/10.3390/app10155126

Adekunle, K. F., & Okolie, J. A. (2015). A Review of Biochemical Process of Anaerobic Digestion. *Advances in Bioscience and Biotechnology*, *06*(03). https://doi.org/10.4236/abb.2015.63020

Adhikari, S., Nam, H., & Chakraborty, J. P. (2018). Conversion of solid wastes to fuels and chemicals through pyrolysis. In *Waste Biorefinery: Potential and Perspectives*. https://doi.org/10.1016/B978-0-444-63992-9.00008-2

Akhtar, A., Krepl, V., & Ivanova, T. (2018). A Combined Overview of Combustion, Pyrolysis, and Gasification of Biomass. *Energy and Fuels*, Vol. 32. https://doi.org/10.1021/acs.energyfuels.8b01678

Akhtar, J., & Amin, N. A. S. (2011). A review on process conditions for optimum bio-oil yield in hydrothermal liquefaction of biomass. *Renewable and Sustainable Energy Reviews*, Vol. 15. https://doi.org/10.1016/j.rser.2010.11.054

Alam, M. S., Bishop, B., Chen, N., Safari, S., Warter, V., Byrne, J. M., … Alessi, D. S. (2020). Reusable magnetite nanoparticles–biochar composites for the efficient removal of chromate from water. *Scientific Reports*, *10*(1). https://doi.org/10.1038/s41598-020-75924-7

Ambuchi, J. J., Zhang, Z., Dong, Y., Huang, L., & Feng, Y. (2018). Hematite and multi-walled carbon nanotubes stimulate a faster syntrophic pathway during methanogenic beet sugar industrial wastewater degradation. *Applied Microbiology and Biotechnology*, *102*(16), 7147–7158.

https://doi.org/10.1007/s00253-018-9100-8

Amonette, J. E., & Joseph, S. (2012). Characteristics of biochar: Microchemical properties. In *Biochar for Environmental Management: Science and Technology*. https://doi.org/10.4324/9781849770552

Anaerobic Digestion. (2018). Biogas Map.

Annamalai, N., Elayaraja, S., Oleskowicz-Popiel, P., Sivakumar, N., & Bahry, S. Al. (2020). Volatile fatty acids production during anaerobic digestion of lignocellulosic biomass. In *Recent Developments in Bioenergy Research*. https://doi.org/10.1016/b978-0-12-819597-0.00012-x

Anukam, A., Mohammadi, A., Naqvi, M., & Granström, K. (2019). A review of the chemistry of anaerobic digestion: Methods of accelerating and optimizing process efficiency. *Processes*, Vol. 7. https://doi.org/10.3390/PR7080504

Apaydin-Varol, E., & Pütün, A. E. (2012). Preparation and characterization of pyrolytic chars from different biomass samples. *Journal of Analytical and Applied Pyrolysis*, *98*. https://doi.org/10.1016/j.jaap.2012.07.001

Appels, L., Baeyens, J., Degrève, J., & Dewil, R. (2008). Principles and potential of the anaerobic digestion of waste-activated sludge. *Progress in Energy and Combustion Science*, Vol. 34. https://doi.org/10.1016/j.pecs.2008.06.002

Appels, L., Lauwers, J., Degrve, J., Helsen, L., Lievens, B., Willems, K., … Dewil, R. (2011). Anaerobic digestion in global bio-energy production: Potential and research challenges. *Renewable and Sustainable Energy Reviews*, Vol. 15. https://doi.org/10.1016/j.rser.2011.07.121

Arauzo, P. J., Atienza-Martínez, M., Ábrego, J., Olszewski, M. P., Cao, Z., & Kruse, A. (2020). Combustion characteristics of hydrochar and pyrochar derived from digested sewage sludge. *Energies*, *13*(6). https://doi.org/10.3390/en13164164

Aravind, S., Kumar, P. S., Kumar, N. S., & Siddarth, N. (2020). Conversion of green algal biomass into bioenergy by pyrolysis. A review. *Environmental Chemistry Letters*, Vol. 18. https://doi.org/10.1007/s10311-020-00990-2

Arenas, C. B., Meredith, W., Snape, C. E., Gómez, X., González, J. F., & Martinez, E. J. (2020). Effect of char addition on anaerobic digestion of animal by-products: evaluating biogas production and process performance. *Environmental Science and Pollution Research*. https://doi.org/10.1007/s11356-020-08828-8

Axel Funke, & Felix Ziegler. (2010). Hydrothermal carbonization of biomass: A summary and discussion of chemical mecha- nisms for process engineering. *Biofuels, Bioproducts and Biorefining*, *4*.

Bacenetti, J., Negri, M., Fiala, M., & González-García, S. (2013). Anaerobic digestion of different feedstocks: Impact on energetic and environmental balances of biogas process. *Science of the Total Environment*, *463–464*. https://doi.org/10.1016/j.scitotenv.2013.06.058

Banks, C. J., Chesshire, M., Heaven, S., & Arnold, R. (2011). Anaerobic digestion of source-segregated domestic food waste: Performance assessment by mass and energy balance. *Bioresource Technology*, *102*(2). https://doi.org/10.1016/j.biortech.2010.08.005

Barry, D., Barbiero, C., Briens, C., & Berruti, F. (2019). Pyrolysis as an economical and ecological treatment option for municipal sewage sludge. *Biomass and Bioenergy*, *122*. https://doi.org/10.1016/j.biombioe.2019.01.041

Barua, S., & Dhar, B. R. (2017). Advances towards understanding and engineering direct interspecies electron transfer in anaerobic digestion. *Bioresource Technology*. https://doi.org/10.1016/j.biortech.2017.08.023

Baştabak, B., & Koçar, G. (2020). A review of the biogas digestate in agricultural framework. *Journal of Material Cycles and Waste Management*, Vol. 22. https://doi.org/10.1007/s10163-020-01056-9

Belmonte, M., Hsieh, C. F., Figueroa, C., Campos, J. L., & Vidal, G. (2011). Effect of free ammonia nitrogen on the methanogenic activity of swine wastewater. *Electronic Journal of Biotechnology*, *14*(3). https://doi.org/10.2225/vol14-issue3-fulltext-11

Bhuvaneshwari, S., Hettiarachchi, H., & Meegoda, J. N. (2019). Crop residue burning in India: Policy challenges and potential solutions. *International Journal of Environmental Research and Public Health*. https://doi.org/10.3390/ijerph16050832

Bi, H., Wang, C., Jiang, X., Jiang, C., Bao, L., & Lin, Q. (2021). Thermodynamics, kinetics, gas emissions and artificial neural network modeling of co-pyrolysis of sewage sludge and peanut shell. *Fuel*, *284*. https://doi.org/10.1016/j.fuel.2020.118988

Bird, L. J., Bonnefoy, V., & Newman, D. K. (2011). Bioenergetic challenges of microbial iron metabolisms. *Trends in Microbiology*, Vol. 19. https://doi.org/10.1016/j.tim.2011.05.001

Bonk, F., Popp, D., Weinrich, S., Sträuber, H., Kleinsteuber, S., Harms, H., & Centler, F. (2018). Ammonia inhibition of anaerobic volatile fatty acid degrading microbial communities. *Frontiers in Microbiology*, *9*(NOV). https://doi.org/10.3389/fmicb.2018.02921

Bora, A. P., Gupta, D. P., & Durbha, K. S. (2020). Sewage sludge to bio-fuel: A review on the sustainable approach of transforming sewage waste to alternative fuel. *Fuel*, Vol. 259. https://doi.org/10.1016/j.fuel.2019.116262

Bourke, J., Manley-Harris, M., Fushimi, C., Dowaki, K., Nunoura, T., & Antal, M. J. (2007). Do all carbonized charcoals have the same chemical structure? 2. A model of the chemical structure of carbonized charcoal. *Industrial and Engineering Chemistry Research*, *46*(18). https://doi.org/10.1021/ie070415u

Bridgwater, A. V. (2007). The production of biofuels and renewable chemicals by fast pyrolysis of biomass. *International Journal of Global Energy Issues*, *27*(2). https://doi.org/10.1504/IJGEI.2007.013654

Bridgwater, A. V. (2012). Review of fast pyrolysis of biomass and product upgrading. *Biomass and Bioenergy*, *38*. https://doi.org/10.1016/j.biombioe.2011.01.048

Bridle, T. R., Hammerton, I., & Hertle, C. K. (1990). Control of heavy metals and organochlorines using the oil from sludge process. *Water Science and Technology*, *22*(12). https://doi.org/10.2166/wst.1990.0119

Buss, W., Graham, M. C., Shepherd, J. G., & Mašek, O. (2016). Suitability of marginal biomass-derived biochars for soil amendment. *Science of the Total Environment*, *547*. https://doi.org/10.1016/j.scitotenv.2015.11.148

Bustamante, M. A., Nogués, I., Jones, S., & Allison, G. G. (2019). The effect of anaerobic digestate derived composts on the metabolite composition and thermal behaviour of rosemary. *Scientific Reports*, *9*(1). https://doi.org/10.1038/s41598-019-42725-6

Cai, Jiao, He, P., Wang, Y., Shao, L., & Lü, F. (2016). Effects and optimization of the use of biochar in anaerobic digestion of food wastes. *Waste Management and Research*, *34*(5). https://doi.org/10.1177/0734242X16634196

Cai, Jingyuan, Zhang, L., Tang, J., & Pan, D. (2019). Adoption of multiple sustainable manure treatment technologies by pig farmers in rural China: A case study of Poyang Lake Region. *Sustainability (Switzerland)*.

https://doi.org/10.3390/su11226458

Calucci, L., Rasse, D. P., & Forte, C. (2013). Solid-state nuclear magnetic resonance characterization of chars obtained from hydrothermal carbonization of corncob and Miscanthus. *Energy and Fuels*, *27*(1). https://doi.org/10.1021/ef3017128

Campos, A. F. C., de Oliveira, H. A. L., da Silva, F. N., da Silva, F. G., Coppola, P., Aquino, R., … Depeyrot, J. (2019). Core-Shell Bimagnetic Nanoadsorbents for Hexavalent Chromium Removal from Aqueous Solutions. *Journal of Hazardous Materials*, *362*. https://doi.org/10.1016/j.jhazmat.2018.09.008

Cao, Z., Wang, S., Wang, T., Chang, Z., Shen, Z., & Chen, Y. (2015). Using Contaminated Plants Involved in Phytoremediation for Anaerobic Digestion. *International Journal of Phytoremediation*, *17*(3). https://doi.org/10.1080/15226514.2013.876967

Caposciutti, G., Baccioli, A., Ferrari, L., & Desideri, U. (2020). Biogas from anaerobic digestion: Power generation or biomethane production? *Energies*, *13*(3). https://doi.org/10.3390/en13030743

Carrère, H., Dumas, C., Battimelli, A., Batstone, D. J., Delgenès, J. P., Steyer, J. P., & Ferrer, I. (2010). Pretreatment methods to improve sludge anaerobic degradability: A review. *Journal of Hazardous Materials*, Vol. 183. https://doi.org/10.1016/j.jhazmat.2010.06.129

Chadwick, D., Wei, J., Yan'an, T., Guanghui, Y., Qirong, S., & Qing, C. (2015). Improving manure nutrient management towards sustainable agricultural intensification in China. *Agriculture, Ecosystems and Environment*. https://doi.org/10.1016/j.agee.2015.03.025

Chambers, B., Nicholson, N., Smith, K., & Pain, B. (2001). Making better use of livestock manures on arable land. *Institute of Grassland and …*.

Chambers, B., Nicholson, N., Smith, K., Pain, B., Cumby, T., & Scotford, I. (2001). Making better use of livestock manures on grassland. *Managing Livestock Manures, Booklet 2*.

Chandel, A. K., da Silva, S. S., Carvalho, W., & Singh, O. V. (2012). Sugarcane bagasse and leaves: Foreseeable biomass of biofuel and bio-products. *Journal of Chemical Technology and Biotechnology*, Vol. 87. https://doi.org/10.1002/jctb.2742

Chen, B., Chen, Z., & Lv, S. (2011). A novel magnetic biochar efficiently sorbs organic pollutants and phosphate. *Bioresource Technology*, *102*(2). https://doi.org/10.1016/j.biortech.2010.08.067

Chen, H., Wang, W., Xue, L., Chen, C., Liu, G., & Zhang, R. (2016). Effects of Ammonia on Anaerobic Digestion of Food Waste: Process Performance and Microbial Community. *Energy and Fuels*, *30*(7). https://doi.org/10.1021/acs.energyfuels.6b00715

Chen, N., Huang, Y., Hou, X., Ai, Z., & Zhang, L. (2017). Photochemistry of Hydrochar: Reactive Oxygen Species Generation and Sulfadimidine Degradation. *Environmental Science and Technology*, *51*(19). https://doi.org/10.1021/acs.est.7b02740

Chen, T., Zhang, Y., Wang, H., Lu, W., Zhou, Z., Zhang, Y., & Ren, L. (2014). Influence of pyrolysis temperature on characteristics and heavy metal adsorptive performance of biochar derived from municipal sewage sludge. *Bioresource Technology*, *164*. https://doi.org/10.1016/j.biortech.2014.04.048

Chen, W., Yang, H., Chen, Y., Xia, M., Chen, X., & Chen, H. (2017). Transformation of Nitrogen and Evolution of N-Containing Species during Algae Pyrolysis. *Environmental Science and Technology*, *51*(11).

https://doi.org/10.1021/acs.est.7b00434

Chen, X., Lin, Q., He, R., Zhao, X., & Li, G. (2017). Hydrochar production from watermelon peel by hydrothermal carbonization. *Bioresource Technology*. https://doi.org/10.1016/j.biortech.2017.04.012

Chen, Y., Yang, G., Sweeney, S., & Feng, Y. (2010). Household biogas use in rural China: A study of opportunities and constraints. *Renewable and Sustainable Energy Reviews*, Vol. 14. https://doi.org/10.1016/j.rser.2009.07.019

Chen, Z., Xiao, X., Chen, B., & Zhu, L. (2015a). Quantification of chemical states, dissociation constants and contents of oxygen-containing groups on the surface of biochars produced at different temperatures. *Environmental Science and Technology*. https://doi.org/10.1021/es5043468

Chen, Z., Xiao, X., Chen, B., & Zhu, L. (2015b). Quantification of Chemical States, Dissociation Constants and Contents of Oxygen-containing Groups on the Surface of Biochars Produced at Different Temperatures. *Environmental Science & Technology*, *49*(1), 309–317. https://doi.org/10.1021/es5043468

Cheng, Q., Xu, C., Huang, W., Jiang, M., Yan, J., Fan, G., … Song, G. (2020). Improving anaerobic digestion of piggery wastewater by alleviating stress of ammonia using biochar derived from rice straw. *Environmental Technology and Innovation*, *19*. https://doi.org/10.1016/j.eti.2020.100948

Chiappero, M., Norouzi, O., Hu, M., Demichelis, F., Berruti, F., Di Maria, F., … Fiore, S. (2020). Review of biochar role as additive in anaerobic digestion processes. *Renewable and Sustainable Energy Reviews*. https://doi.org/10.1016/j.rser.2020.110037

Chowdhury, H., & Loganathan, B. (2019). Third-generation biofuels from microalgae: a review. *Current Opinion in Green and Sustainable Chemistry*, Vol. 20.

https://doi.org/10.1016/j.cogsc.2019.09.003

Chun, L., Wu, X., Lou, X., & Zhang, Y. (2010). Hematite nanoflakes as anode electrode materials for rechargeable lithium-ion batteries. *Electrochimica Acta*, *55*(9). https://doi.org/10.1016/j.electacta.2010.01.016

Cristiani, P., Goglio, A., Marzorati, S., Fest-Santini, S., & Schievano, A. (2020). Biochar-Terracotta Conductive Composites: New Design for Bioelectrochemical Systems. *Frontiers in Energy Research*, *8*. https://doi.org/10.3389/fenrg.2020.581106

Crombie, K., Mašek, O., Sohi, S. P., Brownsort, P., & Cross, A. (2013). The effect of pyrolysis conditions on biochar stability as determined by three methods. *GCB Bioenergy*, *5*(2). https://doi.org/10.1111/gcbb.12030

Cruz Viggi, C., Rossetti, S., Fazi, S., Paiano, P., Majone, M., & Aulenta, F. (2014). Magnetite particles triggering a faster and more robust syntrophic pathway of methanogenic propionate degradation. *Environmental Science and Technology*, *48*(13). https://doi.org/10.1021/es5016789

Cuetos, M. J., Fernández, C., Gómez, X., & Morán, A. (2011). Anaerobic co-digestion of swine manure with energy crop residues. *Biotechnology and Bioprocess Engineering*. https://doi.org/10.1007/s12257-011-0117-4

Dai, X., Duan, N., Dong, B., & Dai, L. (2013). High-solids anaerobic co-digestion of sewage sludge and food waste in comparison with mono digestions: Stability and performance. *Waste Management*. https://doi.org/10.1016/j.wasman.2012.10.018

Daly, C., Halbleib, M. D., Hannaway, D. B., & Eaton, L. M. (2018). Environmental limitation mapping of potential biomass resources across the conterminous United States. *GCB Bioenergy*, *10*(10). https://doi.org/10.1111/gcbb.12496

Dang, Y., Holmes, D. E., Zhao, Z., Woodard, T. L., Zhang, Y., Sun, D., … Lovley, D. R. (2016). Enhancing anaerobic digestion of complex organic waste with carbon-based conductive materials. *Bioresource Technology*. https://doi.org/10.1016/j.biortech.2016.08.114

Dang, Y., Sun, D., Woodard, T. L., Wang, L. Y., Nevin, K. P., & Holmes, D. E. (2017). Stimulation of the anaerobic digestion of the dry organic fraction of municipal solid waste (OFMSW) with carbon-based conductive materials. *Bioresource Technology*, *238*. https://doi.org/10.1016/j.biortech.2017.04.021

Dareioti, M. A., & Kornaros, M. (2014). Effect of hydraulic retention time (HRT) on the anaerobic co-digestion of agro-industrial wastes in a two-stage CSTR system. *Bioresource Technology*, *167*. https://doi.org/10.1016/j.biortech.2014.06.045

Darmstadt, H., Pantea, D., Sümmchen, L., Roland, U., Kaliaguine, S., & Roy, C. (2000). Surface and bulk chemistry of charcoal obtained by vacuum pyrolysis of bark: Influence of feedstock moisture content. *Journal of Analytical and Applied Pyrolysis*, *53*(1). https://doi.org/10.1016/S0165-2370(99)00051-0

Dastgheib, S. A., Ren, J., Rostam-Abadi, M., & Chang, R. (2014). Preparation of functionalized and metal-impregnated activated carbon by a single-step activation method. *Applied Surface Science*, *290*. https://doi.org/10.1016/j.apsusc.2013.11.005

de Bok, F. A. M., Harmsen, H. J. M., Plugge, C. M., de Vries, M. C., Akkermans, A. D. L., de Vos, W. M., & Stams, A. J. M. (2005). The first true obligately syntrophic propionate-oxidizing bacterium, Pelotomaculum schinkii sp. nov., co-cultured with Methanospirillum hungatei, and emended description of the genus Pelotomaculum. *International Journal of Systematic and Evolutionary*

Microbiology, *55*(4). https://doi.org/10.1099/ijs.0.02880-0

de Diego-Díaz, B., Alejandro Cerdán, J. M., Peñas, F. J., & Fernández-Rodríguez, J. (2018). Impact of supplementary nutrients on codigestion of agricultural waste: Study of temperatures. *Food and Bioproducts Processing*, *110*, 120–125. https://doi.org/https://doi.org/10.1016/j.fbp.2018.05.003

De Jong, W., & Van Ommen, J. R. (2014). Biomass as a Sustainable Energy Source for the Future: Fundamentals of Conversion Processes. In *Biomass as a Sustainable Energy Source for the Future: Fundamentals of Conversion Processes* (Vol. 9781118304914). https://doi.org/10.1002/9781118916643

de Souza Souza, C., Bomfim, M. R., Conceição de Almeida, M. da, Alves, L. de S., de Santana, W. N., da Silva Amorim, I. C., & Santos, J. A. G. (2021). Induced changes of pyrolysis temperature on the physicochemical traits of sewage sludge and on the potential ecological risks. *Scientific Reports*, *11*(1). https://doi.org/10.1038/s41598-020-79658-4

Deguchi, S., Tsujii, K., & Horikoshi, K. (2008). Crystalline-to-amorphous transformation of cellulose in hot and compressed water and its implications for hydrothermal conversion. *Green Chemistry*, *10*(2). https://doi.org/10.1039/b713655b

Deublein, D., & Steinhauser, A. (2010). Biogas from Waste and Renewable Resources: An Introduction, Second Edition. In *Biogas from Waste and Renewable Resources: An Introduction, Second Edition*. https://doi.org/10.1002/9783527632794

Devi, P., & Saroha, A. K. (2014). Synthesis of the magnetic biochar composites for use as an adsorbent for the removal of pentachlorophenol from the effluent. *Bioresource Technology*, *169*. https://doi.org/10.1016/j.biortech.2014.07.062

Devi, P., & Saroha, A. K. (2015). Simultaneous adsorption and dechlorination of pentachlorophenol from effluent by Ni-ZVI magnetic biochar composites synthesized from paper mill sludge. *Chemical Engineering Journal*, *271*. https://doi.org/10.1016/j.cej.2015.02.087

Diebold, J. P. (1994). A unified, global model for the pyrolysis of cellulose. *Biomass and Bioenergy*, *7*(1–6). https://doi.org/10.1016/0961-9534(94)00039-V

Dieguez-Alonso, A., Funke, A., Anca-Couce, A., Rombolà, A. G., Ojeda, G., Bachmann, J., & Behrendt, F. (2018). Towards biochar and hydrochar engineering-influence of process conditions on surface physical and chemical properties, thermal stability, nutrient availability, toxicity and wettability. *Energies*. https://doi.org/10.3390/en11030496

Dinjus, E., Kruse, A., & Tröger, N. (2011). Hydrothermal carbonization - 1. Influence of lignin in lignocelluloses. *Chemical Engineering and Technology*, *34*(12). https://doi.org/10.1002/ceat.201100487

Dolling, P. J., & Porter, W. M. (1994). Acidification rates in the central wheatbelt of western australia. 1. on a deep yellow sand. *Australian Journal of Experimental Agriculture*, *34*(8). https://doi.org/10.1071/EA9941155

Dorez, G., Ferry, L., Sonnier, R., Taguet, A., & Lopez-Cuesta, J. M. (2014). Effect of cellulose, hemicellulose and lignin contents on pyrolysis and combustion of natural fibers. *Journal of Analytical and Applied Pyrolysis*, *107*. https://doi.org/10.1016/j.jaap.2014.03.017

Duetz, W. A., Bouwmeester, H., Van Beilen, J. B., & Witholt, B. (2003). Biotransformation of limonene by bacteria, fungi, yeasts, and plants. *Applied Microbiology and Biotechnology*, Vol. 61. https://doi.org/10.1007/s00253-003-1221-y

Dunnigan, L., Morton, B. J., Ashman, P. J., Zhang, X., & Kwong, C. W. (2018). Emission characteristics of a pyrolysis-combustion system for the co-production of biochar and bioenergy from agricultural wastes. *Waste Management*, *77*. https://doi.org/10.1016/j.wasman.2018.05.004

EBA. (2017). European Biogas Association statistical report.

EBA. (2018). EBA Statistical Report 2018, Abbreviated Public Edition. In *Annual Report*.

Edwards, J., Othman, M., & Burn, S. (2015). A review of policy drivers and barriers for the use of anaerobic digestion in Europe, the United States and Australia. *Renewable and Sustainable Energy Reviews*. https://doi.org/10.1016/j.rser.2015.07.112

Elliott, D. C., Biller, P., Ross, A. B., Schmidt, A. J., & Jones, S. B. (2015). Hydrothermal liquefaction of biomass: Developments from batch to continuous process. *Bioresource Technology*, Vol. 178. https://doi.org/10.1016/j.biortech.2014.09.132

Enders, A., & Lehmann, J. (2012). Comparison of Wet-Digestion and Dry-Ashing Methods for Total Elemental Analysis of Biochar. *Communications in Soil Science and Plant Analysis*, *43*(7). https://doi.org/10.1080/00103624.2012.656167

Eom, I. Y., Kim, K. H., Kim, J. Y., Lee, S. M., Yeo, H. M., Choi, I. G., & Choi, J. W. (2011). Characterization of primary thermal degradation features of lignocellulosic biomass after removal of inorganic metals by diverse solvents. *Bioresource Technology*, *102*(3). https://doi.org/10.1016/j.biortech.2010.10.056

Fagbohungbe, M. O., Herbert, B. M. J., Hurst, L., Ibeto, C. N., Li, H., Usmani, S. Q., & Semple, K. T. (2017a). The challenges of anaerobic digestion and the role of

biochar in optimizing anaerobic digestion. *Waste Management*. https://doi.org/10.1016/j.wasman.2016.11.028

Fagbohungbe, M. O., Herbert, B. M. J., Hurst, L., Ibeto, C. N., Li, H., Usmani, S. Q., & Semple, K. T. (2017b). The challenges of anaerobic digestion and the role of biochar in optimizing anaerobic digestion. *Waste Management*. https://doi.org/10.1016/j.wasman.2016.11.028

Fang, J., Zhan, L., Ok, Y. S., & Gao, B. (2018). Minireview of potential applications of hydrochar derived from hydrothermal carbonization of biomass. *Journal of Industrial and Engineering Chemistry*. https://doi.org/10.1016/j.jiec.2017.08.026

Fang, Y., Zhu, W., Gundersen, P., Mo, J., Zhou, G., & Yoh, M. (2009). Large loss of dissolved organic nitrogen from nitrogen-saturated forests in subtropical China. *Ecosystems*, *12*(1). https://doi.org/10.1007/s10021-008-9203-7

Fang, Z., Sato, T., Smith, R. L., Inomata, H., Arai, K., & Kozinski, J. A. (2008). Reaction chemistry and phase behavior of lignin in high-temperature and supercritical water. *Bioresource Technology*, *99*(9). https://doi.org/10.1016/j.biortech.2007.08.008

Fengel, D., & Wegener, G. (2011). Wood: Chemistry, ultrastructure, reactions. In *Wood: Chemistry, Ultrastructure, Reactions*. https://doi.org/10.1515/9783110839654

Fidel, R. B., Laird, D. A., Thompson, M. L., & Lawrinenko, M. (2017). Characterization and quantification of biochar alkalinity. *Chemosphere*, *167*. https://doi.org/10.1016/j.chemosphere.2016.09.151

Foged, Lyngsø, H., Flotats, X., Blasi, A. B., Palatsi, J., Magri, A., & Schelde, K. M. (2011). Inventory of manure processing activities in Europe. *Technical Report No. I Concerning "Manure Processing Activities in Europe" to the European*

Commission, Directorate-General Environment.

Font-Palma, C. (2019). Methods for the Treatment of Cattle Manure—A Review. *C*. https://doi.org/10.3390/c5020027

Font, R., Fullana, A., Conesa, J. A., & Llavador, F. (2001). Analysis of the pyrolysis and combustion of different sewage sludges by TG. *Journal of Analytical and Applied Pyrolysis*, *58–59*. https://doi.org/10.1016/S0165-2370(00)00146-7

Forster-Carneiro, T., Pérez, M., & Romero, L. I. (2008). Anaerobic digestion of municipal solid wastes: Dry thermophilic performance. *Bioresource Technology*, *99*(17). https://doi.org/10.1016/j.biortech.2008.03.021

Freeman, C., Ostle, N., & Kang, H. (2001). An enzymic 'latch' on a global carbon store: A shortage of oxygen locks up carbon in peatlands by restraining a single enzymes. *Nature*, *409*(6817). https://doi.org/10.1038/35051650

Fu, Z., & Holtzapple, M. T. (2010). Anaerobic mixed-culture fermentation of aqueous ammonia-treated sugarcane bagasse in consolidated bioprocessing. *Biotechnology and Bioengineering*, *106*(2). https://doi.org/10.1002/bit.22679

Fuess, L. T., Mazine Kiyuna, L. S., Garcia, M. L., & Zaiat, M. (2016). Operational strategies for long-term biohydrogen production from sugarcane stillage in a continuous acidogenic packed-bed reactor. *International Journal of Hydrogen Energy*, *41*(19). https://doi.org/10.1016/j.ijhydene.2015.10.143

Gabhi, R., Basile, L., Kirk, D. W., Giorcelli, M., Tagliaferro, A., & Jia, C. Q. (2020). Electrical conductivity of wood biochar monoliths and its dependence on pyrolysis temperature. *Biochar*, *2*(3). https://doi.org/10.1007/s42773-020-00056-0

Gabhi, R. S., Kirk, D. W., & Jia, C. Q. (2017). Preliminary investigation of electrical conductivity of monolithic biochar. *Carbon*, *116*.

https://doi.org/10.1016/j.carbon.2017.01.069

Gahlot, P., Ahmed, B., Tiwari, S. B., Aryal, N., Khursheed, A., Kazmi, A. A., & Tyagi, V. K. (2020). Conductive material engineered direct interspecies electron transfer (DIET) in anaerobic digestion: Mechanism and application. *Environmental Technology and Innovation*. https://doi.org/10.1016/j.eti.2020.101056

Gao, L., Volpe, M., Lucian, M., Fiori, L., & Goldfarb, J. L. (2019). Does hydrothermal carbonization as a biomass pretreatment reduce fuel segregation of coal-biomass blends during oxidation? *Energy Conversion and Management*, *181*. https://doi.org/10.1016/j.enconman.2018.12.009

Gao, S., Huang, Y., Yang, L., Wang, H., Zhao, M., Xu, Z., … Ruan, W. (2015). Evaluation the anaerobic digestion performance of solid residual kitchen waste by NaHCO3 buffering. *Energy Conversion and Management*, *93*. https://doi.org/10.1016/j.enconman.2015.01.010

Garcia-Nunez, J. A., Pelaez-Samaniego, M. R., Garcia-Perez, M. E., Fonts, I., Abrego, J., Westerhof, R. J. M., & Garcia-Perez, M. (2017). Historical Developments of Pyrolysis Reactors: A Review. *Energy and Fuels*, Vol. 31. https://doi.org/10.1021/acs.energyfuels.7b00641

Gaskin, J. W., Steiner, C., Harris, K., Das, K. C., & Bibens, B. (2008). Effect of low-temperature pyrolysis conditions on biochar for agricultural use. *Transactions of the ASABE*, *51*(6).

Ghidotti, M., Fabbri, D., Mašek, O., Mackay, C. L., Montalti, M., & Hornung, A. (2017). Source and Biological Response of Biochar Organic Compounds Released into Water; Relationships with Bio-Oil Composition and Carbonization Degree. *Environmental Science and Technology*.

https://doi.org/10.1021/acs.est.7b00520

Gilcreas, F. W. (1967). Future of standard methods for the examination of water and wastewater. *Health Laboratory Science*, *4*(3).

Giorcelli, M., & Bartoli, M. (2019). Development of coffee biochar filler for the production of electrical conductive reinforced plastic. *Polymers*, *11*(12). https://doi.org/10.3390/polym11121916

Giwa, A. S., Xu, H., Chang, F., Wu, J., Li, Y., Ali, N., … Wang, K. (2019). Effect of biochar on reactor performance and methane generation during the anaerobic digestion of food waste treatment at long-run operations. *Journal of Environmental Chemical Engineering*, *7*(4). https://doi.org/10.1016/j.jece.2019.103067

Godlewska, P., Bogusz, A., Dobrzyńska, J., Dobrowolski, R., & Oleszczuk, P. (2020). Engineered biochar modified with iron as a new adsorbent for treatment of water contaminated by selenium. *Journal of Saudi Chemical Society*, *24*(11). https://doi.org/10.1016/j.jscs.2020.07.006

Gómez-Rico, M. F., Font, R., Fullana, A., & Martín-Gullón, I. (2005). Thermogravimetric study of different sewage sludges and their relationship with the nitrogen content. *Journal of Analytical and Applied Pyrolysis*, *74*(1–2). https://doi.org/10.1016/j.jaap.2004.11.029

Gómez, X., Cuetos, M. J., García, A. I., & Morán, A. (2007). An evaluation of stability by thermogravimetric analysis of digestate obtained from different biowastes. *Journal of Hazardous Materials*, *149*(1). https://doi.org/10.1016/j.jhazmat.2007.03.049

Grando, R. L., da Fonseca, F. V., & Antunes, A. M. de S. (2017). Mapping of the Use of Waste as Raw Materials for Biogas Production. *Journal of Environmental*

Protection, *08*(02). https://doi.org/10.4236/jep.2017.82010

Grangeiro, L. C., Almeida, S. G. C. de, Mello, B. S. de, Fuess, L. T., Sarti, A., & Dussán, K. J. (2019). New trends in biogas production and utilization. In *Sustainable Bioenergy: Advances and Impacts*. https://doi.org/10.1016/B978-0-12-817654-2.00007-1

Gronwald, M., Helfrich, M., Don, A., Fuß, R., Well, R., & Flessa, H. (2018). Application of hydrochar and pyrochar to manure is not effective for mitigation of ammonia emissions from cattle slurry and poultry manure. *Biology and Fertility of Soils*, *54*(4). https://doi.org/10.1007/s00374-018-1273-x

Guragain, Y. N., Wilson, J., Staggenborg, S., McKinney, L., Wang, D., & Vadlani, P. V. (2013). Evaluation of pelleting as a pre-processing step for effective biomass deconstruction and fermentation. *Biochemical Engineering Journal*, *77*. https://doi.org/10.1016/j.bej.2013.05.014

Haas, J. R., & Dichristina, T. J. (2002). Effects of FE(III) chemical speciation on dissimilatory FE(III) reduction by shewanella putrefaciens. *Environmental Science and Technology*, *36*(3). https://doi.org/10.1021/es0109287

Hadj, B. E., Astals, S., Galí, A., Mace, S., & Mata-Áivarez, J. (2009). Ammonia influence in anaerobic digestion of OFMSW. *Water Science and Technology*, *59*(6). https://doi.org/10.2166/wst.2009.100

Hafez, H., Nakhla, G., El. Naggar, M. H., Elbeshbishy, E., & Baghchehsaraee, B. (2010). Effect of organic loading on a novel hydrogen bioreactor. *International Journal of Hydrogen Energy*, *35*(1). https://doi.org/10.1016/j.ijhydene.2009.10.051

Hagos, K., Zong, J., Li, D., Liu, C., & Lu, X. (2017). Anaerobic co-digestion process for biogas production: Progress, challenges and perspectives. *Renewable and*

Sustainable Energy Reviews. https://doi.org/10.1016/j.rser.2016.11.184

Hameed, S. A., Riffat, R., Li, B., Naz, I., Badshah, M., Ahmed, S., & Ali, N. (2019). Microbial population dynamics in temperature-phased anaerobic digestion of municipal wastewater sludge. *Journal of Chemical Technology and Biotechnology*, *94*(6). https://doi.org/10.1002/jctb.5955

Hammes, K., Smernik, R. J., Skjemstad, J. O., Herzog, A., Vogt, U. F., & Schmidt, M. W. I. (2006). Synthesis and characterisation of laboratory-charred grass straw (Oryza sativa) and chestnut wood (Castanea sativa) as reference materials for black carbon quantification. *Organic Geochemistry*. https://doi.org/10.1016/j.orggeochem.2006.07.003

Han, Z., Sani, B., Mrozik, W., Obst, M., Beckingham, B., Karapanagioti, H. K., & Werner, D. (2015). Magnetite impregnation effects on the sorbent properties of activated carbons and biochars. *Water Research*, *70*. https://doi.org/10.1016/j.watres.2014.12.016

Hao, Z., Wang, C., Yan, Z., Jiang, H., & Xu, H. (2018). Magnetic particles modification of coconut shell-derived activated carbon and biochar for effective removal of phenol from water. *Chemosphere*, *211*. https://doi.org/10.1016/j.chemosphere.2018.08.038

Hashaikeh, R., Fang, Z., Butler, I. S., Hawari, J., & Kozinski, J. A. (2007). Hydrothermal dissolution of willow in hot compressed water as a model for biomass conversion. *Fuel*. https://doi.org/10.1016/j.fuel.2006.11.005

Hassan, M., Liu, Y., Naidu, R., Parikh, S. J., Du, J., Qi, F., & Willett, I. R. (2020). Influences of feedstock sources and pyrolysis temperature on the properties of biochar and functionality as adsorbents: A meta-analysis. *Science of the Total Environment*, Vol. 744. https://doi.org/10.1016/j.scitotenv.2020.140714

Hatfield, R., & Fukushima, R. S. (2005). Can lignin be accurately measured? *Crop Science*. https://doi.org/10.2135/cropsci2004.0238

He, Z., Mao, J., Honeycutt, C. W., Ohno, T., Hunt, J. F., & Cade-Menun, B. J. (2009). Characterization of plant-derived water extractable organic matter by multiple spectroscopic techniques. *Biology and Fertility of Soils*, *45*(6). https://doi.org/10.1007/s00374-009-0369-8

Helffrich, D., & Oechsner, H. (2003). The Hohenheim biogas yield test: comparison of different laboratory techniques for the digestion of biomass. *Agrartechnische Forschung*, *9*(1/3).

Helms, J. R., Stubbins, A., Ritchie, J. D., Minor, E. C., Kieber, D. J., & Mopper, K. (2008). Absorption spectral slopes and slope ratios as indicators of molecular weight, source, and photobleaching of chromophoric dissolved organic matter. *Limnology and Oceanography*, *53*(3). https://doi.org/10.4319/lo.2008.53.3.0955

Hernandez-Eugenio, G., Fardeau, M. L., Cayol, J. L., Patel, B. K. C., Thomas, P., Macarie, H., … Ollivier, B. (2002). Sporanaerobacter acetigenes gen. nov., sp. nov., a novel acetogenic, facultatively sulfur-reducing bacterium. *International Journal of Systematic and Evolutionary Microbiology*, *52*(4). https://doi.org/10.1099/ijs.0.01992-0

Hoffmann, V., Jung, D., Zimmermann, J., Correa, C. R., Elleuch, A., Halouani, K., & Kruse, A. (2019). Conductive carbon materials from the hydrothermal carbonization of vineyard residues for the application in electrochemical double-layer capacitors (EDLCs) and direct carbon fuel cells (DCFCs). *Materials*, *12*(10). https://doi.org/10.3390/MA12101703

Hossain, M. K., Strezov Vladimir, V., Chan, K. Y., Ziolkowski, A., & Nelson, P. F. (2011). Influence of pyrolysis temperature on production and nutrient properties

of wastewater sludge biochar. *Journal of Environmental Management*, *92*(1). https://doi.org/10.1016/j.jenvman.2010.09.008

Hosseini Koupaie, E., Azizi, A., Bazyar Lakeh, A. A., Hafez, H., & Elbeshbishy, E. (2019). Comparison of liquid and dewatered digestate as inoculum for anaerobic digestion of organic solid wastes. *Waste Management*. https://doi.org/10.1016/j.wasman.2019.02.014

Hou, Y., Velthof, G. L., Lesschen, J. P., Staritsky, I. G., & Oenema, O. (2017). Nutrient Recovery and Emissions of Ammonia, Nitrous Oxide, and Methane from Animal Manure in Europe: Effects of Manure Treatment Technologies. *Environmental Science and Technology*. https://doi.org/10.1021/acs.est.6b04524

Huang, C., Liu, C., Sun, X., Sun, Y., Li, R., Li, J., … Wang, L. (2015). Hydrolysis and volatile fatty acids accumulation of waste activated sludge enhanced by the combined use of nitrite and alkaline pH. *Environmental Science and Pollution Research*, *22*(23). https://doi.org/10.1007/s11356-015-4822-y

Huang, J., Kankanamge, N. R., Chow, C., Welsh, D. T., Li, T., & Teasdale, P. R. (2018). Removing ammonium from water and wastewater using cost-effective adsorbents: A review. *Journal of Environmental Sciences (China)*, Vol. 63. https://doi.org/10.1016/j.jes.2017.09.009

Hussain, M., Choa, Y. H., & Niihara, K. (2001). Fabrication process and electrical behavior of novel pressure-sensitive composites. *Composites - Part A: Applied Science and Manufacturing*, *32*(12). https://doi.org/10.1016/S1359-835X(01)00035-5

Intergovernmental Panel on Climate Change. (2014). Climate Change 2014 Mitigation of Climate Change. In *Climate Change 2014 Mitigation of Climate*

Change. https://doi.org/10.1017/cbo9781107415416

International Energy Agency. (2011). Key World Energy Statistics. *Statistics*.

International Energy Agency. (2017). World Energy Outlook 2017 - Chapter 1: Introduction and scope. *World Energy Outlook 2017*.

IPCC, Masson-Delmotte, V., Zhai, P., Pirani, A., Connors, S. L., Péan, C., … B., Z. (2021). Climate Change 2021: The Physical Science Basis. Contribution of Working Group I to the Sixth Assessment Report of the Intergovernmental Panel on Climate Change. In *Cambridge University Press*.

Ippolito, J. A., Cui, L., Kammann, C., Wrage-Mönnig, N., Estavillo, J. M., Fuertes-Mendizabal, T., … Borchard, N. (2020). Feedstock choice, pyrolysis temperature and type influence biochar characteristics: a comprehensive meta-data analysis review. *Biochar*, Vol. 2. https://doi.org/10.1007/s42773-020-00067-x

István, P. (2020). The European environment-state and outlook 2020. Knowledge for transition to a sustainable Europe. *Teruleti Statisztika*. https://doi.org/10.15196/TS600305

Jahn, L., Baumgartner, T., Krampe, J., & Svardal, K. (2020). Effect of NH3 and organic loading on the inhibition of mesophilic high-solid digestion. *Journal of Chemical Technology and Biotechnology*, *95*(3). https://doi.org/10.1002/jctb.6252

Jain, A., Balasubramanian, R., & Srinivasan, M. P. (2016). Hydrothermal conversion of biomass waste to activated carbon with high porosity: A review. *Chemical Engineering Journal*, Vol. 283. https://doi.org/10.1016/j.cej.2015.08.014

Jain, N., Bhatia, A., & Pathak, H. (2014). Emission of air pollutants from crop residue burning in India. *Aerosol and Air Quality Research*.

https://doi.org/10.4209/aaqr.2013.01.0031

Jang, H. M., Choi, Y. K., & Kan, E. (2018). Effects of dairy manure-derived biochar on psychrophilic, mesophilic and thermophilic anaerobic digestions of dairy manure. *Bioresource Technology*, *250*. https://doi.org/10.1016/j.biortech.2017.11.074

Ji, M., Sang, W., Tsang, D. C. W., Usman, M., Zhang, S., & Luo, G. (2020). Molecular and microbial insights towards understanding the effects of hydrochar on methane emission from paddy soil. *Science of the Total Environment*, *714*. https://doi.org/10.1016/j.scitotenv.2020.136769

Jiang, Y., McAdam, E., Zhang, Y., Heaven, S., Banks, C., & Longhurst, P. (2019). Ammonia inhibition and toxicity in anaerobic digestion: A critical review. *Journal of Water Process Engineering*, Vol. 32. https://doi.org/10.1016/j.jwpe.2019.100899

Jie, W., Peng, Y., Ren, N., & Li, B. (2014). Volatile fatty acids (VFAs) accumulation and microbial community structure of excess sludge (ES) at different pHs. *Bioresource Technology*, *152*. https://doi.org/10.1016/j.biortech.2013.11.011

Johnson, O. A., & Affam, A. C. (2019). Petroleum sludge treatment and disposal: A review. *Environmental Engineering Research*, *24*(2). https://doi.org/10.4491/EER.2018.134

Jung, D., Zimmermann, M., & Kruse, A. (2018). Hydrothermal Carbonization of Fructose: Growth Mechanism and Kinetic Model. *ACS Sustainable Chemistry and Engineering*, *6*(11). https://doi.org/10.1021/acssuschemeng.8b02118

Kambo, H. S., & Dutta, A. (2015). A comparative review of biochar and hydrochar in terms of production, physico-chemical properties and applications. *Renewable and Sustainable Energy Reviews*. https://doi.org/10.1016/j.rser.2015.01.050

Kang, S., Li, X., Fan, J., & Chang, J. (2012a). Characterization of hydrochars produced by hydrothermal carbonization of lignin, cellulose, d-xylose, and wood meal. *Industrial and Engineering Chemistry Research*. https://doi.org/10.1021/ie300565d

Kang, S., Li, X., Fan, J., & Chang, J. (2012b). Characterization of Hydrochars Produced by Hydrothermal Carbonization of Lignin, Cellulose, d-Xylose, and Wood Meal. *Industrial & Engineering Chemistry Research*, *51*(26), 9023–9031. https://doi.org/10.1021/ie300565d

Kapoor, R., Ghosh, P., Kumar, M., Sengupta, S., Gupta, A., Kumar, S. S., … Pant, D. (2020). Valorization of agricultural waste for biogas based circular economy in India: A research outlook. *Bioresource Technology*. https://doi.org/10.1016/j.biortech.2020.123036

Kappler, A., Wuestner, M. L., Ruecker, A., Harter, J., Halama, M., & Behrens, S. (2014). Biochar as an Electron Shuttle between Bacteria and Fe(III) Minerals. *Environmental Science and Technology Letters*. https://doi.org/10.1021/ez5002209

Kariyama, I. D., Zhai, X., & Wu, B. (2018). Influence of mixing on anaerobic digestion efficiency in stirred tank digesters: A review. *Water Research*, Vol. 143. https://doi.org/10.1016/j.watres.2018.06.065

Kavamura, V. N., & Esposito, E. (2010). Biotechnological strategies applied to the decontamination of soils polluted with heavy metals. *Biotechnology Advances*, Vol. 28. https://doi.org/10.1016/j.biotechadv.2009.09.002

Keiluweit, M., Nico, P. S., Johnson, M., & Kleber, M. (2010). Dynamic molecular structure of plant biomass-derived black carbon (biochar). *Environmental Science and Technology*. https://doi.org/10.1021/es9031419

Kelessidis, A., & Stasinakis, A. S. (2012). Comparative study of the methods used for treatment and final disposal of sewage sludge in European countries. *Waste Management*, *32*(6). https://doi.org/10.1016/j.wasman.2012.01.012

Kérouel, R., & Aminot, A. (1997). Fluorometric determination of ammonia in sea and estuarine waters by direct segmented flow analysis. *Marine Chemistry*, *57*(3–4). https://doi.org/10.1016/S0304-4203(97)00040-6

Khan, M. A., Ngo, H. H., Guo, W., Chang, S. W., Nguyen, D. D., Varjani, S., … Cheng, C. (2019). Selective production of volatile fatty acids at different pH in an anaerobic membrane bioreactor. *Bioresource Technology*, *283*. https://doi.org/10.1016/j.biortech.2019.03.073

Khan, Z. H., Gao, M., Qiu, W., & Song, Z. (2020). Properties and adsorption mechanism of magnetic biochar modified with molybdenum disulfide for cadmium in aqueous solution. *Chemosphere*, *255*. https://doi.org/10.1016/j.chemosphere.2020.126995

Khanal, S. K., Surampalli, R. Y., Zhang, T. C., Lamsal, B. P., Tyagi, R. D., & Kao, C. M. (2010). Bioenergy and biofuel from biowastes and biomass. In *Bioenergy and Biofuel from Biowastes and Biomass*. https://doi.org/10.1061/9780784410899

Khelaifia, S., Raoult, D., & Drancourt, M. (2013). A Versatile Medium for Cultivating Methanogenic Archaea. *PLoS ONE*, *8*(4). https://doi.org/10.1371/journal.pone.0061563

Kim, W., Suh, C. Y., Cho, S. W., Roh, K. M., Kwon, H., Song, K., & Shon, I. J. (2012). A new method for the identification and quantification of magnetite-maghemite mixture using conventional X-ray diffraction technique. *Talanta*, *94*. https://doi.org/10.1016/j.talanta.2012.03.001

Kinuthia, G. K., Ngure, V., Beti, D., Lugalia, R., Wangila, A., & Kamau, L. (2020).

Levels of heavy metals in wastewater and soil samples from open drainage channels in Nairobi, Kenya: community health implication. *Scientific Reports*, *10*(1). https://doi.org/10.1038/s41598-020-65359-5

Kizito, S., Wu, S., Kipkemoi Kirui, W., Lei, M., Lu, Q., Bah, H., & Dong, R. (2015). Evaluation of slow pyrolyzed wood and rice husks biochar for adsorption of ammonium nitrogen from piggery manure anaerobic digestate slurry. *Science of the Total Environment*, *505*. https://doi.org/10.1016/j.scitotenv.2014.09.096

Klüpfel, L., Keiluweit, M., Kleber, M., & Sander, M. (2014). Redox properties of plant biomass-derived black carbon (biochar). *Environmental Science and Technology*, *48*(10). https://doi.org/10.1021/es500906d

Klüpfel, L., Piepenbrock, A., Kappler, A., & Sander, M. (2014). Humic substances as fully regenerable electron acceptors in recurrently anoxic environments. *Nature Geoscience*, *7*(3). https://doi.org/10.1038/ngeo2084

Kominko, H., Gorazda, K., & Wzorek, Z. (2017). The Possibility of Organo-Mineral Fertilizer Production from Sewage Sludge. *Waste and Biomass Valorization*, *8*(5). https://doi.org/10.1007/s12649-016-9805-9

Krongthamchat, K., Riffat, R., & Dararat, S. (2006). Effect of trace metals on halophilic and mixed cultures in anaerobic treatment. *International Journal of Environmental Science and Technology*, *3*(2). https://doi.org/10.1007/BF03325913

Kumar, A. S. K., & Jiang, S. J. (2017). Synthesis of magnetically separable and recyclable magnetic nanoparticles decorated with β-cyclodextrin functionalized graphene oxide an excellent adsorption of As(V)/(III). *Journal of Molecular Liquids*, *237*. https://doi.org/10.1016/j.molliq.2017.04.093

Labatut, R. A., & Pronto, J. L. (2018). Sustainable waste-to-energy technologies:

Anaerobic digestion. In *Sustainable Food Waste-to-Energy Systems*. https://doi.org/10.1016/B978-0-12-811157-4.00004-8

Lalman, J. A., & Bagley, D. M. (2001). Anaerobic degradation and methanogenic inhibitory effects of oleic and stearic acids. *Water Research*, *35*(12). https://doi.org/10.1016/S0043-1354(00)00593-5

Lee, S. Y., Sankaran, R., Chew, K. W., Tan, C. H., Krishnamoorthy, R., Chu, D.-T., & Show, P.-L. (2019). Waste to bioenergy: a review on the recent conversion technologies. *BMC Energy*, *1*(1). https://doi.org/10.1186/s42500-019-0004-7

Lehmann, J. (2007). A handful of carbon. *Nature*. https://doi.org/10.1038/447143a

Lehmann, J., Rillig, M. C., Thies, J., Masiello, C. A., Hockaday, W. C., & Crowley, D. (2011). Biochar effects on soil biota - A review. *Soil Biology and Biochemistry*, Vol. 43. https://doi.org/10.1016/j.soilbio.2011.04.022

Lei, Z., Li, Q., Song, X., Wang, W., Zhang, Z., Peng, C., & Tian, L. (2018). Biochar mitigates dissolved organic carbon loss but does not affect dissolved organic nitrogen leaching loss caused by nitrogen deposition in Moso bamboo plantations. *Global Ecology and Conservation*, *16*. https://doi.org/10.1016/j.gecco.2018.e00494

Lewandowski, W. M., Ryms, M., & Kosakowski, W. (2020). Thermal biomass conversion: A review. *Processes*, *8*(5). https://doi.org/10.3390/PR8050516

Li, D., Song, L., Fang, H., Li, P., Teng, Y., Li, Y. Y., … Niu, Q. (2019). Accelerated bio-methane production rate in thermophilic digestion of cardboard with appropriate biochar: Dose-response kinetic assays, hybrid synergistic mechanism, and microbial networks analysis. *Bioresource Technology*, *290*. https://doi.org/10.1016/j.biortech.2019.121782

Li, H., Mahyoub, S. A. A., Liao, W., Xia, S., Zhao, H., Guo, M., & Ma, P. (2017).

Effect of pyrolysis temperature on characteristics and aromatic contaminants adsorption behavior of magnetic biochar derived from pyrolysis oil distillation residue. *Bioresource Technology*, *223*. https://doi.org/10.1016/j.biortech.2016.10.033

Li, J. H., Lv, G. H., Bai, W. B., Liu, Q., Zhang, Y. C., & Song, J. Q. (2016). Modification and use of biochar from wheat straw (Triticum aestivum L.) for nitrate and phosphate removal from water. *Desalination and Water Treatment*, *57*(10). https://doi.org/10.1080/19443994.2014.994104

Li, J., Zhang, M., Ye, Z., & Yang, C. (2019). Effect of manganese oxide-modified biochar addition on methane production and heavy metal speciation during the anaerobic digestion of sewage sludge. *Journal of Environmental Sciences (China)*. https://doi.org/10.1016/j.jes.2018.05.009

Li, K., Liu, R., Cui, S., Yu, Q., & Ma, R. (2018). Anaerobic co-digestion of animal manures with corn stover or apple pulp for enhanced biogas production. *Renewable Energy*, *118*. https://doi.org/10.1016/j.renene.2017.11.023

Li, K., Liu, R., Yu, Q., & Ma, R. (2018). Removal of nitrogen from chicken manure anaerobic digestion for enhanced biomethanization. *Fuel*, *232*. https://doi.org/10.1016/j.fuel.2018.05.142

Li, Q., Xu, M., Wang, G., Chen, R., Qiao, W., & Wang, X. (2018). Biochar assisted thermophilic co-digestion of food waste and waste activated sludge under high feedstock to seed sludge ratio in batch experiment. *Bioresource Technology*, *249*. https://doi.org/10.1016/j.biortech.2017.11.002

Li, X. Q., Brown, D. G., & Zhang, W. X. (2007). Stabilization of biosolids with nanoscale zero-valent iron (nZVI). *Journal of Nanoparticle Research*, *9*(2). https://doi.org/10.1007/s11051-006-9187-1

Li, Yanfei, Zimmerman, A. R., He, F., Chen, J., Han, L., Chen, H., … Gao, B. (2020). Solvent-free synthesis of magnetic biochar and activated carbon through ball-mill extrusion with Fe3O4 nanoparticles for enhancing adsorption of methylene blue. *Science of the Total Environment*, *722*. https://doi.org/10.1016/j.scitotenv.2020.137972

Li, Yin, Meas, A., Shan, S., Yang, R., & Gai, X. (2016). Production and optimization of bamboo hydrochars for adsorption of Congo red and 2-naphthol. *Bioresource Technology*. https://doi.org/10.1016/j.biortech.2016.02.012

Libra, J. A., Ro, K. S., Kammann, C., Funke, A., Berge, N. D., Neubauer, Y., … Emmerich, K. H. (2011). Hydrothermal carbonization of biomass residuals: A comparative review of the chemistry, processes and applications of wet and dry pyrolysis. *Biofuels*. https://doi.org/10.4155/bfs.10.81

Liebetrau, J., Kleinsteuber, S., Jacobi, F., & Pfeiffer, D. (2018). Monitoring and Process Control of Anaerobic Digestion Plants. *Chemical Engineering and Technology*, Vol. 41. https://doi.org/10.1002/ceat.201870045

Lim, H. Y., Yusup, S., Loy, A. C. M., Samsuri, S., Ho, S. S. K., Manaf, A. S. A., … Rianawati, E. (2020). Review on Conversion of Lignin Waste into Value-Added Resources in Tropical Countries. *Waste and Biomass Valorization*. https://doi.org/10.1007/s12649-020-01307-8

Limayem, A., & Ricke, S. C. (2012). Lignocellulosic biomass for bioethanol production: Current perspectives, potential issues and future prospects. *Progress in Energy and Combustion Science*, Vol. 38. https://doi.org/10.1016/j.pecs.2012.03.002

Lin, J. C., Mariuzza, D., Volpe, M., Fiori, L., Ceylan, S., & Goldfarb, J. L. (2021). Integrated thermochemical conversion process for valorizing mixed agricultural

and dairy waste to nutrient-enriched biochars and biofuels. *Bioresource Technology*, *328*. https://doi.org/10.1016/j.biortech.2021.124765

Lin, L., Yan, R., Liu, Y., & Jiang, W. (2010). In-depth investigation of enzymatic hydrolysis of biomass wastes based on three major components: Cellulose, hemicellulose and lignin. *Bioresource Technology*, *101*(21). https://doi.org/10.1016/j.biortech.2010.05.084

Lishan, X., Tao, L., Yin, W., Zhilong, Y., & Jiangfu, L. (2018). Comparative life cycle assessment of sludge management: A case study of Xiamen, China. *Journal of Cleaner Production*, *192*. https://doi.org/10.1016/j.jclepro.2018.04.171

Liu, C. H., Chu, W., Li, H., Boyd, S. A., Teppen, B. J., Mao, J., … Zhang, W. (2019). Quantification and characterization of dissolved organic carbon from biochars. *Geoderma*, *335*. https://doi.org/10.1016/j.geoderma.2018.08.019

Liu, C., Wang, H., Li, P., Xian, Q., & Tang, X. (2019). Biochar's impact on dissolved organic matter (DOM) export from a cropland soil during natural rainfalls. *Science of the Total Environment*, *650*. https://doi.org/10.1016/j.scitotenv.2018.09.356

Liu, D., Yu, S., Shen, Y., Chen, H., Shen, Z., Zhao, S., … Bao, B. (2015). Polyaniline Coated Boron Doped Biomass Derived Porous Carbon Composites for Supercapacitor Electrode Materials. *Industrial and Engineering Chemistry Research*, *54*(50). https://doi.org/10.1021/acs.iecr.5b02507

Liu, Jingyong, Huang, L., Xie, W., Kuo, J., Buyukada, M., & Evrendilek, F. (2019). Characterizing and optimizing (co-)pyrolysis as a function of different feedstocks, atmospheres, blend ratios, and heating rates. *Bioresource Technology*, *277*. https://doi.org/10.1016/j.biortech.2019.01.003

Liu, Jiwei, Jiang, J., Aihemaiti, A., Meng, Y., Yang, M., Xu, Y., … Chen, X. (2019).

Removal of phosphate from aqueous solution using MgO-modified magnetic biochar derived from anaerobic digestion residue. *Journal of Environmental Management*, *250*. https://doi.org/10.1016/j.jenvman.2019.109438

Liu, T., Liu, Z., Zheng, Q., Lang, Q., Xia, Y., Peng, N., & Gai, C. (2018). Effect of hydrothermal carbonization on migration and environmental risk of heavy metals in sewage sludge during pyrolysis. *Bioresource Technology*, *247*. https://doi.org/10.1016/j.biortech.2017.09.090

Liu, Y., Ngo, H. H., Guo, W., Peng, L., Wang, D., & Ni, B. (2019). The roles of free ammonia (FA) in biological wastewater treatment processes: A review. *Environment International*, Vol. 123. https://doi.org/10.1016/j.envint.2018.11.039

Liu, Z., Quek, A., Kent Hoekman, S., & Balasubramanian, R. (2013). Production of solid biochar fuel from waste biomass by hydrothermal carbonization. *Fuel*, *103*. https://doi.org/10.1016/j.fuel.2012.07.069

Liu, Z., & Zhang, F. S. (2009). Removal of lead from water using biochars prepared from hydrothermal liquefaction of biomass. *Journal of Hazardous Materials*. https://doi.org/10.1016/j.jhazmat.2009.01.085

Lü, F., Hao, L., Guan, D., Qi, Y., Shao, L., & He, P. (2013). Synergetic stress of acids and ammonium on the shift in the methanogenic pathways during thermophilic anaerobic digestion of organics. *Water Research*, *47*(7). https://doi.org/10.1016/j.watres.2013.01.049

Lü, F., He, P. J., Shao, L. M., & Lee, D. J. (2007). Effects of ammonia on hydrolysis of proteins and lipids from fish residues. *Applied Microbiology and Biotechnology*, *75*(5). https://doi.org/10.1007/s00253-007-0935-7

Lü, F., Luo, C., Shao, L., & He, P. (2016). Biochar alleviates combined stress of ammonium and acids by firstly enriching Methanosaeta and then

Methanosarcina. *Water Research*, *90*. https://doi.org/10.1016/j.watres.2015.12.029

Lu, L., Yu, W., Wang, Y., Zhang, K., Zhu, X., Zhang, Y., … Chen, B. (2020). Application of biochar-based materials in environmental remediation: from multi-level structures to specific devices. *Biochar*, Vol. 2. https://doi.org/10.1007/s42773-020-00041-7

Lu, Xiaofei, Wang, H., Ma, F., Zhao, G., & Wang, S. (2017). Enhanced anaerobic digestion of cow manure and rice straw by the supplementation of an iron oxide-zeolite system. *Energy and Fuels*, *31*(1). https://doi.org/10.1021/acs.energyfuels.6b02244

Lu, Xiaowei, Jordan, B., & Berge, N. D. (2012). Thermal conversion of municipal solid waste via hydrothermal carbonization: Comparison of carbonization products to products from current waste management techniques. *Waste Management*, *32*(7). https://doi.org/10.1016/j.wasman.2012.02.012

Luo, C., Lü, F., Shao, L., & He, P. (2015). Application of eco-compatible biochar in anaerobic digestion to relieve acid stress and promote the selective colonization of functional microbes. *Water Research*. https://doi.org/10.1016/j.watres.2014.10.052

Ma, J., Pan, J., Qiu, L., Wang, Q., & Zhang, Z. (2019). Biochar triggering multipath methanogenesis and subdued propionic acid accumulation during semi-continuous anaerobic digestion. *Bioresource Technology*, *293*. https://doi.org/10.1016/j.biortech.2019.122026

MacHala, L., Tuček, J., & Zbořil, R. (2011). Polymorphous transformations of nanometric iron(III) oxide: A review. *Chemistry of Materials*, Vol. 23. https://doi.org/10.1021/cm200397g

Magdalena, J. A., Ballesteros, M., & González-Fernandez, C. (2018). Efficient anaerobic digestion of microalgae biomass: Proteins as a key macromolecule. *Molecules*, Vol. 23. https://doi.org/10.3390/molecules23051098

Mai, D., Wen, R., Cao, W., Yuan, B., Liu, Y., Liu, Q., & Qian, G. (2017). Effect of Heavy Metal (Zn) on Redox Property of Hydrochar Produced from Lignin, Cellulose, and d-Xylose. *ACS Sustainable Chemistry and Engineering*, *5*(4). https://doi.org/10.1021/acssuschemeng.7b00204

Malherbe, S., & Cloete, T. E. (2002). Lignocellulose biodegradation: Fundamentals and applications. *Reviews in Environmental Science and Biotechnology*, Vol. 1. https://doi.org/10.1023/A:1020858910646

Manara, P., & Zabaniotou, A. (2012). Towards sewage sludge based biofuels via thermochemical conversion - A review. *Renewable and Sustainable Energy Reviews*, Vol. 16. https://doi.org/10.1016/j.rser.2012.01.074

Martínez, E. J., Rosas, J. G., Sotres, A., Moran, A., Cara, J., Sánchez, M. E., & Gómez, X. (2018). Codigestion of sludge and citrus peel wastes: Evaluating the effect of biochar addition on microbial communities. *Biochemical Engineering Journal*, *137*. https://doi.org/10.1016/j.bej.2018.06.010

Masebinu, S. O., Akinlabi, E. T., Muzenda, E., & Aboyade, A. O. (2019a). A review of biochar properties and their roles in mitigating challenges with anaerobic digestion. *Renewable and Sustainable Energy Reviews*. https://doi.org/10.1016/j.rser.2018.12.048

Masebinu, S. O., Akinlabi, E. T., Muzenda, E., & Aboyade, A. O. (2019b). A review of biochar properties and their roles in mitigating challenges with anaerobic digestion. *Renewable and Sustainable Energy Reviews*, Vol. 103. https://doi.org/10.1016/j.rser.2018.12.048

Mašek, O., Bogush, A., Jayakumar, A., Wurzer, C., & Peters, C. (2020). Biochar characterization methods. In *Biochar*. https://doi.org/10.1088/978-0-7503-2660-5ch5

Mašek, O., Brownsort, P., Cross, A., & Sohi, S. (2013). Influence of production conditions on the yield and environmental stability of biochar. *Fuel*, *103*. https://doi.org/10.1016/j.fuel.2011.08.044

Mašek, O., Buss, W., Brownsort, P., Rovere, M., Tagliaferro, A., Zhao, L., … Xu, G. (2019). Potassium doping increases biochar carbon sequestration potential by 45%, facilitating decoupling of carbon sequestration from soil improvement. *Scientific Reports*. https://doi.org/10.1038/s41598-019-41953-0

Mašek, O., Buss, W., & Sohi, S. (2018). Standard Biochar Materials. *Environmental Science and Technology*. https://doi.org/10.1021/acs.est.8b04053

Mateos, R., Escapa, A., Vanbroekhoven, K., Patil, S. A., Moran, A., & Pant, D. (2018). Microbial electrochemical technologies for CO2 and its derived products valorization. In *Biomass, Biofuels, Biochemicals: Microbial Electrochemical Technology: Sustainable Platform for Fuels, Chemicals and Remediation*. https://doi.org/10.1016/B978-0-444-64052-9.00032-7

McGlade, C., & Ekins, P. (2015). The geographical distribution of fossil fuels unused when limiting global warming to 2°C. *Nature*, *517*(7533). https://doi.org/10.1038/nature14016

Meegoda, J. N., Li, B., Patel, K., & Wang, L. B. (2018). A review of the processes, parameters, and optimization of anaerobic digestion. *International Journal of Environmental Research and Public Health*, Vol. 15. https://doi.org/10.3390/ijerph15102224

Méndez, A., Gascó, G., Ruiz, B., & Fuente, E. (2019). Hydrochars from industrial

macroalgae “Gelidium Sesquipedale” biomass wastes. *Bioresource Technology*, *275*. https://doi.org/10.1016/j.biortech.2018.12.074

Meng, F., Wang, D., & Zhang, M. (2021). Effect of ultrasonic vibration-assisted pelleting of biomass on biochar properties. *Journal of Cleaner Production*, *279*. https://doi.org/10.1016/j.jclepro.2020.123900

Mészáros, E., Jakab, E., Várhegyi, G., Bourke, J., Manley-Harris, M., Nunoura, T., & Antal, M. J. (2007). Do all carbonized charcoals have the same chemical structure? 1. Implications of thermogravimetry-mass spectrometry measurements. *Industrial and Engineering Chemistry Research*, *46*(18). https://doi.org/10.1021/ie0615842

Mia, S., Singh, B., & Dijkstra, F. A. (2017). Aged biochar affects gross nitrogen mineralization and recovery: a 15N study in two contrasting soils. *GCB Bioenergy*, *9*(7). https://doi.org/10.1111/gcbb.12430

Millati, R., Cahyono, R. B., Ariyanto, T., Azzahrani, I. N., Putri, R. U., & Taherzadeh, M. J. (2019). Agricultural, Industrial, Municipal, and Forest Wastes. In *Sustainable Resource Recovery and Zero Waste Approaches*. https://doi.org/10.1016/b978-0-444-64200-4.00001-3

Minor, E. C., Swenson, M. M., Mattson, B. M., & Oyler, A. R. (2014). Structural characterization of dissolved organic matter: A review of current techniques for isolation and analysis. *Environmental Sciences: Processes and Impacts*, Vol. 16. https://doi.org/10.1039/c4em00062e

Minyuk, P. S., Subbotnikova, T. V., & Plyashkevich, A. A. (2011). Measurements of thermal magnetic susceptibility of hematite and goethite. *Izvestiya, Physics of the Solid Earth*, *47*(9). https://doi.org/10.1134/S1069351311080052

Mittal, S., Ahlgren, E. O., & Shukla, P. R. (2018). Barriers to biogas dissemination in

India: A review. *Energy Policy*, *112*. https://doi.org/10.1016/j.enpol.2017.10.027

Mohan, D., Sarswat, A., Ok, Y. S., & Pittman, C. U. (2014). Organic and inorganic contaminants removal from water with biochar, a renewable, low cost and sustainable adsorbent - A critical review. *Bioresource Technology*, *160*. https://doi.org/10.1016/j.biortech.2014.01.120

Mohubedu, R. P., Diagboya, P. N. E., Abasi, C. Y., Dikio, E. D., & Mtunzi, F. (2019). Magnetic valorization of biomass and biochar of a typical plant nuisance for toxic metals contaminated water treatment. *Journal of Cleaner Production*, *209*. https://doi.org/10.1016/j.jclepro.2018.10.215

Mok, W. S. L., & Antal, M. J. (1992). Uncatalyzed Solvolysis of Whole Biomass Hemicellulose by Hot Compressed Liquid Water. *Industrial and Engineering Chemistry Research*, *31*(4). https://doi.org/10.1021/ie00004a026

Möller, K., & Müller, T. (2012). Effects of anaerobic digestion on digestate nutrient availability and crop growth: A review. *Engineering in Life Sciences*, Vol. 12. https://doi.org/10.1002/elsc.201100085

Momayez, F., Karimi, K., & Taherzadeh, M. J. (2019). Energy recovery from industrial crop wastes by dry anaerobic digestion: A review. *Industrial Crops and Products*, Vol. 129. https://doi.org/10.1016/j.indcrop.2018.12.051

Morrish, A. H. (2001). The physical principles of magnetism. In *The Physical Principles of Magnetism*. https://doi.org/10.1109/9780470546581

Mosier, N., Wyman, C., Dale, B., Elander, R., Lee, Y. Y., Holtzapple, M., & Ladisch, M. (2005). Features of promising technologies for pretreatment of lignocellulosic biomass. *Bioresource Technology*, *96*(6). https://doi.org/10.1016/j.biortech.2004.06.025

Mudhoo, A., & Kumar, S. (2013). Effects of heavy metals as stress factors on

anaerobic digestion processes and biogas production from biomass. *International Journal of Environmental Science and Technology*, Vol. 10. https://doi.org/10.1007/s13762-012-0167-y

Mukherjee, A., & Zimmerman, A. R. (2013). Organic carbon and nutrient release from a range of laboratory-produced biochars and biochar-soil mixtures. *Geoderma*, *193–194*. https://doi.org/10.1016/j.geoderma.2012.10.002

Mukome, F. N. D., Zhang, X., Silva, L. C. R., Six, J., & Parikh, S. J. (2013). Use of chemical and physical characteristics to investigate trends in biochar feedstocks. *Journal of Agricultural and Food Chemistry*. https://doi.org/10.1021/jf3049142

Mullen, C. A., Boateng, A. A., Goldberg, N. M., Lima, I. M., Laird, D. A., & Hicks, K. B. (2010). Bio-oil and bio-char production from corn cobs and stover by fast pyrolysis. *Biomass and Bioenergy*, *34*(1). https://doi.org/10.1016/j.biombioe.2009.09.012

Mumme, J., Eckervogt, L., Pielert, J., Diakité, M., Rupp, F., & Kern, J. (2011). Hydrothermal carbonization of anaerobically digested maize silage. *Bioresource Technology*. https://doi.org/10.1016/j.biortech.2011.06.099

Mumme, J., Srocke, F., Heeg, K., & Werner, M. (2014). Use of biochars in anaerobic digestion. *Bioresource Technology*, *164*, 189–197. https://doi.org/10.1016/j.biortech.2014.05.008

Munar-Florez, D. A., Varón-Cardenas, D. A., Ramírez-Contreras, N. E., & García-Núñez, J. A. (2021). Adsorption of ammonium and phosphates by biochar produced from oil palm shells: Effects of production conditions. *Results in Chemistry*, *3*. https://doi.org/10.1016/j.rechem.2021.100119

Mutegoa, E., Hilonga, A., & Njau, K. N. (2020). Approaches to the mitigation of

ammonia inhibition during anaerobic digestion – A review. *Water Practice and Technology*, Vol. 15. https://doi.org/10.2166/wpt.2020.047

Náthia-Neves, G., Berni, M., Dragone, G., Mussatto, S. I., & Forster-Carneiro, T. (2018). Anaerobic digestion process: technological aspects and recent developments. *International Journal of Environmental Science and Technology*, Vol. 15. https://doi.org/10.1007/s13762-018-1682-2

Navia, R., & Mittelbach, M. (2012). Could sewage sludge be considered a source of waste lipids for biodiesel production? *Waste Management and Research*, Vol. 30. https://doi.org/10.1177/0734242X12458074

Nges, I. A., & Liu, J. (2010). Effects of solid retention time on anaerobic digestion of dewatered-sewage sludge in mesophilic and thermophilic conditions. *Renewable Energy*, *35*(10). https://doi.org/10.1016/j.renene.2010.02.022

Nizamuddin, S., Baloch, H. A., Griffin, G. J., Mubarak, N. M., Bhutto, A. W., Abro, R., … Ali, B. S. (2017). An overview of effect of process parameters on hydrothermal carbonization of biomass. *Renewable and Sustainable Energy Reviews*, Vol. 73. https://doi.org/10.1016/j.rser.2016.12.122

Noori, A., Bartoli, M., Frache, A., Piatti, E., Giorcelli, M., & Tagliaferro, A. (2020). Development of pressure-responsive polypropylene and biochar-based materials. *Micromachines*, *11*(4). https://doi.org/10.3390/MI11040339

Ogwang, I., Kasedde, H., Nabuuma, B., Kirabira, J. B., & Lwanyaga, J. D. (2021). Characterization of Biogas Digestate for Solid Biofuel Production in Uganda. *Scientific African*, *12*. https://doi.org/10.1016/j.sciaf.2021.e00735

Ok, Y. S., Chang, S. X., Gao, B., & Chung, H. J. (2015). SMART biochar technology-A shifting paradigm towards advanced materials and healthcare research. *Environmental Technology and Innovation*, Vol. 4.

https://doi.org/10.1016/j.eti.2015.08.003

Özçimen, D., & Ersoy-Meriçboyu, A. (2010). Characterization of biochar and bio-oil samples obtained from carbonization of various biomass materials. *Renewable Energy*, *35*(6). https://doi.org/10.1016/j.renene.2009.11.042

Paksung, N., Pfersich, J., Arauzo, P. J., Jung, D., & Kruse, A. (2020). Structural Effects of Cellulose on Hydrolysis and Carbonization Behavior during Hydrothermal Treatment. *ACS Omega*, *5*(21). https://doi.org/10.1021/acsomega.0c00737

Pan, J., Ma, J., Zhai, L., Luo, T., Mei, Z., & Liu, H. (2019). Achievements of biochar application for enhanced anaerobic digestion: A review. *Bioresource Technology*, Vol. 292. https://doi.org/10.1016/j.biortech.2019.122058

Park, J. H., Wang, J. J., Xiao, R., Tafti, N., DeLaune, R. D., & Seo, D. C. (2018). Degradation of Orange G by Fenton-like reaction with Fe-impregnated biochar catalyst. *Bioresource Technology*, *249*. https://doi.org/10.1016/j.biortech.2017.10.030

Parliament. (1989). The Sludge (Use in Agriculture) Regulations 1989, No 1263.

Pastor-Poquet, V., Papirio, S., Steyer, J. P., Trably, E., Escudié, R., & Esposito, G. (2018). High-solids anaerobic digestion model for homogenized reactors. *Water Research*, *142*. https://doi.org/10.1016/j.watres.2018.06.016

Pathak, V. M., & Navneet. (2017). Review on the current status of polymer degradation: a microbial approach. *Bioresources and Bioprocessing*. https://doi.org/10.1186/s40643-017-0145-9

Patinvoh, R. J., & Taherzadeh, M. J. (2019). Challenges of biogas implementation in developing countries. *Current Opinion in Environmental Science and Health*, Vol. 12. https://doi.org/10.1016/j.coesh.2019.09.006

Pattanotai, T., Watanabe, H., & Okazaki, K. (2013). Experimental investigation of intraparticle secondary reactions of tar during wood pyrolysis. *Fuel*, *104*. https://doi.org/10.1016/j.fuel.2012.08.047

Pattanotai, T., Watanabe, H., & Okazaki, K. (2015). Effects of particle aspect ratio on pyrolysis and gasification of anisotropic wood cylinder. *Fuel*, *150*. https://doi.org/10.1016/j.fuel.2015.02.017

Paul, S., & Dutta, A. (2018). Challenges and opportunities of lignocellulosic biomass for anaerobic digestion. *Resources, Conservation and Recycling*, Vol. 130. https://doi.org/10.1016/j.resconrec.2017.12.005

Pearse, L. F., Hettiaratchi, J. P., & Kumar, S. (2018). Towards developing a representative biochemical methane potential (BMP) assay for landfilled municipal solid waste – A review. *Bioresource Technology*, Vol. 254. https://doi.org/10.1016/j.biortech.2018.01.069

Pellera, F. M., & Gidarakos, E. (2016). Effect of substrate to inoculum ratio and inoculum type on the biochemical methane potential of solid agroindustrial waste. *Journal of Environmental Chemical Engineering*, *4*(3). https://doi.org/10.1016/j.jece.2016.05.026

Peng, H., Zhang, Y., Tan, D., Zhao, Z., Zhao, H., & Quan, X. (2018). Roles of magnetite and granular activated carbon in improvement of anaerobic sludge digestion. *Bioresource Technology*. https://doi.org/10.1016/j.biortech.2017.10.047

Peng, L., Ren, Y., Gu, J., Qin, P., Zeng, Q., Shao, J., … Chai, L. (2014). Iron improving bio-char derived from microalgae on removal of tetracycline from aqueous system. *Environmental Science and Pollution Research*, *21*(12). https://doi.org/10.1007/s11356-014-2677-2

Perea-Moreno, M. A., Samerón-Manzano, E., & Perea-Moreno, A. J. (2019). Biomass as renewable energy: Worldwide research trends. *Sustainability (Switzerland)*, *11*(3). https://doi.org/10.3390/su11030863

Pereira, R. C., Arbestain, M. C., Sueiro, M. V., & Maclá-Agulló, J. A. (2015). Assessment of the surface chemistry of wood-derived biochars using wet chemistry, Fourier transform infrared spectroscopy and X-ray photoelectron spectroscopy. *Soil Research*, *53*(7). https://doi.org/10.1071/SR14194

Perlack, R. D. (2005). Biomass as feedstock for a bioenergy and bioproducts industry: the technical feasibility of a billion-ton annual supply. In *Agriculture*.

Petersen, S. O., Sommer, S. G., Béline, F., Burton, C., Dach, J., Dourmad, J. Y., … Mihelic, R. (2007). Recycling of livestock manure in a whole-farm perspective. *Livestock Science*. https://doi.org/10.1016/j.livsci.2007.09.001

Petersen, Søren O. (2018). Greenhouse gas emissions from liquid dairy manure: Prediction and mitigation. *Journal of Dairy Science*. https://doi.org/10.3168/jds.2017-13301

Petropoulos, E., Dolfing, J., Davenport, R. J., Bowen, E. J., & Curtis, T. P. (2017). Developing cold-adapted biomass for the anaerobic treatment of domestic wastewater at low temperatures (4, 8 and 15 °C) with inocula from cold environments. *Water Research*, *112*. https://doi.org/10.1016/j.watres.2016.12.009

Petropoulos, E., Shamurad, B., Tabraiz, S., Yu, Y., Davenport, R., Curtis, T. P., & Dolfing, J. (2021). Sewage treatment at 4 °c in anaerobic upflow reactors with and without a membrane-performance, function and microbial diversity. *Environmental Science: Water Research and Technology*, *7*(1). https://doi.org/10.1039/d0ew00753f

Pham, C. H., Triolo, J. M., Cu, T. T. T., Pedersen, L., & Sommer, S. G. (2013). Validation and recommendation of methods to measure biogas production potential of animal manure. *Asian-Australasian Journal of Animal Sciences*, *26*(6). https://doi.org/10.5713/ajas.2012.12623

Pham Van, D., Takeshi, F., Hoang Minh, G., & Pham Phu, S. T. (2020). Comparison Between Single and Two-Stage Anaerobic Digestion of Vegetable Waste: Kinetics of Methanogenesis and Carbon Flow. *Waste and Biomass Valorization*, *11*(11). https://doi.org/10.1007/s12649-019-00861-0

Pignatello, J. J. (2011). Interactions of Anthropogenic Organic Chemicals with Natural Organic Matter and Black Carbon in Environmental Particles. In *Biophysico-Chemical Processes of Anthropogenic Organic Compounds in Environmental Systems*. https://doi.org/10.1002/9780470944479.ch1

Pooja, N. S., Sajeev, M. S., Jeeva, M. L., & Padmaja, G. (2018). Bioethanol production from microwave-assisted acid or alkali-pretreated agricultural residues of cassava using separate hydrolysis and fermentation (SHF). *3 Biotech*, *8*(1). https://doi.org/10.1007/s13205-018-1095-4

Qambrani, N. A., Rahman, M. M., Won, S., Shim, S., & Ra, C. (2017). Biochar properties and eco-friendly applications for climate change mitigation, waste management, and wastewater treatment: A review. *Renewable and Sustainable Energy Reviews*. https://doi.org/10.1016/j.rser.2017.05.057

Qian, Y., Song, K., Hu, T., & Ying, T. (2018). Environmental status of livestock and poultry sectors in China under current transformation stage. *Science of the Total Environment*. https://doi.org/10.1016/j.scitotenv.2017.12.045

Qiang, H., Niu, Q., Chi, Y., & Li, Y. (2013). Trace metals requirements for continuous thermophilic methane fermentation of high-solid food waste. *Chemical*

Engineering Journal, *222*. https://doi.org/10.1016/j.cej.2013.02.076

Qin, Y., Wang, H., Li, X., Cheng, J. J., & Wu, W. (2017). Improving methane yield from organic fraction of municipal solid waste (OFMSW) with magnetic rice-straw biochar. *Bioresource Technology*, *245*, 1058–1066. https://doi.org/10.1016/j.biortech.2017.09.047

Qu, X., Fu, H., Mao, J., Ran, Y., Zhang, D., & Zhu, D. (2016). Chemical and structural properties of dissolved black carbon released from biochars. *Carbon*, *96*. https://doi.org/10.1016/j.carbon.2015.09.106

Racek, J., Sevcik, J., Chorazy, T., Kucerik, J., & Hlavinek, P. (2020). Biochar – Recovery Material from Pyrolysis of Sewage Sludge: A Review. *Waste and Biomass Valorization*, Vol. 11. https://doi.org/10.1007/s12649-019-00679-w

Rajagopal, R., Massé, D. I., & Singh, G. (2013). A critical review on inhibition of anaerobic digestion process by excess ammonia. *Bioresource Technology*. https://doi.org/10.1016/j.biortech.2013.06.030

Rajkovich, S., Enders, A., Hanley, K., Hyland, C., Zimmerman, A. R., & Lehmann, J. (2012). Corn growth and nitrogen nutrition after additions of biochars with varying properties to a temperate soil. *Biology and Fertility of Soils*, *48*(3). https://doi.org/10.1007/s00374-011-0624-7

Rana, M. S., Bhushan, S., & Prajapati, S. K. (2020). New insights on improved growth and biogas production potential of Chlorella pyrenoidosa through intermittent iron oxide nanoparticle supplementation. *Scientific Reports*, *10*(1). https://doi.org/10.1038/s41598-020-71141-4

Rasapoor, M., Young, B., Brar, R., Sarmah, A., Zhuang, W. Q., & Baroutian, S. (2020). Recognizing the challenges of anaerobic digestion: Critical steps toward improving biogas generation. *Fuel*. https://doi.org/10.1016/j.fuel.2019.116497

Ratasuk, N., & Nanny, M. A. (2007). Characterization and quantification of reversible redox sites in humic substances. *Environmental Science and Technology*, *41*(22). https://doi.org/10.1021/es071389u

Reibe, K., Götz, K. P., Roß, C. L., Döring, T. F., Ellmer, F., & Ruess, L. (2015). Impact of quality and quantity of biochar and hydrochar on soil Collembola and growth of spring wheat. *Soil Biology and Biochemistry*. https://doi.org/10.1016/j.soilbio.2015.01.014

Ren, J., Wang, F., Zhai, Y., Zhu, Y., Peng, C., Wang, T., … Zeng, G. (2017). Effect of sewage sludge hydrochar on soil properties and Cd immobilization in a contaminated soil. *Chemosphere*, *189*. https://doi.org/10.1016/j.chemosphere.2017.09.102

Ren, S., Usman, M., Tsang, D. C. W., O-Thong, S., Angelidaki, I., Zhu, X., … Luo, G. (2020). Hydrochar-Facilitated Anaerobic Digestion: Evidence for Direct Interspecies Electron Transfer Mediated through Surface Oxygen-Containing Functional Groups. *Environmental Science and Technology*. https://doi.org/10.1021/acs.est.0c00112

Reza, M. T., Rottler, E., Tölle, R., Werner, M., Ramm, P., & Mumme, J. (2015). Production, characterization, and biogas application of magnetic hydrochar from cellulose. *Bioresource Technology*. https://doi.org/10.1016/j.biortech.2015.03.044

Reza, M. T., Uddin, M. H., Lynam, J. G., & Coronella, C. J. (2014). Engineered pellets from dry torrefied and HTC biochar blends. *Biomass and Bioenergy*, *63*. https://doi.org/10.1016/j.biombioe.2014.01.038

Roubík, H., Mazancová, J., Le Dinh, P., Dinh Van, D., & Banout, J. (2018). Biogas quality across small-scale biogas plants: A case of central vietnam. *Energies*,

11(7). https://doi.org/10.3390/en11071794

Routledge, S. J., Hewitt, C. J., Bora, N., & Bill, R. M. (2011). Antifoam addition to shake flask cultures of recombinant Pichia pastoris increases yield. *Microbial Cell Factories*, *10*. https://doi.org/10.1186/1475-2859-10-17

Saha, N., Saba, A., & Reza, M. T. (2019). Effect of hydrothermal carbonization temperature on pH, dissociation constants, and acidic functional groups on hydrochar from cellulose and wood. *Journal of Analytical and Applied Pyrolysis*, *137*. https://doi.org/10.1016/j.jaap.2018.11.018

Saha, N., Xin, D., Chiu, P. C., & Reza, M. T. (2019). Effect of Pyrolysis Temperature on Acidic Oxygen-Containing Functional Groups and Electron Storage Capacities of Pyrolyzed Hydrochars. *ACS Sustainable Chemistry and Engineering*. https://doi.org/10.1021/acssuschemeng.9b00024

Salimova, A., Zuo, J., Liu, F., Wang, Y., Wang, S., & Verichev, K. (2020). Ammonia and phosphorus removal from agricultural runoff using cash crop waste-derived biochars. *Frontiers of Environmental Science and Engineering*, *14*(3). https://doi.org/10.1007/s11783-020-1225-1

Sanahuja-Parejo, O., Veses, A., Navarro, M. V., López, J. M., Murillo, R., Callén, M. S., & García, T. (2019). Drop-in biofuels from the co-pyrolysis of grape seeds and polystyrene. *Chemical Engineering Journal*, *377*. https://doi.org/10.1016/j.cej.2018.10.183

Sánchez-González, J., MacÍas-García, A., Alexandre-Franco, M. F., & Gómez-Serrano, V. (2005). Electrical conductivity of carbon blacks under compression. *Carbon*, *43*(4). https://doi.org/10.1016/j.carbon.2004.10.045

Santhoshkumar, A., & Anand, R. (2019). Microwave-assisted fast pyrolysis of hazardous waste engine oil into green fuels. In *Advances in Eco-Fuels for a*

Sustainable Environment. https://doi.org/10.1016/b978-0-08-102728-8.00005-x

Saratale, G. D., Saratale, R. G., Banu, J. R., & Chang, J.-S. (2019). Biohydrogen Production From Renewable Biomass Resources. In *Biohydrogen*. https://doi.org/10.1016/b978-0-444-64203-5.00010-1

Sarfaraz, Q., Silva, L., Drescher, G., Zafar, M., Severo, F., Kokkonen, A., … Solaiman, Z. (2020). Characterization and carbon mineralization of biochars produced from different animal manures and plant residues. *Scientific Reports*, *10*(1). https://doi.org/10.1038/s41598-020-57987-8

Sarkar, N., Ghosh, S. K., Bannerjee, S., & Aikat, K. (2012). Bioethanol production from agricultural wastes: An overview. *Renewable Energy*, Vol. 37. https://doi.org/10.1016/j.renene.2011.06.045

Sarkhot, D. V., Ghezzehei, T. A., & Berhe, A. A. (2013). Effectiveness of Biochar for Sorption of Ammonium and Phosphate from Dairy Effluent. *Journal of Environmental Quality*, *42*(5). https://doi.org/10.2134/jeq2012.0482

Sawatdeenarunat, C., Surendra, K. C., Takara, D., Oechsner, H., & Khanal, S. K. (2015). Anaerobic digestion of lignocellulosic biomass: Challenges and opportunities. *Bioresource Technology*, Vol. 178. https://doi.org/10.1016/j.biortech.2014.09.103

Schink, B. (1997). Energetics of syntrophic cooperation in methanogenic degradation. *Microbiology and Molecular Biology Reviews : MMBR*, *61*(2). https://doi.org/10.1128/.61.2.262-280.1997

Schwanninger, M., Rodrigues, J. C., Pereira, H., & Hinterstoisser, B. (2004). Effects of short-time vibratory ball milling on the shape of FT-IR spectra of wood and cellulose. *Vibrational Spectroscopy*, *36*(1). https://doi.org/10.1016/j.vibspec.2004.02.003

Schwertmann, U. (1971). Transformation of hematite to goethite in soils [4]. *Nature*, Vol. 232. https://doi.org/10.1038/232624a0

Şengör, S. S., Barua, S., Gikas, P., Ginn, T. R., Peyton, B., Sani, R. K., & Spycher, N. F. (2009). Influence of heavy metals on microbial growth kinetics including lag time: Mathematical modeling and experimental verification. *Environmental Toxicology and Chemistry*, *28*(10). https://doi.org/10.1897/08-273.1

Serrano-Ruiz, J. C., West, R. M., & Dumesic, J. A. (2010). Catalytic conversion of renewable biomass resources to fuels and chemicals. *Annual Review of Chemical and Biomolecular Engineering*, *1*. https://doi.org/10.1146/annurev-chembioeng-073009-100935

Sevilla, M., & Fuertes, A. B. (2009). The production of carbon materials by hydrothermal carbonization of cellulose. *Carbon*. https://doi.org/10.1016/j.carbon.2009.04.026

Sevilla, Marta, Maciá-Agulló, J. A., & Fuertes, A. B. (2011). Hydrothermal carbonization of biomass as a route for the sequestration of CO2: Chemical and structural properties of the carbonized products. *Biomass and Bioenergy*, *35*(7). https://doi.org/10.1016/j.biombioe.2011.04.032

Sewu, D. D., Tran, H. N., Ohemeng-Boahen, G., & Woo, S. H. (2020). Facile magnetic biochar production route with new goethite nanoparticle precursor. *Science of the Total Environment*, *717*. https://doi.org/10.1016/j.scitotenv.2020.137091

Shakeri Yekta, S., Gonsior, M., Schmitt-Kopplin, P., & Svensson, B. H. (2012). Characterization of dissolved organic matter in full scale continuous stirred tank biogas reactors using ultrahigh resolution mass spectrometry: A qualitative overview. *Environmental Science and Technology*, Vol. 46.

https://doi.org/10.1021/es3024447

Sharma, H. B., Panigrahi, S., & Dubey, B. K. (2019). Hydrothermal carbonization of yard waste for solid bio-fuel production: Study on combustion kinetic, energy properties, grindability and flowability of hydrochar. *Waste Management*, *91*. https://doi.org/10.1016/j.wasman.2019.04.056

Sharma, P., Gaur, V. K., Kim, S. H., & Pandey, A. (2020). Microbial strategies for bio-transforming food waste into resources. *Bioresource Technology*. https://doi.org/10.1016/j.biortech.2019.122580

Sharma, R. K., Wooten, J. B., Baliga, V. L., Lin, X., Chan, W. G., & Hajaligol, M. R. (2004). Characterization of chars from pyrolysis of lignin. *Fuel*, *83*(11–12). https://doi.org/10.1016/j.fuel.2003.11.015

Shen, Y., Linville, J. L., Ignacio-de Leon, P. A. A., Schoene, R. P., & Urgun-Demirtas, M. (2016). Towards a sustainable paradigm of waste-to-energy process: Enhanced anaerobic digestion of sludge with woody biochar. *Journal of Cleaner Production*, *135*. https://doi.org/10.1016/j.jclepro.2016.06.144

Shen, Y., Linville, J. L., Urgun-Demirtas, M., Schoene, R. P., & Snyder, S. W. (2015). Producing pipeline-quality biomethane via anaerobic digestion of sludge amended with corn stover biochar with in-situ CO2 removal. *Applied Energy*. https://doi.org/10.1016/j.apenergy.2015.08.016

Shi, X., Lin, J., Zuo, J., Li, P., Li, X., & Guo, X. (2017). Effects of free ammonia on volatile fatty acid accumulation and process performance in the anaerobic digestion of two typical bio-wastes. *Journal of Environmental Sciences (China)*, *55*. https://doi.org/10.1016/j.jes.2016.07.006

Show, K.-Y., Yan, Y., & Lee, D.-J. (2019). Bioreactor and Bioprocess Design for Biohydrogen Production. In *Biohydrogen*. https://doi.org/10.1016/b978-0-444-

64203-5.00016-2

Siddique, N. I., & Zularisam, A. W. (2012). Renewable methane from ammonium bicarbonate supplemented petrochemical wastewater treatment during anaerobic co-digestion in CSTR. *Procedia Engineering*, *50*. https://doi.org/10.1016/j.proeng.2012.10.017

Sika, M. P., & Hardie, A. G. (2014). Effect of pine wood biochar on ammonium nitrate leaching and availability in a South African sandy soil. *European Journal of Soil Science*, *65*(1). https://doi.org/10.1111/ejss.12082

Silber, A., Levkovitch, I., & Graber, E. R. (2010). PH-dependent mineral release and surface properties of cornstraw biochar: Agronomic implications. *Environmental Science and Technology*, *44*(24). https://doi.org/10.1021/es101283d

Silva, T. C. F., Vergütz, L., Pacheco, A. A., Melo, L. F., Renato, N. S., & Melo, L. C. A. (2020). Characterization and application of magnetic biochar for the removal of phosphorus from water. *Anais Da Academia Brasileira de Ciencias*, *92*(3). https://doi.org/10.1590/0001-3765202020190440

Singh, B., Camps-Arbestain, M., Lehmann, J., & CSIRO (Australia). (2017). Biochar: A Guide to Analytical Methods. In *Csiro publishing*.

Singh, B., Singh, B. P., & Cowie, A. L. (2010). Characterisation and evaluation of biochars for their application as a soil amendment. *Australian Journal of Soil Research*, *48*(6–7). https://doi.org/10.1071/SR10058

Singh Karam, D., Nagabovanalli, P., Sundara Rajoo, K., Fauziah Ishak, C., Abdu, A., Rosli, Z., … Zulperi, D. (2021). An overview on the preparation of rice husk biochar, factors affecting its properties, and its agriculture application. *Journal of the Saudi Society of Agricultural Sciences*. https://doi.org/10.1016/j.jssas.2021.07.005

Sipra, A. T., Gao, N., & Sarwar, H. (2018). Municipal solid waste (MSW) pyrolysis for bio-fuel production: A review of effects of MSW components and catalysts. *Fuel Processing Technology*, Vol. 175. https://doi.org/10.1016/j.fuproc.2018.02.012

Skomski, R. (2010). Simple Models of Magnetism. In *Simple Models of Magnetism* (Vol. 9780198570752). https://doi.org/10.1093/acprof:oso/9780198570752.001.0001

Smith, K. A., & Williams, A. G. (2016). Production and management of cattle manure in the UK and implications for land application practice. *Soil Use and Management*. https://doi.org/10.1111/sum.12247

Smoliński, A., Karwot, J., Bondaruk, J., & Bak, A. (2019). The bioconversion of sewage sludge to bio-fuel: The environmental and economic benefits. *Materials*, *12*(15). https://doi.org/10.3390/ma12152417

Sohi, S. P., Krull, E., Lopez-Capel, E., & Bol, R. (2010). A review of biochar and its use and function in soil. In *Advances in Agronomy*. https://doi.org/10.1016/S0065-2113(10)05002-9

Song, J., Jiang, H., Shi, D. L., Feng, X. Q., Huang, Y., Yu, M. F., & Hwang, K. C. (2006). Stone-Wales transformation: Precursor of fracture in carbon nanotubes. *International Journal of Mechanical Sciences*, *48*(12). https://doi.org/10.1016/j.ijmecsci.2006.03.019

Stams, A. J. M., & Plugge, C. M. (2009). Electron transfer in syntrophic communities of anaerobic bacteria and archaea. *Nature Reviews Microbiology*, Vol. 7. https://doi.org/10.1038/nrmicro2166

Su, L., Shi, X., Guo, G., Zhao, A., & Zhao, Y. (2013). Stabilization of sewage sludge in the presence of nanoscale zero-valent iron (nZVI): Abatement of odor and improvement of biogas production. *Journal of Material Cycles and Waste*

Management, *15*(4). https://doi.org/10.1007/s10163-013-0150-9

Suberu, M. Y., Bashir, N., & Mustafa, M. W. (2013). Biogenic waste methane emissions and methane optimization for bioelectricity in Nigeria. *Renewable and Sustainable Energy Reviews*, Vol. 25. https://doi.org/10.1016/j.rser.2013.05.017

Sun, J., Norouzi, O., & Mašek, O. (2021). A state-of-the-art review on algae pyrolysis for bioenergy and biochar production. *Bioresource Technology*. https://doi.org/10.1016/j.biortech.2021.126258

Sun, K., Kang, M., Zhang, Z., Jin, J., Wang, Z., Pan, Z., … Xing, B. (2013). Impact of deashing treatment on biochar structural properties and potential sorption mechanisms of phenanthrene. *Environmental Science and Technology*, *47*(20). https://doi.org/10.1021/es4026744

Sun, R. (2010). Cereal straw as a resource for sustainable biomaterials and biofuels: chemistry, extractives, lignins, hemicelluloses and cellulose. *Concrete*.

Sun, T., Levin, B. D. A., Guzman, J. J. L., Enders, A., Muller, D. A., Angenent, L. T., & Lehmann, J. (2017). Rapid electron transfer by the carbon matrix in natural pyrogenic carbon. *Nature Communications*, *8*. https://doi.org/10.1038/ncomms14873

Syed-Hassan, S. S. A., Wang, Y., Hu, S., Su, S., & Xiang, J. (2017). Thermochemical processing of sewage sludge to energy and fuel: Fundamentals, challenges and considerations. *Renewable and Sustainable Energy Reviews*, Vol. 80. https://doi.org/10.1016/j.rser.2017.05.262

Taghizadeh-Toosi, A., Clough, T. J., Sherlock, R. R., & Condron, L. M. (2012). Biochar adsorbed ammonia is bioavailable. *Plant and Soil*, *350*(1–2). https://doi.org/10.1007/s11104-011-0870-3

Taha, M., Foda, M., Shahsavari, E., Aburto-Medina, A., Adetutu, E., & Ball, A.

(2016). Commercial feasibility of lignocellulose biodegradation: Possibilities and challenges. *Current Opinion in Biotechnology*, Vol. 38. https://doi.org/10.1016/j.copbio.2016.02.012

Takada, M., Minami, E., & Saka, S. (2018). Decomposition behaviors of the lignocellulosics as treated by semi-flow hot-compressed water. *Journal of Supercritical Fluids*, Vol. 133. https://doi.org/10.1016/j.supflu.2017.07.007

Takaya, C. A., Fletcher, L. A., Singh, S., Anyikude, K. U., & Ross, A. B. (2016). Phosphate and ammonium sorption capacity of biochar and hydrochar from different wastes. *Chemosphere*. https://doi.org/10.1016/j.chemosphere.2015.11.052

Tan, X., Liu, Y., Zeng, G., Wang, X., Hu, X., Gu, Y., & Yang, Z. (2015). Application of biochar for the removal of pollutants from aqueous solutions. *Chemosphere*, Vol. 125. https://doi.org/10.1016/j.chemosphere.2014.12.058

Tang, Y., Alam, M. S., Konhauser, K. O., Alessi, D. S., Xu, S., Tian, W. J., & Liu, Y. (2019). Influence of pyrolysis temperature on production of digested sludge biochar and its application for ammonium removal from municipal wastewater. *Journal of Cleaner Production*. https://doi.org/10.1016/j.jclepro.2018.10.268

Theerarattananoon, K., Xu, F., Wilson, J., Staggenborg, S., Mckinney, L., Vadlani, P., … Wang, D. (2012). Effects of the pelleting conditions on chemical composition and sugar yield of corn stover, big bluestem, wheat straw, and sorghum stalk pellets. *Bioprocess and Biosystems Engineering*, *35*(4). https://doi.org/10.1007/s00449-011-0642-8

Titirici, M. M., & Antonietti, M. (2010). Chemistry and materials options of sustainable carbon materials made by hydrothermal carbonization. *Chemical Society Reviews*, *39*(1). https://doi.org/10.1039/b819318p

Tomczyk, A., Sokołowska, Z., & Boguta, P. (2020). Biochar physicochemical properties: pyrolysis temperature and feedstock kind effects. *Reviews in Environmental Science and Biotechnology*, Vol. 19. https://doi.org/10.1007/s11157-020-09523-3

Torri, C., & Fabbri, D. (2014). Biochar enables anaerobic digestion of aqueous phase from intermediate pyrolysis of biomass. *Bioresource Technology*. https://doi.org/10.1016/j.biortech.2014.09.021

Tradler, S. B., Mayr, S., Himmelsbach, M., Priewasser, R., Baumgartner, W., & Stadler, A. T. (2018). Hydrothermal carbonization as an all-inclusive process for food-waste conversion. *Bioresource Technology Reports*. https://doi.org/10.1016/j.biteb.2018.04.009

Triolo, J. M., Pedersen, L., Qu, H., & Sommer, S. G. (2012). Biochemical methane potential and anaerobic biodegradability of non-herbaceous and herbaceous phytomass in biogas production. *Bioresource Technology*, *125*. https://doi.org/10.1016/j.biortech.2012.08.079

Tripathi, M., Sahu, J. N., & Ganesan, P. (2016). Effect of process parameters on production of biochar from biomass waste through pyrolysis: A review. *Renewable and Sustainable Energy Reviews*, Vol. 55. https://doi.org/10.1016/j.rser.2015.10.122

Tripathi, N., Hills, C. D., Singh, R. S., & Atkinson, C. J. (2019). Biomass waste utilisation in low-carbon products: harnessing a major potential resource. *Npj Climate and Atmospheric Science*. https://doi.org/10.1038/s41612-019-0093-5

Tu, C., Wei, J., Guan, F., Liu, Y., Sun, Y., & Luo, Y. (2020). Biochar and bacteria inoculated biochar enhanced Cd and Cu immobilization and enzymatic activity in a polluted soil. *Environment International*, *137*.

https://doi.org/10.1016/j.envint.2020.105576

Uchimiya, M., Hiradate, S., & Antal, M. J. (2015). Influence of carbonization methods on the aromaticity of pyrogenic dissolved organic carbon. *Energy and Fuels*, *29*(4). https://doi.org/10.1021/acs.energyfuels.5b00146

Usman, M., Shi, Z., Ren, S., Ngo, H. H., Luo, G., & Zhang, S. (2020). Hydrochar promoted anaerobic digestion of hydrothermal liquefaction wastewater: Focusing on the organic degradation and microbial community. *Chemical Engineering Journal*. https://doi.org/10.1016/j.cej.2020.125766

van Dijk, K. C., Lesschen, J. P., & Oenema, O. (2016). Phosphorus flows and balances of the European Union Member States. *Science of the Total Environment*. https://doi.org/10.1016/j.scitotenv.2015.08.048

Velthof, G. L., Lesschen, J. P., Webb, J., Pietrzak, S., Miatkowski, Z., Pinto, M., … Oenema, O. (2014). The impact of the Nitrates Directive on nitrogen emissions from agriculture in the EU-27 during 2000-2008. *Science of the Total Environment*. https://doi.org/10.1016/j.scitotenv.2013.04.058

Villalobos, M., Escobar-Quiroz, I. N., & Salazar-Camacho, C. (2014). The influence of particle size and structure on the sorption and oxidation behavior of birnessite: I. Adsorption of As(V) and oxidation of As(III). *Geochimica et Cosmochimica Acta*, *125*. https://doi.org/10.1016/j.gca.2013.10.029

Voet, A., Whitten, W. N., & Cook, F. R. (1964). 169. The electrical conductance of carbon blacks. *Carbon*, *1*(3). https://doi.org/10.1016/0008-6223(64)90460-9

Wainaina, S., Lukitawesa, Kumar Awasthi, M., & Taherzadeh, M. J. (2019). Bioengineering of anaerobic digestion for volatile fatty acids, hydrogen or methane production: A critical review. *Bioengineered*, Vol. 10. https://doi.org/10.1080/21655979.2019.1673937

Wambugu, C. W., Rene, E. R., van de Vossenberg, J., Dupont, C., & van Hullebusch, E. D. (2019). Role of biochar in anaerobic digestion based biorefinery for food waste. *Frontiers in Energy Research*. https://doi.org/10.3389/fenrg.2019.00014

Wang, D., Ai, J., Shen, F., Yang, G., Zhang, Y., Deng, S., … Song, C. (2017). Improving anaerobic digestion of easy-acidification substrates by promoting buffering capacity using biochar derived from vermicompost. *Bioresource Technology*. https://doi.org/10.1016/j.biortech.2016.12.060

Wang, G., Li, Q., Gao, X., & Wang, X. C. (2018). Synergetic promotion of syntrophic methane production from anaerobic digestion of complex organic wastes by biochar: Performance and associated mechanisms. *Bioresource Technology*, *250*. https://doi.org/10.1016/j.biortech.2017.12.004

Wang, G., Li, Q., Gao, X., & Wang, X. C. (2019). Sawdust-Derived Biochar Much Mitigates VFAs Accumulation and Improves Microbial Activities to Enhance Methane Production in Thermophilic Anaerobic Digestion. *ACS Sustainable Chemistry and Engineering*. https://doi.org/10.1021/acssuschemeng.8b04789

Wang, Jia, Liao, Z., Ifthikar, J., Shi, L., Chen, Z., & Chen, Z. (2017). One-step preparation and application of magnetic sludge-derived biochar on acid orange 7 removal via both adsorption and persulfate based oxidation. *RSC Advances*, *7*(30). https://doi.org/10.1039/c7ra01425b

Wang, Jin, Li, L., Wong, C. L., Sun, L., Shen, Z., & Madhavi, S. (2013). Controlled synthesis of α-FeOOH nanorods and their transformation to mesoporous α-Fe2O3, Fe3O4@C nanorods as anodes for lithium ion batteries. *RSC Advances*, *3*(35). https://doi.org/10.1039/c3ra41886c

Wang, K., Yin, J., Shen, D., & Li, N. (2014). Anaerobic digestion of food waste for

volatile fatty acids (VFAs) production with different types of inoculum: Effect of pH. *Bioresource Technology*, *161*. https://doi.org/10.1016/j.biortech.2014.03.088

Wang, M., Zhao, Z., Niu, J., & Zhang, Y. (2019). Potential of Crystalline and Amorphous Ferric Oxides for Biostimulation of Anaerobic Digestion. *ACS Sustainable Chemistry and Engineering*, *7*(1). https://doi.org/10.1021/acssuschemeng.8b04267

Wang, M., Zhao, Z., & Zhang, Y. (2021). Magnetite-contained biochar derived from fenton sludge modulated electron transfer of microorganisms in anaerobic digestion. *Journal of Hazardous Materials*, *403*. https://doi.org/10.1016/j.jhazmat.2020.123972

Wang, P., Peng, H., Adhikari, S., Higgins, B., Roy, P., Dai, W., & Shi, X. (2020). Enhancement of biogas production from wastewater sludge via anaerobic digestion assisted with biochar amendment. *Bioresource Technology*, *309*. https://doi.org/10.1016/j.biortech.2020.123368

Wang, T., Zhai, Y., Zhu, Y., Li, C., & Zeng, G. (2018). A review of the hydrothermal carbonization of biomass waste for hydrochar formation: Process conditions, fundamentals, and physicochemical properties. *Renewable and Sustainable Energy Reviews*, Vol. 90. https://doi.org/10.1016/j.rser.2018.03.071

Wang, X. J., Wang, Y., Wang, X., Liu, M., Xia, S. Q., Yin, D. Q., … Zhao, J. F. (2011). Microwave-assisted preparation of bamboo charcoal-based iron-containing adsorbents for Cr(VI) removal. *Chemical Engineering Journal*, *174*(1). https://doi.org/10.1016/j.cej.2011.09.044

Wang, X., Zhao, J., Yang, Q., Sun, J., Peng, C., Chen, F., … Zeng, G. (2017). Evaluating the potential impact of hydrochar on the production of short-chain fatty acid from sludge anaerobic digestion. *Bioresource Technology*.

https://doi.org/10.1016/j.biortech.2017.07.051

Wang, Zhiwen, Li, J., Zhang, G., Zhi, Y., Yang, D., Lai, X., & Ren, T. (2020). Characterization of acid-aged biochar and its ammonium adsorption in an aqueous solution. *Materials*. https://doi.org/10.3390/ma13102270

Wang, Ziqi, Yun, S., Xu, H., Wang, C., Zhang, Y., Chen, J., & Jia, B. (2019). Mesophilic anaerobic co-digestion of acorn slag waste with dairy manure in a batch digester: Focusing on mixing ratios and bio-based carbon accelerants. *Bioresource Technology*, *286*. https://doi.org/10.1016/j.biortech.2019.121394

Weber, K. A., Achenbach, L. A., & Coates, J. D. (2006). Microorganisms pumping iron: Anaerobic microbial iron oxidation and reduction. *Nature Reviews Microbiology*, Vol. 4. https://doi.org/10.1038/nrmicro1490

Wei, J., Liang, G., Alex, J., Zhang, T., & Ma, C. (2020). Research progress of energy utilization of agricultural waste in China: Bibliometric analysis by citespace. *Sustainability (Switzerland)*. https://doi.org/10.3390/su12030812

Wei, W., Guo, W., Ngo, H. H., Mannina, G., Wang, D., Chen, X., … Ni, B. J. (2020). Enhanced high-quality biomethane production from anaerobic digestion of primary sludge by corn stover biochar. *Bioresource Technology*, *306*. https://doi.org/10.1016/j.biortech.2020.123159

Wei, W., Zhou, X., Wang, D., Sun, J., & Wang, Q. (2017). Free ammonia pre-treatment of secondary sludge significantly increases anaerobic methane production. *Water Research*, *118*. https://doi.org/10.1016/j.watres.2017.04.015

Weiner, B., Poerschmann, J., Wedwitschka, H., Koehler, R., & Kopinke, F. D. (2014). Influence of process water reuse on the hydrothermal carbonization of paper. *ACS Sustainable Chemistry and Engineering*, *2*(9). https://doi.org/10.1021/sc500348v

Wellinger, A., Murphy, J., & Baxter, D. (2013). The Biogas Handbook: Science, Production and Applications. In *The Biogas Handbook: Science, Production and Applications*. https://doi.org/10.1533/9780857097415

Wendt, H. (1988). K. Kinoshita: Carbon, Electrochemical and Physical Properties , John Wiley + Sons, Chichester, New York, Brisbane, Toronto 1988. 533 Seiten, Preis: £ 65.- . *Berichte Der Bunsengesellschaft Für Physikalische Chemie*, *92*(9). https://doi.org/10.1002/bbpc.198800269

Westerholm, M., Hansson, M., & Schnürer, A. (2012). Improved biogas production from whole stillage by co-digestion with cattle manure. *Bioresource Technology*, *114*. https://doi.org/10.1016/j.biortech.2012.03.005

Wiedemeier, D. B., Abiven, S., Hockaday, W. C., Keiluweit, M., Kleber, M., Masiello, C. A., … Schmidt, M. W. I. (2015). Aromaticity and degree of aromatic condensation of char. *Organic Geochemistry*. https://doi.org/10.1016/j.orggeochem.2014.10.002

Wiedner, K., Naisse, C., Rumpel, C., Pozzi, A., Wieczorek, P., & Glaser, B. (2013). Chemical modification of biomass residues during hydrothermal carbonization - What makes the difference, temperature or feedstock? *Organic Geochemistry*. https://doi.org/10.1016/j.orggeochem.2012.10.006

Wirth, B., & Mumme, J. (2014). Anaerobic Digestion of Waste Water from Hydrothermal Carbonization of Corn Silage. *Applied Bioenergy*. https://doi.org/10.2478/apbi-2013-0001

Wu, H., Zhao, Y., Long, Y., Zhu, Y., Wang, H., & Lu, W. (2011). Evaluation of the biological stability of waste during landfill stabilization by thermogravimetric analysis and Fourier transform infrared spectroscopy. *Bioresource Technology*, *102*(20). https://doi.org/10.1016/j.biortech.2011.07.029

Wu, S., Fang, G., Wang, Y., Zheng, Y., Wang, C., Zhao, F., … Zhou, D. (2017). Redox-Active Oxygen-Containing Functional Groups in Activated Carbon Facilitate Microbial Reduction of Ferrihydrite. *Environmental Science and Technology*, *51*(17). https://doi.org/10.1021/acs.est.7b01854

Wurzer, C., & Mašek, O. (2021). Feedstock doping using iron rich waste increases the pyrolysis gas yield and adsorption performance of magnetic biochar for emerging contaminants. *Bioresource Technology*, *321*. https://doi.org/10.1016/j.biortech.2020.124473

Wüst, D., Rodriguez Correa, C., Suwelack, K. U., Köhler, H., & Kruse, A. (2019). Hydrothermal carbonization of dry toilet residues as an added-value strategy – Investigation of process parameters. *Journal of Environmental Management*, *234*. https://doi.org/10.1016/j.jenvman.2019.01.005

Xiao, K., Liu, H., Li, Y., Yi, L., Zhang, X., Hu, H., & Yao, H. (2018). Correlations between hydrochar properties and chemical constitution of orange peel waste during hydrothermal carbonization. *Bioresource Technology*, *265*. https://doi.org/10.1016/j.biortech.2018.06.014

Xiao, X., Chen, B., Chen, Z., Zhu, L., & Schnoor, J. L. (2018). Insight into Multiple and Multilevel Structures of Biochars and Their Potential Environmental Applications: A Critical Review. *Environmental Science and Technology*, Vol. 52. https://doi.org/10.1021/acs.est.7b06487

Xiao, X., Chen, Z., & Chen, B. (2016). H/C atomic ratio as a smart linkage between pyrolytic temperatures, aromatic clusters and sorption properties of biochars derived from diverse precursory materials. *Scientific Reports*, *6*. https://doi.org/10.1038/srep22644

Xing, M., Li, X., Yang, J., Huang, Z., & Lu, Y. (2012). Changes in the chemical

characteristics of water-extracted organic matter from vermicomposting of sewage sludge and cow dung. *Journal of Hazardous Materials*, *205–206*. https://doi.org/10.1016/j.jhazmat.2011.11.070

Xu, J., Lin, H., & Sheng, K. (2021). Effects of Hydrothermal Pretreatment and Hydrochar Addition on the Performance of Pig Carcass Anaerobic Digestion. *Frontiers in Microbiology*, *12*. https://doi.org/10.3389/fmicb.2021.622235

Xu, N., Liu, S., Xin, F., Zhou, J., Jia, H., Xu, J., … Dong, W. (2019). Biomethane production from lignocellulose: Biomass recalcitrance and its impacts on anaerobic digestion. *Frontiers in Bioengineering and Biotechnology*, *7*(AUG). https://doi.org/10.3389/fbioe.2019.00191

Xu, S., Wang, C., Duan, Y., & Wong, J. W. C. (2020). Impact of pyrochar and hydrochar derived from digestate on the co-digestion of sewage sludge and swine manure. *Bioresource Technology*, *314*. https://doi.org/10.1016/j.biortech.2020.123730

Xu, Z., Xu, X., Zhang, Y., Yu, Y., & Cao, X. (2020). Pyrolysis-temperature depended electron donating and mediating mechanisms of biochar for Cr(VI) reduction. *Journal of Hazardous Materials*, *388*. https://doi.org/10.1016/j.jhazmat.2019.121794

Yaashikaa, P. R., Kumar, P. S., Varjani, S., & Saravanan, A. (2020). A critical review on the biochar production techniques, characterization, stability and applications for circular bioeconomy. *Biotechnology Reports*, Vol. 28. https://doi.org/10.1016/j.btre.2020.e00570

Yaman, S. (2004). Pyrolysis of biomass to produce fuels and chemical feedstocks. *Energy Conversion and Management*, *45*(5). https://doi.org/10.1016/S0196-8904(03)00177-8

Yan, Y., Ma, X., Cao, W., Zhang, X., Zhou, J., Liu, Q., & Qian, G. (2018). Identifying the reducing capacity of biomass derived hydrochar with different post-treatment methods. *Science of the Total Environment*, *643*. https://doi.org/10.1016/j.scitotenv.2018.06.232

Yang, G., Xu, Q., Wang, D., Tang, L., Xia, J., Wang, Q., … Li, X. (2018). Free ammonia-based sludge treatment reduces sludge production in the wastewater treatment process. *Chemosphere*, *205*. https://doi.org/10.1016/j.chemosphere.2018.04.140

Yang, H., Yan, R., Chen, H., Lee, D. H., & Zheng, C. (2007). Characteristics of hemicellulose, cellulose and lignin pyrolysis. *Fuel*, *86*(12–13). https://doi.org/10.1016/j.fuel.2006.12.013

Yang, L., He, L., Xue, J., Wu, L., Ma, Y., Li, H., … Zhang, Z. (2019). Highly efficient nickel (II) removal by sewage sludge biochar supported α-Fe2O3 and α-FeOOH: Sorption characteristics and mechanisms. *PLoS ONE*, *14*(6). https://doi.org/10.1371/journal.pone.0218114

Yi, Y., Huang, Z., Lu, B., Xian, J., Tsang, E. P., Cheng, W., … Fang, Z. (2019). Magnetic biochar for environmental remediation: A review. *Bioresource Technology*. https://doi.org/10.1016/j.biortech.2019.122468

Ying, S. C., Kocar, B. D., & Fendorf, S. (2012). Oxidation and competitive retention of arsenic between iron- and manganese oxides. *Geochimica et Cosmochimica Acta*, *96*. https://doi.org/10.1016/j.gca.2012.07.013

Yu, D., & Dai, L. (2010). Self-assembled graphene/carbon nanotube hybrid films for supercapacitors. *Journal of Physical Chemistry Letters*, *1*(2). https://doi.org/10.1021/jz9003137

Yu, L., Yuan, Y., Tang, J., Wang, Y., & Zhou, S. (2015). Biochar as an electron

shuttle for reductive dechlorination of pentachlorophenol by Geobacter sulfurreducens. *Scientific Reports*, *5*. https://doi.org/10.1038/srep16221

Yu, Q., Sun, C., Liu, R., Yellezuome, D., Zhu, X., Bai, R., … Sun, M. (2021). Anaerobic co-digestion of corn stover and chicken manure using continuous stirred tank reactor: The effect of biochar addition and urea pretreatment. *Bioresource Technology*, *319*. https://doi.org/10.1016/j.biortech.2020.124197

Yu, Z., Qiu, W., Wang, F., Lei, M., Wang, D., & Song, Z. (2017). Effects of manganese oxide-modified biochar composites on arsenic speciation and accumulation in an indica rice (Oryza sativa L.) cultivar. *Chemosphere*, *168*. https://doi.org/10.1016/j.chemosphere.2016.10.069

Yu, Z., Zhou, L., Huang, Y., Song, Z., & Qiu, W. (2015). Effects of a manganese oxide-modified biochar composite on adsorption of arsenic in red soil. *Journal of Environmental Management*, *163*. https://doi.org/10.1016/j.jenvman.2015.08.020

Yuan, H. Y., Ding, L. J., Zama, E. F., Liu, P. P., Hozzein, W. N., & Zhu, Y. G. (2018). Biochar Modulates Methanogenesis through Electron Syntrophy of Microorganisms with Ethanol as a Substrate. *Environmental Science and Technology*, *52*(21). https://doi.org/10.1021/acs.est.8b04121

Yuan, Haiping, & Zhu, N. (2016). Progress in inhibition mechanisms and process control of intermediates and by-products in sewage sludge anaerobic digestion. *Renewable and Sustainable Energy Reviews*, Vol. 58. https://doi.org/10.1016/j.rser.2015.12.261

Yuan, Haoran, Lu, T., Huang, H., Zhao, D., Kobayashi, N., & Chen, Y. (2015). Influence of pyrolysis temperature on physical and chemical properties of biochar made from sewage sludge. *Journal of Analytical and Applied Pyrolysis*,

112. https://doi.org/10.1016/j.jaap.2015.01.010

Yue, Y., Yao, Y., Lin, Q., Li, G., & Zhao, X. (2017). The change of heavy metals fractions during hydrochar decomposition in soils amended with different municipal sewage sludge hydrochars. *Journal of Soils and Sediments*. https://doi.org/10.1007/s11368-015-1312-2

Zaied, B. K., Nasrullah, M., Siddique, M. N. I., Zularisam, A. W., Singh, L., & Krishnan, S. (2020). Co-digestion of palm oil mill effluent for enhanced biogas production in a solar assisted bioreactor: Supplementation with ammonium bicarbonate. *Science of the Total Environment*, *706*. https://doi.org/10.1016/j.scitotenv.2019.136095

Zboril, R., Mashlan, M., & Petridis, D. (2010). ChemInform Abstract: Iron(III) Oxides from Thermal Processes-Synthesis, Structural and Magnetic Properties, Moessbauer Spectroscopy Characterization, and Applications. *ChemInform*, *33*(21). https://doi.org/10.1002/chin.200221225

Zhan, W., Tian, Y., Zhang, J., Zuo, W., Li, L., Jin, Y., … Zhang, X. (2021). Mechanistic insights into the roles of ferric chloride on methane production in anaerobic digestion of waste activated sludge. *Journal of Cleaner Production*, *296*. https://doi.org/10.1016/j.jclepro.2021.126527

Zhang, Jie, Liu, J., & Liu, R. (2015). Effects of pyrolysis temperature and heating time on biochar obtained from the pyrolysis of straw and lignosulfonate. *Bioresource Technology*, *176*. https://doi.org/10.1016/j.biortech.2014.11.011

Zhang, Jin, Jin, J., Wang, M., Naidu, R., Liu, Y., Man, Y. B., … Shan, S. (2020). Co-pyrolysis of sewage sludge and rice husk/ bamboo sawdust for biochar with high aromaticity and low metal mobility. *Environmental Research*, *191*. https://doi.org/10.1016/j.envres.2020.110034

Zhang, Jing, Dong, H., Liu, D., Fischer, T. B., Wang, S., & Huang, L. (2012). Microbial reduction of Fe(III) in illite-smectite minerals by methanogen Methanosarcina mazei. *Chemical Geology*, *292–293*. https://doi.org/10.1016/j.chemgeo.2011.11.003

Zhang, Miao, Lin, Q., Rui, J., Li, J., & Li, X. (2017). Ammonium inhibition through the decoupling of acidification process and methanogenesis in anaerobic digester revealed by high throughput sequencing. *Biotechnology Letters*, *39*(2). https://doi.org/10.1007/s10529-016-2241-x

Zhang, Min, Li, J., Wang, Y., & Yang, C. (2019). Impacts of different biochar types on the anaerobic digestion of sewage sludge. *RSC Advances*, *9*(72). https://doi.org/10.1039/c9ra08700a

Zhang, Min, Yang, C., Jing, Y., & Li, J. (2016). Effect of energy grass on methane production and heavy metal fractionation during anaerobic digestion of sewage sludge. *Waste Management*, *58*. https://doi.org/10.1016/j.wasman.2016.09.040

Zhang, Ming, Gao, B., Varnoosfaderani, S., Hebard, A., Yao, Y., & Inyang, M. (2013). Preparation and characterization of a novel magnetic biochar for arsenic removal. *Bioresource Technology*, *130*. https://doi.org/10.1016/j.biortech.2012.11.132

Zhang, Mingyuan, & Zang, L. (2019). A review of interspecies electron transfer in anaerobic digestion. *IOP Conference Series: Earth and Environmental Science*, *310*(4). https://doi.org/10.1088/1755-1315/310/4/042026

Zhang, W., Guo, J., Wu, S., Dong, R., Zhou, J., Lang, Q., … Wang, B. (2012). Effects of Fe 2+ on the anaerobic digestion of chicken manure: A batch study. *Proceedings - 2012 3rd International Conference on Digital Manufacturing and Automation, ICDMA 2012*. https://doi.org/10.1109/ICDMA.2012.259

Zhang, W. M., Wu, X. L., Hu, J. S., Guo, Y. G., & Wan, L. J. (2008). Carbon coated Fe3O4 nanospindles as a superior anode material for lithium-ion batteries. *Advanced Functional Materials*, *18*(24). https://doi.org/10.1002/adfm.200801386

Zhang, Y., Xu, X., Cao, L., Ok, Y. S., & Cao, X. (2018). Characterization and quantification of electron donating capacity and its structure dependence in biochar derived from three waste biomasses. *Chemosphere*, *211*. https://doi.org/10.1016/j.chemosphere.2018.08.033

Zhang, Y., Xu, X., Zhang, P., Ling Zhao, Qiu, H., & Cao, X. (2019). Pyrolysis-temperature depended quinone and carbonyl groups as the electron accepting sites in barley grass derived biochar. *Chemosphere*, *232*. https://doi.org/10.1016/j.chemosphere.2019.05.225

Zhang, Zengsheng, Wang, X., Wang, Y., Xia, S., Chen, L., Zhang, Y., & Zhao, J. (2013). Pb(II) removal from water using Fe-coated bamboo charcoal with the assistance of microwaves. *Journal of Environmental Sciences (China)*, *25*(5). https://doi.org/10.1016/S1001-0742(12)60144-2

Zhang, Zhikun, Zhu, Z., Shen, B., & Liu, L. (2019). Insights into biochar and hydrochar production and applications: A review. *Energy*, Vol. 171. https://doi.org/10.1016/j.energy.2019.01.035

Zhao, Y., Zhang, R., Liu, H., Li, M., Chen, T., Chen, D., … Frost, R. L. (2019). Green preparation of magnetic biochar for the effective accumulation of Pb(II): Performance and mechanism. *Chemical Engineering Journal*, *375*. https://doi.org/10.1016/j.cej.2019.122011

Zhao, Z., Zhang, Y., Holmes, D. E., Dang, Y., Woodard, T. L., Nevin, K. P., & Lovley, D. R. (2016). Potential enhancement of direct interspecies electron transfer for syntrophic metabolism of propionate and butyrate with biochar in up-flow

anaerobic sludge blanket reactors. *Bioresource Technology*. https://doi.org/10.1016/j.biortech.2016.03.005

Zhao, Z., Zhang, Y., Wang, L., & Quan, X. (2015). Potential for direct interspecies electron transfer in an electric-anaerobic system to increase methane production from sludge digestion. *Scientific Reports*, *5*. https://doi.org/10.1038/srep11094

Zheng, L., Gao, Y., Du, J., Zhang, W., Huang, Y., Wang, L., … Pan, X. (2020). A novel, recyclable magnetic biochar modified by chitosan-EDTA for the effective removal of Pb(ii) from aqueous solution. *RSC Advances*, *10*(66). https://doi.org/10.1039/d0ra07499c

Zhong, D., Li, J., Ma, W., & Qian, F. (2020). Clarifying the synergetic effect of magnetite nanoparticles in the methane production process. *Environmental Science and Pollution Research*, *27*(14). https://doi.org/10.1007/s11356-020-07828-y

Zhou, Yi, Liu, G., Liu, J., Xiao, Y., Wang, T., & Xue, Y. (2021). Magnetic biochar prepared by electromagnetic induction pyrolysis of cellulose: Biochar characterization, mechanism of magnetization and adsorption removal of chromium (VI) from aqueous solution. *Bioresource Technology*, *337*. https://doi.org/10.1016/j.biortech.2021.125429

Zhou, Ying, Engler, N., Li, Y., & Nelles, M. (2020). The influence of hydrothermal operation on the surface properties of kitchen waste-derived hydrochar: Biogas upgrading. *Journal of Cleaner Production*, *259*. https://doi.org/10.1016/j.jclepro.2020.121020

Zhu, L., Lei, H., Wang, L., Yadavalli, G., Zhang, X., Wei, Y., … Ahring, B. (2015). Biochar of corn stover: Microwave-assisted pyrolysis condition induced changes in surface functional groups and characteristics. *Journal of Analytical and*

Applied Pyrolysis, *115*. https://doi.org/10.1016/j.jaap.2015.07.012

Zhu, T., Curtis, J., & Clancy, M. (2019). Promoting agricultural biogas and biomethane production: Lessons from cross-country studies. *Renewable and Sustainable Energy Reviews*. https://doi.org/10.1016/j.rser.2019.109332

Appendix

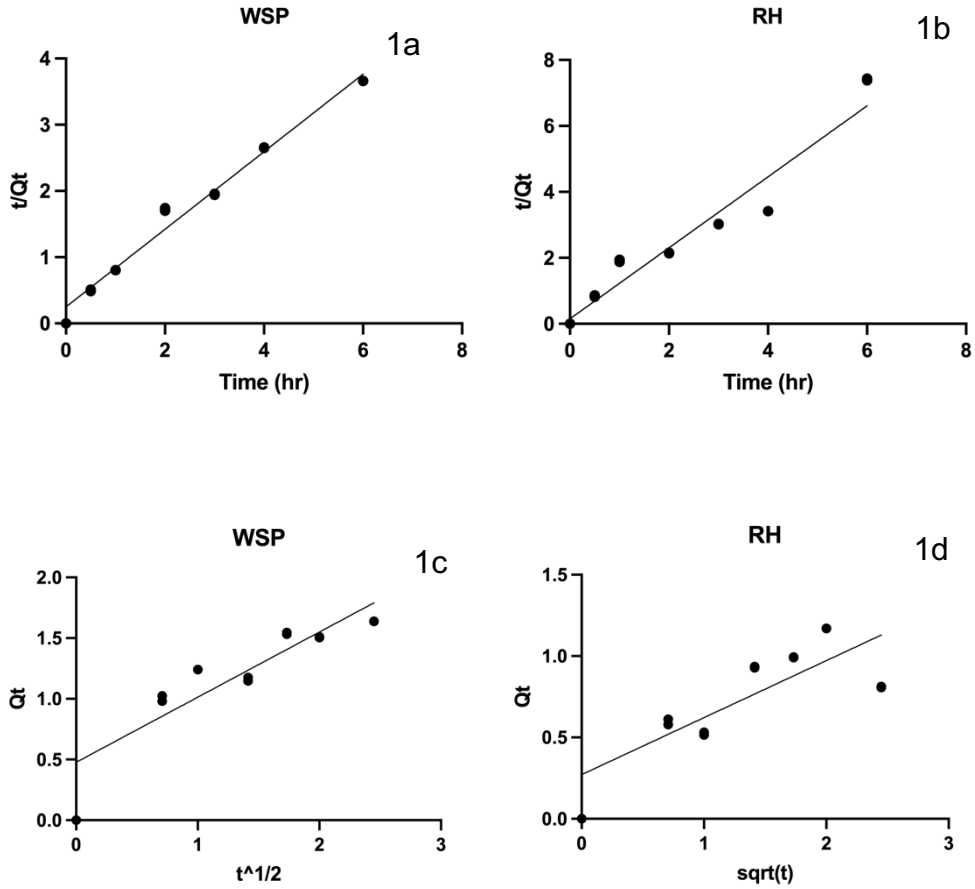

Appendix Figure 1. Kinetic data of ammonium adsorption on RH and WSP biochar (1a, 1b) Pseudo 2nd order kinetic model; (1c, 1d) Intra-particle diffusion model. More detailed information on adsorption kinetic models is listed in Table 3-4.

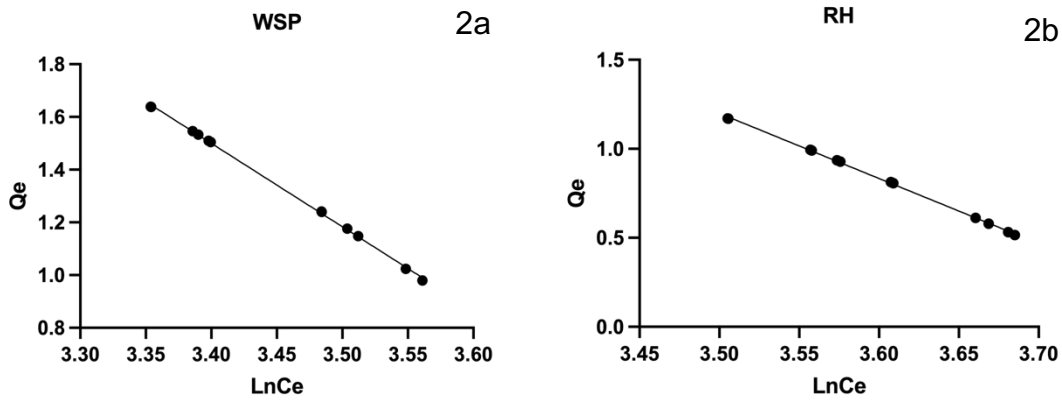

Appendix Figure 2. Adsorption isothermals of biochar by fitting Temkin isotherm models. More detailed information of isothermal models is summarized in Table 3-2.